UNIVERSITY OF CALGARY

Extended Distillation and Property Correlations for Heavy Oil

by

Maria Catalina Sanchez Lemus

A THESIS

SUBMITTED TO THE FACULTY OF GRADUATE STUDIES

IN PARTIAL FULFILMENT OF THE REQUIREMENTS FOR THE

DEGREE OF DOCTOR OF PHILOSOPHY

GRADUATE PROGRAM IN CHEMICAL AND PETROLEUM ENGINEERING

CALGARY, ALBERTA

DECEMBER, 2015

Abstract

A previously developed Deep Vacuum Fractionation Apparatus (DVFA) was modified and improved to provide reproducible and consistent distillation data and samples of cuts with reproducible physical properties. The apparatus can distill up to 50 wt% of a bitumen compared to the 25% typically obtained with a conventional vacuum distillation. An interconversion method was implemented to obtain the Normal Boiling Points (NBP) of the distillation fractions. The physical properties of the distillation cuts collected were measured and used to improve and develop correlations to predict the normal boiling point (NBP), specific gravity (SG), molecular weight (MW), heat capacity, heat of vaporization, and heat of combustion of heavy distillation cuts. In addition, two methods were developed to generate property distributions from only bulk properties and distillation data. The extensive property measurements for the heavy distillation cuts provide a unique property database. The correlations developed in this thesis form the basis of an improved characterization procedure that requires only conventional distillation data and bulk specific gravity.

Executive Summary

The simulation of refining and recovery processes requires models to describe petroleum fluid phase behavior and the associated physical properties. The input to these models is a fluid characterization based on pseudo-components representing the distribution of properties within the fluid. The characterization is typically based on distillation or GC data and well established methodologies exist for conventional oils for which the distillable fraction represents the majority of the fluid. However, these techniques are not necessarily accurate for heavy crude oils because less than 30% of the whole heavy oil can be distilled and property extrapolation over the residue introduces considerable uncertainty. To improve the characterization, an extended distillation curve is required for heavy oils as well as physical property measurements of distillation cuts from the extended distillation region.

A Deep Vacuum Fractionation Apparatus (DVFA), originally designed to measure vapor pressure and previously shown capable of fractionating heavy oils and bitumen (Castellanos, 2012), was modified and improved to provide reproducible and consistent distillation data and samples of cuts with reproducible physical properties. After modifications, the DVFA apparatus was able to distill a set of seven bitumen and heavy oil samples, sourced from Europe, North, Central, and South America, up to 50 wt% without generating cracked samples. The repeatability for all tested oils was less than 1.8% for the distillation curve, 0.2% for the density of the cuts, and 3% for the molecular weight of the cuts.

The interconversion of the boiling temperatures measured in the DVFA to True Boiling Point (TBP) was required for use in oil characterization procedures. An interconversion method based on the simultaneous fitting of vapor pressure and heat capacity with the Cox vapor pressure equation was successfully applied to the DVFA data. During this process, it was confirmed that maltene distillation cuts follow a Gaussian distribution, which validates the characterization methodology for heavy oils proposed by Castellanos *et al.* (2011). Additionally, a simplified interconversion method was developed to predict distillation curves of heavy oils from bulk properties.

Correlations to predict normal boiling point (NBP), specific gravity (SG) and molecular weight (MW) of heavy distillation cuts were developed. A modified version of Soreide's correlation was

implemented to better estimate NBP and MW. The average relative deviations before and after modification are as follows:

	NBP %ARD*		MW %ARD*	
	Original	Modified	Original	Modified
Development Dataset (DDS)	3.0	2.0	7.8	5.3
Test Dataset (TDS)	2.5	2.3	5.4	5.1

**ARD average Relative Deviation*

A new correlation was proposed to predict SG from the H/C ratio and MW. The average relative deviations were less than 0.8% for the DDS and 1.4% for the TDS, compared with 1.7% and 3.1%, respectively, for the best performing correlation in the literature. A simple correlation between refractive index and SG was proposed that fitted the development dataset with an error less than 1.2%.

A new vapor pressure correlation was developed based on the trends found between the Cox vapor pressure constants and molecular weight. The new equation improved the vapor pressure predictions for the heavier oils and bitumen with an AARD within 50% for the DDS. The Maxwell-Bonnell equations performed better for the light cuts with a deviation of 41% compared with 44% from the correlation developed in this study. For the TDS, the deviations were decreased from 200% to 50%.

The Tsonopoulos (1986) heat capacity correlation was modified to better fit the data collected in this thesis: first, with the Watson Factor and the SG of the cuts as input; second, with the H/C ratio and SG of the cuts as input. Both versions improved the heat capacity prediction compared to the original correlation, reducing the AARD from 4.5 to 1.0% for the DDS and from 6.0 to 1.1% for the TDS.

Using the direct relationship between vapor pressure and enthalpy of vaporization from the Clapeyron equation, the previously obtained Cox constants were used to estimate enthalpy of vaporization values. Although the data cannot be regarded as experimental results, these calculated values are the only estimate available for heats of vaporization of heavy distillation cuts. A new correlation to calculate the enthalpy of vaporization at the normal boiling point was constructed based on the calculated "data". The overall AARD for the DDS was 7.5% compared with 9.5% from the best literature correlation. In this case, the TDS was the development dataset used for the

best performing correlation (Fang, 2011); therefore, the proposed method had a slightly higher error of 0.3% compared with Fang's correlation.

The heats of combustion of some cuts were measured and the data was used to test the accuracy of current correlations based on the elemental analysis. The Tsonopoulos (1986) and Yan *et al.* (1988) correlations predicted the heats of combustion (HHV) for heavy distillation cuts to within 1%.

In practice, often only a distillation curve and bulk properties are available to construct an oil characterization. Two methods were developed to generate property distributions from only bulk properties and TBP data. The first method was a modified version of the Katz-Firoozabadi correlation that included a new generalization of a correction proposed by Satyro and coworkers (2011). The second method was an equation developed specifically for heavy oils and bitumen samples, excluding pure components. Both methods showed an improvement from literature correlations, decreasing the deviations from 2.8% to 1.3% for the modified K-F method and to 0.8% for the new correlation.

The final contribution of this study was in simulated distillation, which has proven to be faster and more economical than physical distillation. Beyond 30 wt% distilled, simulated distillation from ASTM D7169 diverged from the boiling point distribution obtained from the DVFA apparatus and corroborated with a Gaussian extrapolation of the Spinning Band Distillation (SBD) data. A preliminary correction factor based on the bulk molar volume was recommended for simulated distillation data above 30 wt% distilled.

The correlations developed in this thesis form the basis of an improved characterization procedure that requires only conventional distillation data and bulk specific gravity. It is recommended to use a Gaussian extrapolation to obtain a complete distillation curve for the deasphalted fraction of the oil. Then, the specific gravity distribution is determined using the correlations developed in this work and the molecular weight distribution is determined using the modified version of Soreide correlation. Additionally, vapor pressure and thermal properties can be determined from the known and calculated physical properties. Note, a separate characterization for the asphaltenes is recommended; since asphaltene self-associate, they are not expected to follow the same trends as the non-associated maltenes. An asphaltene molecular weight distribution is calculated from a Gamma distribution function and existing correlations are used for their specific gravity and

boiling point. Common correlations to predict critical properties (such as the Lee-Kesler correlations) are used to complete the characterization. This characterization procedure can provide more accurate property predictions for heavy oils and their fractions than the currently used methods.

Acknowledgements

First of all, I am thankful to God for always lining up my path in the best possible way and never leaving me wishing for something better.

To my supervisor, Dr. Harvey Yarranton, saying thank you wouldn't be enough to express the immense gratitude I have for his guidance and support. All the time he put in meetings, practice presentations, discussions, answering emails, rewording convoluted Spanish-like sentences, a difficult task I must say, and many other time-consuming but invaluable efforts, not only made this thesis possible, but also made me a much better person. A great teacher is one who teaches with love, patience, dedication, inspires and brings the best out of their students. As part of my gratitude, I want to say that Harvey did a great job in making me realize how incomplete my definition of a great teacher was.

A fruitful work is always the result of contributions by many people. A part of my awesome team was my co-supervisor, Dr. Shawn Taylor. Once again, saying thanks seems a bit shorthanded. It is highly appreciated all the time he gave to my project in useful discussions that left me wondering if I knew what I was doing. Also very valued is the professional advice he was always ready to provide and the times he had to fly to Calgary to check on my 'great' progress (and all the other students) on the not so great 5 am flight.

To Elaine and Florian I offer my apologies for breaking so much stuff in the lab and complaining about leaks that were technically inexistent, but terribly annoying for my experiments. I would like to thank them for the lab support and insightful discussions about my project and also about life. They made possible the construction of all the tables and figures in this thesis by teaching me how to use a huge number of lab equipment.

I also want to extend my gratitude to Dr. Marco Satyro and Dr. Orlando Castellanos. They were also big contributors to this work and part of my awesome team. I thank them for always giving me valuable advice and answering the questions I was shy to ask to my supervisor (because I thought I was supposed to know that). Thanks to them, there was a big idea and an apparatus I used to complete this work.

Thank you also to the NSERC Industrial Research Chair in Heavy Oil Properties and Processing, Shell Canada, Schlumberger, Suncor Energy, Petrobras, Nexen Energy ULC, and Virtual Materials Group for providing the funding and make this project possible.

I cannot finish this section before thanking the most important people in my life: my future hubby, my mom, my daddy, and my brother. To my parents, I owe them everything I have learnt and I will be forever in debt with them for giving me the best they had to make me the person I am today. To my brother, I want to say that life acts in very strange ways, but the results are always rewarding if you put your heart and mind in what you do. Last, but by no means least, I want to thank my best friend and love of my life, Anthony, for supporting me through this path, for wiping my tears when the VPO didn't work and for being so caring and loving when I most needed it.

Dedication

This thesis is dedicated to God and the parents, brother and husband He gave me to give purpose to my life.

Table of Contents

List of Tables

List of Figures and Illustrations

List of Symbols, Abbreviations and Nomenclature

Symbols	Definition	Units
$\Delta C^{'}$	Change in Heat Capacity Defines as $\left(d\Delta H_{vap}/dT\right)_{Sat}$	
$\Delta H^{'}$	Ratio defined as $\frac{\Delta H_{vap}}{\Delta z}$	
ΔH_{vap}	Heat of Vaporization	kJ/mol
ΔU^{0}	Heat of Combustion	kJ/g
ΔV	Difference of Voltage	Volts
Δz	Compressibility Factor Difference in Vapor and Liquid Phase	
A	Integrated Value of the Differential Heat Flow (Eq. 3.5) Coefficient in VPO Calibration Equation (Eq. 3.1) Ideal Gas Heat Capacity Constant (Eq. 5.6)	
A_0	First Adjustable Parameter in Cox Vapor Pressure Equation	
A_1	Second Adjustable Parameter in Cox Vapor Pressure Equation	K^{-1}
A_2	Third Adjustable Parameter in Cox Vapor Pressure Equation	K^{-2}
B	Second Virial Coefficient Ideal Gas Heat Capacity Constant (Eq. 5.6)	
C	Concentration (Eq. 3.1) Ideal Gas Heat Capacity Constant (Eq. 5.6)	kg/m^3, NA
C_f	Soreide Characterization Factor	
CN	Carbon Number	
C_p	Specific Heat Capacity	kJ/g K
d	Standard Deviation	
dr	Relative Standard Deviation	

e	Heat Of Combustion Correction Factor	kJ/g
F_{RI}	Function of Refractive Index defined as $\frac{n^2-1}{n^2+2}$	
J_a	Jacoby Characterization Factor	
K	VPO Calibration Constant	
K_c	Weighting Factor	
K_w	Watson Factor	
MW	Molecular Weight	g/mol
n	Refractive Index	
N_A	Avogadro's Number	
NBP	Normal Boiling Point	K
P	Pressure	Pa
P_0	Reference Pressure in cox Equation	Pa
P_b	Atmospheric Pressure	Pa
P^{vap}	Vapor Pressure	Pa
R	Universal Gas Constant	kJ m^3/mol K
R_m	Molar Refraction	m^3/mol
SG	Specific Gravity	
T	Temperature	K
T_b	Boiling Temperature	K
v	Molar Volume	m^3/mol
w	Mass fraction	
w%	Weight Percent	
W_c	Calorimeter Heat Capacity	kJ/K
z	Mole fraction	
Z	Standard Normal Distribution Parameter	

Subscripts	**Definition**
mix	Mixture Property
ss	Heat Capacity Reference Substance

vap	Vapor Phase
liq	Liquid Phase
sat	Saturated Conditions
bulk	Bulk Property of the Oil
i	Pseudocomponent i

Superscripts	**Definition**
0	Ideal Gas
l	Saturated Liquid
calc	Calculated Value
exp	Experimental Value

Greek Symbols	**Definition**	**Units**
ρ	Density	kg/m^3
τ	Polarizability	
α	Similarity Variable	
Δ	Difference	

Abbreviations	**Definition**	**Units**
AAAD	Overall Average Absolute Deviation	
AAD	Average Absolute Deviation	
AARD	Overall Average Absolute Relative Deviation	
AET	Atmospheric Equivalent Temperature	K
ARD	Average Relative Deviation	
ASTM	American Society for Testing Materials	

CEOS	Cubic Equation of State	
CF	Correction Factor	
DFVA	Deep Vacuum Fractionation Apparatus	
GC	Gas Chromatography	
HHV	High Heating Value	kJ/g
LHV	Low Heating Value	kJ/g
MAAD	Maximum Average Absolute Deviation	
MARD	Maximum Average Relative Deviation	
OF	Optimization Function	
PHAs	Polyaromatic Hydrocarbons	
PID	Proportional-Integral-Derivative Controller	
SBD	Spinning Band Distillation	
SimDist	Simulated Distillation	
TBP	True Boiling Point	
VPO	Vapor Pressure Osmometry	

CHAPTER ONE: INTRODUCTION

1.1 Background

The steady increase in global demand for oil and the depletion of conventional oil reserves has created a transition from conventional to non-conventional oil. In this environment, heavy oil and oil sands are expected to become a major source of energy and could potentially extend the world's energy reserves by 15 years (SER, 2010) if they can be recovered and transformed into final products at a rate and price competitive with other energy sources (Chopra *et al.*, 2010). Heavy oil and oil sands have been found in countries such as Russia, United States, Mexico, China and some regions in the Middle East. The largest deposits are located in Venezuela and Canada with an oil-in-place equaling the world's reserves of conventional oil. In Canada, unconventional oil is mainly located in three areas: Peace River, Athabasca, and Cold Lake (Chopra *et al.*, 2010). Alberta has heavy oil and mineable oil sands reserves of 27 billion cubic meters (168 billion barrels) and approximately 202 billion cubic meters (1.7 trillion barrels) of heavy oil-in-place. A general overview of the global oil reserves is presented in Figure 1.1 (BP statistical Review of World energy, 2015).

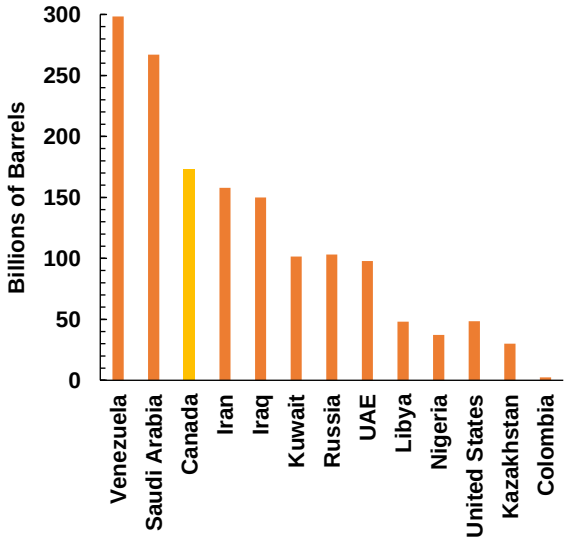

Figure 1.1 World oil reserves in billions of barrels (Reproduced from BP, 2015).

Heavy oil and bitumen have significantly higher viscosity, density, and concentrations of nitrogen, sulfur, oxygen, and heavy metals compared to conventional oil (BP-Heavy Oil, 2011), Figure 1.2. These differences pose technological, economic, and environmental challenges in both downstream and upstream processes. Over the past few decades, the industry has been seeking and applying innovative extraction techniques and technological breakthroughs to recover heavy oil with less energy usage while maintaining cost effectiveness, product quality, and minimizing environmental impacts.

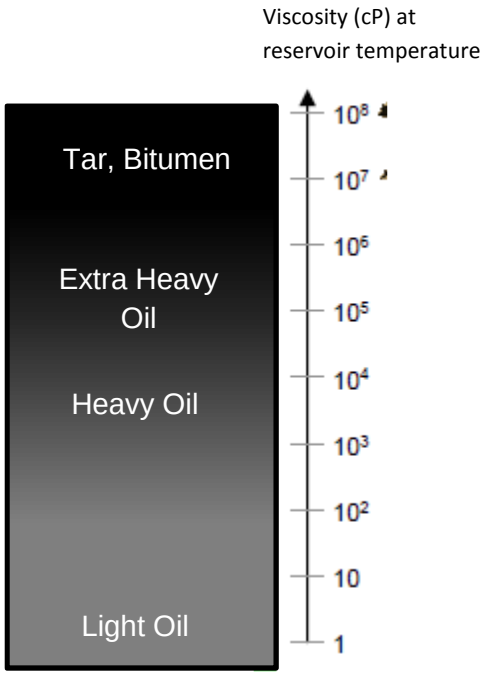

Figure 1.2. Viscosity transition from light oil to oil sands. Adapted from source BP-Heavy Oil, (2011).

The main issue is the reduction of viscosity for the purposes of improving mobility for recovery, transportation, and processing, which is most commonly facilitated by heating or dilution. For heavy oil recovery processes, a solvent (usually an *n*-alkane) can be used directly, as in the VAPEX process (Butler and Mokrys, 1989), or together with steam as in the ES-SAGD (Nars and Ayodele, 2006), N-SOL (Nenniger, 2005), SAP (Gupta *et al*, 202), LASER (Leaute, 202) and SAS (Zhao, 2004) processes. However, mixtures of solvent and heavy oil are challenging from a fluid modeling perspective because they can form more than one liquid phase (Mehrotra *et al*, 1985) and may experience asphaltene precipitation (Alboudwarej *et al*, 2005). In order to design and optimize

these methods, an accurate phase behavior model is required that is based on a more rigorous characterization of heavy oil than is usually required for thermal processes.

For phase behavior and property prediction, cubic equations of state (CEOS) and property correlations are used in the majority of commercial simulators. The fluid must first be characterized for input into the CEOS. The fluid is represented as a mixture of pseudo-components, each with an assigned mass fraction and measured or calculated specific gravity, molecular weight, and boiling point. The mass fractions as well as physical and critical properties of the pseudo-components are the required inputs for the phase behavior calculation. Critical properties are calculated since they cannot be measured for heavy petroleum fractions. Mixing rules are applied to predict the properties of the phases formed from the crude oil/solvent systems at any given pressure, temperature, and compositional conditions (Riazi, 2005).

This characterization methodology is commonly based on a distillation curve, which can be obtained from either chromatographic techniques or direct distillation. Chromatographic techniques are simple, fast, reproducible, and more economical than a laboratory-scale physical distillation. However, the calibration is based on the retention time of normal paraffins and their respective boiling points. The results for a heavy oil or bitumen must be interpreted with caution as these samples are known to have large amounts of aromatic compounds. Direct distillations techniques are abundant for crude oils (Riazi, 2005; Speight, 2001) and can be classified as atmospheric and vacuum distillations. The maximum distillation temperature is limited by the temperature (300ºC) at which the *sigma* bonds between carbons start to break and the chemical composition of the crude oil is modified. The choice of distillation method is usually dictated by the volatility of the oil; for example, an atmospheric distillation is sufficient for a light oil or condensate liquid while a vacuum distillation is required for conventional and heavier oils. The vacuum allows more liquid to be distilled below the 300°C limit.

The use of distillation curves together with cubic equations of state have proven sufficient to predict conventional oil phase behavior in most petroleum related applications (Riazi, 2005). However, there are several challenges when attempting to apply this established characterization approach to bitumen/solvent mixtures.

1. Their phase behavior is often complex and requires a more rigorous characterization.

2. Only a small fraction of the fluid is distillable, limiting the ability to characterize it. Although there is a wide range of distillation methods, most can only fractionate up to 30 wt % of the bitumen sample before reaching 300ºC even at vacuum conditions. Hence, there is considerable uncertainty in extrapolating the distillation curve over the whole oil.
3. There is a lack of data for heavy petroleum fractions limiting the ability to correlate properties. Since no heavy cuts can be collected with conventional distillation, there are few physical and thermal property data available for heavy fractions. Currently, the only option is to use the correlations developed for lighter oils which do not account for the higher aromaticity and heteroatom content of the heavier cuts.

These challenges not only require adjustments in the models used to predict the behavior of the mixtures, but also necessitate the development of alternative distillation techniques for characterization of bitumen and heavy oils and collection of data in heavier regions not explored before. A recently developed deep vacuum apparatus (DVA), originally designed to measure vapor pressure of compounds with low volatility (Castellanos, 2012), provided an opportunity to overcome the lack of data and incomplete characterization of heavy oils. The apparatus has the potential to fractionate heavy oils at pressures lower than the current vacuum techniques ($1x10^{-9}$ kPa) and to provide physical samples of heavy distillation fractions for property measurements.

1.2 Objectives

The goal of this work is to improve the characterization of bitumen and heavy oils samples by: 1) developing a reproducible deep vacuum batch fractionation technique to generate distillation curves beyond current commercial assays, and; 2) producing light and heavy fractions that can be physically characterized and compared with the results of current physical correlations.

The specific objectives of this study are as follows:

a) Modify the deep vacuum apparatus to fractionate heavy oils and bitumen samples. Develop and standardize the procedure to generate reproducible distillation data.
b) Develop an inter-conversion method to estimate the normal boiling point of the fractions collected in the deep vacuum apparatus.

c) Propose a simplified inter-conversion method that is based on readily measurable physical properties of the fractions.
d) Test the accuracy of a Gaussian extrapolation of conventional distillation curves (spinning band method) towards non-distillable regions based on the inter-converted data collected in this work for the heavy ends.
e) Fractionate heavy oils and bitumen samples from different geographic regions. The diversity of origins creates a broader spectrum of data that can be generalized for heavy oils and bitumens and is not limited to a specific region or extraction technique.
f) Measure the properties, including density, molecular weight, refractive index, vapor pressure, heat capacity, heat of combustion, and elemental analysis of the fractions obtained from the different oils. Use this data to tune and modify existing correlations (or propose new correlations) to improve their predictive behavior for samples with high content of aromatic and heteroatoms compounds. Determine the enthalpy of vaporization from the heat capacity data.
g) Propose a characterization technique that requires a minimum amount of physical bulk or fractional information for bitumen and heavy oils.
h) Compare the simulated distillation (ASTM D-7169) results with the distillation assay obtained using the deep vacuum fractionation. Simulated distillation is a chromatographic method commonly used to characterize crude oils. Incorporate adjustments to the calibration techniques used in simulated distillation assays to better characterize bitumen and heavy oil samples.

Seven bitumen and heavy oil samples from different geographic locations were used to develop the fractionation method and their distillation cuts were used for physical and thermal property measurements.

1.3 Outline

The thesis is divided into nine chapters each of which is described below.

Chapter Two reviews the basics of petroleum chemistry including their chemical compositions and properties. It also reviews of the most common distillation techniques and presents a summary

of the characterization methods for heavy components. A summary of the correlations currently available in the literature to predict physical and thermal properties is presented.

Chapter Three describes the experimental procedures related to the collection of physical properties such as density, molecular weight, liquid heat capacity, vapor pressure, elemental analysis, and refractive index. A description of the original version of the deep vacuum apparatus is also presented and the steps prior to fractionation are explained.

Chapter Four presents the modifications made on the deep vacuum apparatus including a detailed description of the advantages of the new apparatus and the reason for the modifications. The chapter finishes with a description of the standard procedure developed in this study and the statistics corresponding to repeatability of the distillation procedure.

Chapter Five presents the inter-conversion techniques developed to obtain normal boiling points based on the measured boiling temperature at low pressure, measured vapor pressure, and liquid heat capacity. The inter-conversion technique is constrained by the use of a vapor pressure equation to fit vapor pressure and heat capacity data simultaneously. A simplified, less data intensive inter-conversion method is also developed. Finally, a correlation for the normal boiling point of heavy oil and bitumen cuts is proposed based only on specific gravity of the maltenes and specific gravity of the fractions.

Chapter Six summarizes all the property data collected for the seven oils and their fractions. Here the most common physical property correlations are assessed and modifications are proposed to improve predictions of physical properties for heavy oils and bitumens. Also, additional properties such as refractive index and elemental analysis are discussed and their correlation with other physical properties is determined for heavy fractions.

Chapter Seven introduces the thermal property correlations available in the literature and their deviations from measured values. Proposed correlations are introduced to improve predictions of vapor pressure and liquid heat capacity. The enthalpy of vaporization is estimated from vapor pressure data and recommendations to predict this value from correlations available in the literature are presented.

Chapter Eight presents a new characterization methodology for heavy oils and bitumen samples that uses only a distillation curve and bulk properties. This methodology is compared with other techniques such as the constant Watson factor and Katz Firoozabadi tuning method.

Chapter Nine summarizes the major conclusions of this study and presents recommendations for future research.

CHAPTER TWO: LITERATURE REVIEW

This chapter presents a review of petroleum chemistry, petroleum characterization methods and the associated correlations. In particular, different approaches to classify crude oils and to measure their property distributions are discussed. The methods used to represent their property distributions for input into phase behavior models are presented including pseudo-component generation and property correlations.

2.1 Petroleum Definition

Petroleum is a naturally occurring mixture of gas, liquid and solid hydrocarbons, which contains varying amounts of oxygen, nitrogen, sulfur and metals such as vanadium and nickel (Speight, 2001; Altgelt and Boduszynski, 1994; McKenna *et al*., 2011). Petroleum, along with coal and shale oils, consists of millions (perhaps many millions) of chemical compounds (Tsonopoulos *et al.*, 1986; Strausz and Lown, 2003; McKenna *et al*., 2011). Its composition mainly varies with the source (Speight, 2001) and these differences are a result of processes such as biodegradation, water washing, oxidation, deasphalting/evaporation and preferential migration of lighter components (Deroo *et al*., 1977) that occurs during the migration of the oil and its subsequent accumulation in the reservoir. All of these factors can have a significant effect on the final composition of the fluid. The oil ultimately discovered in the reservoir rock may have mainly low boiling point components, as is the case of light oils, or high concentrations of high boiling point components as occurs in heavy oil and bitumen.

Crude oils can be classified according to recovery method. When conventional techniques (vertical or horizontal wells under primary or waterflood recovery) are used to recover the crude oil from the subsurface, the oil is categorized as conventional oil. However, if significant technical effort and cost is required to recover the oil (such as thermal methods and multi-frac technology), then the oil is categorized as an unconventional oil.

Crude oils can also be classified according to their fluid properties as depicted in Figure 2.1. On the basis of API gravity, crude oil can be classified into the following categories: light (API> 31.1),

medium (22.3<API<31.1), heavy (API<22.3), and extra heavy or bitumen (API<10). The viscosity at the reservoir conditions of light or medium crude oil ranges from 10 to 1,000 cP, heavy oils from 1,000 to 10,000 cP, and bitumen from 10,000 cP to 1,000,000+ cP. The quality of the crude oils are also classified based on sulfur content (Speight, 2001; Banerjee, 2012) as "sweet" (sulfur content less than 1 wt%) or "sour" (sulfur content more than 1 wt%).

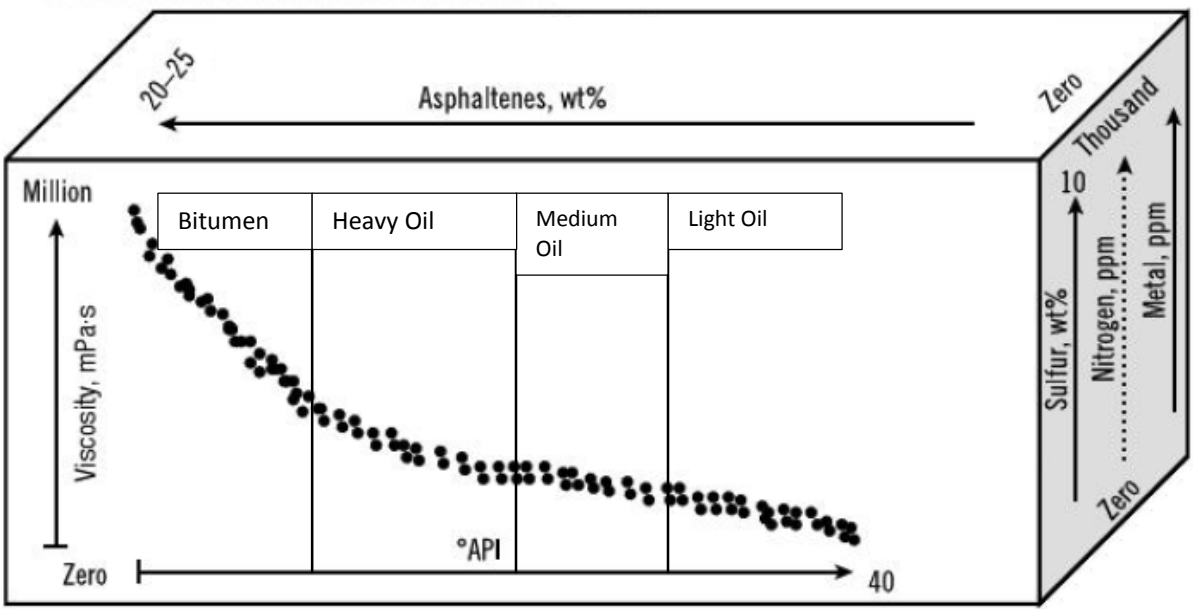

Figure **2.1. Property variation of crude oil with API (modified from Banerjee, 2012).**

Figure 2.1 also shows the trends in composition through the oil classes. The asphaltene, sulfur, nitrogen, and metals content increases from lighter to heavier crude oils. The variation in properties indicated above is a consequence of differences in the chemical constituents in different types of crude oils. For example, heavy oils and bitumens are deficient in hydrogen content (high aromaticity) and have high contents of carbon, sulfur, nitrogen, and metal compounds. Density and viscosity tend to increase with aromaticity. Bitumen is an oil that has been microbiologically degraded (Larter and Head, 2014) and therefore is strongly depleted in straight chain paraffinic components and relatively abundant in the naphthenic and aromatic classes. As a result, it is an extremely viscous material.

A relation between carbon number and boiling point was presented by Altgelt and Boduszynski, (1994), Figure 2.2. Denser components tend to have higher boiling points (lower volatility). Hence, heavier oils contain less volatile and distillable components. Also, as the molecular weight increases, the number of species that fall into the same carbon number or boiling interval increases dramatically. Hence, heavier oils are not only less volatile but are more complex mixtures than light oils, and therefore are more challenging to characterize.

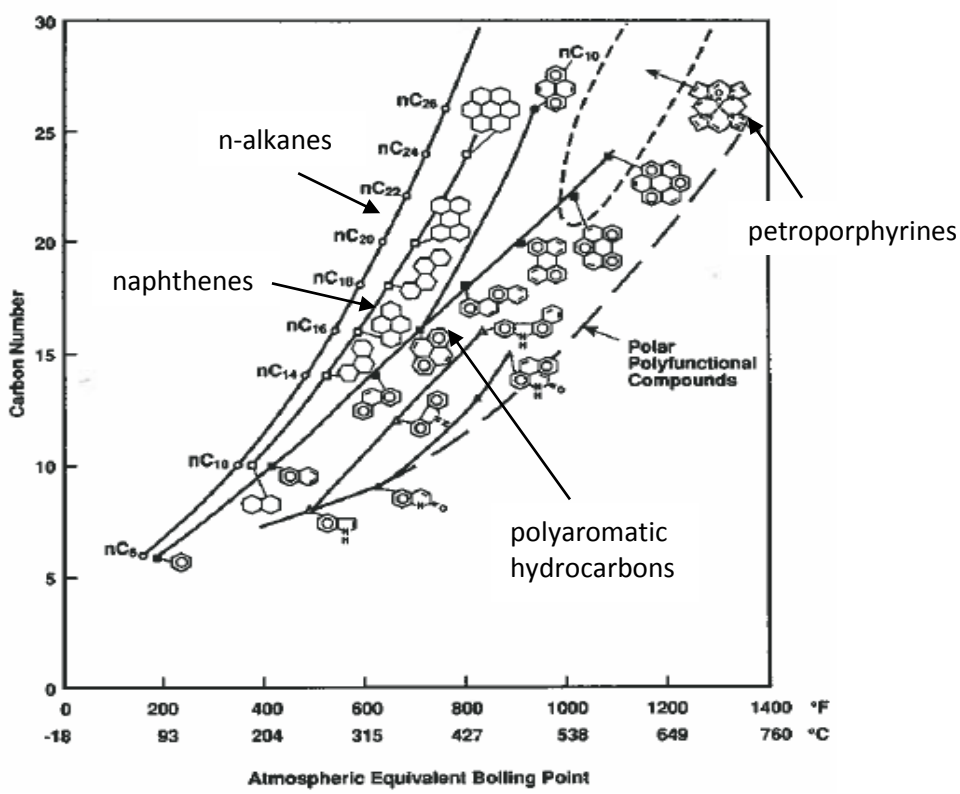

Figure 2.2. Effect of carbon number and structure in boiling point. (Modified from Altgelt and Boduszynski, 1994).

Crude oils can also be considered as a mixture of chemical families which include paraffins, iso-paraffins, oleofins, naphthenes, and aromatics. These families each encompass a very broad range of molecular weights and heteroatomic sub-families. From a solubility point of view, the paraffins and naphthenes are commonly lumped as saturates. The aromatics are divided into simple aromatics (e.g. mono-, di-, and tri-ring), resins, and asphaltenes. Insoluble material (carbenes and

carboids) are also part of the heavy oil feedstock. Figure 2.3 presents a flow chart for the separation of solubility classes from a crude oil.

There is no direct relationship between boiling point and solubility classes. However, the saturates and simple aromatics consist of the species with the lowest molecular weight, density, and boiling point, Figure 2.4. The aromatic species increase in polydispersity, density, molecular weight, heteroatom content, polarity, and boiling point from resins to asphaltenes. Hence, low boiling cuts consist primarily of saturates and aromatics and high boiling cuts consist primarily of resins and asphaltenes.

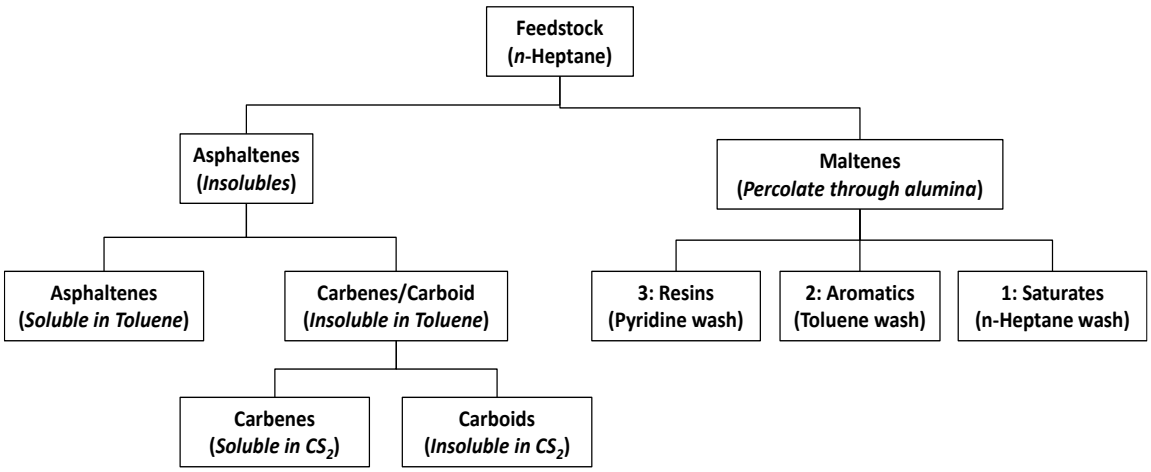

Figure 2.3 Fractionation scheme for crude oil samples based on solubility. (Modified from Speight, 2001).

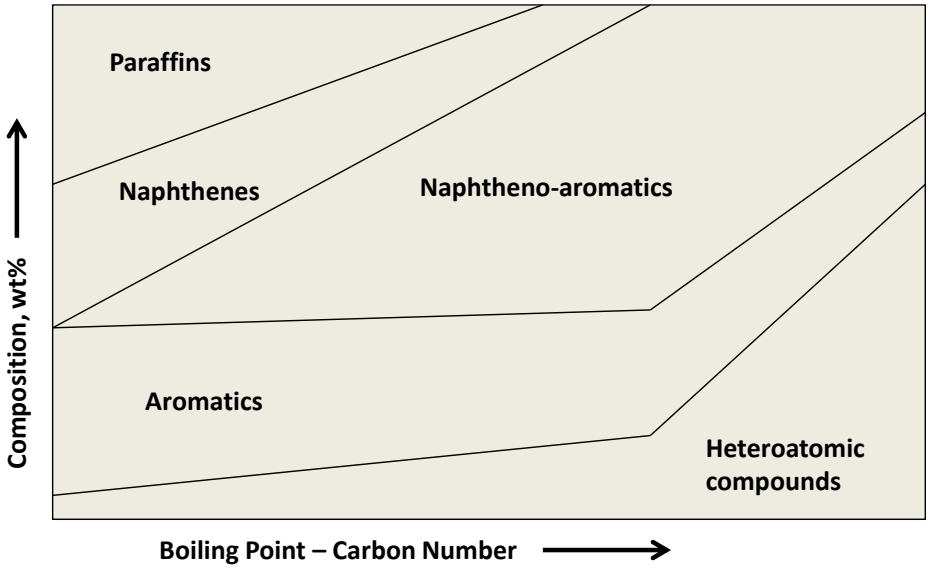

Figure 2.4. Distribution of main compound classes within the different types of crude oil. (Modified from Speight, 2001).

2.2 Heavy Oil and Bitumen Chemistry

Elemental and Heteroatomic Composition

Typical elemental analysis for heavy oil and bitumen is provided in Table 2.1. Their H/C ratio ranges from 1.4 to 1.6 consistent with low paraffin and high naphthene and aromatic content. For context, the H/C ratio of benzene, *n*-heptane, and a typical light conventional oil are 1, 2.3 and 1.9, respectively. Heavy oil and bitumen have a narrow range for their elemental composition (Altgelt and Boduszynski, 1994; Speight, 2001; Strausz and Lown, 2003; Read and Whiteoak, 2003). Recall that these fluids are defined by their relatively high density and viscosity. Higher H/C ratios are only observed in less dense oils. Bitumen is approaching the lower limit of aromaticity that is observed in naturally occurring liquid hydrocarbons; and, therefore, the lower range of the H/C ratios is also limited.

Table 2.1 Standard compositional ranges for CHSN and O for heavy oil and bitumen.

Element	Range	Atomic Ratio	Average Value
Carbon	83.1 ± 3	-	-
Hydrogen	10.3 ± 0.5	H/C	1.48
Nitrogen	0.5 ± 0.2	N/C	0.005
Oxygen	1.1 ± 0.3	O/C	0.009
Sulfur	0.05 to 14	S/C	0.02
Metals (Ni and V)	>1000 ppm	-	-

Sulfur compounds are distributed in the whole range of boiling fractions with a content varying from 0.05 to about 14%. Sulfur content tends to increase monotonically from the low boiling to the high and non-distillable fractions. The distillable fraction of sulfur is found in the form of sulfoxides. In the heavier fractions, where more than half of the total sulfur is present, the sulfur is in the form of thiophene derivatives. Small amounts of sulfides and sulfoxides are also present in the heavier petroleum fractions (Boduszynski, 1987; Strausz and Lown, 2003; Speight, 2001).

Oxygen is the second most abundant heteroatom in bitumen and heavy oils, with a concentration usually less than 2%. However, the concentration may vary if the oil is exposed to air. The most common compounds are phenols, carboxylic acids, esters, ketones, ethers, amides (with nitrogen), and sulfoxides (with sulfur). The oxygen compounds are concentrated in the most polar fractions of the resins and their concentrations can be as high at 10% (Strausz and Lown, 2003).

Nitrogen is the least abundant heteroatom in heavy oil and bitumen, ranging from 0.1 to 0.7 wt% and its concentration increases as molecular weight increases. The types of nitrogen in petroleum are classified as neutral (mostly indoles, acridines and hydroxypyridines), basic (pyridine derivaties, quinolones, indolines) and acid (pyrrole, carbazoles, benzocarbazoles). Identification of nitrogen components provides crucial information in refinery operations, even in low concentrations, since they may poison cracking catalysts and their elimination requires severe hydrogenation conditions (Strauz and Lown, 2003; Gray, 1994; Speight, 2001).

Other non-hydrocarbon compounds include metals such as iron, nickel and vanadium and occur primarily in the asphaltene fraction of the oil. Studies of different oils have shown that the most

predominant metal is vanadium, followed by nickel and in a minor concentration iron (Abu-Elgheit *et al.*, 1981; Altgelt and Boduszynski, 1994; Hodgson and Baker, 1957). The forms in which the metals occur in the oils are called petroporphyrins, although some authors (Dunning *et al.*, 1960; Dickson *et al.*, 1972; Reynolds and Biggs, 1985) believe that they are also present as metallo-nonporphyrins. The petroporphyrins consist of four pyrrole units bonded by methine carbons with a chelated metal. Their presence in petroleum fluids provided a definitive proof for their biological nature (Treibs, 1934). The presense of metalloporphyrins has negative effects during upgrading and refining processes since they cause reduction of performance and durability of catalysts used in catalytic cracking and hydrodesulfurization due to deposition of the metals when porphyrins thermally decompose (Speight, 2001; Dunning *et al.*, 1960).

Hydrocarbon Composition

In heavy oil and bitumen, the aliphatic hydrocarbons or saturate region can be divided into two groups: the low boiling saturates and the high boiling saturates. Several studies of different heavy oil and bitumen samples from Canada and Venezuela have shown that the low boiling point saturates are mainly paraffins with some mono- and di-naphthenes (Boduszynsky, 1987; Payzant *et al.*, 1985; Setti *et al.*, 1992) followed by tri- and tetracyclic compounds depending on the level of biodegradation that the precursor oil experienced (Strausz and Lown, 2003; Johns, 1986). Interestingly, a comparison made between the cyclic compounds found and the cyclic terpenoid hydrocarbon biological marker molecules showed that the low boiling point saturate region contained the rearranged and partly degraded original biomarker. On the other hand, the high boiling point saturates were comprised of the same base structures as low boiling point saturates, but with a significantly higher amount of side-chains (Altgelt and Boduszynsky, 1994; Strausz and Lown, 2003). This increase in side chains increases the paraffinic nature of the naphthenic structures.

By definition, aromatic hydrocarbons have at least one aromatic ring attached to their molecular structure. In general, the aromatic compounds in heavy oils and bitumens range from alkylbenzenes to large condensed polyaromatic and heteroatomic molecules. Several studies have revealed that the aromatic structures are mixtures of mono- to tetra-aromatics and some penta-aromatic hydrocarbons (Payzant *et al.*, 1985; Mojelshy *et al.*, 1986; Poirier and Bas, 1984;

Boduszynski, 1987). Most importantly, aromatics contain substantial amounts of hetero-compounds such as nitrogen (carbazoles), nitrogen (thiophenes) and oxygen (carboxylic acids). The majority of the aromatic rings are fused to a minimum of one naphthenic ring and contain considerable amounts of carbon as alkyl chains.

Resins are mainly a mixture of molecules that can be acidic, basic, or amphoteric (Strausz and Lown, 2003). This fraction, along with the aromatic fraction, also contains a significant amount of heteroatoms and have low H/C ratios. Since resins are a very poly-dispersed system, their characterization requires combinations of efficient fractionation techniques and high resolution analytical methods (Rodgers and McKenna, 2011; Merdrignac and Espinat, 2007; Payzant *et al.*, 1985). Some possible structures found in the resins are described later in this section.

Asphaltenes are defined as the fraction of the bitumen that is insoluble in *n*-alkanes, but is soluble in more polar solvents such as toluene or benzene. In terms of volatility, they are part of the non-distillable fraction of the crude oil. They are comprised of a large amount of hetero-compounds that may contain more than one heteroatom per molecule and contain most of the metals in the crude oil (Speight, 2001; Strausz and Lown, 2003; Altget and Boduszynski, 1994). The amount and composition of asphaltenes vary based on the origin of the crude oil. Due to all the operational problems this fraction causes during extraction transportation and refining processes, myriads of studies have been devoted to understand their behavior (Shaw, 2002; Zou and Shaw, 2004, Kokal *et al.*, 1992; Mansoori, 1997; Maham *et al.*, 2005; Anderson and Speight, 1999), molecular composition and structure (Mullins, 2008; Mullins and Sheu, 1998), and physical properties (Escobedo and Mansoori, 1998; Barrera *et al.*, 2013; Parkash *et al.*, 1979). It is important to note that because asphaltenes are a solubility class, their yield and composition depend on the method and conditions used to remove them from the oil including the amount and type of solvent, temperature, pressure, time, and washing procedure (Alboudwarej *et al*., 2003, ASTM D2007M).

The structure of asphaltenes is widely debated and difficult to determine due to their polydispersity. Two main structures have been postulated: the archipelago structure (polyaromatic nuclei interconnected with aliphatic chains) and the continent structure (flat disk shape with dominant aromatic core). Given their polydispersity, it is likely that both structures are present.

Asphaltene molecular weight has been of particular interest due to the tendency of asphaltenes to self-aggregate. The molecular weight of the monomers has been reported to be in the order of 1000 g/mol, while aggregate molecular weight can be as high as 30,000 g/mol (Barrera *et al.*, 2013). Asphaltene molecules appear to be structures with active sites through which they interact with similar molecules to form nano-aggregates (Mullins *et al.*, 2007; Yarranton *et al.*, 2007, Barrera *et al.*, 2013, McKenna *et al.*, 2013).

A common method to obtain the fractions is SARA fractionation. Through this method the oil is separated based on the solubility and polarity of these fractions in different solvents and media. Table 2.2 shows the SARA analysis of some heavy oils and bitumen.

Table 2.2. SARA compositional analysis for bitumen samples and heavy oils (Akbarzadeh, *et al.*, 2005).

Fraction (wt%)	Athabasca Bitumen	Peace River Bitumen	Venezuelan Heavy Oil
Saturates	16.3	18.2	15.4
Aromatics	39.8	42.7	44.4
Resins	28.5	21.5	25
Asphaltenes	14.7	17.6	15

2.3 Petroleum Characterization

The phase behavior and physical properties of heavy oils and bitumen during extraction, production and refining are essential inputs for the adaptation and development of new technologies. However, their prediction for multicomponent mixtures is complex and poses significant experimental and modelling challenges. Prediction of phase behavior and physical properties is typically accomplished with Equations of State (EoS) or generalized correlations. The required inputs to perform phase behavior calculations with an EoS are the critical temperature and pressure and acentric factors of each component, as well as binary interaction parameters for each pair of components in the mixture.

The critical properties of most petroleum components are pseudo-critical properties that cannot be measured (Aladwani and Riazi, 2005). Instead, their critical properties are estimated from

correlations of their measurable properties, usually boiling point, density, and molecular weight. It is impractical, if not impossible, to estimate these EoS parameters for each single component in a heavy crude oil. Therefore, to study and characterize the physical and chemical behavior of heavy oil and bitumen, a preliminary step of matrix simplification is recommended. In other words, the mixture is divided into a set of pseudo-components that represent the distribution of properties in the mixture. Oil characterization is the process of dividing the fluid into components and pseudo-components and assigning properties to each of these components.

2.3.1 Characterization Assays

There are three main approaches to divide a petroleum fluid into pseudo-components: solubility assays, chromatography, and distillation. Mass spectrometric techniques have been proposed as a characterization technique (Espinat and Mendrignac, 2007); however, practical use of these data is still under development.

Solubility Assays

Solubility assays include fractionation of the oil into:

- paraffins, iso-paraffins, olefins, naphthenes, and aromatics (PIONA), or
- paraffins, olefins, naphthenes, and aromatics (PONA), or
- paraffins, naphthenes, and aromatics (PNA), or
- saturates, aromatics, resins, and asphaltenes (SARA).

Solubility separation is particularly useful since asphaltenes can be separated from the oil to facilitate the characterization of the maltene fraction. Removing the asphaltenes lowers the oil viscosity and facilitates distillation. Several standard methods are used to precipitate the asphaltenes and fractionate the deasphalted heavy oil (ASTM D-2006; ASTM D-2007; ASTM D-4124; IP-143). For heavy oils and bitumen, the most common fractionation technique is SARA fractionation. To obtain the SARA fractions, techniques such as high-performance liquid chromatography or thin-layer chromatography with flame ionization detector have been implemented (Vela *et al*, 1998). Although, the chemical information provided by this type of fractionation provides some information for characterization of heavy oils and bitumen, the boiling point, a critical property for characterization cannot be obtained this way.

Gas Chromatography Assays

Gas chromatography is used to separate individual hydrocarbon components by their retention time which correlates to their carbon number or boiling point. A distillation curve produced by GC is called a simulated distillation curve. This method is simple, fast, reproducible and more economical than a laboratory-scale physical distillation. Currently, there are four commonly used ASTM methods for characterization of heavy fractions: D2887, D5307, D6352, and D7169. ASTM D7169 extends the applicability of simulated distillation to petroleum samples that do not elute completely from the system, normally referred to as the residue. This method covers a wide temperature boiling range, up to 993 K, which represents the elution of *n*-C_{100} (Vickers, 2002)

Although GC analysis provides fast and economical results, this technique requires calibration in order to identify the components and the equivalent boiling points. Calibration is based on the retention time of the normal paraffins and their respective boiling points. The interpretation of the results for a heavy oil or bitumen must be done with caution as these samples are known to have large amounts of aromatic compounds. Therefore, the boiling point of a given paraffin may not correspond to that of the aromatic fraction that elutes at the same time.

Distillation Assays

Distillation is the most common approach to characterizing oils. It provides the boiling point distribution of the sample and generates fractions that have a reduced molecular weight range and a variety of chemical groups (Aladwani and Riazi, 2005). Distillation separates the oil components by the differences in their vapor pressure, which decreases with increasing molecular weight. Note, intermolecular forces also play an important role in the heat of vaporization, causing molecules of similar molecular weight but different structure or atomic make-up to boil at a higher or lower temperature. These forces are particularly important for compounds with high polarity.

Based on the continuum concept proposed by Boduszynsky (1987) distillation will provide fractions of increasing average molecular weight, aromaticity, and heteroatom content. Figure 2.5 depicts how distillation fractionates the compositional matrix. Note how, although the average

molecular weight of the distillation cuts increases with their average boiling point, the range of molecular weight and chemical groups in each distillation cut can still be quite broad, particularly for heavier cuts.

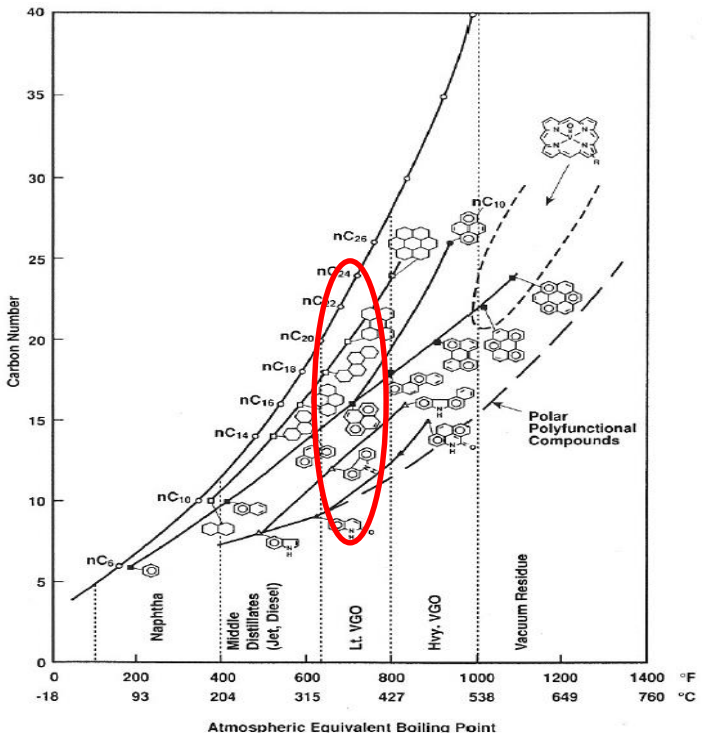

Figure 2.5. Distillation fractions and their distribution of molecular weights and chemical families. (Altgelt and Boduszynski, 1994).

A large number of crude oil distillation methods have been developed for different applications (Riazi, 2005; Villalanti, 1995; Nji, 2008; Nji, 2009; Sbaite 2006; Fuhr, 2008). Some of the common methods for crude oil distillation are listed below:

ASTM 86 is one of the oldest methods used to characterize petroleum products, such as naphthas, gasolines, kerosenes, gas oils and fuel oils. It is conducted at atmospheric pressure and has limited application for heavy oils due to their low volatility. The amount that can be distilled is limited by the cracking temperature of the oil components which is approximately 300°C (Carbognani *et al.*, 2007; Speight and Ozum, 2002; Gray, 1994). Material is distillable

up to approximately 250ºC with this atmospheric pressure method. Since this method does not represent actual boiling point of components in a petroleum fraction interconversion to true boiling point data (TBP) is required using the correlation proposed by Riazi (2005), Equation 2.1.

ASTM D1160 was developed to extend the applicability of ASTM D86 to heavier petroleum products. The distillation is carried out at 0.133 kPa with a separation equivalent to one theoretical plate. Material is distillable up to approximately 400ºC Atmospheric Equivalent Temperature (AET). When this technique is used for heavy oils and bitumen only 20 to 25% of the original volume can be distilled before reaching the cracking temperature; hence far more than half of the sample is left uncharacterized. Since this method is performed at sub-atmospheric pressures, Maxwell and Bonnell correlation (1957) is used to convert the actual distillation temperature to AET. To convert the AET distillation curves to TBP a two-step procedure needs to be carried out to first get TBP at 10 mmHg and then TBP at 760 mmHg (Edmister and Okamoto, 1959; Riazi, 2005).

ASTM D2892 is also called the TBP method or 15/5. The distillation is carried out at atmospheric pressure first and then pressure is dropped to 0.25 kPa with a separation equivalent of 14 to 18 theoretical plates (nominally 15). A reflux ratio of 5:1 is used. Material is distillable up to about 400ºC AET. The actual distillation temperature is kept below the cracking temperature but is equivalent to a higher temperature at atmospheric pressure. When vacuum is used the vapor temperatures are converted to AET using Maxwell and Bonnell (1957) correlations. The AET obtained in this method correspond to TBP data.

ASTM 5236 is an extension of ASTM D2892 and operates at pressures as low as 0.0133 kPa. This method can be applied to heavy hydrocarbons with an initial boiling point higher than 150ºC and distills material up to approximately 565ºC AET. If the sample has low boiling material, it is required to first run ASTM D2892 and then ASTM D5236. Hence, a large volume sample (4 L) is required to run the distillation. The Maxwell and Bonnell correlation (1957) is used to convert the actual distillation temperature to AET. The calculated AET temperature are reported as TBP data because the measured temperatures correspond to a true thermodynamic state point (Satyro and Yarranton, 2009). The drawback is that this method does not have the

same fractionation capabilities as ASTM D2892; therefore, the TBP temperatures are higher than they would be if a more efficient fractionation was performed (Golden, 2012).

Spinning Band Distillation (SBD) operates with a spiral Teflon or metal band that increases the liquid-vapor contact and can achieve efficiency of 50 theoretical plates in a 100 cm length column. The reflux ratio can be adjusted to the desired value, but is normally operated at 5:1 if distillation is performed to simulate ASTM D2892. The distillation pressure can also be adjusted with a minimum value of 0.13kPa (1 mmHg). The system is equipped with four receivers that allow collection of the distilled fractions. Heavy oils and bitumen can be distilled using this technique to remove the light distillable fraction; however, approximately 35% of the initial volume can be distilled leaving 65% of the oil uncharacterized. As in any other distillation procedure, at atmospheric or vacuum condition, the pot temperature should not exceed 300 ºC to avoid thermal decomposition of the sample. The AET reaches values up to 450ºC. The vapor temperatures are converted to AET using the correlations developed by Maxwell and Bonnell (1957). A discussion about the validity of this method as TBP data will be presented in Appendix A.

Short path distillation (HV-SPD) is a proposed ASTM method for molecular distillation. The separation is carried out at 0.0001 kPa to approximately 650ºC AET. In this method, the sample flows at constant rate over a hot surface at high vacuum, where temperature and pressure are fixed. The system is equipped with rollers that assure a thin film on the wall and the collector device is closely place so the evaporated molecules condense in the cold finger. For every run only one fraction and a residue are obtained. Simulated distillation is performed to determine the TBP temperatures of the obtained fractions.

A summary of the boiling ranges covered by the most commonly used GC and physical distillation techniques is compared in Figure 2.6.

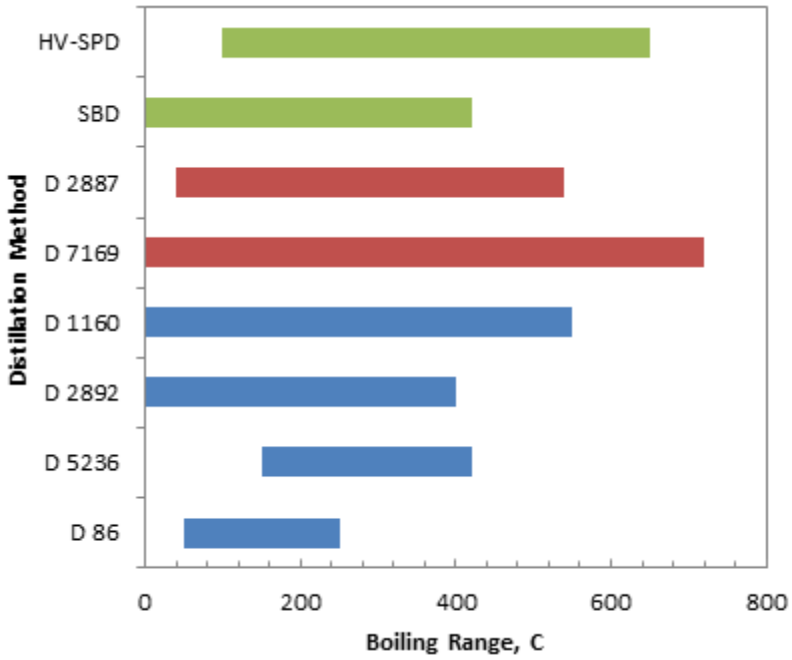

Figure 2.6 Summary of the boiling ranges of physical and simulated distillation techniques. (Modified from Villalanti *et al.*, 2000). Bottom four blue bars are standard physical distillation methods, two middle red bars are standard simulated distillation methods, and two upper green bars are alternative non-standard physical distillation methods.

The distillation curve obtained from any of these methods (GC or physical distillation) is then extrapolated over the residue (the fraction of the oil that was not distilled) using a Gaussian extrapolation (Castellanos *et al.*, 2011). The completed curve is divided into pseudo-components and each of them has an assigned set of physical properties that can be measured if fractions are available. If fractions are not available, the physical properties can be estimated from correlations and property distributions. Finally, critical properties and acentric factors of the pseudo-components are estimated from correlations. Figure 2.7 present a summary of the characterization procedure based on a distillation assay.

The approach depicted in Figure 2.7 has been extensively used for conventional oils and has been extended to characterize heavy oils (Castellanos, 2012). For both conventional and unconventional

oils, the distillation assay is limited by the cracking temperature at atmospheric and vacuum conditions. Light conventional oils can be accurately characterized using the steps presented in Figure 2.7 because most of their constituents can be distilled. The pseudo-components and their property distributions represent more than 90% of the oil and only small extrapolations are required. Furthermore, detailed studies have been performed to obtain generalized correlations to accurately predict critical properties.

However, for heavy crude oils these techniques are inadequate because no more than 40% of the whole crude oil can be distilled and property extrapolation over the residue introduces considerably uncertainty. Additionally, most of the correlations used to estimate critical properties are biased to paraffinic oils and may be inaccurate or not applicable for high molecular weight compounds that are commonly encountered in heavy crudes. Deep vacuum distillation has the potential to distill a greater fraction of heavy oil without thermal cracking. However, a completely new design is required to reach lower pressures, avoid high pressures drops, read thermodynamic boiling points, and generate fractions to measure physical, thermal or optical properties.

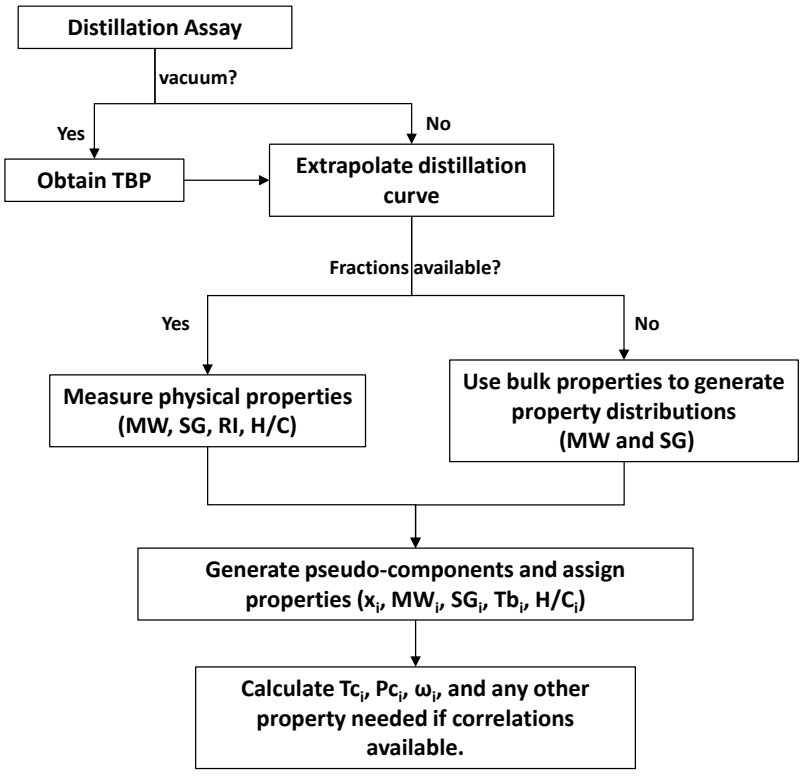

Figure 2.7 Flow chart for petroleum characterization.

New Method: Deep Vacuum Fractionation Apparatus (DVFA). Castellanos *et al.* (2012) designed and constructed an apparatus to measure vapor pressure using a static technique in which the sample is placed under vacuum conditions at constant temperature in a closed vessel and the pressure exerted by the vapor is directly measured. The DVFA apparatus consists on a liquid-trap section, a turbo molecular pump and two thermocouples connected to a temperature controller. The turbo molecular pump can reach pressures as low as $1 \cdot 10^{-9}$ kPa at clean conditions; therefore, the implementation of this system as a distillation technique could allow distillation data for heavy oil and bitumen to be extended to an uncharted region. Castellanos *et al.* (2012) proved that distillation of up to approximately 50 wt% of a bitumen can be performed using the newly developed apparatus. An important feature of the DVFA is the liquid-trap section, which if maintained at low temperatures can condense the vapor produced in the sample vessel allowing for distillation cuts to be captured.

However, the implementation of this technique as a distillation assay required modifications to the apparatus and in the fractionation procedure. Also, since the temperature range of pressure gauges did not allow the collection of pressure readings during distillation, the DVFA required an alternative inter-conversion method to that of Maxwell and Bonnell to obtain TBP data.

2.3.2 Inter-conversion Methods to Obtain AET and TBP

True boiling points are required for the correlations used to predict other physical and thermodynamic properties. Since actual TBP data is very difficult to measure in terms of time and cost, alternative distillation procedures have been developed to replace the TBP experimental approach. For atmospheric distillation, such as ASTM D86, the measured boiling points are converted to TBP using empirical correlations. If the distillation is undertaken at sub-atmospheric pressures, it is also necessary to convert low pressure temperatures to atmospheric equivalent temperatures (AET) and then determine if they correspond to TBP data. Note, AET are equivalent to TBP if the measured temperatures correspond to an actual thermodynamic state.

Most of the ASTM distillation techniques have their own inter-conversion method which uses the available distillation temperature and specific gravity of the fraction as inputs to estimate the TBP data.

$$T_i(desired) = a(T_i(available))^b SG^c \quad (2.1)$$

The coefficients *a*, *b*, and *c* for each ASTM method were determined by Riazi and Daubert and can be found elsewhere (Riazi, 2005). This equation can be applied for a distillation performed at atmospheric conditions.

To interconvert boiling points at reduced pressures to atmospheric equivalent boiling points (AET), a vapor pressure correlation is required. The vapor pressure correlation developed for petroleum fractions by Maxwell and Bonnell (1957) is the accepted industry standard. Other vapor pressure correlations proposed by Myers and Fenske (1955) and Van Kranen and Van Nes (1951) are less commonly used for inter-conversion.

When vapor pressure data are available, there are two other alternatives for inter-conversion. The first option is to model the experimental vapor pressure of the cut with an equation of state and then predict the normal boiling point with the tuned model. Using an equation of state and mixing rules can be a very accurate way to estimate boiling points from vapor pressure. However, critical properties and interaction parameters are also required and these values are rarely, if ever, available for heavy fractions.

The second option involves the extrapolation of sub-atmospheric vapor pressures towards higher pressures. Ruzicka (1993; 1994) developed a simultaneous treatment of vapor pressure and related heat capacity data between the triple and normal boiling temperature for *n*-alkanes. Heat capacity is related to vapor pressure through the Clausius-Clapeyron equation and can be used to constrain the extrapolation of low temperature range vapor pressure measurements with heat capacity measured over a broader temperature range. Different vapor pressure equations were tested by Ruzicka (1996) and the best performance in the fitting and extrapolation of vapor pressure and heat capacity data was obtained with the Cox equation (Ruzicka and Majer, 1986; 1994; 1996).

2.3.3 Generation of Crude Oil Pseudo-Components: Splitting and Lumping

For modelling purposes, the crude oil can be lumped or split into pseudo-components. Pseudo-components are a way to simplify the characterization of crude oils, as they represent narrow boiling range cuts with a known composition and physical properties. The number of pseudo-components is normally defined between five and twenty depending on the process being simulated (Whitson and Brule, 2000). Lumping is usually only used for chromatographic characterizations. Some of the light components such as *i*-butane, *n*-butane, *i*-pentane, *n*-pentane, are typically lumped into carbon number ranges such as C4-C6, C7-C10. The uncharacterized part of the assay (e.g. C30+) can be split into a number of pseudo-components.

Splitting is always used for distillation based characterizations. The distillation curve is divided into pseudo-components with an assigned set of average properties such as density, molecular weight, normal boiling point, elemental composition, thermal properties, and critical properties. The TBP curve can be split using temperature intervals or mass fraction intervals, Figure 2.8. The assigned average boiling point for a mass fraction interval is given as:

$$T_{bi} = \frac{1}{w_i - w_{i-1}} \int_{w_{i-1}}^{w_i} T_{TBP}(w)dw \tag{2.2}$$

where the terms *w* and *T* stand for the mass fraction and temperature respectively.

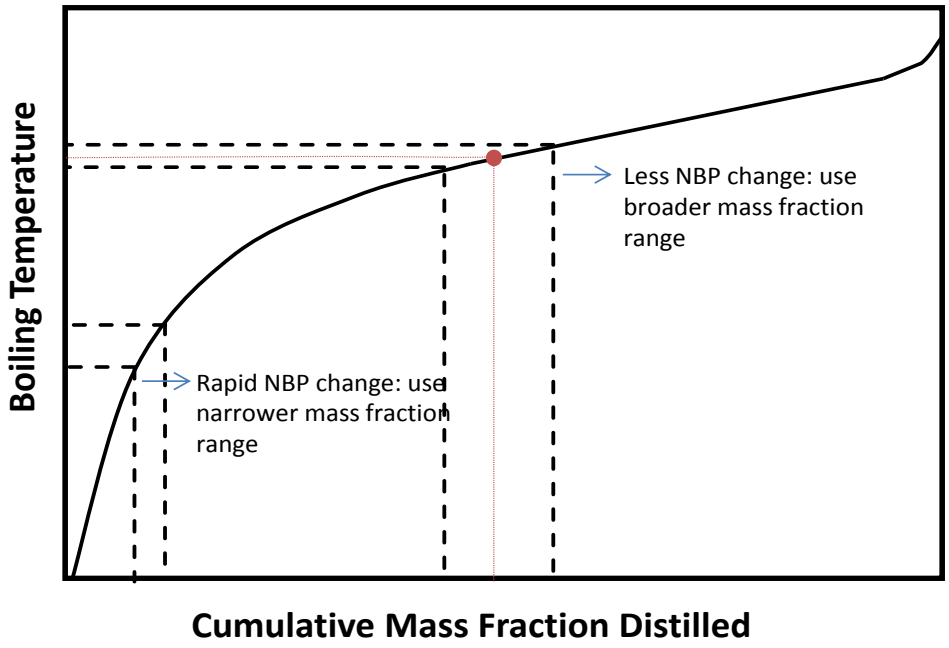

Figure 2.8. Approach to split a TBP curve into pseudo-components.

2.4 Physical and Thermal Property Correlation

Once the distillation curve is divided into cuts, the physical, thermal, and critical properties must be determined. The first three properties to be determined are specific gravity, molecular weight, and boiling point (Smith and Watson, 1937; Whitson, 1982). These physical properties are important in their own right and, because they are readily measured, they have been used as correlating parameters for many other properties. Usually either carbon number (molecular weight) or boiling point distributions are measured and the other two properties are determined for each from correlations. Sometimes refractive index is used in place of specific gravity.

Vapor pressure and thermal properties are also required since they constitute the backbone of thermodynamic equilibrium calculations as well as mass and energy balances required to design process units. Thermal data, in this study, includes liquid heat capacity, enthalpy of vaporization and heat of combustion. The liquid heat capacity, as well as enthalpy or heat of vaporization, play a significant role in determining the amounts of energy required to operate petroleum processing units such as distillation units and in general any process involving heating and cooling of the

crude oil (Parhizgar *et al.*, 2013; Kikic and Vetere, 2011). Heat of combustion constitutes a crucial property for hydrocarbons because its value helps to identify the quality of the hydrocarbon as a fuel source and it is also used to derive the heat of formation for reaction enthalpy calculations (Tsonopoulos, 1986; Strausz and Low, 2003). Several correlations are available in the literature to predict these properties; usually, the inputs for these correlations are the specific gravity, molecular weight and normal boiling point.

Critical properties are required for equation of state models. Since it is particularly difficult to measure the critical state of complex mixtures, several methods and correlations to predict critical properties of hydrocarbon mixtures have been developed (Anselme and Teja, 1990; Gambill, 1959; King, 1957; Lixiong and Kiran, 1990; Zais, 1972; Whitson and Brule, 2000; Riazi, 2005). Most of the correlations are polynomial or exponential equations based on one or more properties that can be measured directly. The best option to determine the critical properties for pseudo-components is to tune them to match phase behavior or vapor pressure data using equations of state.

Since pseudo-component critical properties cannot be measured, correlations cannot be validated and are not considered in this thesis. The correlations for physical, thermal properties and vapor pressure are summarized below.

Note, most of the correlations presented below apply only to compounds with molecular weight less than 700 g/mol or normal boiling points less than 800 K. Furthermore, the majority of the correlations are biased toward paraffins and light to medium oils due to availability of experimental data used to build the generalized correlations.

Also note that whatever correlations are selected, the characterization procedure is subject to the constraint that the appropriately weighted average of the pseudo-component properties should result in the known bulk property of the crude oil as described in the following equations:

$$1 = \sum_{i=1}^{N} z_i \tag{2.3}$$

and

$$SG_{Bulk} = \left(\sum_{i=1}^{N} \frac{w_i}{SG_i} \right)^{-1}, MW_{Bulk} = \sum_{i=1}^{N} z_i MW_i \tag{2.4}$$

where *z* is the moles of pseudo-component *i*, *N* is the total number of pseudo-components, and the subscript *Bulk* indicates the properties of the whole oil sample.

2.4.1 Physical Properties

Normal Boiling Point, T_b

The prediction of T_b is required when performing characterizations based on calculated molar distributions, solubility class separations (SARA, PIONA), or when density and molecular weight of the fractions are available. A common factor in the majority of the correlations to predict this property is the use of *MW* and SG as input parameters. This is because the *MW* is a good parameter to characterize compounds within the same hydrocarbon family, whereas *SG* is a property that makes a distinction between hydrocarbon families. Their combinations provide a suitable pair of input parameters that, combined in different forms, can be used to predict the normal boiling point of a wide range of structures.

These correlations are very useful when expensive and time consuming distillations assays are not available. However, all the correlations that have been developed to predict the normal boiling point are mainly based on data for light to medium oils and pure components. Therefore, their application for heavy oils and bitumen may be accurate for low boiling cuts, but may be biased towards paraffinic properties for the heavier and more aromatic fractions. Table 2.3 presents the most common correlations to estimate T_b from molecular weight, *MW*, and specific gravity, *SG*. Note that some of the correlations were designed to predict *MW* from T_b and are implicit in T_b.

Table 2.3. Summary of correlations to estimate normal boiling point.

Source	Correlation	Range of Applicability	Eq.
Soreide (1989)	$T_b = [1928.3 - 169500 * MW^{-0.03522} * SG^{3.266} D]/1.8$	$361 < T_b < 830$	(2.5)

	$D = \exp(-0.004922 * MW - 4.7685 * SG + 0.003462 * MW * SG)$		
Kesler and Lee (1976) Implicit in Tb	$MW = [D] + \frac{[A]}{T_b} + \frac{[B]}{{T_b}^3}$ $D = -12272.6 + 9486.4 * SG + (4.6523 - 3.3287 * SG) * T_b$ $A = (1 - 0.77084 * SG - 0.02058 * SG^2) * \left(1.3437 - \frac{720.79}{T_b}\right) * 10^7$ $B = (1 - 0.80882 * SG + 0.02226 * SG^2) * \left(1.8828 - \frac{181.92}{T_b}\right) * 10^{12}$	T_b<750	(2.6)
Riazi and Daubert (1980) Implicit in Tb	$MW = 0.000045673 * {T_b}^{2.1962} * SG^{-1.0164}$	300< T_b<610	(2.7)
Riazi and Daubert (1986)	For MW<300 $T_b = 3.76587 * D * MW^{0.40167} * SG^{-1.58262}$ $D = \exp(0.0037741MW + 2.98404SG - 0.00425288MWSG)$ For MW>300 $T_b = 9.3369 * D * MW^{0.5369} * SG^{-0.7276}$ $D = \exp(0.00016414MW + 1.4103SG - 0.00075152MWSG)$	200< T_b<610	(2.8)
API (1977)	$MW = 204.38 * {T_b}^{0.118} * SG^{1.88} * \exp(0.00218 * T_b - 3.07 * SG)$	309< T_b<900	(2.9)
Rao and Bardon (1985)	$ln\, MW = (1.27 + 0.071K_w) ln\left(\frac{1.8T_b}{22.31 + 1.68K_w}\right)$	361< T_b<830	(2.10)

Twu *et al.* (1984)	$T_b = exp\left(5.1264 + 2.71579\beta - 0.28659\beta^2 - \frac{29.8544}{\beta} - \frac{0.122488}{\beta^2}\right) - 13.7512\beta + 19.6197\beta^2$ $\beta = \ln(M°)$ $M° = \frac{T_b}{5.8 - 0.0052T_b}$ *as a starting iterating point*	MW<600	(2.11)
Nji *et al.* (2010)	$T_b = \left(477.63 * \ln\left(\frac{w + 88.51}{w + 1007}\right) + 1214.4\right) * \left(\frac{1 + 2 * x}{1 - 2 * x}\right)^2$ $w = -0.07412 * \Delta SG^2 - 0.0075041 * \Delta SG - 2.6031 * \Delta MW^2 + 0.090188 * \Delta MW - 1.0482 * \Delta SG * \Delta MW$ $\Delta SG = \ln\left[\frac{0.83 + \frac{89.9513}{w} - \frac{139.6612}{(w + 3.2033)^{1.0564}}}{SG}\right]$ $\Delta MW = \ln\left(\frac{w}{MW}\right)$ $w = 14 * CN + 2$	200< T_b<900	(2.12)

Molecular Weight

Molecular weight is a very useful property that can be used not only for critical property prediction, but to convert from mole to mass units for equipment design. Additionally, molecular weight values have impact on chemical equilibrium, vapor density calculations and hydrocarbon processing systems (Schneider, 1998; Goossens, 1996). However, the measurement of molecular weight is not simple and depending on the method used, either vapor pressure osmometry or freezing point depression, some discrepancies may arise (Altgelt and Boduszynski, 1994). These

differences can be attributed to the assumptions that have to be made in the experimental techniques and the association effects that solvents and temperature may have on the molecular weight of complex mixtures. This property has the highest measurement uncertainty of the three main physical properties.

Most of the correlations presented in Table 2.3 were developed for light to medium oils; therefore, their application for heavy oils and bitumen may be accurate for low boiling cuts but may be biased towards paraffinic properties for the heavier more aromatic fractions. Note that the application of correlations in Table 2.4 is limited to deasphalted fractions. Asphaltenes self-associate and their associated molecular weight is higher than the trend extrapolated from the non-associating maltenes.

Table 2.4. Summary of correlations to estimate molecular weight.

Source	**Correlation**	**Range of Applicability**	**Eq.**
Soreide (1989)	See Equation 2.5	361< T_b<830	(2.5)
Kesler and Lee (1976)	See Equation 2.6	T_b<750	(2.6)
Riazi and Daubert (1980)	See Equation 2.7	300< T_b<610	(2.7)
Riazi and Daubert (1986)	See Equation 2.8	300< T_b<610	(2.8)
Rao and Bardon (1985)	See Equation 2.10	361< T_b<830	(2.10)
Twu (1984)	$\ln(M) = lnM°[(1+2f_M)/(1-2f_M)]^2$ $f_M = \Delta SG_M\left[\chi + (-0.0175691 + 0.143979/T_b^{1/2})\Delta SG_M\right]$ $\chi = \left\lvert 0.012342 - 0.2445541/T_b^{1/2}\right\rvert$ $\Delta SG_M = exp[5(SG° - SG)] - 1$ $SG° = 0.843593 - 0.128624\alpha - 3.36159\alpha^3 - 13749.5\alpha^{12}$ $\alpha = 1 - T_b/T_c^{\circ}$	MW<600	(2.13)

	$T_c^{\circ} = T_b(0.533273 + 0.34383x10^{-3}T_b + 2.52617x10^{-7}{T_b}^2 - 1.658481x10^{-10}{T_b}^3 + 4.60776x10^{24}{T_b}^{-13})^{-1}$		
Goosens (1996)	$MW = \frac{0.01077 * {T_b}^x}{\rho}$ $x = 1.52869 + 0.06486 * ln(\frac{T_b}{1087 - T_b})$	300< T_b<900	(2.14)
Hariu and Sage (1969)	$MW = 0.6670202 + 0.1552531Kw - 0.005378496Kw^2 * 0.004583705T_bKw + 0.00002500584T_bKw^2 + 0.000002698693{T_b}^2 + 0.0000387595{T_b}^2Kw - 0.00000001566228{T_b}^2 * Kw^2$	30< T_b<800	(2.15)
Katz and Firoozabadi (1978)	$MW = -0.000005763156 * (CN - 5)^5 + 0.0007293105 * (CN - 5)^4 - 0.03341596 * (CN - 5)^3 + 0.5740517 * (CN - 5)^2 + 10.24725 * (CN - 5) + 72.53757$	C_N<45	(2.16)

Specific Gravity

As discussed previously, specific gravity is used to classify crude oils. It is also used to convert from mass to volume for process calculations. Density seems to correlate to many different properties including sulfur content, viscosity, nitrogen content, H/C ratio, and refractive index. Several correlations for SG are based on MW and a characterization factor which is tuned to fit the correlation to the bulk density (Jacoby, 1952; Soreide, 1989; Whitson, 1983). Other correlations relate SG to carbon number alone (Katz and Firoozabadi, 1978) or to refractive index

and either MW or NBP (Riazi and Daubert, 2005). For these correlations, there is no tuning to assure that the predicted bulk density matches the measured value. Gray's correlation (Gray, 2002) relates product quality with elemental composition and was developed mainly to predict the product quality of upgrading processes. The described SG correlations are presented in Table 2.5. Note that most of these correlations were developed from the properties of pure hydrocarbons and light to medium petroleum cuts and therefore may not apply to heavy oils.

Table 2.5. Summary of correlations to estimate specific gravity.

Source	**Correlation**	**Range of Applicability**	**Eq.**
Soreide (1989)	$SG = 0.28554 + Cf * (MW - 65.94185)^{0.129969}$	300<MW<600	(2.17)
Whitson (1983)	$SG = 6.0108 * MW^{0.17947} * K_W{}^{-1.18241}$	MW<250	(2.18)
Jacoby (1952)	$SG = 0.8468 - \frac{15.8}{MW} + Ja * \left(0.2456 - \frac{1.77}{MW}\right)$		(2.19)
Katz and Firoozabadi (1978)	$SG = 0.6839638(CN - 5)^{0.08661026}$	C_6<C_N<C_{45}	(2.20)
Riazi and Daubert (2005)	$SG = 24381000 * D * T_b{}^{-0.3418} * RI^{6.9195}$ $D = \exp(-0.0004194T_b - 23.5535n + 0.0039874T_b n)$	300<MW<700	(2.21)
Riazi and Daubert (2005)	$SG = 1128400 * D * MW^{-0.0771} * RI^{6.3028}$ $D = \exp(-0.001588 * MW - 20.594 * n + 0.007344 * MW * n)$	70<MW<700	(2.22)
Gray (2002)	$SG = (1033 - 13.69 * H + 13.85 * S + 115.7 * N)/(1000 * 0.998207)$	Only for petroleum fractions	(2.23)

Refractive Index

The refractive index (n) is a property that, like density, gives information about the intermolecular interactions in a system. Since hydrocarbons do not have a significant amount of polar compounds, the major molecular interactions can be attributed to the London dispersion forces which can be described through polarizability by the following equation:

$$\tau = \left(\frac{3}{4\pi N_A}\right)\left(\frac{n^2-1}{n^2+2}\right)\left(\frac{MW}{\rho}\right) \tag{2.24}$$

where, τ is the polarizability, N_A is the Avogadro's number, n is the refractive index, MW is the molecular weight and ρ is the density. The last two terms in Equation 2.22 are defined as the molar refraction, R_m, as follows:

$$R_m = F_{RI}\left(\frac{MW}{\rho}\right) \tag{2.25}$$

where F_{RI} is a function of the refractive index, $F_{RI} = (n^2 - 1)/(n^2 + 2)$. From Equations 2.24 and 2.25, it is evident there is a relationship between polarizability and molar refraction. These relationships indicate that refractive index can describe the intermolecular forces of nonpolar hydrocarbons, as density does. As with density, the refractive index could be correlated to an additional energy parameter such as boiling point temperature and hence can be used as a correlating parameter for the characterization of fossil fuels.

It has been noted by several authors that there is strong correlation between density and the refractive index or F_{RI}, and that refractive index can be used as a substitute for density in equation of state modelling (Riazi and Yousef, 2001). Others have found a direct relation between F_{RI} and solubility parameter and have used this relationship to develop a method to predict the onset of asphaltene precipitation from the refractive index of the mixture (Vargas and Chapman, 2010; Taylor *et al.*, 2001). In this thesis, the focus is on the relationship between refractive index and density.

Vargas and Chapman (2010) used the relation presented in Equation 2.24 to propose a simple relation between F_{RI} and density. They plotted the molar refraction as a function of the molecular weight and found that the slope of the curve approximated a constant value of 1/3 for all pure components. This relationship is shown for pure hydrocarbons and petroleum solubility cuts in

Figure 2.9. It follows from this proportionality and from Eq. 2.24 that the F_{RI} can be determined simply by dividing the density by 3. This method is known as the one-third rule.

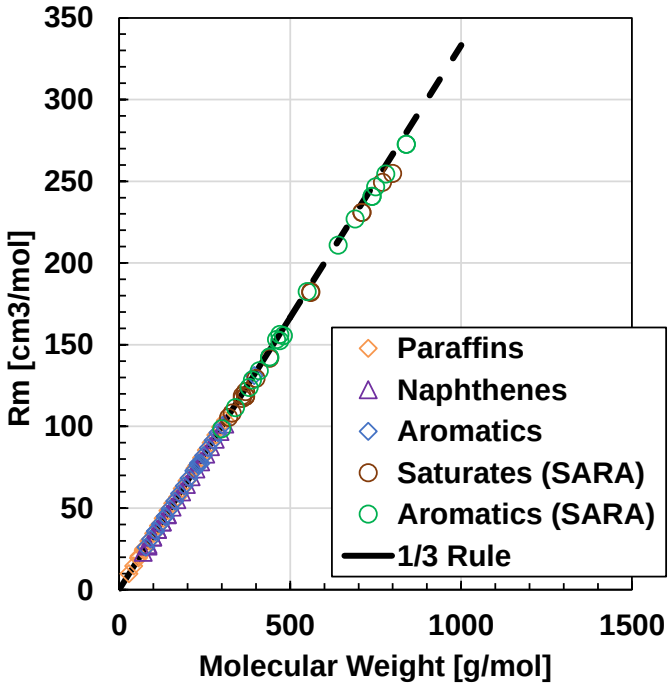

Figure 2.9. Molar refractivity versus molecular weight for pure components and petroleum saturate and aromatic cuts. SARA fractions from Powers (2014) and pure components from NIST.

Although R_m and MW have nearly the same ratio for all components, the density predictions using the one-third rule are not accurate for the lightest and heaviest petroleum components. Angle *et al.* (2006) proposed a linear correlation between density and refractive index. Vargas and Chapman (2010) proposed a cubic equation to account for the deviations observed from the one-third rule. The above correlations related to the refractive index are summarized in Table 2.6.

Table 2.6. Summary of correlations to estimate refractive index.

Source	Correlation	Range of Applicability	Eq.
One Third Rule	$\frac{FRI}{\rho} = 1/3$		(2.26)

Vargas and Chapman (2010)	$\frac{FRI}{\rho} = 0.5054 - 0.3951\rho + 0.2314\rho^2$	Pure Components	(2.27)
Angle *et al.* (2006)	$FRI = \left(\frac{\rho + 0.0647}{3.24}\right)$	Petroleum fractions	(2.28)

2.4.2 Vapor Pressure and Thermal Properties

Several correlations to estimate vapor pressure, liquid heat capacity, enthalpy of vaporization and heats of combustion have been developed using either critical values or easily obtainable parameters such as the normal boiling point and molecular weight. Since critical values for petroleum fractions are unknown, correlations using physical properties have been reported as more accurate and practical for thermal property estimation (Riazi, 2005; Vetere, 1979, 1995). The most well-known correlations for vapor pressure and thermal properties are discussed below.

Vapor Pressure

Vapor pressure constitutes the backbone of thermodynamic equilibrium calculations. It is used to check the consistency of phase equilibrium calculations and is frequently used together with liquid density to determine equation of state parameters. The equilibrium provided by vapor pressure is a requirement for design and operation of several refinery units such as atmospheric and vacuum distillation columns.

One approach to determining the vapor pressure is through equations of state. However, a major disadvantage of CEOS in predicting vapor pressure is that the main inputs for equations of state are the critical temperature, critical pressure, and acentric factor. These values are not available for complex mixtures and cannot be measured for heavy components. Therefore, values for critical temperature, critical pressure, and acentric factor, must be estimated from correlations, introducing additional uncertainty in the model predictions.

Other options to predict vapor pressure are generalized correlations. A plethora of vapor pressure correlations have been developed to both fit and predict vapor pressure data of pure fluids. The basis of most predictive methods follows from corresponding states theory and the Clapeyron equation. These equations normally have a high degree of accuracy over a moderate range of

temperatures, but their reliability decreases significantly in the very low temperature range (Velasco *et al.*, 2008; Vetere, 1991).

The most commonly used predictive correlations used for pure hydrocarbons and narrow petroleum fractions are the equations developed by Korsten (2000), Lee-Kesler (1975), and Ambrose and Walton (1989). These equations are recommended when reliable critical properties are available. Since these equations were developed using the principle of corresponding states, the quality of the prediction is markedly affected by the quality of the critical properties. Consequently, the major application of these equations is for light hydrocarbons, while their application to complex systems such as hetero-atomic and highly aromatic petroleum fractions is questionable.

A more general set of correlations were developed by Maxwell and Bonnell (1957) and Riazi (2005). These equations have the advantage over the above correlations in that they were developed using petroleum fraction vapor pressures and their inputs are measurable physical properties. The Maxwell and Bonnell (M-B) is the most common method used to estimate vapor pressures of petroleum fractions and to interconvert boiling temperatures at vacuum conditions. This correlation is also known to perform well at subatmospheric pressures ($P < 1atm$). The M-B correlation was developed using *n*-hexane as a reference compound; a temperature correction factor is required for more aromatic fractions where the Watson Factor is less than 12. Tsonopoulos and coworkers (1986) determined that the linear temperature dependence proposed by M-B for the temperature correction factor is not accurate for more complex systems such as coal liquids. They proposed a quadratic temperature dependence for the temperature correction factor based on a dataset with *Kw* between 8.3 and 11.1. The new temperature correction factor improved the vapor pressure predictions for the subatmospheric and super-atmospheric pressure ranges.

Riazi (2005) proposed one of the simplest equations for vapor pressures using only the normal boiling point. The accuracy of this correlation for pure components is around 1% and is recommended when data near the boiling temperature are available. All of the vapor pressure correlations tested in this project are summarized in Table 2.7.

Table 2.7. Summary of correlations to estimate vapor pressure.

Source	Correlation	Range of Applicability	Eq.
Maxwell and Bonnell (1957)	$\log_{10} P^{vap} = \frac{3000.538Q - 6.761560}{43Q - 0.987672}$ $Q = \frac{\frac{T_b'}{T} - 0.00051606T_b'}{748.1 - 0.3861T_b'}$ $T_b' = T_b - 1.3889F(K_w - 12)\log_{10}\frac{P^{vap}}{760}$ $F = -3.2985 + 0.009T_b$	$12<K_w<13$ and $P^{vap}<1$ atm	(2.29)
Riazi and Daubert (2005)	$\log_{10} P^{vap} = 3.2041\left(1 - 0.998\frac{T_b - 41}{T - 41}\frac{1393 - T}{1393 - T_b}\right)$	For T close to T_b	(2.30)

Liquid Heat Capacity

Accurate correlation of the liquid heat capacity is required to determine the net heat fluxes for any process where heating and cooling take place. For heavy oil in particular, the liquid heat capacity is used to estimate the amount of heat required to preheat a heavy oil or bitumen during recovery.

For petroleum fractions, liquid heat capacity is normally estimated from physical using the Lee-Kesler (1976) and Tsonopoulos (1986) correlations. The Lee-Kesler correlation was specifically developed for petroleum fractions and is recommended for the range shown in Table 2.8. Tsonopoulos developed a correlation to predict liquid heat capacity of coal liquids and aromatic compounds, and Riazi (2005) showed that the Tsonopoulos correlation is also able to predict the liquid heat capacity of hydrocarbons with good accuracy (4%).

Dagostar (2013) developed a correlation based on the principle that the energy requirements of fundamental structures are due to the internal energy of the molecule (vibrational, rotational, and translational modes). He demonstrated that for the types of molecules found in petroleum, these energy modes depended mainly on the atomic composition and were less sensitive to the molecular

structure. He then developed a correlation for the liquid heat capacity based on elemental analysis. The correlation retained the quadratic form of the Lee-Kesler correlation but the parameters were redefined as a function of the similarity variable (α) which is function of elemental analysis. All of the liquid heat capacity correlations presented above are summarized in Table 2.8.

Table 2.8. Summary of correlations to estimate specific liquid heat capacity

Source	Correlation	Range of Applicability	Eq.
Dagostar (2013)	$C_p^{liq} = A_1 + A_2 T + A_3 T^2$ $A_1 = 24.5(-0.3416\alpha + 2.2671\alpha^2)$ $A_2 = 0.1064\alpha - 0.3874\alpha^2$ $A_3 = \alpha + 2.2671\alpha^2$	T_r<0.95	(2.31)
Tsonopoulos (1986)	$C_p^{liq} = B * [0.645 - 0.05959SG + D]$ $B = (0.28299 + 0.23605K_w)$ $D = (2.32056 - 0.94752SG)\left(\frac{T}{1000} - 0.25537\right)$	Coal liquids and aromatics	(2.32)
Lee-Kesler (1976)	$C_p^{liq} = A + B \times 10^{-4} T + C \times 10^{-7} T^2$ $A = -4.90383 + (.099319 + 0.104281SG)K_w + \left(\frac{4.81407 - 0.194833K_w}{SG}\right)$ $B = (7.53624 + 6.214610K_w)\left(1.12172 - \frac{0.27634}{SG}\right)$ $C = -(1.35652 + 1.11863K_w)\left(2.9027 - \frac{0.70958}{SG}\right)$	T_r<0.85	(2.33)

Heat of Vaporization

Along with heat capacity, the heat of vaporization plays an important role in determining the amounts of energy required to operate petroleum processing units such as distillation columns. For petroleum fractions, the enthalpy of vaporization decreases with increasing temperature and at the critical temperature, where H^V and H^L become the same, its value is zero. To determine the enthalpy of vaporization at a given temperature, the enthalpy at a defined temperature, usually the normal boiling temperature (ΔH_{nbp}^{vap}) is first calculated. Then, the value at the desired temperature is calculated from the change in sensible heat (i.e. from the liquid and vapor heat capacities). Hence, most correlations are for the heat of vaporization at the normal boiling point.

Several correlations have been proposed to predict the ΔH_{nbp}^{vap} for petroleum fractions (Parhizgar *et al.*, 2013; Kikic and Vetere, 2011). In general, there are two groups of equations. One group uses the critical properties and normal boiling point as inputs. The second group uses empirical correlations that try to relate ΔH_{nbp}^{vap} with easily obtainable parameters such as specific gravity, molecular weight, and normal boiling point. Since critical properties are not available for the petroleum cuts used in this study, the second group of correlations was tested.

The simplest of these correlations is Trouton's rule where it is assumed that, for any pure component, the ratio $\Delta H_{nbp}^{vap}/T_b$ is a constant. This ratio has been modified for the correlations for petroleum cuts with expressions based on MW, SG, and/or T_b. Riazi (2005) proposed a correlation based on the normal boiling point and the specific gravity, but it was developed using only pure hydrocarbons and its application is limited to low molecular weight components. Vetere (1979 and 1995) also developed correlations based only on pure components. Gopinathan and Saraf (2001) and Fang *et al.* (2003) published similar correlations, but these correlations were developed with data from petroleum cuts. The above correlations for the heat of vaporization are summarized in Table 2.9.

Table 2.9. Summary of correlations to estimate heats of vaporization at the normal boiling point.

Source	Correlation	Range of Applicability	Eq.
Riazi and Daubert (2005)	$\Delta H_{nbp}^{vap} = 37.32315\ {T_b}^{1.14086}\ SG^{0.00977089}$	70<MW<300	(2.34)
Vetere (1979)	$\Delta H_{nbp}^{vap} = \frac{T_b}{MW}\ (58.20 + 5.94 lnMW - (6.485[T_b - 263MW^{0.581}]^{1.037}))$	Pure compounds	(2.35)
Vetere (1995)	$\Delta H_{nbp}^{vap} = 4.1868T_b \left(9.08 + 4.36\ lnT_b + 0.0068\frac{T_b}{MW} + 0.0009\frac{{T_b}^2}{MW}\right)$	Pure compounds	(2.36)
Gopinathan and Saraf (2001)	$\Delta H_{nbp}^{vap} = 1081 + (SG^{-0.01418}T_b) * F$ $F = 31.98\ lnT_b + \frac{22.12{T_b}^{-1.573}}{MW}$	245<T_b<1321	(2.37)
Fang (2003)	$\Delta H_{nbp}^{vap} = T_b(9.549 + 14.811\ lnT_b + 19.334\ lnSG + F)$ $F = 12.346\frac{T_b}{MW} - 0.06662\frac{{T_b}^2}{MW} + 7.833 \times 10^{-5}\frac{{T_b}^3}{MW}$	350<T_b<650	(2.38)

Heat of Combustion

The heat of combustion is determined as the amount of heat evolved by the combustion of a quantity of fuel in the presence of oxygen under standard conditions. It represents an important property for hydrocarbons because it helps to identify the quality of the hydrocarbon as a fuel source. Heat of combustion is also used to derive the heat of formation for reaction enthalpy calculations (Tsonopoulos, 1986; Strausz and Low, 2003). For a simple hydrocarbon the combustion reaction can be expressed as:

$$C_aH_b + (a + b/4)O_2(g) \rightarrow aCO_2(g) + (b/2)H_2O\ (l\ or\ g) \quad (2.37)$$

For a precise definition for the heat of combustion, it is important to specify whether the value is obtained at constant volume (ΔU°) or at constant pressure (ΔH°) and whether the water is in a liquid *(l)* or gas phase *(g)*. If the water is in a liquid phase, the measurement corresponds to the gross or high heating value (HHV). If the water is in the gas phase the value represents the low or net heating value (LHV) (Bruno and Smith, 2006). Since the amount of water produced depends on the hydrogen content of the fuel, the relation between LHV and HHV is given as (Riazi, 2004):

$$LHV = HHV - 0.22H\% \quad (2.38)$$

where *H%* is the hydrogen content weight percent.

In this work, the values reported correspond to the heat released at constant volume (ΔU°) and water is in the liquid phase (HHV).

There are two types of correlations for predicting the heat of combustion of fossil fuels. The first type are correlations to SG or the Watson Factor. These correlations are infrequently used because they are empirical and do not account for the presence of heteroatoms in the molecules. The second type are correlations based on modifications of the model proposed by Dulong (Tsonoupolos, 1986) where the heat of combustion is calculated based upon elemental composition. Improvements in the original model attempt to account for the presence of S, N and O in the mixture (Ringen *et al.*, 1979; Lloyd and Davenport, 1980; Jain and Sundararajan, 1981). More recent correlations are those developed by Tsonoupolos and coworkers (1986) and Yan *et al.* (1988). The above correlations for the heat of combustion are summarized in Table 2.10.

Table 2.10. Summary of correlations to estimate heats of combustion from elemental analysis.

Source	**Correlation**	**Range of Applicability**	**Eq.**
Yan (1987)	$\Delta U^\circ = -0.347(\%C) - 1.1696(\%H) - 0.1507(\%S) + 0.1927(\%O + \%N)$	Heavy Oil/Bitumen	(2.39)

Tsonopoulos (1986)	$\Delta U^{\circ} = 0.3506(\%C) + 1.1453(\%H) + 0.2054(\%S) + 0.0617(\%O) - 0.0873(\%N)$	Coal Liquids	(2.40)

CHAPTER THREE: EXPERIMENTAL METHODS

This chapter describes the samples used in this project, sample preparation, and the experimental methods used to characterize the distillation fractions. Sample preparation includes dewatering (if required), deasphalting (asphaltene precipitation), and distillation of the de-asphalted bitumen. The characterization measurements include molecular weight, density, refractive index, vapor pressure, liquid heat capacity, enthalpies of combustion, and elemental analysis for all collected fractions. All measurements were performed by the author except for the liquid heat capacity and enthalpies of combustion (measured at the Institute of Chemical Technology, Prague) and the elemental analysis (carried out by the University of Alberta Analytical & Instrumentation Laboratory). All procedures except for the elemental analysis (a standard method) are described below. Details of the apparatus and procedures for the deep vacuum fractionation method developed in this thesis are described in Chapter 4

3.1 Materials

Seven different heavy oils and bitumen samples from five geographical regions were distilled and characterized. The native samples were provided by Shell Canada Ltd. and Schlumberger Ltd. Table 3.1 lists the samples used in this project. The nomenclature for the samples is as follows: the first term indicates the country of origin (WC = Western Canada, CO = Colombia, MX = Mexico, US = United States, RO = Romania); the second term indicates the type of oil (B = bitumen, HO = heavy oil), and the third term indicates the reservoir and sample number. The samples provided by Shell Canada Ltd. were obtained using VAPEX extraction. The samples provided by Schlumberger Ltd. were obtained through a one-zone, one-well cold production method. Once received in the laboratory, the samples were refrigerated and were stored in sealed containers with nitrogen caps.

Prior to distillation the samples were checked for water content. Once the water was removed, the crude oils were deasphalted. The asphaltenes were washed to remove solids and the deasphalted and water-free crude oil was distilled using both spinning band distillation and deep vacuum

fractionation. The fractions obtained from the deep vacuum fractionation apparatus were characterized by measuring density, molecular weight, refractive index, elemental analysis, vapor pressure and liquid heat capacity. All the experimental methods related to this workflow are described in the following sections.

Table 3.1. Bitumen and heavy oils used in this thesis

Sample Name	API Gravity	nC5 Asphaltene Content wt%	Elemental Analysis wt%	Source
WC-B-B1	9.7	17.4	C:82.3 H:10.1 N:0.47 S:6.01 O:0.85	Shell
CO-B-A1	9.2	25.8	C:85.1 H:10.21 N:0.71 S:3.21 O:0.60	Schlumberger
MX-HO-A1	13.2	21.2	C:83.4 H:10.5 N:0.55 S:5.32 O:0.48	Schlumberger
CO-B-B1	10.9	22.7	C:86.1 H:10.57 N:0.59 S:2.59 O:0.57	Schlumberger
US-HO-A1	15.5	12.7	C:84.1 H:11.12	Schlumberger

			N:0.81 S:2.37 O:1.61	
WC-B-D1	10.4	16.2	C:84.6 H:10.8 N:0.36 S:3.26 O:0.35	Schlumberger
RO-HO-A1	15.4	6.5	C:86.8 H:11.6 N:0.77 S:0.19 O:0.56	Schlumberger

3.2 Sample Preparation: Water Content Determination and Dewatering

In any case where the water content of the oil sample was greater than 1%, the sample was dewatered. Removing the water was necessary to obtain a correct distribution of boiling points for the heavy oil and bitumen samples. The water content was initially determined by Karl Fisher titration (Metrohm 787KF Titrino). The Karl Fisher procedure involved first filling the titration vessel with a solvent mixture of 26 vol% 2-propanol and 74 vol% toluene, both ACS grade and dried using molecular sieves. A pre-titration was carried out using Aqualine Complete 5 by EMD supplied from VWR International. The crude oil was diluted with the same solvent mixture and sonicated. Then a syringe with diluted sample was weighed before and after injection into the titration vessel. The water content of the sample was then calculated from a calibration curve of titrant volume versus water. Most of the samples had low water content except CO-B-A1, US-HO-A1, and US-HO-A1 which had a water content higher than 3 wt%.

To remove water, the sample was placed in a separatory funnel and wrapped with heating tape to warm the sample to 50 ºC. The temperature of the heating tape was controlled with a thermostat. Upon heating, the water would coalesce and sediment at the bottom of the funnel where it could be removed. The sample was heated until no more water was observed at the bottom of the funnel. To determine the final water content, the sample was tested again by Karl Fischer titration. All the samples had less than 1 wt% water after the dewatering process.

3.3 Sample Preparation: Deasphalting

Maltenes are required for the deep vacuum fractionation method and they were obtained by de-asphalting the bitumen sample using *n*-pentane. The asphaltene precipitation was a modified version of ASTM D2007. A known amount of bitumen was mixed with *n*-pentane at a ratio of 40 mL of solvent per 1 g of bitumen. The mixture was sonicated for 60 minutes and left to settle for a total contact time of 24 hours. Then, the supernatant was decanted and filtered through a 24 cm Whatman #2 filter. *n*-Pentane was then added to the sediment at an amount equivalent to 10 vol% of the initial *n*-pentane added. The mixture was sonicated for 45 minutes and left to settle. After 16 hours of settling, the solution was filtered through the same filter used previously.

The filter cake was washed with *n*-pentane until the filtrate was colorless and then it was dried for 8 days at 333 K. The filter cake includes asphaltenes and any co-precipitated material and is termed asphaltene/solids. Finally, all of the filtrate was rotoevaporated at 323 K and atmospheric pressure to remove solvent to recover the maltenes.

To remove solids from the asphaltene/solids, mixtures of toluene and asphaltenes/solids were prepared. The solution was sonicated for 45 min and left to settle for 60 minutes. Then, the solution was centrifuged for 5 min at 4000 rpm (1780 RCF). The centrifuged solution was decanted into a beaker and left to dry in a fume hood. A mass balance was performed to determine the amount of solids. Negligible amounts of solids were observed in the asphaltenes/solids from all of the oils used in this study.

3.4 Spinning Band Distillation

Distillations were performed using a BR Instruments model number 18-100-M-250 spinning band distillation apparatus (SBD). This apparatus consists of a 200 cm^3 round bottom flask, a heating mantle, a spinning band equivalent to 200 theoretical plates, an automatically controlled reflux valve, two thermocouples, a vacuum pump, a condenser bath and four receivers, Figure 3.1. The temperature of the flask is controlled with the heating mantle. The thermocouples read the temperatures of the vapor and liquid during the distillation. The receivers collect the fractions at the desired temperature intervals set for the distillation. If distillation is undertaken at vacuum conditions pressure is set to a desired value and controlled with a VAC-1000 vacuum system that integrates a pressure sensor, control valve, cold trap and vacuum pump.

To start a distillation, 0.1 kg of dewatered bitumen was placed in the round bottom flask and continuously heated until both liquid and vapor flows were observed, as indicated by one drop per second of liquid exiting the condenser. The temperature of the condenser was set at 278 K. A period of 40 minutes was required to equilibrate the liquid and vapor flows within the system. Then the reflux valve was opened to a reflux ratio of 5:1. To increase the temperature of the system the heating rate was set initially at 10% and after equilibration time it was increased to maintain the liquid and vapor temperature curves parallel to each other throughout the distillation until the cracking temperature (573 K) was reached. The operating pressure was maintained at 390 Pa (3 mmHg).

Four cuts were collected in the receivers for each distillation and the upper temperatures for each cut were set to obtain a separation indicating a color change in the cuts collected. Once 573 K was reached in the boiling flask, the distillation was stopped. The temperatures of the vapor and boiling liquid sample were recorded before and after each cut was recovered. The Atmospheric Equivalent Temperature (AET) of the vapor was calculated using the Maxwell-Bonnell inter-conversion method for reduced distillations. Mass balances were performed to determine the amount of bitumen distilled.

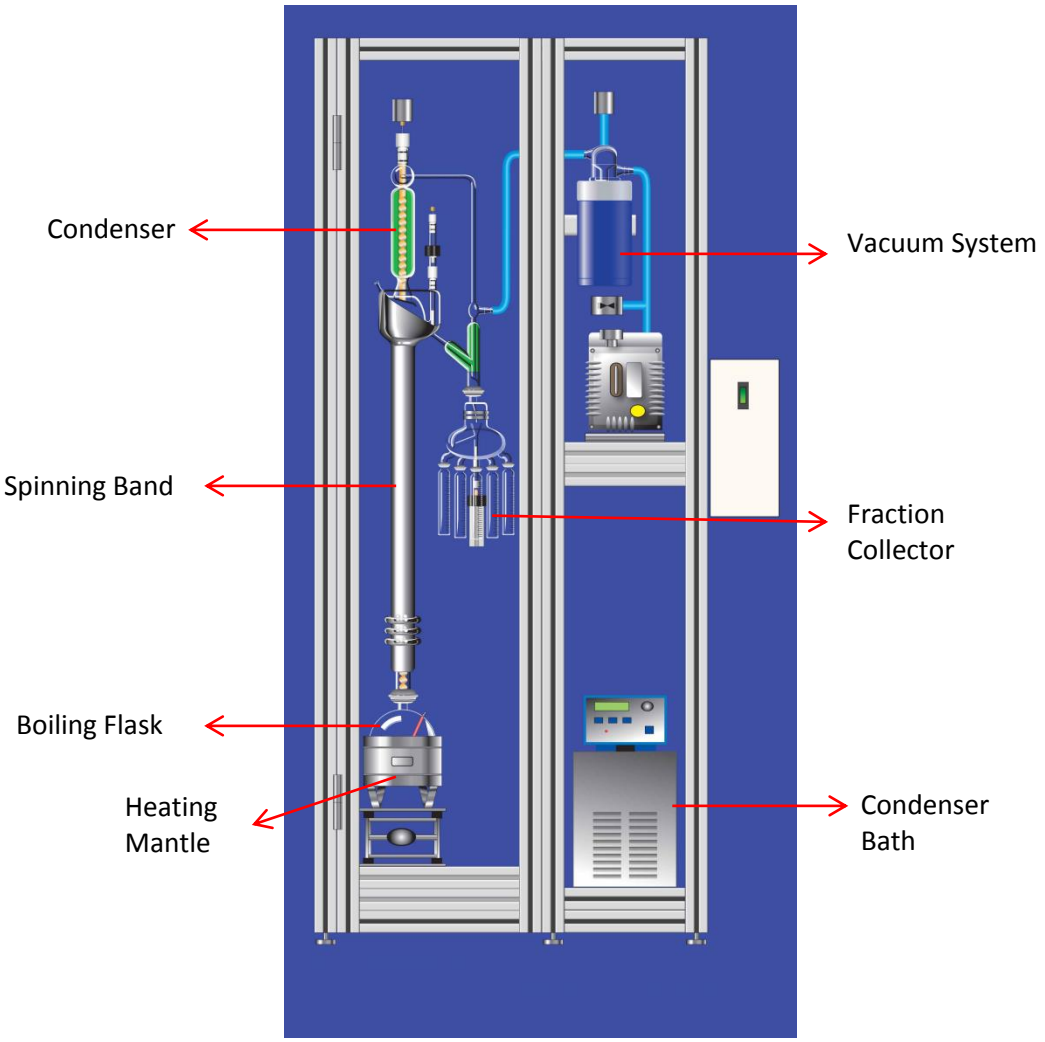

Figure 3.1. Layout of the spinning band distillation apparatus (adapted from the BR Instruments manual).

3.5 Property Measurement of Crude Oil Fractions

The most commonly used properties used to supplement distillation-based characterizations are molecular weight and density. Additional properties such as refractive index, elemental analysis and thermal properties were measured to aid the inter-conversion methodology developed in Chapter 5. The experimental methods used for each property are presented in the following thesis section.

3.5.1 Molecular Weight

Molecular weights of the bitumen and its distillation cuts were measured in toluene at 323 K using a Jupiter Model 833 vapor pressure osmometer calibrated with sucrose octaacetate. Briefly, the osmometer measures the voltage difference between a thermistor contacted with solvent and a thermistor contacted with a solution of the same solvent and the solute of interest. Figure 3.2 shows a schematic representation of the apparatus.

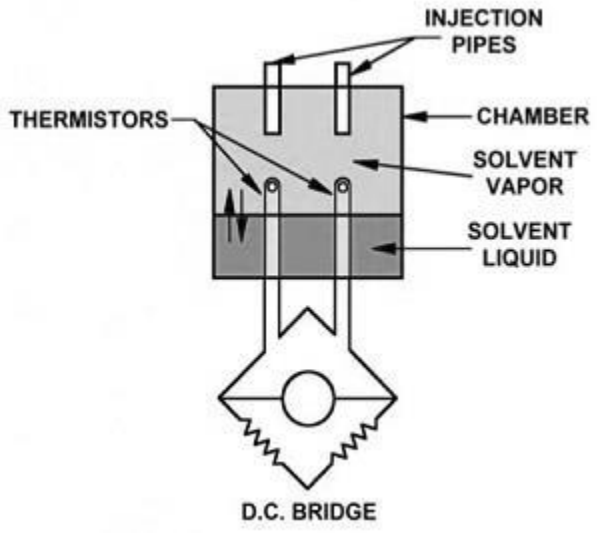

Figure 3.2. Vapor Pressure Osmometer Diagram (adapted from Jupiter VPO manual).

The difference in voltage is the result of differences in vapor pressure between the two thermistors. The relation between voltage difference and molecular weight is given by:

$$\frac{\Delta V}{C_2} = K\left(\frac{1}{MW_2} + A_1 C_2 + A_2 {C_2}^2 + \cdots\right) \tag{3.1}$$

where ΔV is the voltage difference, C_2 is the solute concentration in g/L, K is a calibration constant and A_1, A_2 are constants to account for non-ideal behavior of the solution. At low concentrations, the higher order terms (A_2 plus) are negligible and the equation reduces to:

$$\frac{\Delta V}{C_2} = K\left(\frac{1}{MW_2} + A_1 C_2\right) \tag{3.2}$$

To determine the molecular weight of a substance, the voltage difference is measured for a series of solutions of different concentrations of the test substance in the reference solvent (toluene). The voltage difference/concentration ratios are linearly extrapolated versus solute concentration and the y-intercept is converted to molecular weight as follows:

$$MW_2 = \frac{K}{\left(\frac{\Delta V}{C_2}\right)} \tag{3.3}$$

The instrument was calibrated with sucrose octaacetate (679 g/mol) and the calibration was confirmed with octacosane (395 g/mol). The measured molecular weight of octacosane was within 4% of the correct value.

For each bitumen and distillation cut sample, a series of solutions were prepared at concentrations of 0.001, 0.002, 0.005, 0.010 and 0.020 g/cm³. The repeatability of the cut molecular weights was ±15%. These errors are possibly due to fluctuations in temperature, pressure, and humidity between experiments.

3.5.2 Density

The densities of bitumen and the distillation cuts were measured with an Anton Paar DMA 4500M density meter at 293 K. The instrument precision was ±0.01 kg/m³. The densities of pure solvents and the light distillation fractions were measured directly. The repeatability of the direct measurements was ±0.05 kg/m³.

For bitumen, denser and more viscous fractions, the density was determined indirectly by linearly extrapolating the density of the sample at higher temperatures down to 20ºC. To validate the linear extrapolation, the same procedure was used on several light fractions. Figure 3.3 shows the extrapolated density at 20ºC versus the directly measured density for the first four fractions of four different heavy oil and bitumen samples. The extrapolated densities at 293 K were within the experimental error (±0.05 kg/m³) of the densities measured directly at 293 K.

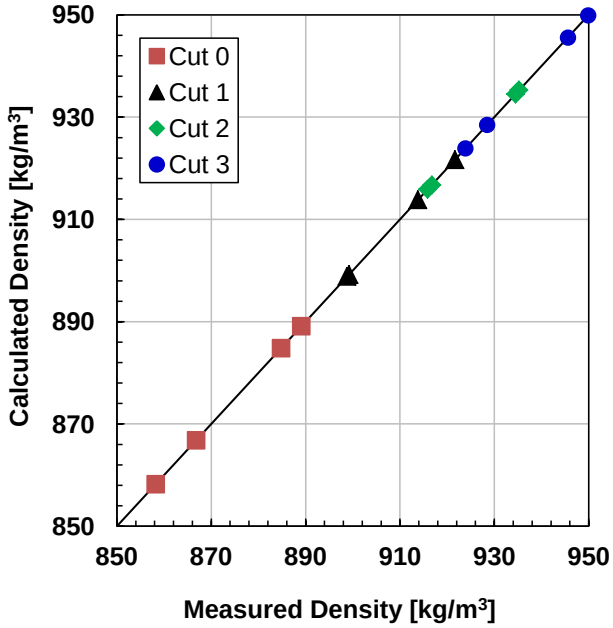

Figure 3.3. Measured and predicted density at 20°C for the initial four distillation fractions of four bitumen samples.

In the case of the distillation residue, the viscosity did not decrease enough to allow density measurement at higher temperatures. Instead, solutions of the sample in toluene at concentrations from 0.001 to 0.02 kg/L were prepared. The density of the residue was calculated using a mixing rule (Powers, 2014)

Since the residue contains highly aromatic structures it is expected that a mixtures of residue and toluene form nearly ideal solutions (Powers, 2014). Therefore, the density of the mixture is given by:

$$\rho_{Mix} = \left[\frac{w_1}{\rho_1} + \frac{w_2}{\rho_2}\right]^{-1} \tag{3.4}$$

where w is the mass fraction, ρ is the density, and subscripts *Mix*, *1*, and *2* denote the mixture and Components 1 and 2, respectively. Equation 3.4 was least squares fitted to the density data of the mixtures of residue and toluene to obtain the residue density.

3.5.3 Refractive Index

Refractive index was measured with an Anton Paar Abbemat-WR refractometer. The apparatus includes a measuring prism made of an isotropic crystal of a high refractive index (YAG -Yttrium-Aluminum-Garnet). The refractometer is designed to be used with samples with a lower refractive index than the prism. A liquid sample in contact with the prism is illuminated by an LED and the critical angle of the total reflection at 589.3 nm sodium D wavelength is measured with a high-resolution sensor array. The refractive index (n_D) is calculated from this value. The instrument has a precision of ±0.00002.

To measure the refractive index, the sample was placed on the measuring prism and after allowing stabilization of the reading and temperature (30 to 60 seconds) the value was recorded. The measurements were performed at 293 K and room pressure for samples with low viscosity. The repeatability of the refractive index from direct measurements was ±0.0002.

Very viscous samples were warmed to 333 K in an oven prior to measurements to facilitate sample placement and measurements at higher temperatures were linearly extrapolated to the refractive index at a desired temperature. As with density, the extrapolated values at 293 K were compared with the measured values for light fractions, thus testing the accuracy of the extrapolation. Figure 3.4 shows the measured and predicted value for four different fractions of two bitumen samples. The extrapolated refractive indices at 293 K were within the experimental error (±0.0002) of the indices measured directly at 293 K.

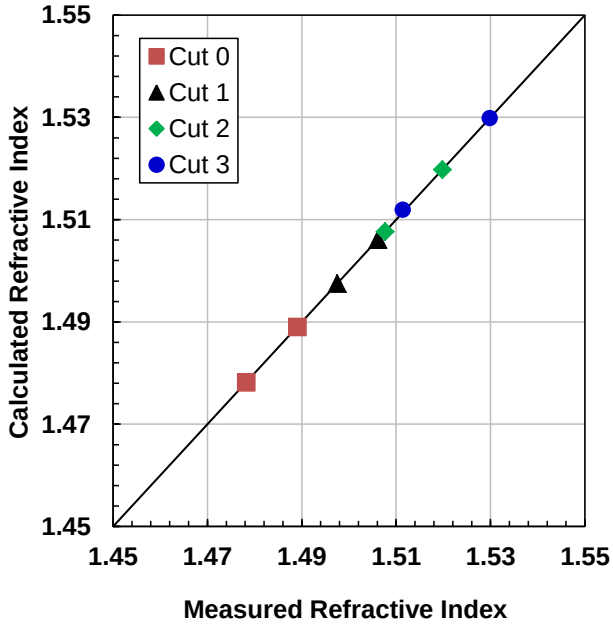

Figure 3.4. Measured and predicted refractive index at 293 K for the initial four distillation fractions of two bitumen samples

3.5.4 Elemental Analysis

The elemental composition of the boiling fractions was determined via combustion using a Carlo Erba EA 1108 elemental analyzer that simultaneously determines the total carbon, nitrogen, hydrogen and sulfur based on the composition of the sample's combustion products. Oxygen is measured separately based on its conversion to carbon monoxide over a nickel carbon phase. Standards fall within 0.3% of the theoretical values. These measurements were performed by the Department of Chemistry at the University of Alberta (Moffat, 2012)

3.5.5 Vapor Pressure

The vapor pressure of the fractions was measured using a static method developed by Castellanos *et al*. (2012) that was designed to achieve pressures below 0.1 Pa. The principle is simple: a liquid sample is allowed to equilibrate with its vapor at a fixed volume and temperature. Note, since the heavy oils are multi-component mixtures, the saturation pressure measured is not technically a vapor pressure. However, the term vapor pressure is often used in the literature in this situation and we have continued with this convention.

DVFA-I Apparatus. The apparatus consists of a sample vessel, two valves used to control the operating cycles, a diaphragm gauge, a liquid trap and a turbomolecular pump, Figure 3.5. The pressure readings were measured with an Inficon diaphragm gauge capable to measure pressures in the 0.1-133 Pa range. Readouts of pressure gauge are recorded in a digital file using LabView 8.6 (2008). The desired temperature is attained using electric heating tapes which are uniformly wrapped on the apparatus. J-type thermocouples are attached to the pipes to read the temperature and PID temperature controllers maintain the temperature within ±0.1 K.

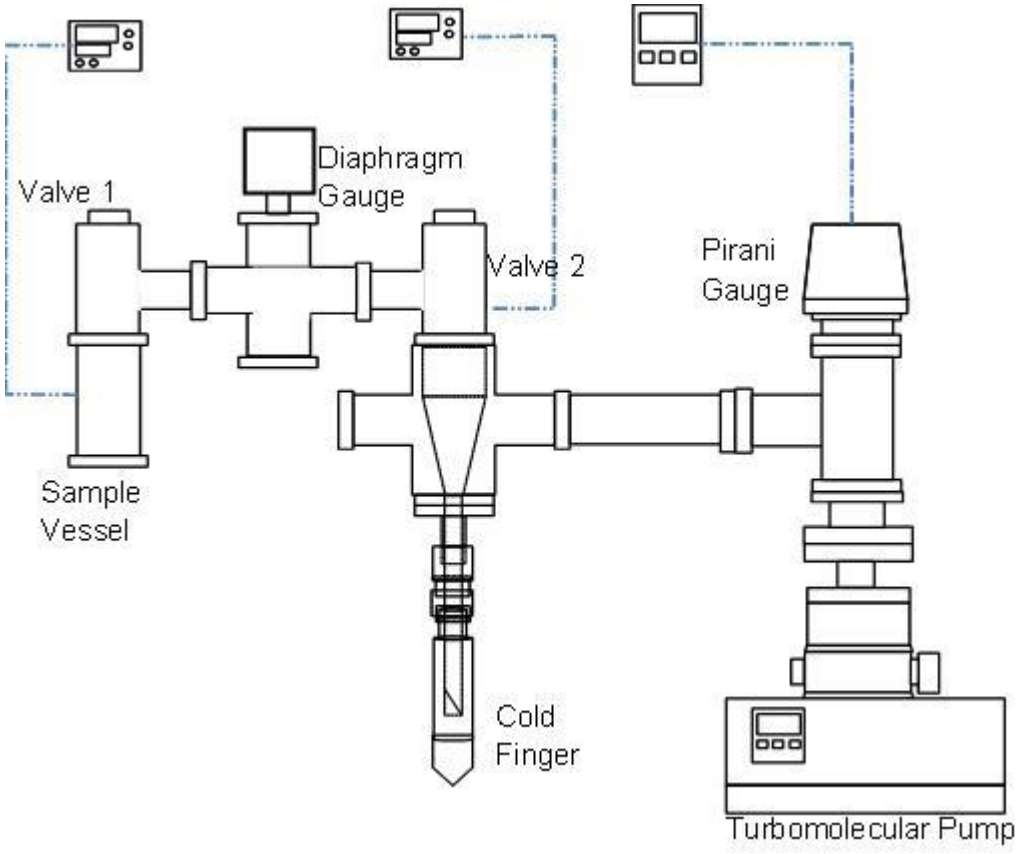

Figure 3.5. Simplified schematic of the deep vacuum apparatus (DVFA-I) in configuration to measure vapor pressure

Measurement. Baking out of the empty apparatus and degassing of the samples are required to eliminate contaminants that invalidate vapor pressure readings. The degassing process was carried out at 313 K to minimize possible fractionation of the cuts. Note the fractions were stored in sealed

vials under nitrogen at 273 K in order to minimize any potential contamination prior to the vapor pressure measurement.

After degassing, the vapor pressure was measured using the following procedure. The liquid sample was placed in the sample vessel and the apparatus was heated up to the desired temperature. The pump was switched on and once the apparatus reached the minimum pressure given by the turbo-molecular pump (or baseline), the vapor pressure was measured at the test section between Valves 1 and 2 in cycles. First, the test section was opened to the pump (open Valve 2 keeping Valve 1 closed) for two minutes. Then the test section was isolated from the pump and opened to the sample (close Valve 2 and open Valve 1) until the pressure reached a constant value. Finally, Valve 1 was closed to isolate the sample and Valve 2 was opened to begin a new cycle. The cycles were repeated until the peak pressures of at least three consecutive cycles were constant. To account for the leak rate, the pressure readings for each cycle were corrected by extrapolating the pressure back to the time when the cycle started.

The repeatability of the measurements was within 3%. The measured vapor pressures for naphthalene and *n*-hexadecane were within 13% and 4%, respectively, of the literature values (Castellanos-Diaz, 2012). The error in the vapor pressure measurements for the boiling fractions is expected to have a maximum uncertainty of 13%.

3.5.6 Liquid Heat Capacity

The liquid heat capacities of the boiling fractions were measured at the Institute of Chemical Technology in Prague (Ruzicka, 2015), with a Tian-Calvet calorimeter (Setaram μDSC IIIa) in the range from 258 to 355 K using an incremental temperature scanning mode with 5 K steps and a heating rate of 0.3 K/min followed by isothermal delays of 2600 seconds. A synthetic sapphire, NIST Standard Reference Material No.720, was used as the reference material. The typical mass of samples was 0.4 to 1 g. The combined uncertainty (0.95 level of confidence) of heat capacity measurements was estimated to be 1%. Details of the calorimeter, measurement procedure and its calibration can be found elsewhere (Straka *et al*., 2007; Fulem *et al*., 2008).

The measurement of heat capacity for the boiling fractions was carried out after three successive runs: 1) empty measuring cell; 2) cell filled with the reference material; 3) cell was filled with the boiling fraction. The second vessel, the reference vessel, was empty during all three runs. Heat capacity was calculated as follows.

$$C_{p,f} = \frac{m_{ss} C_{p,ss} (A_f - A_e)}{m_f (A_{ss} - A_e)} \quad (3.5)$$

where $C_{p,f}$ is the specific heat capacity of the boiling fraction; $C_{p,ss}$ is the specific heat capacity of the reference substance (synthetic sapphire); m_f is the mass of the boiling fraction; m_{ss} is the mass of the reference substance; A_f is the integrated value of the differential heat flow when the measuring vessel contains the sample; A_{ss} is the integrated value of the differential heat flow when the measuring vessel contains the reference substance; and A_e is the integrated value of the differential heat flow when the measuring vessel is empty.

3.5.7 Heat of Combustion

The heat of combustion of the boiling fractions was measured at the Institute of Chemical Technology, Prague, with a Parr 1356 Isoperibol Bomb Calorimeter at constant volume. In "isoperibol" operation, the temperature of the jacket is held constant through the measurement while the temperature of the bucket rises. To compensate for the heat flow within the calorimeter, an automated correction is applied using a microprocessor controller. The energy equivalent of the calorimeter was determined using 1.0 g pellets of benzoic acid. The precision of the standard measurement was below 0.3%. A run with benzoic acid was performed before each measurement to improve precision of the measurements. Since the amount of the distillation cut used for the measurement was less than 0.5 g, a spiking material (benzoic acid) was used to drive the combustion process to completion. Details for this method are provided elsewhere (Mahnel, 2015).

The results obtained from the bomb calorimeter represent the gross or high heat of combustion of the cuts, which includes the heat of vaporization of the condensed water. The heat of combustion was calculated as follows.

$$HHV = \frac{W_c \Delta T - e_N - e_S - e_F}{m} \quad (3.9)$$

where *HHV* is the gross heat of combustion of the distillation fraction in kJ/g, W_c is the heat capacity of the calorimeter being used in kJ/˚C, ΔT is the temperature rise in ˚C, *m* is the mass of the sample in grams, e_N is a correction factor for the heat produced by burning nitrogen to form nitric acid, e_S is a correction factor for the heat produced by burning sulfur to form sulfuric acid, and e_F is a correction factor for the heat produced by the burning fuse.

CHAPTER FOUR: MODIFIED DEEP VACUUM FRACTIONATION APPARATUS AND STANDARDIZED PROCEDURE

The original deep vacuum fractionation apparatus (DVFA-I) was designed to measure vapor pressure. Its capability to distill heavy oil was evaluated in a proof of concept test and the results of this test are presented in this chapter. Then, a modified version (DFVA-II) of the DFVA-I is introduced along with the reasoning for the modifications. A new procedure to operate DVFA-II to consistently distill deasphalted bitumen and heavy oil samples is presented and evaluated. The WC-B-B1 bitumen is used to demonstrate the differences and improvements between DVFA-I and DVFA-II. A summary of repeatability of the fractionations for the other six oils is presented at the end of the chapter. The apparatus was also designed so that physical cuts could be collected for property measurements. The properties measured in this thesis are summarized at the end of the chapter but are discussed in detail in subsequent chapters.

4.1 Proof of Concept for Extended Distillation

The proof of concept test was performed with the static deep vacuum apparatus (DVFA-I) developed by Castellanos-Diaz (2012) for the measurement of vapor pressure of heavy oils and bitumen. In this case, the apparatus was operated as a batch distillation with no reflux and one theoretical plate. The apparatus was described in Chapter 3 and its configuration is shown again in Figure 4.1, for the reader's convenience.

To fractionate a bitumen sample using the DVFA-I, the sample temperature was raised to the initial condition at T_1. The initial temperature of fractionation was the temperature at which a detectable amount of condensate was visually observed in the cold finger after gradual heating. At this point, the sample was left open to pump suction by leaving all the connecting valves open. The upper DVFA-I section, above the sample vessel, was left at a temperature 20 K higher than T_1 to facilitate vapor transportation and avoid condensation in the inner pipe.

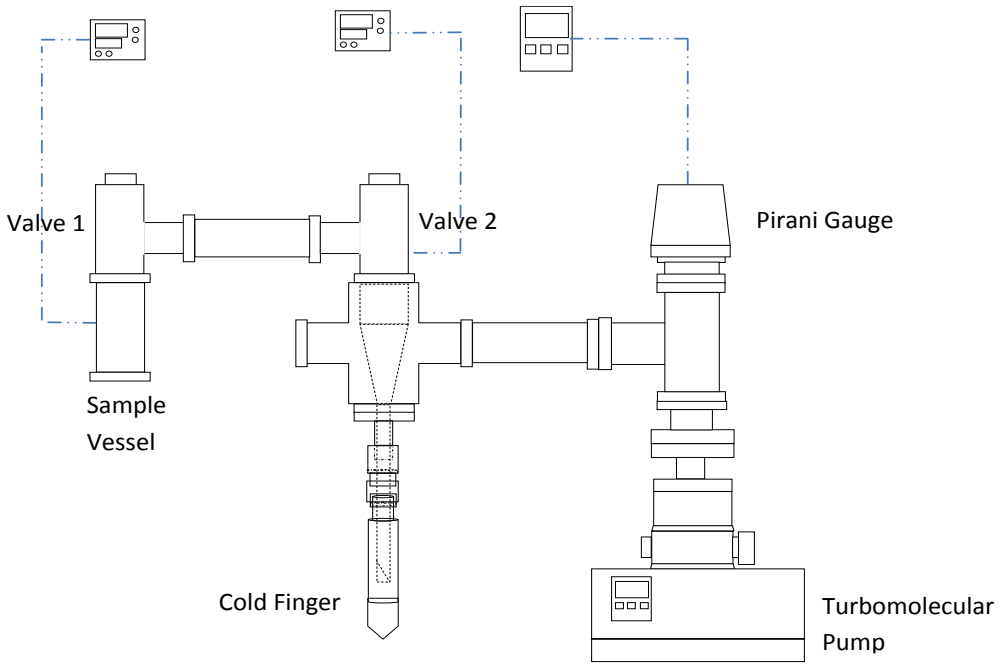

Figure 4.1. Simplified schematics of the deep vacuum apparatus (DVFA-I).

Each cut was collected by condensation in the cold finger which was replaced when the fractionation process at T_1 stops. To determine when the fractionation at a given temperature was complete, the volume of the accumulating cut was measured over time. If the volume of the cut did not change during 72 hours, the cut was considered to be complete. Then, the sample vessel was isolated and the temperature is raised to a value T_2, higher than T_1. Once the temperature was constant to within ± 0.1 K, the fractionation process was repeated. A set of cuts was collected at temperatures between 413 and 563 K. Note, the pressure during fractionations was lower than the minimum operational range of the Pirani gauge placed on top of the pump; therefore, the distillation pressure could not be measured. Even if a wider-pressure-range gauge were available, at pressures below 10^{-5} kPa, leaks and absorption/desorption phenomena will affect the pressure readouts. Since pressure could not be measured during the experiments, an interconversion method for the temperature, independent of the pressure, was required.

Deep vacuum fractionations were performed on maltenes instead of the whole bitumen. Asphaltenes are non-distillable and contribute significantly to the high viscosity of the oil. Removing the asphaltenes reduced the sample viscosity and thereby enhanced mass transfer which

is expected to decrease the distillation time, improve the separation, and possibly increase the amount of oil that can be distilled.

Two fractionations were performed on WC-B-B1 maltenes in the proof-of-concept test. The results are listed in Table 4.1 and Figure 4.2 shows a photo of the five cuts collected for Fractionation 1. Note that as the boiling point of the cut increased, the color of the cut changed from light, transparent amber to dark greenish brown, ending in an opaque black for the residue. In addition, as expected the measured density (Table 4.1) of the cuts increased from the first to the last cut. Slower flow was also observed as the separation proceeded, suggesting that the viscosity increased from the first to last cut. These changes in physical properties indicate that a qualitatively successful fractionation was achieved.

Table 4.1. WC-B-B1 maltene cuts obtained using the DVFA-I.

Trial	Cut	Temperature [K]	Cumulative wt% Bitumen Distilled	Density at 293 K [kg/m^3]
Fractionation 1	1	423	10.4	933.9
	2	463	22.8	952.0
	3	493	29.7	982.3
	4	533	46.4	998.6
	5	563	**56.9**	1018.5
	Residue	>563		1055.1
Fractionation 2	1	423	5.51	918.1
	2	443	17.72	958.1
	3	463	27.79	959.1
	4	483	34.53	999.1
	5	503	41.29	1001.5
	6	523	45.43	1005.0
	7	543	50.00	1016.3
	8	573	**56.08**	1013.1
	Residue	>573		1050

Figure 4.2. Photograph of five different cuts and residue of WC-B-B1 maltenes from Fractionation 1 (DVFA-I) proof-of-concept test.

The data from Table 4.1 are plotted as a boiling curve (at the apparatus pressure) in Figure 4.3. The cumulative mass percent of the maltenes distilled is 67 to 68 wt% (55 to 56 wt% bitumen based) compared with 26 wt% distilled of bitumen using spinning band distillation, Table 4.2. Hence, the deep vacuum method approximately doubles the distillable portion of the bitumen. The repeatability of the fractionation was estimated by fitting the Fractionation 1 data and then determining the deviation of the Fractionation 2 data from the fitted curve, Figure 4.2. The average deviation of the distillation data was ±4.3 cumulative wt%.

Table 4.2. Spinning Band Distillation (SBD) assay of WC-B-B1.

Normal Boiling Temperature [K]	Cumulative wt % Distilled
511	3.2
526	4.9
541	6.5
552	8.1
563	9.7
575	11.4

587	13
597	14.6
613	17.9
623	19.5
631	21.1
640	22.7
648	24.3
653	26

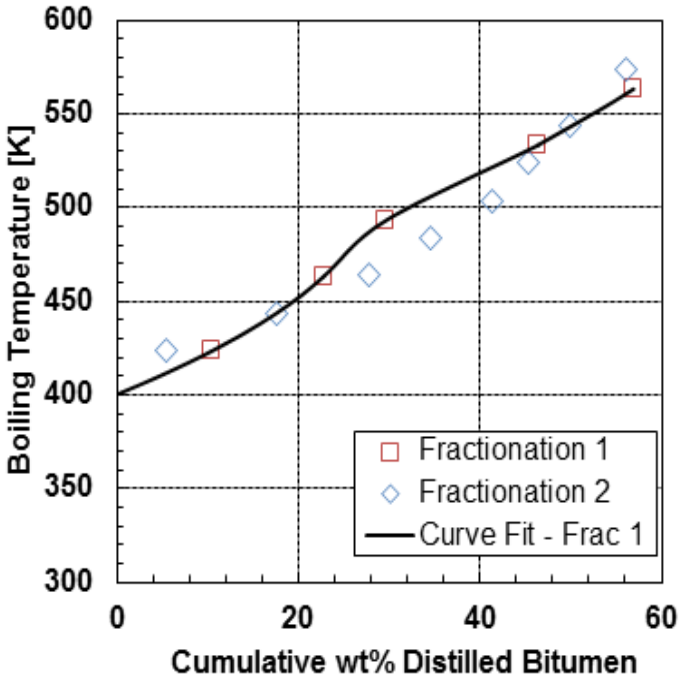

Figure 4.3. Boiling point profiles for WC-B-B1 bitumen at DVFA-I apparatus pressure; symbols are data and line is cubic spline fit to Fractionation 1 data.

The results from the proof-of-concept using DVFA-I were encouraging. However, the DVFA-I posed several significant challenges: a very long experimental time per cut, potential sample entrainment, and insufficient amounts of cut sample collected for further analysis. To overcome these challenges and standardize the DVFA, a second apparatus (DVFA-II) was developed utilizing the same basis of design of the DVFA-I.

4.2 Modification of Original Deep Vacuum Apparatus

The original DVFA-I had a capacity for a sample volume of 20 cm^3 with a 5 cm^3 volume capacity for condensate collection. Given that 8 cuts were desired for the oil characterization and at least 7 cm^3 of each cut was required for property measurements, the volume of the initial configuration was insufficient. In addition, due to the small diameter of the sample vessel and high viscosity of the fluid, many days were required for each cut to diffuse through the de-asphalted heavy oil, making the complete procedure very time consuming (2 months per fractionation). Simply increasing the length of the cylindrical sample vessel to obtain larger cuts would increase the height of the fluid and the corresponding mass transfer resistance, leading to an increase in the distillation time per cut.

Another issue was the proximity of the sample vessel to the collector device and the absence of a physical barrier to avoid entrainment. Coloring of the light cuts was observed, indicating overlapping and splashing of the sample, Figure 4.2. An important constraint is that additional fittings and seals would increase the apparatus leak rate, which increased the pressure of the system and therefore decreased the ability of the DVFA to extend the distillation of heavy oils.

To solve these issues without adding significantly more fittings, the original cylindrical sample vessel was replaced with a tee-shaped fitting and two additional concentric reducers. The new configuration used Swagelok fittings and the same metal gasket seals to minimize leaks. It provided a larger sample volume (110 cm^3) to obtain the desired cut volumes as well as a larger sample surface area in order to reduce mass transfer resistance and therefore produce a corresponding increase in mass transfer rate. Reducers above the tee-shaped sample vessel were required to couple the tee diameter with the diameter of Valve 1. Due to their conical shape, the reducers also act as a barrier for the entrained liquid when vapor is produced during the distillation, Figure 4.4. When assembled and in the absence of fluid, the system is able to achieve pressures as low as $1x10^{-7}$ Pa.

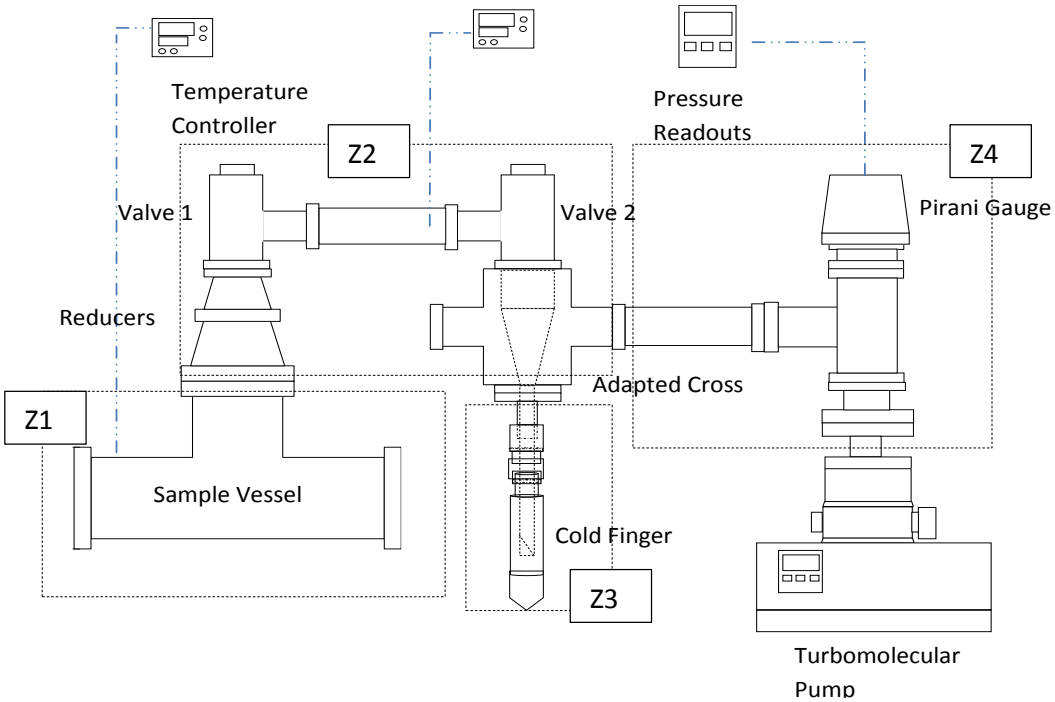

Figure 4.4. Simplified schematics of the modified deep vacuum apparatus (DVFA-II).

Figure 4.5 presents a comparison of the time required to collect the same volume of a cut with a boiling range between 443 to 463 K using the same initial amount of oil (0.11 kg) using the original (DVFA-I) and modified (DVFA-II) sample vessels. With this change, the total time of the distillation for WC-B-B1 was halved. The fractionation of all the oils listed in Table 3.1 were performed within a month, indicating that modifications in DFVA-I successfully overcame the issues present in DVFA-I. Table 4.3 summarizes the distillation time for each sample and the final wt% distilled.

The completed DVFA-II has four different temperature zones. The first zone (Z1) corresponds to the temperature at which each distillation cut is obtained; the second zone (Z2) is always 20 K higher than Z1 to avoid condensation of vapor in the pipes; the third zone (Z3) is maintained at 253 K to assure condensation; and the fourth zone (Z4) is left at room temperature to avoid overheating of the bearings of the pump. Note the temperatures of Z1 and Z2 are controlled during the distillation procedure.

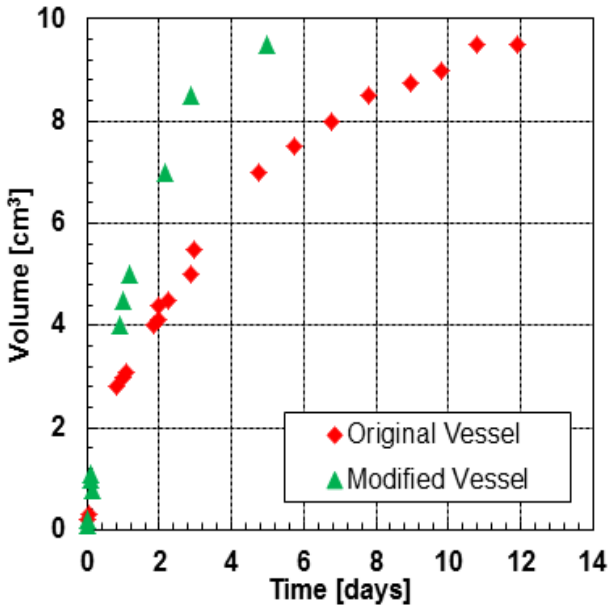

Figure 4.5. Effect of the modified sample vessel design on distillation time for the 443 to 463 K cut.

Table 4.3. Distillation time and wt% distilled of bitumen for each sample used in this work

Sample	Distillation Time (days)	Cumulative wt% Bitumen Distilled*
WC-B-B1	30	51.7
CO-B-A1	31	42.8
MX-HO-A1	28	41.4
CO-B-B1	30	46.0

US-HO-A1	27	53.4
WC-B-D1	30	41.8
RO-HO-A1	25	62.2

*Mass balance normalized based on the losses

4.3 Standardization of Fractionation Using DVFA-II

The next step was to define an initial sample volume, cut point temperature, and number of cuts as part of a standard procedure. To finalize the standardization of the distillation process, two fractionations using DVFA-II were performed for a Western Canadian Bitumen (WC-B-B1). Table 4.4 presents the distillation data collected for the maltenes as well as the density and molecular weight of each cut. The repeatability of the DVFA-II fractionations was within an average deviation of ±1.5 wt%, Figure 4.6. The distillations curves were fitted using cubic splines to avoid discontinuities for the sole purpose of providing an exact as possible comparison between curves where data points do not fall on the same X or Y coordinate. Note, the 0 wt% to 20 wt% distilled seemed to have a discontinuity; however, this is an artifact introduced due to the fitting process and scatter of the data but does not represent the nature of the data. The spinning band distillation of this sample and the DVFA fractionations of other samples did not show this discontinuity. Potential sources of error are considered below.

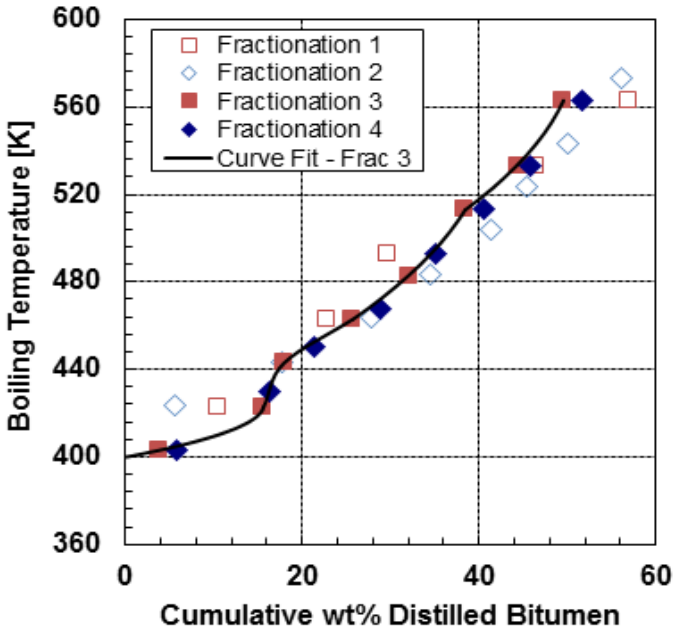

Figure 4.6. Boiling point profiles for WC-B-B1 bitumen in DVFA-II at apparatus pressure (Fractionations 3 and 4) compared with profiles from DVFA-I (Fractionations 1 and 2). Symbols are data; line is cubic spline fit to Fractionation 3 data.

Table 4.4. Distillation data using DVFA-II for WC-B-B1

Trial	Cut	Temperature [K]	Cumulative wt% Bitumen Distilled	Molecular Weight [g/mol]	Density at 293 K [kg/m^3]
Fractionation 3	0	403	3.7	209	890.1
	1	423	15.6	242	920.4
	2	443	18.0	283	954.8
	3	463	25.7	293	970.9
	4	483	32.1	331	977.9
	5	513	38.4	380	987.5
	6	533	44.3	460	998.5
	7	563	**49.5**	496	1001.1
	res	>563		1023	1028.5
Fractionation 4	0	403	5.8	213	893.3
	1	430	16.3	247	920.6

2	450	21.4	272	961.9
3	468	28.8	327	973.2
4	493	35.0	352	982.2
5	513	40.5	362	992.0
6	533	45.9	480	999.6
7	563	**51.7**	490	1016.8
res	>563		1010	1035.0

4.3.1 Sources of Error

Some of the possible sources of error during the distillation are discussed below. The final standardized procedure was design to minimize overlapping between cuts and light end losses as well as to increase repeatability of the distillation curve and the properties of each cut.

Entrainment: One of the major issues with the initial apparatus was significant entrainment of liquid droplets in the boiling vapor. To assess the impact of the modified apparatus on entrainment, the distillation curves from the standardized fractionations are compared with the proof-of-concept fractionations in Figure 4.6. Note, the amount of bitumen distilled using DVFA-II is 7 wt% less than that obtained with DVFA-I apparatus. While a lower distillation of the sample does not sound like an improvement, it is in fact evidence of a cleaner separation and reduction in entrainment. Consider the early stage of the distillation: comparing Figures 4.1 and 4.7, a lighter color is observed for the first cuts, Figure 4.7, when the modified DFVA-II was used. Also, the difference between the wt% distilled for the first cut in Fractionations 1 and 2 in the proof-of-concept tests was 4.9 wt%, whereas the difference for the first cut in Fractionations 3 and 4 in the standardized procedure was only 2.1 wt%.

Figure 4.7 is a photo of the maltene cuts of the WC-B-B1 from Fractionation 4. The progressive changes in color and viscosity were similar to the initial fractionations, but there are clearly sharper distinctions in color between the cuts confirming that entrainment has been reduced or eliminated. Finally, the gas chromatography (GC) assays of the initial cuts from Fractionation 4 are shown in Figure 4.8. The carbon number in Figure 4.8 is an ‘equivalent carbon number’ corresponding to the carbon number of a paraffin that elutes at the same retention time. The cuts show a near

Gaussian distribution of carbon numbers with no suggestion of entrainment of heavy components. The distribution of density and molecular weights will be discussed later, although it is worth noting that both values show smooth trends and no evidence of entrainment effects. Hence, entrainment has been reduced to negligible levels.

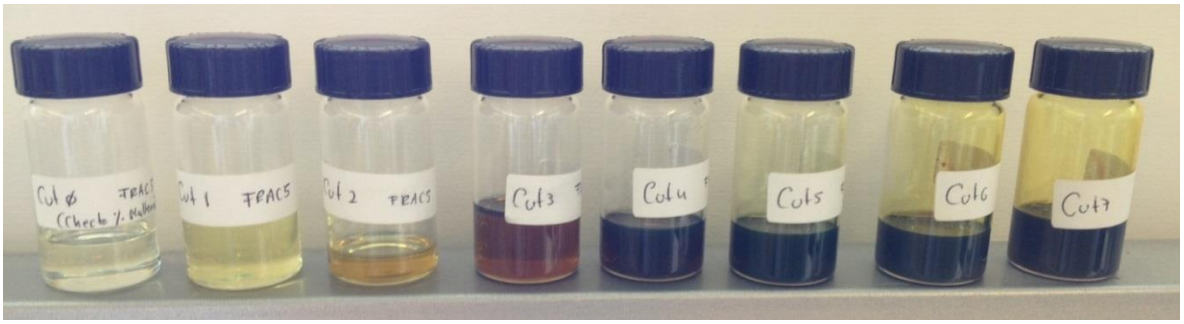

Figure 4.7. Photograph of the seven different cuts of WC-B-B1 maltenes from Fractionation 4 (DVFA-II).

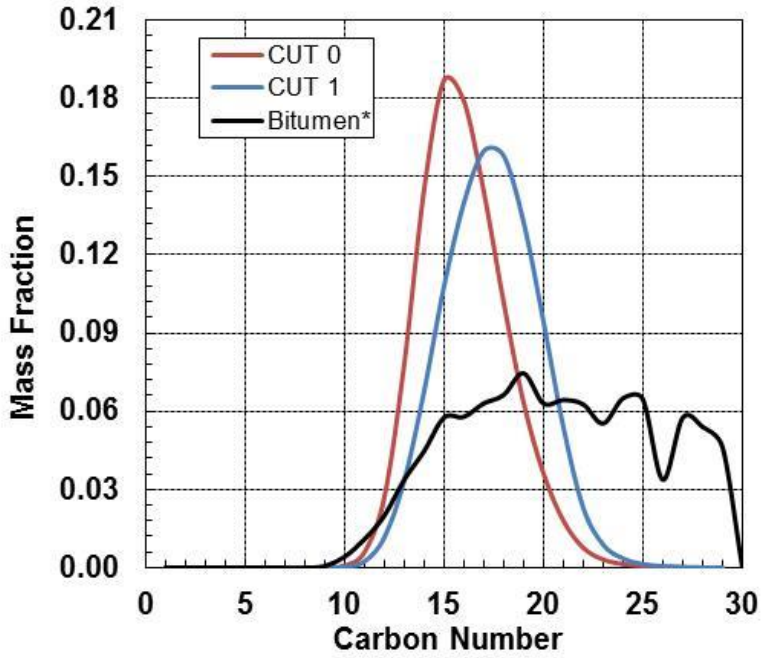

Figure 4.8. Carbon number distribution for the first two boiling cuts from Fractionation 4 and whole WC-B-B1 bitumen (free of C30+ compounds).

Residual Pentane from De-asphalting of Maltenes: The GC assays for the first cuts (Cut 0 and Cut 1) from Fractionation 4 show no traces of pentane, Figure 4.8. The chromatographic results also show the expected overlapping of compounds as a consequence of the compositional complexity of the oil and the absence of reflux in the batch distillation. Finally, when compared to the assay for the whole bitumen, it appears that the small amount of material in the C_{10} to C_{11} range may have been partially stripped off during the asphaltene precipitation procedure. However, these losses are negligible and correspond to approximately 0.006% of the total bitumen sample. This mass fraction was calculated as the difference between the amounts of lightest components (from C_9 to C_{11}) reported in the GC assay of the whole bitumen and the corresponding components in the GC of the initial two cuts.

Losses: During fractionation there were two sources of losses during sample distillation: 1) the escape of light components through the pump during the initial stages of the fractionation; 2) the condensation of heavy boiling cuts in the lines during the final stages of the fractionation. The latter losses were determined from the mass change of the DVFA-II fittings. The former were determined from the difference between the initial mass sample and the sum of the masses of residue, cuts, and condensed material on the fittings. On average, the total losses for all the 14 distillations were less than 3.2% of the initial sample mass.

Leak Rate: In all vacuum systems, air enters the apparatus through imperfect seals and limits the ultimate vacuum pressure achievable. However, pressure cannot be monitored during the fractionation due to temperature limitations in the pressure gauges and may be a source of systematic error. Since the leak rate will vary from run to run (tightness of seals will vary), the distillation pressure will also vary and therefore the amount distilled will be different. Any differences in the leak rates will only be detectable at the higher temperatures where the leak rate is largest. Despite the leak rate error, the average repeatability of the procedure was only 2% of the cumulative weight percent collected for a given boiling point range, which is in within the repeatability range of standard atmospheric and vacuum distillation methods.

4.3.2 Distillation Procedure using DVFA-II

Based on the previous results, the finalized distillation procedure can be divided into three general steps: preparation of the apparatus, degassing and fractionation. Each step is discussed below.

Preparation of the Apparatus

Before starting the fractionation, all the fittings are washed with toluene and left in a vacuum oven for 24 hours at 373 K and 8000 Pa. After cleaning, all parts are weighed and then assembled together and connected to the pump as shown in Figure 4.1. The empty DVFA-II is baked-out at 573 K for one day to avoid contamination of the sample and cuts collected; contaminants are collected in the cold finger. The main purpose is to clean the surface of the pipes by removing the remaining contaminants and water vapor by desorption.

Degassing

Degassing of the sample begins by disconnecting the sample vessel, weighing it once more to check for any major change in mass due to desorption of contaminants, and then 0.11 kg of de-asphalted bitumen are added into the sample vessel. It is then reconnected to DVFA-II and two thermocouples are placed on the outside wall of the sample vessel. Next, the cold finger that was used to collect the contaminants is removed and replaced by a new, pre-weighed cold finger. Heating and insulation tape are then uniformly wrapped over the entire DVFA-II apparatus except for the cold finger. The heating tape provides temperature control for all of the non-cold finger parts of DVFA-II. A bath of oil and dry ice is placed around the cold finger section to maintain its temperature at 253 K. All the fittings after Valve 1 are heated to 30 K higher than the sample temperature in order to avoid condensation in the pipes and to enhance the mobility of the produced vapor as it travels toward the collector device. Once the DVFA-II apparatus is reassembled, both Valves 1 and 2 are opened and the turbomolecular pump is switched on.

Degassing of *n*-pentane from the oil sample is achieved by holding the sample vessel at 323 K for 6 hours. After this time, the cold finger is replaced once again with a new, pre-weighed cold finger. The sample vessel is disconnected and weighed to determine the remaining mass. A temperature of 323 K is used to avoid losses of light ends from the oil.

Note, this temperature was found to be sufficient to remove the residual *n*-pentane from the de-asphalting procedure used to prepare the maltenes. At the end of the degassing process, approximately 0.01 to 0.22 wt% of the initial maltenes were collected in the cold finger. Gas chromatography (GC) assays confirmed that this distilled material was almost entirely *n*-pentane. GC assays of the subsequent lightest cuts confirmed that all of the pentane had been removed. Potential losses of light ends will be discussed later.

Fractionation

Following degassing of the sample, the sample vessel is reconnected and fractionation initiated by increasing the temperature at a rate of 10 K/h until the desired cut temperature is achieved. The temperature is then held constant until the volume in the cold finger does not change for 24 hours. Cuts are collected at temperature intervals of 20 K. The 20 K interval was selected because it balanced the required sample volume for each cut with a reasonable number of cuts to use in the oil characterization. Also, two to three of the lightest cuts had to overlap the distillable region of the SBD in order to validate the method. For heavy oils, the first cut occurred at approximately 403 K and the fractionation produced 8 cuts plus a residue.

The following three steps are repeated for every cut collected:

i. Set the cut temperature
ii. Run distillation for the cut until volume in the cold finger does not change for 24 hours
iii. Close valves, turn off pump, disconnect cold finger, weight it, and replace it with a new, pre-weighed cold finger

The maximum cut temperature is 563 K in order to avoid thermal cracking of the sample. At the end of the distillation, the pump is switched off, all fittings are disassembled, and the mass of every fitting is recorded. Any change in the mass of fitting is likely caused by condensation of the heavier cuts and is used in the determination of losses during the procedure, as will be discussed later. The collected cuts are stored in glass vials with nitrogen caps and then refrigerated until needed for property analysis. The cleaning procedure is then repeated to prepare the apparatus for the next sample.

The remaining six deasphalted oils were distilled by this procedure. Two fractionations were performed for each sample and the density and molecular weight measured for all of the cuts. Table 4.5 summarizes the average deviation of the distillation curves for a given sample following the cubic spline approach. The deviations of the measured density and molecular weight of each cut are also summarized.

The final test was to compare the results from the standardized fractionation with results from a conventional vacuum distillation such as spinning band distillation. This comparison will be detailed in Chapter Five after the low pressure boiling points are converted to atmospheric equivalent boiling points.

Table 4.5. Repeatability obtained for density molecular weight and boiling point of seven oils following the standardized procedure for DVFA-II

Sample	Distillation Curve ARD %	Density ARD %	Molecular Weight ARD %
WC-B-B1	2.3	0.18	4.0
CO-B-A1	0.8	0.10	1.2
MX-HO-A1	1.5	0.21	2.8
CO-B-B1	2.6	0.25	3.4
US-HO-A1	2.5	0.17	4.1
WC-B-D1	0.9	0.12	2.6
RO-HO-A1	2.5	0.27	3.6

4.3.3 Cut Property Measurements

A significant contribution from the deep fractionation apparatus is the ability to collect cuts, including heavy fractions, for property measurements. In addition to the properties measured to test the repeatability of the fractionation (density and molecular weight), the following properties were measured for the distillation cuts: refractive index, elemental analysis, liquid heat capacity, vapor pressure, and heat of combustion. The physical properties are presented and discussed in Chapter 6.Vapor pressure and the thermal properties are presented and discussed in Chapter 7.

CHAPTER FIVE: INTERCONVERSION METHOD DEVELOPED FOR THE DEEP VACUUM FRACTIONATION APPARATUS

In this chapter, a methodology to obtain an equivalent atmospheric temperature (AET) for each boiling fraction from the deep vacuum apparatus is developed. The proposed methodology requires vapor pressure and heat capacity data which were collected in this study and are presented here. A new correlation for liquid heat capacity (presented in Chapter 7) is used for cases where data are unavailable. The interconversion results for all seven oil samples considered in this thesis are presented. The AET values are compared with the TBP data obtained from spinning band distillations, and the use of the Gaussian distribution to extrapolate these distillation curves is assessed. A simpler interconversion method to TBP data using only the bulk specific gravity and actual distillation temperature for inputs is proposed. Finally a correlation of TBP to cumulative wt% distilled is introduced to determine the whole distillation curve for heavy oils and bitumen up to the asphaltene fraction with only bulk specific gravity as an input.

5.1 Interconversion Methodology

5.1.1 General Concept

The proposed interconversion approach is illustrated in Figure 5.1. The left plot demonstrates how the measured vapor pressure in the low pressure region of a single cut is extrapolated to the boiling point at 1atm. The extrapolation is made with a correlation constrained to fit both thermal and vapor pressure data as a function of temperature. The AET from the extrapolations of all of the cuts are then assembled to create the desired boiling point curve, as demonstrated on the right plot of Figure 5.1.

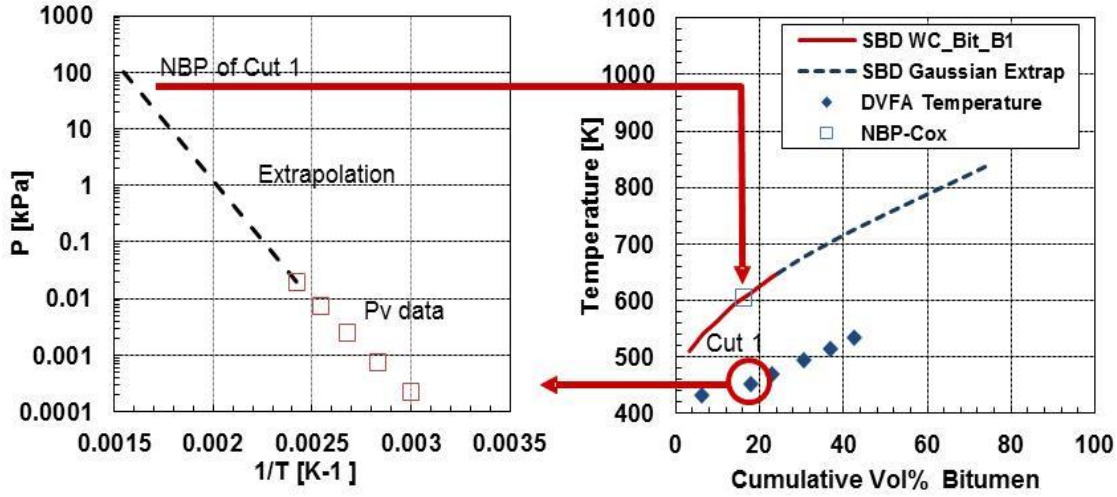

Figure 5.1. Proposed Interconversion Methodology for Deep Vacuum Distillation using DVFA-II

The key to the method is the relationship between vapor pressure, enthalpy of vaporization and heat capacity. This relationship has been extensively studied, not only as an extrapolation technique, but also as a methodology to assess the quality of the available experimental data for pure compounds (Ruzicka and Majer, 1993). The thermodynamic relationship between vapor pressure and caloric properties is given by the Clapeyron equation:

$$RT^2\left(\frac{d\ln P}{dT}\right)_{sat} = \frac{\Delta H_{vap}}{\Delta z_{vap}} = \Delta H' \qquad (5.1)$$

where R is the gas constant, T is the absolute temperature, P is vapor pressure, ΔH_{vap} is the enthalpy of vaporization, and Δz_{vap} stands for the difference between the compressibility factors of the saturated vapor and the saturated liquid. $\Delta H'$ represents the ratio of the enthalpy of vaporization to the difference in compressibility factors. Given an expression for vapor pressure as a function of temperature, Equation 5.1 allows the simultaneous correlation of enthalpy of vaporization and vapor pressure as a function of temperature using only one set of constraints.

In this case, the available thermal data are heat capacities and a relationship between vapor pressure and heat capacity is required. First, the change in heat capacity, $\Delta C'$, is defined as follows:

$$\Delta C' = \left(\frac{d\Delta H'}{dT} \right)_{sat} = \frac{d}{dT} \left[RT^2 \left(\frac{d \ln P}{dT} \right) \right]_{sat} \tag{5.2}$$

where the second equality comes from Equation 1. Equation 5.1 is introduced into Eq. 5,2 and the compressibility factor is expressed in terms of a volume explicit virial expansion truncated after the second virial coefficient to obtain the following expression (Ruzicka and Majer, 1993):

$$\Delta C' = \Delta C^0_{vap} - TP_{sat} \frac{d^2 B}{dT^2} - 2T \frac{d(B - v^l)}{dT} \left(\frac{dP}{dT} \right)_{sat} - T(B - v^l) \left(\frac{d^2 P}{dT^2} \right)_{sat} \tag{5.3}$$

where ΔC^0_{vap} is the difference in the heat capacities of the saturated phases, B is the second virial coefficient, and v^l is the molar volume of the liquid phase. However, the last three terms of Equation 5.3 are only significant at higher vapor pressure values (P >5000 Pa). At low pressures, the enthalpy of vaporization and the change in heat capacity expressions reduce to:

$$\Delta H' = \Delta H_{vap} \tag{5.4}$$

$$\Delta C' = \Delta C^0_{vap} = C^0_p - C^l_p \tag{5.5}$$

where C^0_p is the heat capacity of the ideal gas and C^l_p is the heat capacity of the saturated liquid. This approach has been mainly used to extrapolate vapor pressure in the middle pressure range (between 1000 and 200000 Pa) towards the triple point; hence, the accuracy of the extrapolation towards the boiling point is unknown.

The required elements for this method are then: a correlation of vapor pressure to temperature, vapor pressure data, enthalpy of vaporization and/or liquid heat capacity data, and the ideal gas heat capacity. Therefore, before developing the method it was required to collect experimental data for each cut including vapor pressure, liquid heat capacity, elemental analysis, and molecular weight. The following steps are required to complete the interconversion method:

1) Calculate the ideal gas heat capacity for each cut using Laštovka's equation and the elemental analysis of the cut
2) Select a vapor pressure equation

3) Regress the vapor pressure and heat capacity data with an appropriate optimization function and initial guesses.
4) Validate the calculated AET versus the data obtained from a spinning band distillation.

Data collection was described in Chapter Three. The remaining steps are described below using the WC-B-B1 bitumen as an example.

5.1.2 Ideal Gas Heat Capacity

The ideal gas heat capacity is the amount of heat required to increase one mole of sample by 1 K assuming that there are no intermolecular forces that may increase or decrease the internal energy of the molecules in the mixture. Laštovka *et al*. (2013) studied available correlations for predicting ideal gas heat capacity and proposed a correlation for ill-defined hydrocarbons that had better predictive capabilities. Laštovka *et al*.'s correlation for specific ideal gas heat capacity is a function of temperature and elemental analysis. It was developed based on the principle that the effect of fundamental vibrations of the atoms in a molecule (which determine heat capacity) are not significantly altered by relatively small difference in the structure of the molecule. They developed two correlations:

1. for aromatic hydrocarbons,

$$C_{P1}^{0} = A_2 + \frac{(A_1 - A_2)}{1+\exp\left\{(\alpha - A_3)/A_4\right\}} + \left(B_{11} + B_{12}\alpha\right)\left(\frac{C_{11} + C_{12}\alpha}{T}\right)^2 \frac{\exp\left\{-(C_{11} + C_{12}\alpha)/T\right\}}{1-\exp\left\{-(C_{11} + C_{12}\alpha)/T\right\}} + \left(B_{21} + B_{22}\alpha\right)\left(\frac{C_{21} + C_{22}\alpha}{T}\right)^2 \frac{\exp\left\{-(C_{21} + C_{22}\alpha)/T\right\}}{1-\exp\left\{-(C_{21} + C_{22}\alpha)/T\right\}} \quad (5.6)$$

2. for aliphatic hydrocarbons,

$$C_{P2}^{0} = A_1 + A_2\alpha + \left(B_{11} + B_{12}\alpha\right)\left(\frac{C_{11} + C_{12}\alpha}{T}\right)^2 \frac{\exp\left\{-\left(C_{11} + C_{12}\alpha\right)/T\right\}}{1 - \exp\left\{-\left(C_{11} + C_{12}\alpha\right)/T\right\}} + \left(B_{21} + B_{22}\alpha\right)\left(\frac{C_{21} + C_{22}\alpha}{T}\right)^2 \frac{\exp\left\{-\left(C_{21} + C_{22}\alpha\right)/T\right\}}{1 - \exp\left\{-\left(C_{21} + C_{22}\alpha\right)/T\right\}} \quad (5.7)$$

where *A*, *B* and *C* are constants and α is the similarity variable, which is given by:

$$\alpha = \frac{\sum_{i=1}^{5} \frac{w_i}{M_i}}{\sum_{i=1}^{5} w_i} \quad (5.8)$$

where w_i and M_i are the mass fraction and molecular mass of hydrogen, oxygen, nitrogen, sulfur and carbon (i = 1-5), respectively. The values of the constants are provided in Table 5.1. The reported relative deviations were 2.9% for aromatic and acyclic aliphatic hydrocarbons and 2.5% cyclic aliphatic hydrocarbons.

Table 5.1 Parameters for predictive ideal gas heat capacity correlations

Parameter	Eq 5.6	Eq 5.7
A_1	0.58	-0.17935
A_2	1.25	3.869444
A_3	0.17338	-
A_4	0.014	-
B_{11}	0.739174	-0.08053
B_{12}	8.883089	9.699713
C_{11}	1188.281	686.4342
C_{12}	1813.046	1820.466

B_{21}	0.048302	-0.99964
B_{22}	4.356567	17.26243
C_{21}	2897.019	1532.256
C_{22}	5987.804	5974.871

The ideal gas heat capacity of each cut was determined from a weighted average of C_p^0 obtained from Equations 5.6 and 5.7:

$$C_{Pi}^{o} = w_1 C_{P1i}^{o} + w_2 C_{P2i}^{o} \tag{5.9}$$

where, if $(H/C)_i$ <1.5, $w_1 = [(H/C)_i - 1]$ and $w_2 = 1 - w_1$ and, if $(H/C)_i > 1.5$, $w_2 = [2 - (H/C)_i]$ and $w_1 = 1 - w_2$. This weighting is based on a maximum *H/C* ratio of 2 for 100% paraffinic compounds and minimum *H/C* atomic ratio of 1 for highly aromatic petroleum compounds (Strausz and Lown, 2003). The accuracy of the predicted ideal heat capacity for the cuts is unknown, but it is expected to be within the accuracy reported by Laštovka (within 3%). The liquid and ideal gas specific heat capacities were then converted to molar heat capacities using the measured molecular weights of each cut.

5.1.3 Vapor Pressure Equation

Five different vapor pressure equations were tested for the extrapolation of the vapor pressure data: the Antoine, the Quasi-Polynomial with two and three adjustable parameters, the Cox and the Korsten equations. The criteria to select an appropriate equation were a low number of fitting parameters and an accurate fit of the trends for experimental vapor pressure and heat capacity with temperature. The best result was obtained for the three-parameter Cox equation, Equation 5.10:

$$ln P^{calc} = \ln P_b + \left(1 - \frac{T_b}{T}\right) exp(A_0 + A_1 T + A_0 T^2) \tag{5.10}$$

where P^{calc} is the calculated saturation pressure, T is the absolute temperature at the saturation pressure, P_b is the atmospheric pressure. T_b is the absolute boiling temperature at atmospheric conditions or AET and A_0, A_1 and A_2 are the adjustable parameters in the Cox equation.

Ruzicka and Majer (1996) previously studied the performance of the Cox equation and concluded that this mathematical relation between pressure and temperature had the best performance for extrapolation purposes. Their findings were corroborated in this work. Additional advantages of the Cox equation are that it does not depend on critical properties and the reference states can be modified based on the need of the extrapolation.

The corresponding equation obtained from the relationship of heat capacity to vapor pressure from Equation 5.2 is given in Equation 5.11:

$$\Delta C'^{\,calc} = RTexp(A_0 + A_1T + A_2T^2)[2A_1 + 4A_2T + (T - T_0) * (2A_2 + (A_1 + 2A_2T)^2] \quad (5.11)$$

where superscript *calc* indicates a calculated value. The Cox equation has 4 fitting parameters: A_0, A_1, A_2 and T_b which are the same parameters as in Equation 5.10.

5.1.4 Regression Method

The regression is a least squares minimization of the following objective function by adjusting the constants in the Cox equation:

$$OF = \sum_{i=1}^{n}\left(\frac{\ln P_i^{\exp} - \ln P_i^{calc}}{\ln P_i^{\exp}}\right)^2 + K_c\sum_{i=1}^{m}\left(\frac{\Delta C_i'^{\exp} - \Delta C_i'^{calc}}{\Delta C_i'^{\exp}}\right)^2 \quad (5.12)$$

where *n* and *m* are the number of experimental values for vapor pressure and $\Delta C'$ respectively, *OF* stands for optimization function, the subscripts *calc* and *exp* correspond to the calculated and experimental values of the corresponding variables and K_c is a weighting factor. The experimental vapor pressures were measured directly and the experimental $\Delta C'$ was determined using Equation 5.5. A K_c of unity was found to provide the best match to the spinning band distillation data and was used for all cuts while minimizing *OF*. The optimization is sensitive to the initial guess and a

single step procedure was found to be slow and not always stable. Therefore, the following multistep procedure was adopted:

1) Initialize the optimization with constants fitted to eicosane vapor pressure, Table 5.2, and heat capacity data from Růžička and Majer (1994). The vapor pressure of eicosane is similar to the vapor pressure of the lightest cuts.

2) Optimize the Cox constants for vapor pressure only (first term in Equation5.12). The optimized constants are the initial condition for the next step.

3) Simultaneously optimize vapor pressure and heat capacity for all terms in Equation 5.12.

4) Initialize the regression for the next cut using the constants calculated for the previous cut.

The deviations in the fits to the data are reported as standard deviations:

$$d = \left[\frac{1}{n} \sum_{i=1}^{n} \left(X_i^{calc} - X_i^{\exp} \right)^2 \right]^{1/2} \tag{5.13}$$

and relative standard deviations:

$$d_r = \left[\frac{1}{n} \sum_{i=1}^{n} \left(\frac{X_i^{calc} - X_i^{\exp}}{X_i^{\exp}} \right)^2 \right]^{1/2} \tag{5.14}$$

where n is the number of data points, X indicates either $\Delta C'$ or $\ln P$, and superscripts *exp* and *calc* indicate the measured and calculated values, respectively.

Table 5.2 Vapor pressure of eicosane measured in DVFA-I.

Temperature [K]	Pressure [Pa]
323	0.3
338	0.8
353	2.2
368	5.6
383	13.9
398	33.1

413	84.8

5.2 Vapor Pressure and Heat Capacity Data for DVFA Cuts

Liquid heat capacity and vapor pressure data were collected for all the distillation cuts of the seven oils and are provided in Appendix D and E, respectively. The estimated ideal gas heat capacity (Equation 5.8) for the distillation cuts are summarized in Appendix C. The data for bitumen WC-B-B1 are presented below as an example. The data for all samples are summarized in section 5.5 when the results from the interconversion method are presented.

The vapor pressures of the WC-B-B1 cuts, measured with the Deep Vacuum apparatus, are provided in Table 5.3. Each cut has a different temperature range. The lower limit was selected based on minimum gauge resolution (low volatility range) and the upper limit was selected to avoid significant losses of the lower boiling components which would alter the cut composition. For instance, if the boiling range of a cut was between 453 and 473 K, the maximum temperature at which vapor pressure was measured was 373 K, 80 K below the initial cut temperature. The precision of the vapor pressure measurements for the set of 6 cuts was within 2.2% based on the pressure differences obtained from the last five cycles for a given temperature. While the accuracy of the cut vapor pressures cannot be confirmed, the measured eicosane vapor pressures were within 8% of literature data (Castellanos, 2012).

The temperature range for which vapor pressure can be measured is limited to some extent for less volatile cuts; for example, only three data points were collected for Cut 6. The range is limited by: 1) the lower limit of the gauge readouts; 2) the maximum operating temperature of the gauge (463 K); 3) the maximum temperature that can be used to measure vapor pressure before the loss of lower boiling components.

Table 5.3. Measured vapor pressure of WC-B-B1 boiling cuts

Cut	T [K]	P [Pa]	Cut	T [K]	P [Pa]	Cut	T [K]	P [Pa]
1	313.2	0.5	2	333.2	0.06	3	323.2	0.002
1	333.2	2.5	2	353.2	0.6	3	353.2	0.05

1	343.2	5.3	2	373.2	2.3	3	393.2	2.2
1	353.2	11.7	2	393.2	8.6	3	413.2	7.2
1	363.2	25.5	2	413.2	33.8	3	433.2	23.0
4	403.2	0.7	5	423.2	2.2	6	433.2	1.3
4	413.2	1.3	5	433.2	3.6	6	443.2	2.1
4	423.2	2.2	5	443.2	6.0	6	453.2	3.5
4	433.2	3.8	5	458.2	12.1			
4	443.2	6.4						

The liquid and ideal gas heat capacities of each cut are provided in Tables 5.4 and 5.5. Table 5.6 shows the $\Delta C'^{exp}$ values obtained from experimental liquid heat capacity and the calculated ideal gas heat capacity (Eq. 5.8). The values for $\Delta C^{'exp}$ have four main sources of error (here shown for the mass based $\Delta C^{'exp}$): 1) the error in the measured liquid heat capacity, estimated to be 1%; 2) the error in the elemental analysis, estimated to be 0.3 wt%; 3) the error in the measured molecular weight, estimated to be 3.2%, and; 4) the error in the ideal gas heat capacity calculated using Laštovka correlation, reported to have a maximum deviation of 2.8% for ill-defined hydrocarbons. The overall error for $\Delta C^{'exp}$ was determined using a Monte Carlo sampling of the error distributions and was found to be 3.9% for the mass based $\Delta C^{'exp}$ and 2.1% for the molar $\Delta C^{'exp}$.

Table 5.4. Measured liquid heat capacity of WC-B-B1boiling cuts.

Temperature [K]	**C_p^l [J mol^{-1} K^{-1}]**					
	Cut 1	**Cut 2**	**Cut 3**	**Cut 4**	**Cut 5**	**Cut 6**
258.1	420.9	459.8	536.7	612.4	692.3	775.7
263.2	425.5	464.7	542.4	619.0	698.6	782.7
268.3	430.0	469.6	548.1	625.5	705.4	790.4
273.4	434.6	474.5	553.8	632.0	711.7	797.4
278.5	439.1	479.4	559.5	638.5	718.6	805.1
283.6	443.7	484.3	565.3	645.1	725.5	812.9

288.7	448.2	489.2	571.0	651.6	732.4	820.6
293.8	452.8	494.1	576.7	658.1	739.8	828.9
298.9	457.3	499.0	582.4	664.6	746.0	835.9
304.0	461.8	503.9	588.1	671.2	752.7	843.4
309.1	466.4	508.8	593.8	677.7	759.7	851.2
314.3	470.9	513.6	599.6	684.2	766.7	859.1
319.4	475.5	518.5	605.3	690.8	773.9	867.1
324.5	480.0	523.4	611.0	697.3	781.3	875.4
329.6	484.6	528.3	616.7	703.8	788.4	883.4
334.7	489.1	533.2	622.4	710.3	795.7	891.5
339.8	493.7	538.1	628.1	716.9	803.2	899.9
344.9	498.2	543.0	633.9	723.4	810.5	908.1
350.0	502.8	547.9	639.6	729.9	817.9	916.5
355.1	507.3	552.8	645.3	736.5	825.0	924.4

Table 5.5. Calculated ideal gas heat capacity of WC-B-B1boiling cuts.

Temperature [K]	C_p^{ig} **[J mol^{-1} K^{-1}]**					
	Cut 1	**Cut 2**	**Cut 3**	**Cut 4**	**Cut 5**	**Cut 6**
258.1	281.7	302.6	349.4	398.5	452.6	493.9
263.2	287.5	308.8	356.6	406.7	461.6	504.0
268.3	293.2	314.9	363.6	414.7	470.6	514.0
273.4	298.9	321.1	370.7	422.8	479.6	524.1
278.5	304.6	327.2	377.8	430.9	488.6	534.1
283.6	310.3	333.4	384.9	438.9	497.6	544.1
288.7	315.9	339.5	392.0	447.0	506.5	554.1
293.8	321.6	345.6	399.0	455.0	515.5	564.1
298.9	327.3	351.7	406.1	463.0	524.4	574.1
304.0	332.9	357.8	413.1	471.1	533.3	584.1
309.1	338.5	363.9	420.1	479.0	542.2	594.0

314.2	344.2	369.9	427.1	487.0	551.1	604.0
319.4	349.7	376.0	434.1	495.0	559.9	613.8
324.5	355.3	382.0	441.0	502.9	568.7	623.7
329.6	360.9	388.0	448.0	510.8	577.5	633.5
334.7	366.4	393.9	454.9	518.6	586.2	643.3
339.8	371.9	399.9	461.7	526.5	594.9	653.1
344.9	377.4	405.8	468.6	534.3	603.6	662.8
350.0	382.8	411.7	475.4	542.0	612.3	672.4
355.1	388.3	417.6	482.2	549.8	0.0	682.1

Table 5.6. $\Delta C'^{exp}$ of WC-B-B1boiling cuts.

Temperature [K]	**$\Delta C'^{exp}$ [J mol^{-1} K^{-1}]**					
	Cut 1	**Cut 2**	**Cut 3**	**Cut 4**	**Cut 5**	**Cut 6**
258.1	-139.3	-157.2	-187.3	-213.9	-248.8	-281.9
263.2	-138.0	-155.9	-185.8	-212.3	-245.9	-278.7
268.3	-136.9	-154.6	-184.5	-210.8	-243.8	-276.4
273.4	-135.7	-153.4	-183.1	-209.2	-241.1	-273.4
278.5	-134.5	-152.1	-181.7	-207.7	-239.0	-271.1
283.6	-133.4	-150.9	-180.4	-206.2	-236.9	-268.8
288.7	-132.3	-149.7	-179.0	-204.6	-234.8	-266.4
293.8	-131.1	-148.4	-177.7	-203.1	-233.2	-264.7
298.9	-130.0	-147.2	-176.3	-201.6	-230.6	-261.8
304.0	-128.9	-146.0	-175.0	-200.1	-228.3	-259.3
309.1	-127.8	-144.9	-173.7	-198.7	-226.3	-257.2
314.3	-126.8	-143.7	-172.5	-197.2	-224.5	-255.1
319.4	-125.8	-142.6	-171.2	-195.8	-222.8	-253.3
324.5	-124.7	-141.5	-170.0	-194.4	-221.3	-251.7
329.6	-123.7	-140.4	-168.8	-193.0	-219.7	-249.9

334.7	-122.8	-139.3	-167.6	-191.7	-218.2	-248.2
339.8	-121.8	-138.2	-166.4	-190.4	-216.9	-246.9
344.9	-120.9	-137.2	-165.3	-189.1	-215.6	-245.4
350.0	-120.0	-136.2	-164.2	-187.9	-214.3	-244.0
355.1	-119.1	-135.3	-163.1	-186.7	-212.7	-242.3

5.3 Application of Interconversion Method to WC-B-B1 Sample

5.3.1 Optimized Fit of Cox Equations to Vapor Pressure and Heat Capacity Data

The three parameter Cox equation was used to fit both vapor pressure and heat capacity data, Figure 5.2, for the oil WC-B-B1. The fitted vapor pressure parameters of the Cox equation are presented in Table 5.7. Note, the number of significant digits for T_b does not correspond to the accuracy of the calculated AET, but is required for the accuracy of the correlation from a numerical point of view. In general, the magnitude of the parameters increased monotonically from the first cut to the last.

Table 5.8 lists the average standard deviation, d, and the average relative deviation, d_r, of the fitted vapor pressure and heat capacity data for each cut. The average relative standard deviations for vapor pressure and $\Delta C^{'exp}$ were 7% and 1%, respectively. All of the vapor pressure and $\Delta C^{'exp}$ deviations are within experimental error. Note, the sensitivity of the interconversion method increases from Cut 1 to Cut 6 as the vapor pressure data becomes scarce and the low vapor pressure values are less reliable since they are, to some extent, affected by the leak rate of the deep vacuum apparatus.

While not shown explicitly in Table 5.8, the highest errors for each cut were observed in the low and high temperature ranges for both vapor pressure and heat capacity. At low temperatures, accurate readings are hindered by pressure leaks and the low volatility of the distillation cuts. At high temperature, the boiling point of the lighter components in the mixture is approached and the accuracy of the measurements is compromised.

The vapor pressures of Cut 4 and 5 overlap even though their heat capacities do not. Possible explanations are: 1) experimental error associated with the high leak rates when measuring the vapor pressure of these fractions; 2) an error in the fractionation temperature; 3) significant compositional overlap of these cuts which makes the vapor pressure differences too low to be determined using the deep vacuum apparatus. As will be shown later, the extrapolated AET for Cut 5 is off trend from the other cuts indicating that the measured vapor pressure was lower than expected. It is likely that there was an experimental error in the vapor pressure measurement for this cut.

Table 5.7. Parameters for Cox equations used to fit vapor pressure and $\Delta C^{'exp}$ with P_0 set to 101325 Pa.

Cut	A_0	$A_1 \times 10^{-4}$ [K^{-1}]	$A_2 \times 10^{-6}$ [K^{-2}]	T_b [K]
1	3.11221	-22.21270	1.69391	605.031
2	3.21997	-21.65373	1.79536	651.160
3	3.30326	-23.05355	1.82732	690.603
4	3.44185	-22.25477	1.70515	698.031
5	3.51200	-23.61439	1.68252	706.730
6	3.54805	-26.63337	2.03107	743.266

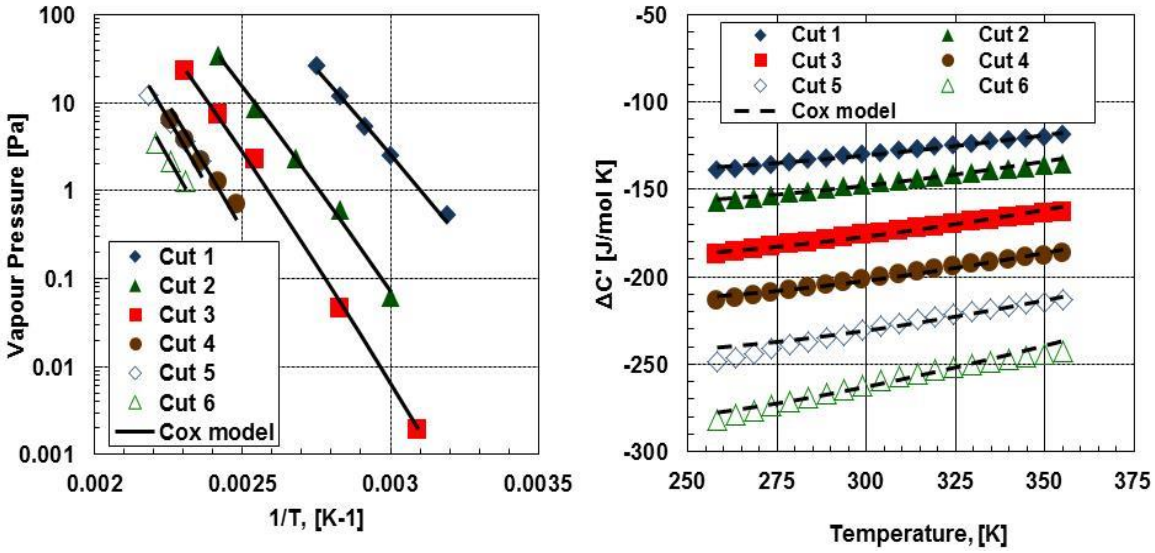

Figure 5.2. Simultaneous fitting of experimental vapor pressure (left) and heat capacity (right) of WC-B-B1 cuts using a three parameter Cox equation.

Table 5.8. Error analysis of the optimized correlation using the Cox equation.

Cut	Vapor Pressure		$\Delta C'^{exp}$	
	d **[Pa]**	***dr*** **%**	***d*** **[J mol^{-1} K^{-1}]**	***dr*** **%**
1	1.1	5.2	0.92	1.0
2	0.5	8.7	1.17	1.0
3	0.2	3.0	1.27	0.8
4	0.1	7.8	1.26	0.6
5	0.3	9.0	3.05	1.3
6	0.1	10.5	2.41	1.0

5.3.2 Interconverted Boiling Points Using Vapor Pressure and Heat Capacity Data

Figure 5.3 presents the measured boiling points at the apparatus pressure and the interconverted AET for WC_Bit_B1. The calculated final values for the optimization functions (*OF*) are presented in Table 5.9. The interconverted boiling points are within experimental error of the

spinning band distillation (SBD) data. The error analysis is presented below and the Gaussian extrapolation is discussed later.

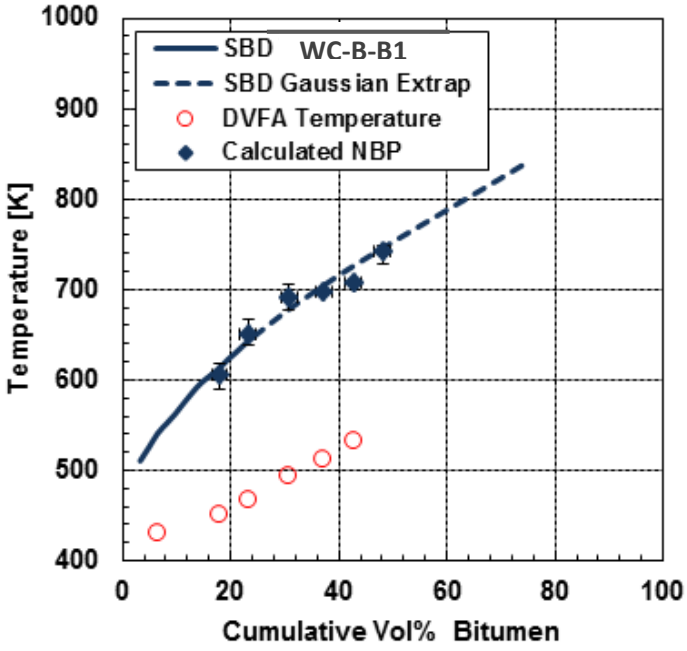

Figure 5.3. Interconverted boiling point from the simultaneous correlation of vapor pressure and heat capacity. The vertical error bars correspond to the maximum and minimum deviation obtained during the error analysis, and the horizontal error bars correspond to the experimental error estimated based on the repeatability of the distillation procedure.

Table 5.9. Sensitivity analysis results after simultaneous correlation of vapor pressure and heat capacity data for the WC-B-B1 sample.

Cut	Calculated TBP [K]	*OF*	Maximum ARD %	Minimum ARD %
1	606	0.003	3.7	4.7
2	651	0.004	4.4	3.6
3	690	0.044	3.6	3.2
4	698	0.009	0.09	0.01
5	707	0.013	0.06	0.00

6	743	0.004	1.1	3.3

A sensitivity analysis was performed to determine how the errors of each property involved in the interconversion method affect the predicted boiling point. The properties involved in the interconversion include vapor pressure, molecular weight, elemental analysis, liquid heat capacity, and gas ideal heat capacity. The value of each property was set to its highest or lowest value within its range of error and the interconverted boiling points were recalculated for all combinations of these values. The error bars in the inter-converted boiling point data, Figure 5.3, represent the maximum and minimum deviation found during the sensitivity analysis. Table 5.9 presents the absolute relative deviations for all the cuts of oil WC-B-B1. The maximum and minimum relative deviations in the AET were 2.2% and -2.5% (corresponding to +8 K and -9 K), respectively.

5.4 Correlation of Liquid Heat Capacity

Liquid heat capacity data were not available for all of the distillation cuts. Therefore, a correlation was required for the liquid heat capacity of heavy oil cuts before the interconversion method could be applied to all seven samples. The proposed correlation is developed in Chapter 7 and has the form:

$$C_p^{liq} = (B_1 + A_2 C_S) * \left[A_3 - A_4 SG + (A_5 - A_6 SG)\left(\frac{T}{1000} - A_7\right)\right] \quad (5.15)$$

where Cp^{liq} is in J g^{-1} K^{-1}, T is in K and Cs is defined in equation 5.16.

$$C_S = \exp\left(-\frac{2.124}{H/C}\right) \quad (5.16)$$

The constants are provided in Table 5.10. Figure 5.4 illustrates the errors obtained for the fitted liquid heat capacity data of the WC-B-B1 oil. Overall the average error for all the WC-B-B1 distillation cuts was less than 1.5% with a maximum deviation of 2.5%. Note, here the specific liquid heat capacity was fitted to the experimental data. However, for the interconversion method the molar liquid heat capacity was used. Therefore, the values obtained using Equation 5.15 were multiplied by the molecular weight.

Using Equation 5.15, the remaining liquid heat capacities of the other distillation cuts (where data was not available) were calculated. Measured and calculated liquid heat capacity data for all the distillation cuts are presented in Appendix D.

Table 5.10. Constants for liquid heat capacity correlation (Equation 5.15).

B_1	1.621
A_2	0.007
A_3	0.733
A_4	0.076
A_5	4.401
A_6	2.341
A_7	0.092

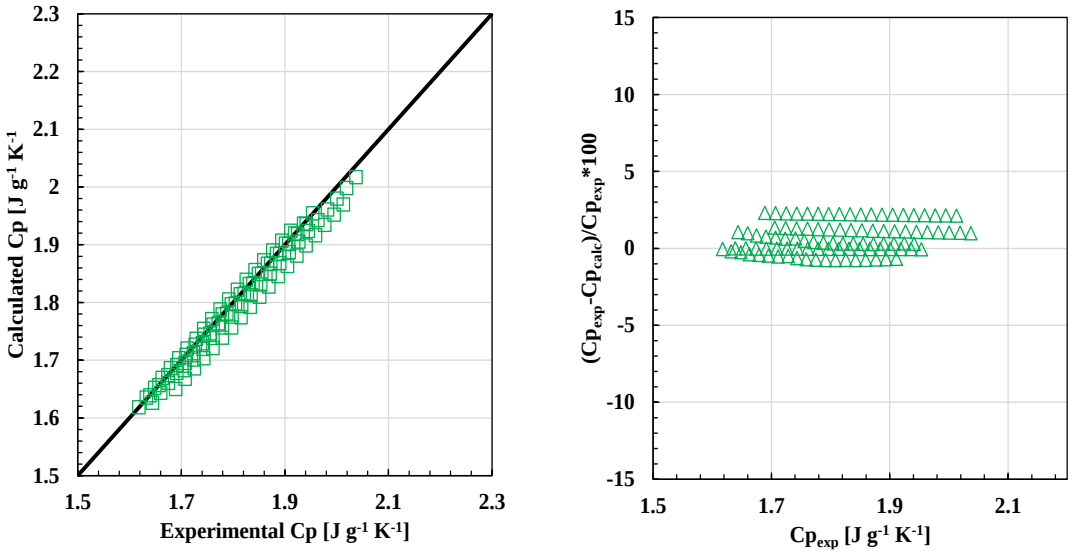

Figure 5.4. Dispersion (left) and relative error (right) plot for the liquid heat capacity of WC-B-B1 using Equation 5.15.

5.5 Interconversion Results for Seven Heavy Oil and Bitumen Samples

The results of the fitting of both vapor pressure and heat capacity for WC-B-B1 were presented in Figure 5.2 and are presented for the other oils in Figures 5.5 to 5.10. The Cox equation constants obtained for each cut along with the boiling temperature are presented in Appendix E. A summary of the average and relative absolute deviations obtained for the distillation cuts of the seven samples is provided in Table 5.12. As mentioned previously in Section 5.4, not all the distillation cuts had experimental liquid heat capacity and Equation 5.15 had to be used to estimate these values. Table 5.11 shows what data were measured and what data were predicted for each of the oils.

Table 5.11. Measured and calculated (Equation 5.15) liquid heat capacities of the distillation cuts of the oils used in this study

Sample	Measured	Calculated
WC-B-B1	1 to 6	
CO-B-A1	0 to 6	
MX-HO-A1	0 to 4	5 to 7
CO-B-B1	0 to 3	4 to 6
US-HO-A1		0 to 7
WC-B-D1		0 to7
RO-HO-A1		0 to 7

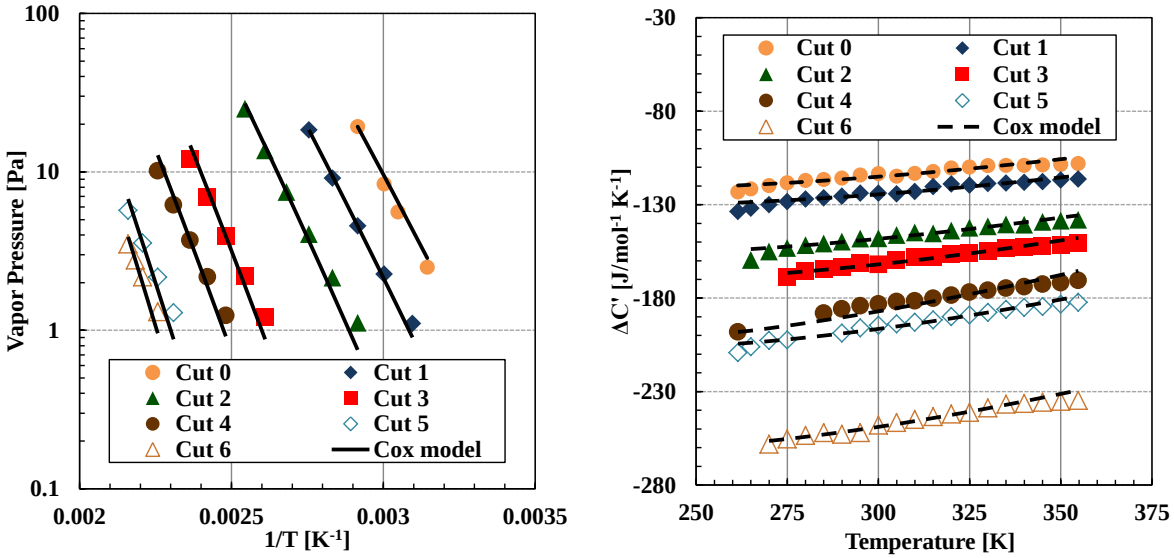

Figure 5.5. Simultaneous fitting of experimental vapor pressure (left) and heat capacity (right) of CO-B-A1using a three parameter Cox equation.

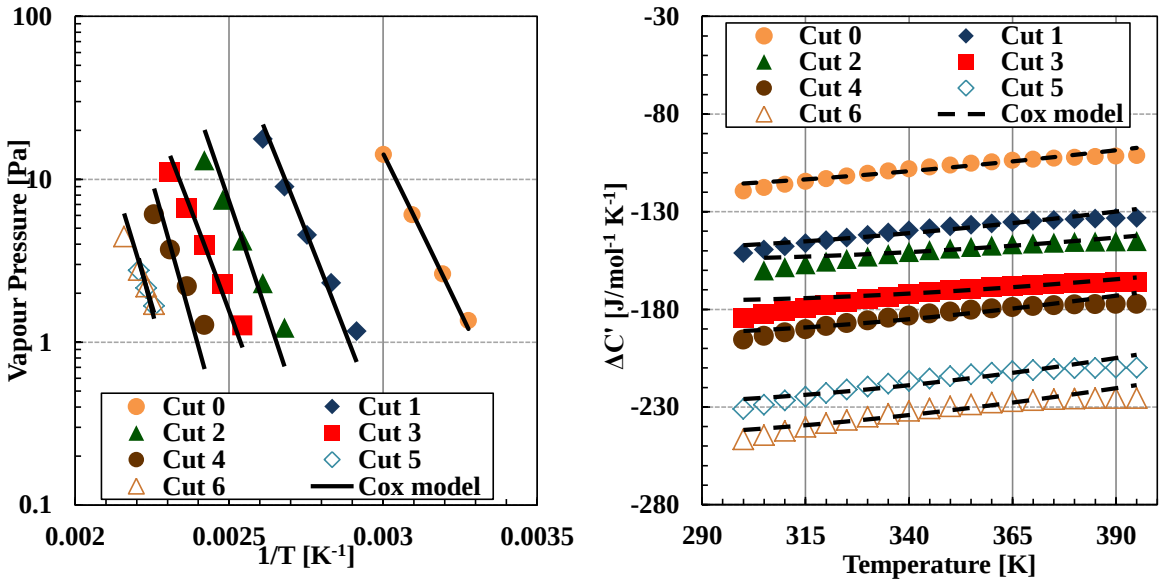

Figure 5.6. Simultaneous fitting of experimental vapor pressure and heat capacity using a three parameter Cox equation for MX-HO-A1.

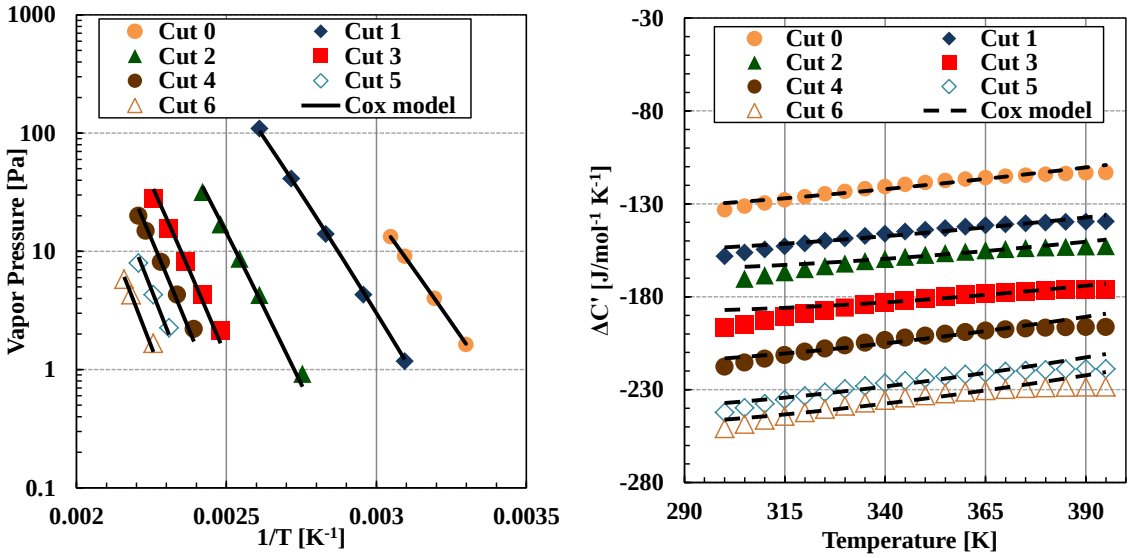

Figure 5.7. Simultaneous fitting of experimental vapor pressure and heat capacity using a three parameter Cox equation for CO-B-B1.

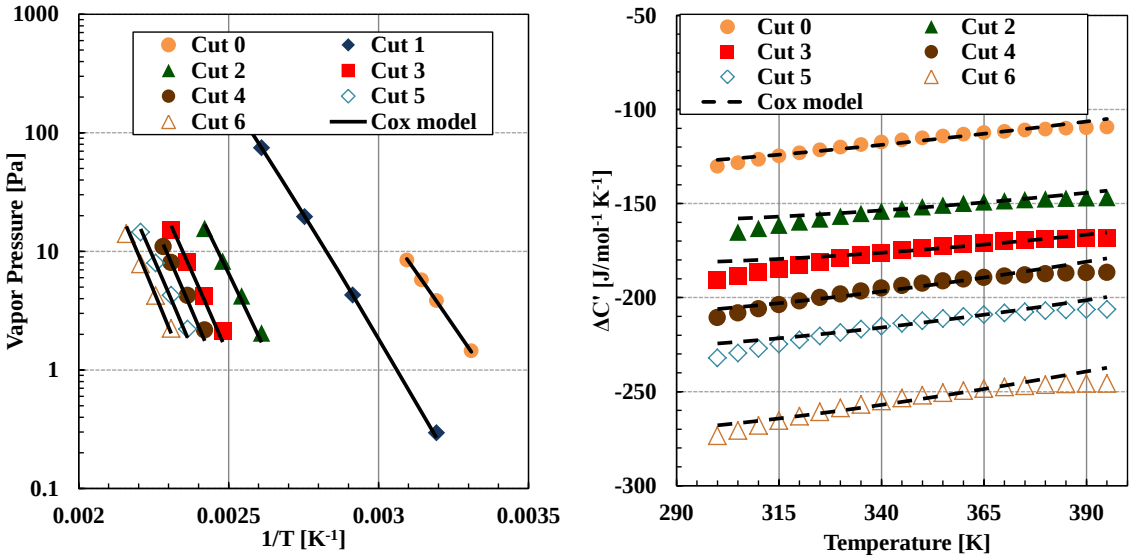

Figure 5.8. Simultaneous fitting of experimental vapor pressure and heat capacity using a three parameter Cox equation for US-HO-A1.

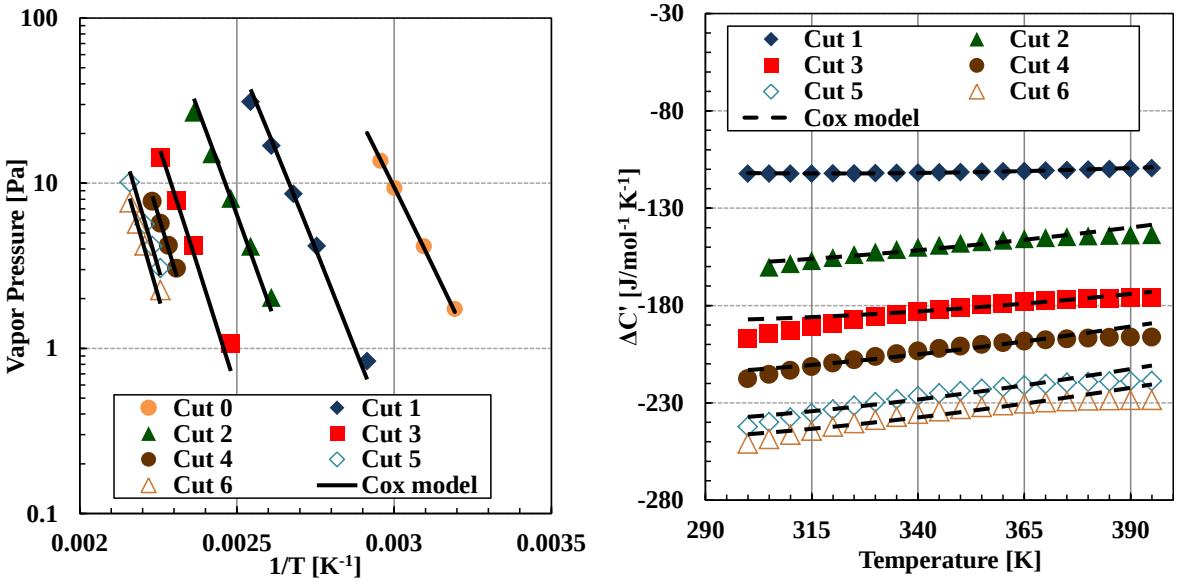

Figure 5.9. Simultaneous fitting of experimental vapor pressure and heat capacity using a three parameter Cox equation for WC-B-D1.

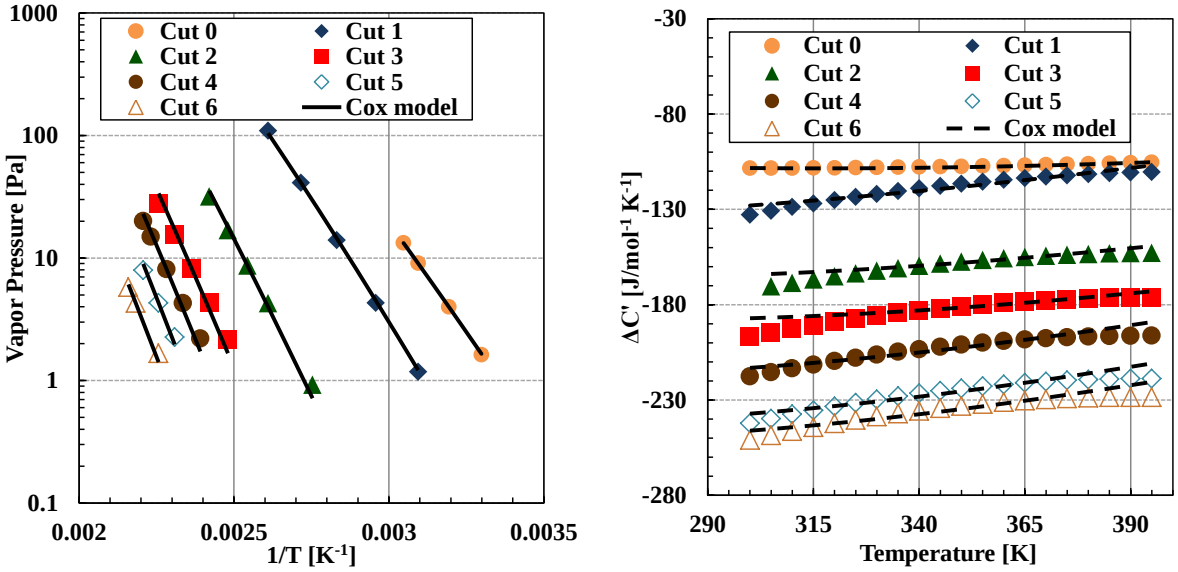

Figure 5.10. Simultaneous fitting of experimental vapor pressure and heat capacity using a three parameter Cox equation for RO-HO-A1.

Table 5.12. Error analysis of the optimized correlation using the Cox equation

Sample	Cut	Vapor Pressure		$\Delta C'^{exp}$	
		***dr* [%]**	***d* [Pa]**	***dr* [%]**	***d* [J mol^{-1} K^{-1}]**
WC-B-B1	1	5.2	1.1	1.0	0.9
	2	8.7	0.5	1.0	1.2
	3	3.0	0.2	0.8	1.3
	4	7.8	0.1	0.6	1.3
	5	9.0	0.3	1.3	3.0
	6	10.5	0.1	1.0	2.4
CO-B-A1	0	6.0	0.5	9.8	1.4
	1	1.3	0.1	9.5	1.7
	2	9.9	0.9	10.1	2.9
	3	12.4	1.2	12.8	5.3
	4	8.4	0.4	12.6	3.5
	5	12.3	0.5	9.4	2.9
	6	7.1	0.2	7.9	2.5
MX-HO-A1	0	5.8	0.1	10.6	1.6
	1	14.0	1.9	9.9	1.7
	2	15.4	0.9	6.0	0.8
	3	14.8	1.4	5.2	0.7
	4	10.8	0.3	9.5	2.1
	5	12.4	0.3	9.4	2.4
	6	8.5	0.2	8.9	2.3
	7	16.4	0.4	8.7	2.5
CO-B-B1	0	0.8	0.0	10.2	1.6
	1	3.2	0.2	9.7	1.8
	2	9.8	0.4	6.1	0.9
	3	12.0	0.8	5.4	0.8

	4	11.6	0.7	9.4	2.3
	5	9.0	0.5	9.3	2.6
	6	8.1	0.2	9.1	2.6
US-HO-A1	0	1.6	0.1	10.4	1.6
	1	4.1	0.1	4.4	0.3
	2	8.3	0.6	6.5	1.0
	3	10.5	0.7	5.6	0.8
	4	9.6	0.3	9.7	2.4
	5	4.9	0.5	9.8	3.0
	6	9.9	1.1	9.2	2.8
	7	6.4	0.3	9.1	2.8
WC-B-D1	0	2.7	0.3	11.3	1.9
	1	14.2	2.8	3.5	0.2
	2	12.3	2.4	10.7	2.2
	3	15.6	0.7	10.3	2.4
	4	6.0	0.3	9.4	2.2
	5	9.7	0.8	9.3	2.6
	6	9.4	0.3	9.9	3.0
	7	8.2	0.4	9.3	2.9
RO-HO-A1	0	0.2	0.0	11.5	2.0
	1	6.4	1.2	5.1	0.3
	2	10.6	2.1	10.9	2.2
	3	11.7	1.9	5.6	3.8
	4	8.3	0.5	11.0	2.9
	5	3.7	0.3	10.6	2.8
	6	5.0	0.3	10.3	3.0
	7	5.0	0.3	10.1	3.3

The interconverted boiling points were compared with spinning band distillation (SBD) data in Figure 5.3 for WC-B-B1 and for the other oils in Figures 5.11 to 5.12. In all cases, the inter-converted data for the light cuts which overlapped the SBD measurement range were in good agreement with the SBD data. Figure 5.13 shows the relative deviations (left) and the dispersion plots (right) of the boiling temperature from the Cox fitting versus the SBD measurement. The error bars on the dispersion plot in figures 5.13 to 5.16 correspond to the maximum deviation expected based on the sensitivity analysis performed on the simultaneous fitting of vapor pressure and heat capacity (Cox equation). The ARD was less than 1.3% which is lower than the expected error in the interconverted boiling temperatures. The maximum deviation was less than 3.6%. The dispersion plot shows that there is no systematic error in the inter-converted data. The spinning band distillation data are summarized in Appendix F.

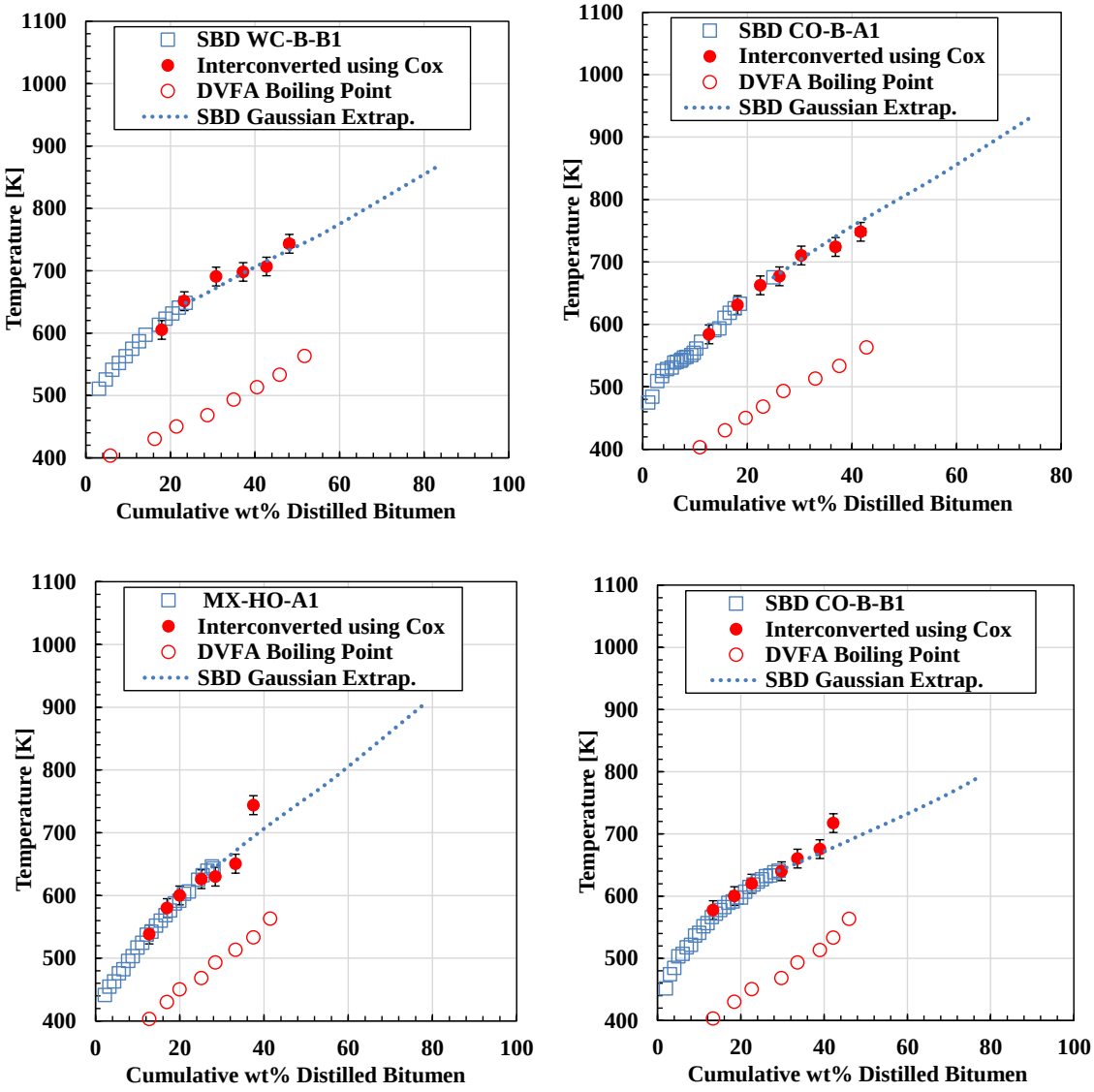

Figure 5.11. Comparison of the boiling temperatures obtained from the Cox equation with the experimental and extrapolated SBD data for the WC-B-B1, CO-B-A1, MX-HO-A1, and CO-B-B1 oils.

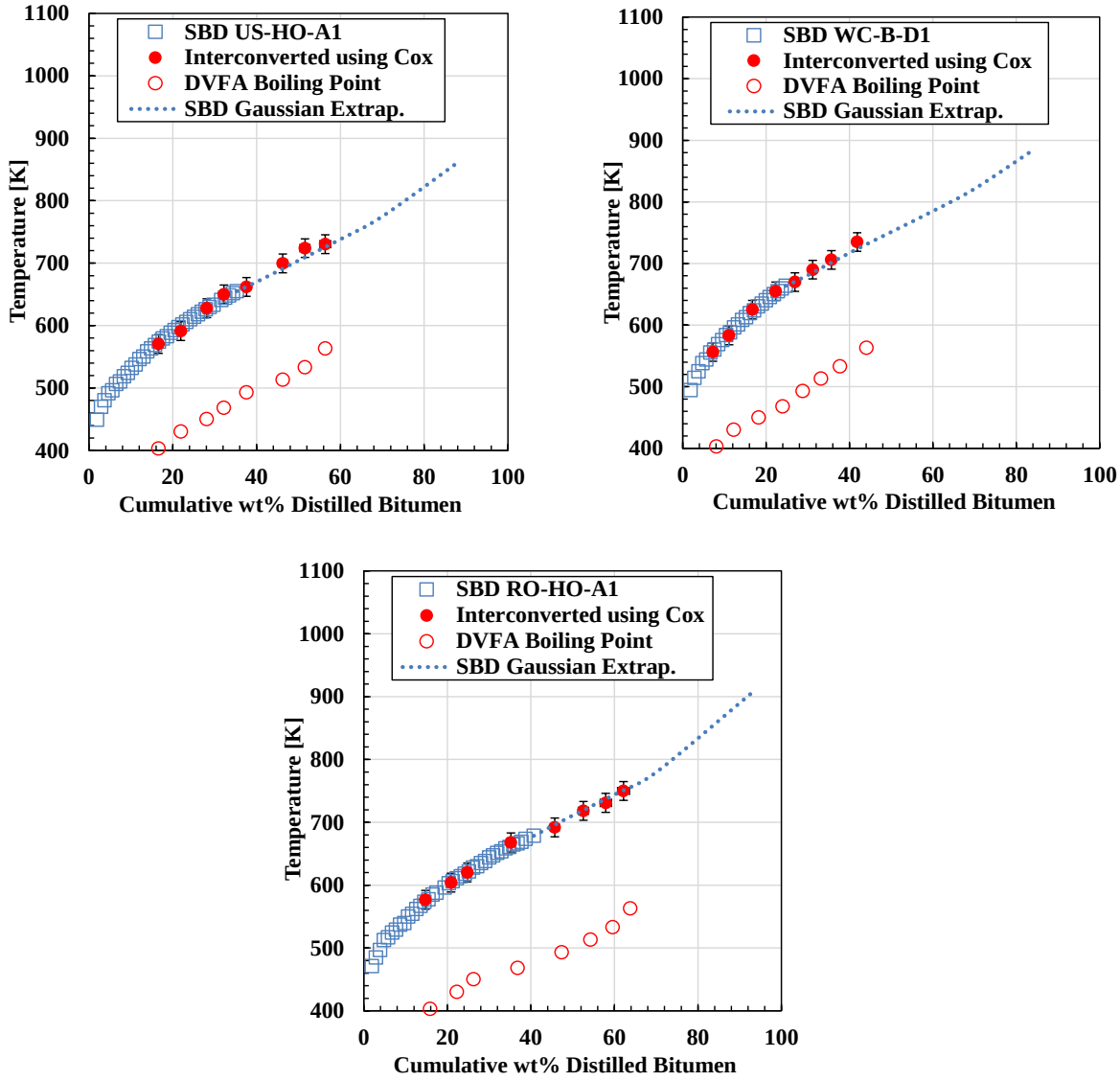

Figure 5.12. Comparison of the boiling temperatures obtained from the Cox equation with the experimental and extrapolated SBD data for the US-HO-A1, WC-B-D1, and RO-HO-A1 oils.

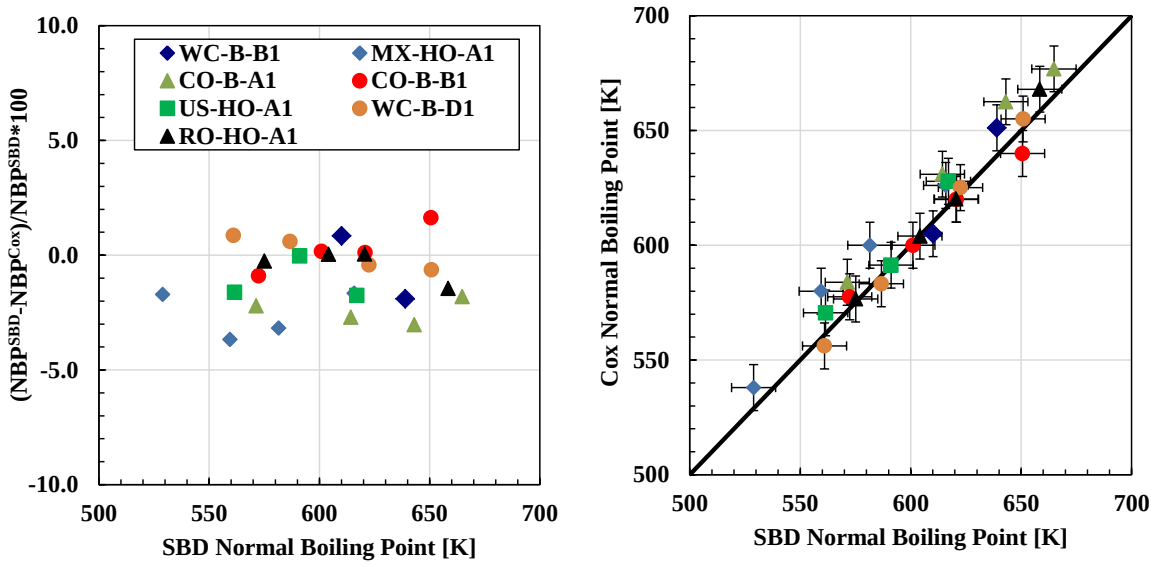

Figure 5.13. left) Relative deviation of the boiling temperature (distillable portion of the oil using SBD) obtained with SBD and Cox fitting and right) dispersion plot of the same data.

5.6 Gaussian Extrapolation Validation

As discussed previously, Castellanos *et al*. (2012) demonstrated that a Gaussian extrapolation of the distillation curve provides the best characterization of heavy oil maltenes in order to match heavy oil saturation pressure and phase behavior with an equation of state. However, no experimental data were available to validate this extrapolation. Therefore, the SBD distillation data for all seven oils were extrapolated and compared with the interconverted DVFA boiling point data, as was shown in Figures 5.3, 5.11 and 5.12.

To perform the extrapolation, the weight percent distilled was transformed iteratively into a cumulative standard normal distribution (mean μ=0; standard deviation σ^2=1) to obtain the corresponding Z value which is implicit in the following equation:

$$w = \frac{1}{2}\left[1 + \mathrm{erf}\left(\frac{Z}{\sqrt{2}}\right)\right] \tag{5.17}$$

where w is the cumulative weight fraction distilled of bitumen and Z is defined as $(x-\mu)^2/\sigma^2$. The measured boiling temperatures were linearly correlated with corresponding Z values. The remaining part of the curve was obtained by extrapolating the linear relation between boiling point

and Z values and converting the Z values back to weight fractions. Note that the extrapolation is only used for the maltenes; the asphaltene are characterized using a different distribution that accounts for self-association.

Figure 5.14 shows the deviation of the extrapolated SBD boiling points from the interconverted DFVA boiling points. Table 5.13 summarizes the average relative deviations and maximum deviations for each oil. Note that for sample MX-HO-A1 there are two possible outliers corresponding to the heaviest cuts. Vapor pressure errors could have significant impact on these values and, since the other cuts follow the Gaussian distribution, it is possible that the two AET values are outliers. The total average relative deviation for all the oils was less than 1.6% and the maximum deviation, excluding the outliers, was 3.4%. In general, the maximum deviations corresponded to the boiling temperature of the heaviest cut. Note, due to the extremely low volatility of the last distillation cuts, vapor pressure and liquid heat capacity values are subject to systematic errors introduced by leaks in the system that may have an order of magnitude similar to the measured property.

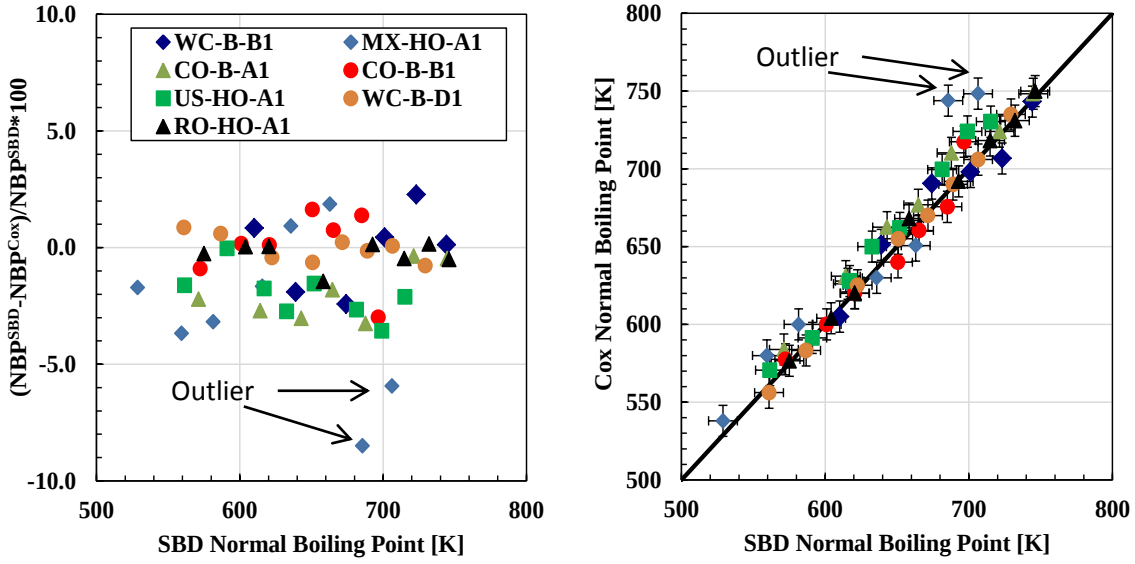

Figure 5.14. Deviation of the boiling points from the Gaussian extrapolation of SBD data versus the interconverted DVFA data: left) relative error versus boiling point; right) dispersion plot.

Table 5.13 ARD and maximum ARD obtained for the comparison between Gaussian extrapolation of SBD data and AET using Cox equation

Sample	ARD [%]	MARD [%]
WC-B-B1	1.3	2.4
CO-B-A1	2.0	3.3
MX-HO-A1	3.4	8.5
CO-B-B1	1.1	3.0
US-HO-A1	2.0	3.6
WC-B-D1	0.5	0.9
RO-HO-A1	0.4	1.5

5.7 Simplified Interconversion Method for DVFA

The data requirements for the above interconversion method are numerous and it is useful to develop a simpler interconversion method. Most of the interconversion methods available in the literature require the pressure at which distillation is performed because the correlations are based on vapor pressure (Maxwell and Bonnell, 1955; Myers and Fenske, 1955; Riazi, 1979; Van Nes and Van Western, 1951). Due to temperature constraints and vacuum detection limits, the DVFA does not have a pressure gauge that allows data recording. Therefore, a different approach was required with the following two main criteria: 1) minimum amount of measurements from distillation cuts, and; 2) no pressure dependent equation.

The first input parameter is the measured boiling point data; that is, the end cut temperature of each cut at the apparatus pressure. A second parameter is required and density was selected because it is one of the most reliable and easy to measure properties that can be obtained for each distillation cut. Finally, the bulk density of the sample distilled (in this case the maltenes) was used to account for differences between different oils. The following interconversion equation, Equation 5.15, was found to match the interconversion method based on vapor pressure and heat capacity data (rigorous method):

$$AET = \frac{{SG_i}^{1.6068}(T_{bi} \cdot SG_{Bulk})^{0.09661} + 260.77}{0.9559\ {SG_{Bulk}}^{0.379}} \tag{5.18}$$

where SG_i is the density of the cut, SG_{Bulk} is the density of the sample distilled using the DVFA and T_{bi} is the end cut temperature of each cut. Table 5.14 provides the absolute relative deviation as well as maximum deviations of the interconverted boiling points from the simple method versus the rigorous method. The relative error and dispersion plots are shown in Figure 5.15. The deviations for each cut are reported in Appendix F. Overall, the average ARD was less than 1.2% with a maximum deviation of 3.0%. In this case since the interconverted data using rigorous method matched the data from SBD assay and its Gaussian extrapolation, the AET points are equivalent to TBP values.

The correlation is very sensitive to specific gravity of the sample distilled, therefore it is recommended to use Equation 5.18 for samples within the specific gravity range of the samples used in this project; that is, from 0.95 to 1.00. Additional data on less dense oils would be required to validate the method beyond this range.

Table 5.14. ARD and maximum ARD obtained for the proposed simplified interconversion method

Sample	ARD [%]	MARD [%]
WC-B-B1	0.6	2.1
CO-B-A1	1.9	3.0
MX-HO-A1	1.6	2.5
CO-B-B1	1.2	2.3
US-HO-A1	1.0	2.3
WC-B-D1	0.6	1.1
RO-HO-A1	1.5	2.6

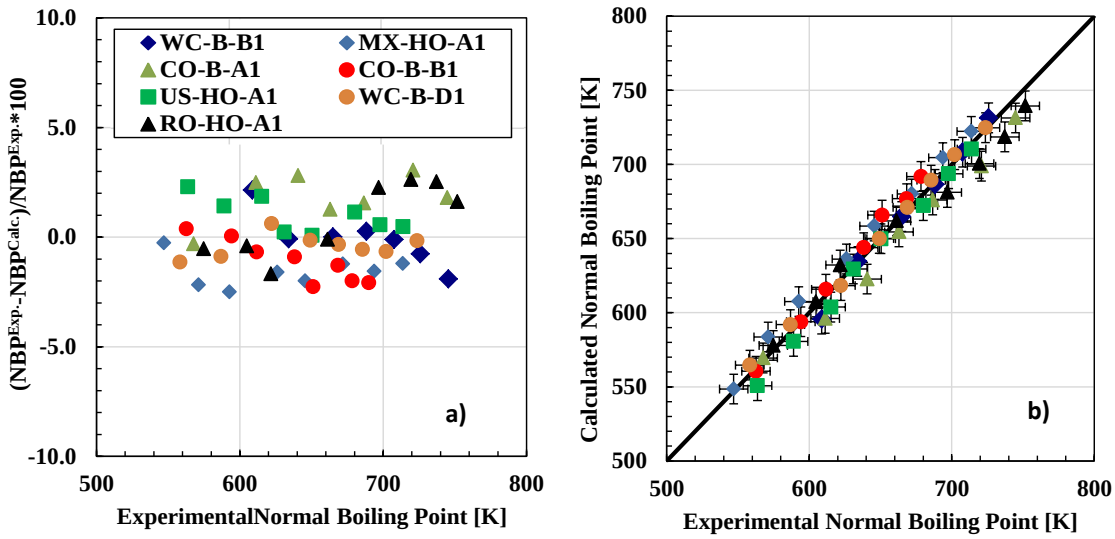

Figure 5.15. Deviation of the DFVA boiling points from simplified interconversion method versus the rigorous method: left) relative error versus boiling point; right) dispersion plot.

5.8 Prediction of Complete Distillation Curves

Distillation data for heavy oils are always incomplete. With SBD, only 25 to 35 wt% of the oil is distilled, Figures 5.11 and 5.12. Even with deep vacuum there is a limit to the amount of sample that can be distilled. Gaussian extrapolation is one approach that can be used to complete the distillation curve. An alternative is to correlate the boiling point at any point within the maltenes to the cumulative weight percent distilled, instead of the end cut temperature. The specific gravity is again used to distinguish between different oils. The following correlation was found to fit the interconverted DVFA distillation data:

$$AET = B * (487.3 + 2.54w_i){w_i}^{0.0503}{SG_{Bulk}}^{1.028} \quad (5.19)$$

$$B = \exp[b_1{SG_{Bulk}}^{b_2}] \quad (5.20)$$

$$b_1 = (7.0973w_i^2 - 81.41w_i + 109.65) \quad (5.21)$$

$$b_2 = (-0.0409w_i^2 + 7.770w_i + 902.48) \quad (5.22)$$

where w_i is the bitumen cumulative weight percent and SG_{Bulk} is the density of the sample distilled (deasphalted oil).

Figure 5.16 presents the relative error and dispersion plot for the correlated versus the measured boiling points for the seven oils from this study. Table 5.15 summarizes the deviation for each oil. The average deviation for all the oils was within 1.2% and the maximum deviation was 4.0%. Note, the residue is included in the error analysis since its weight percent is known. Its 'experimental' TBP was obtained from the Gaussian extrapolation of the SBD data.

Note that sample MX-HO-A1 has the highest deviation. It is possible that, due to its highly paraffinic character, the slope of the curve was distinctly steeper compared with the rest of the oils and possibly an additional variable is required to account for this effect. However, since the fitting gave an error below the experimental error, the correlation was not further modified.

Table 5.15. ARD and MARD for the proposed correlation to obtain complete distillation curves for the seven oils in this study.

Sample	ARD [%]	MARD [%]
WC-B-B1	0.6	1.1
CO-B-A1	0.4	1.7
MX-HO-A1	1.6	7.0
CO-B-B1	0.8	1.8
US-HO-A1	0.7	1.3
WC-B-D1	1.2	2.1
RO-HO-A1	0.5	0.8

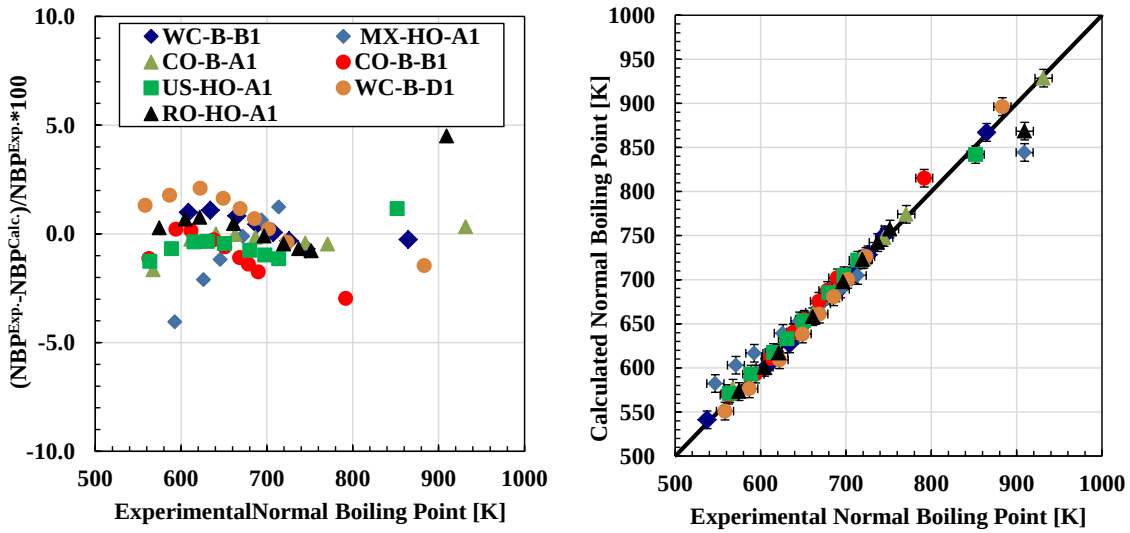

Figure 5.16. Deviation of the correlated versus the measured boiling points for the oils in this study: left) relative error versus boiling point; right) dispersion plot.

The proposed correlation was then tested on an independent dataset extracted from an API technical report (Sturm and Shay, 2000). The dataset included the following three oils which covered a significant specific gravity and aromaticity range: Alaska North Slope (ANS) crude (SG=0.8911), Utah Altamont (ALT) crude (very paraffinic; SG=0.8179), and San Joaquin Valley (SJV) crude (very aromatic; SG=0.9772). Table 5.16 summarizes the deviations of the correlated boiling points for test data set. The test data set had a total average deviation of less than 5.5% and maximum deviation of 14.3%.

It is evident that for the most aromatic oils (Figure 5.17), the correlation was able to predict the TBP with good accuracy. However, for the paraffinic sample, the performance was not as good. This is attributed to the slightly different slope that distillation curves of light oils have compared with those of heavy, aromatic oils. Therefore, the correlation is recommended for samples with SG higher than 0.85; for lighter samples, alternative methods like Riazi method (Riazi, 2005) can be used.

Table 5.16. Deviation between experimental TBP and calculated TBP using Equations 5.19 through 5.22.

Sample	Specific Gravity	ARD [%]	MARD [%]
ANS	0.8911	4.3	8.7
SJV	0.9772	3.3	7.3
ALT	0.8179	9.4	14.4

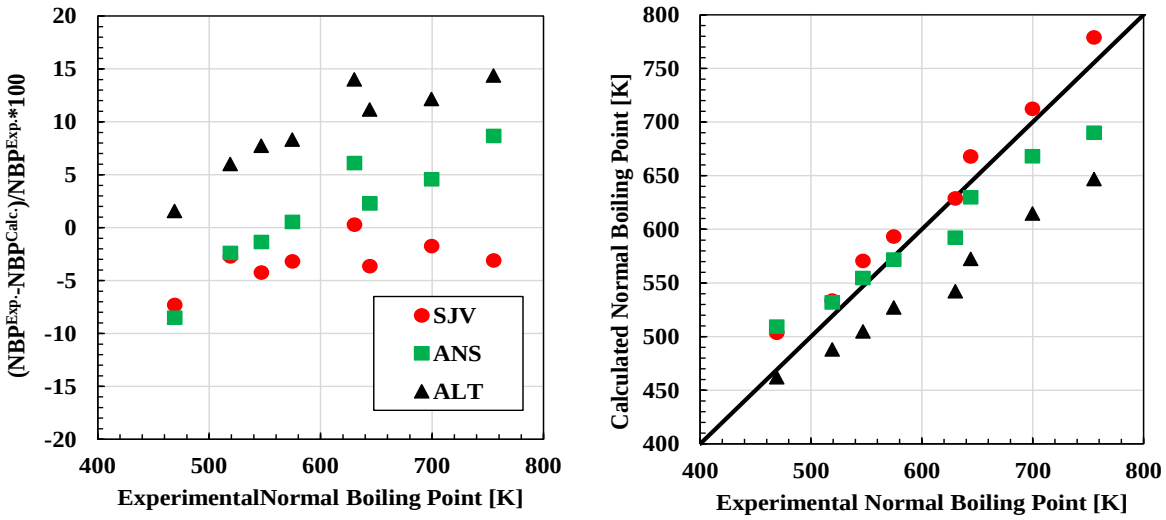

Figure 5.17. Deviation of the correlated versus the measured boiling points for the oils in the test dataset: left) relative error versus boiling point; right) dispersion plot.

CHAPTER SIX: PHYSICAL PROPERTY DISTRIBUTIONS AND THEIR CORRELATION

In this chapter, the physical properties collected for 63 cuts from different oil samples are presented. It is shown that most of the correlations existing in the literature cannot correctly predict the properties of the heavy cuts. New correlations are proposed that can be used when experimental data are not available and predictions must be made. The most commonly employed correlating properties are normal boiling point (NBP), molecular weight (MW), and specific gravity (SG), and their correlations to each other are examined in first three sections of this chapter. Finally, the correlations between specific gravity to the atomic H/C ratio and between specific gravity and the refractive index are provided.

6.1 Normal Boiling Point

As was discussed in Chapter 2, the normal boiling point is usually correlated to MW and SG. For pure paraffins, NBP increases monotonically with MW, Figure 6.1. Naphthenes follow the same trend and aromatics and complex polyaromatic hydrocarbons (PAH) deviate to a higher NBP. Riazi proposed a set of generalized correlations for the NBP (and other properties) of different chemical families using only MW values as an input (Riazi, 2005). However, to correlate NBP when all compound classes are present in a mixture (as is the case for petroleum cuts), a second parameter is required. Typically, this additional correlating variable is SG since it captures the changes that arise when different homologous series are present in a mixture.

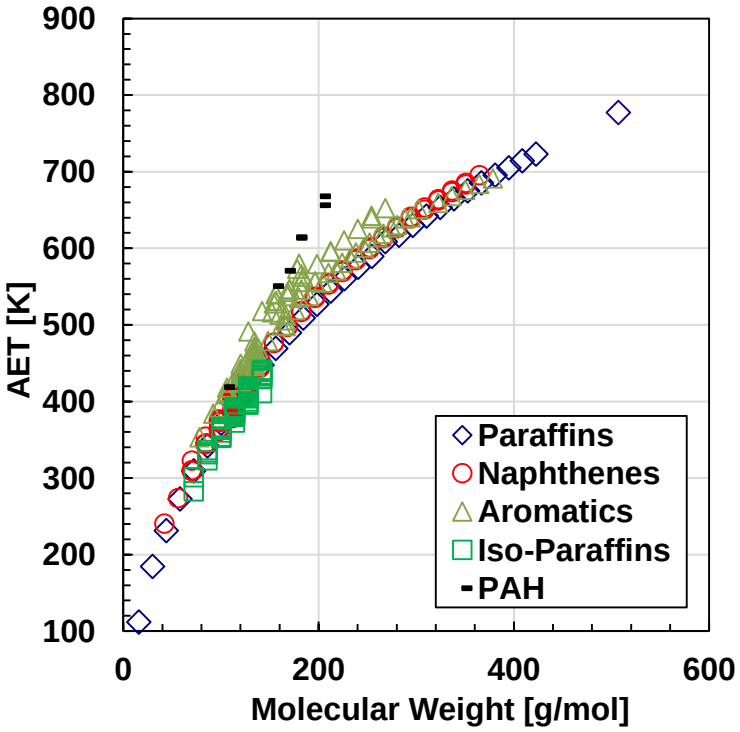

Figure 6.1. Relationship between MW and NBP for different compound classes.

The correlations available in the literature for NBP were given in Table 2.2 and include the: Riazi Daubert (RD), API, Soreide, Nji *et al*., Twu, Rao Bardon (RB), original Riazi Daubert (oldRD), and Lee Kesler (LK) correlations. The correlations were compared to the experimental NBP of the heavy oil cuts using their measured specific gravity and molecular weight as inputs. Measured data are reported in Appendix B. As an example, Figure 6.2 shows the measured and correlated NBP versus MW for the WC-B-B1 distillation cuts as an example. Figure 6.3 presents the deviations for all of the above correlations from the measured TBP for all the oils. The average and maximum absolute and relative deviations and the bias obtained for each correlation are reported in Table 6.1. Detailed results for each sample are summarized in Appendix G.

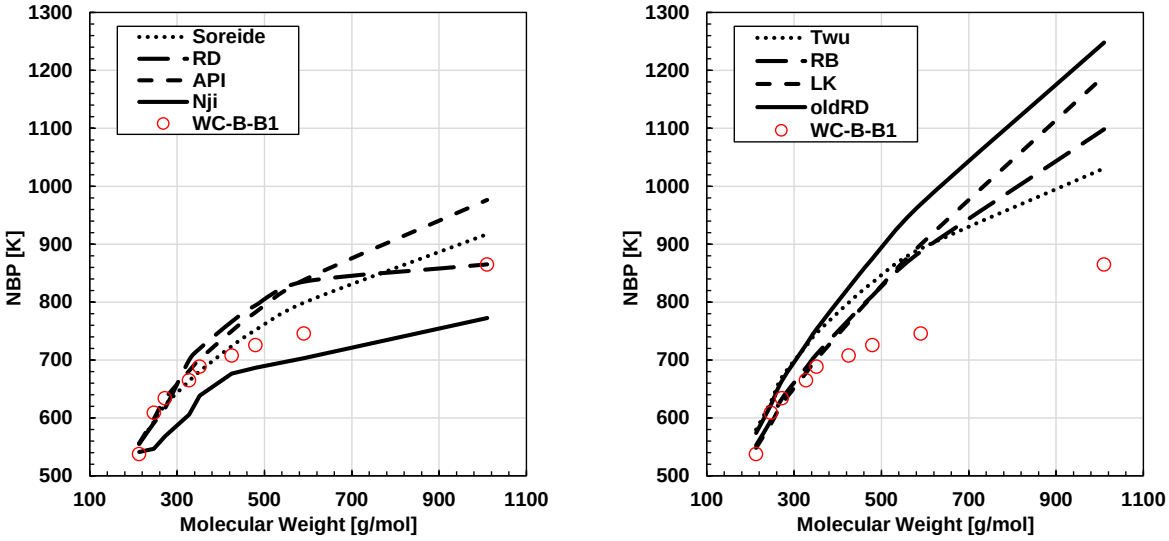

Figure 6.2. Measured and correlated NBP versus MW for the WC-B-B1 distillation cuts: left) Soreide, Riazi Daubert (RD), API, and Nji *et al.* correlations; right) Twu, Rao Bardon (RB), Lee Kesler (LK), and original Riazi Daubert (oldRD) correlations.

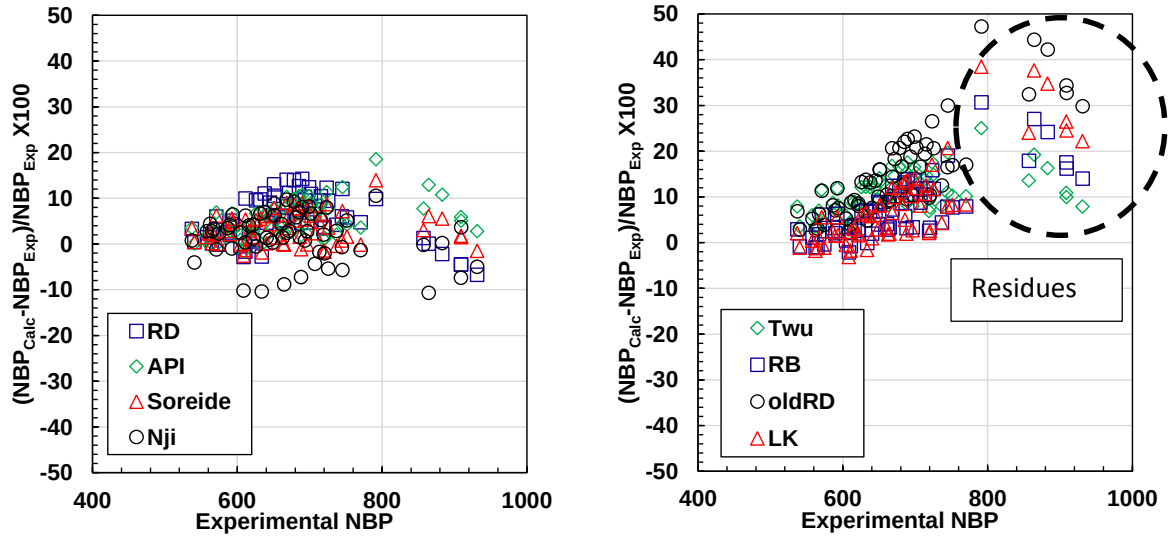

Figure 6.3. Relative error obtained for predicted NBP using experimental density and molecular weight values: left) Riazi Daubert (RD), API, Soreide, and Nji et al. correlations; right) Twu, Rao Bardon (RB), original Riazi Daubert (oldRD), Lee Kesler (LK).

Table 6.1 Average absolute and relative deviations, maximum absolute and relative deviations, and bias for NBP obtained using correlations from literature for the development dataset.

Correlation	AAD [K]	ARD [%]	MAAD [K]	MARD [%]	Bias [%]
Soreide	25	3.7	110	14	3.3
LK	116	8.5	586	39	8.1
RD	43	6.2	98	14	5.4
API	68	5.3	264	19	5.2
oldRD	202	15.4	690	47	15.4
RB	57	7.8	243	31	7.6
Twu	76	10.9	198	25	10.9
Nji	30	4.4	92	11	1.6

The lowest relative deviation, 3.7%, was observed for the Soreide (1989) correlation. The correlation with highest deviation, 15.4%, was the oldRD, the initial version of the correlation proposed by Riazi (2005). This large deviation is not surprising since the oldRD correlation was expected to fail since the heaviest hydrocarbon used to develop the correlation corresponded to carbon numbers up to C_{25}. Interestingly, the Lee-Kesler (1976) correlation, which is one of the most commonly used correlations in simulation software, failed to predict the NBP of high molecular weight distillation cuts and reports an average deviation of 8.5%.

All of the correlations, except for one oil (WC-B-B1) using the Nji *et al.* (2010) equation, have a positive bias of the same magnitude as the relative deviation indicating that the majority of the deviations over-predict the NBP. Also, all of the correlations have an increasing deviation from the low to the high boiling cuts (excluding the residue). These trends are illustrated in the dispersion plot for the best performing correlation (Soreide) in Figure 6.4. These correlations were developed from datasets that included light to medium oils and pure paraffinic components. For example, the development dataset for the Soreide correlation contained mostly North Sea Oils and gas condensates (Soreide, 1989) with API values no lower than 25. These correlations do not account for the higher aromaticity with heteroatom content of the heavier cuts. Since the

correlations are being used outside the range where they accurately predict the NBP, the higher deviations for heavy cuts and residue are to be expected. Therefore, it is proposed to develop a new correlation to address the consistent deviation observed for the higher boiling cuts.

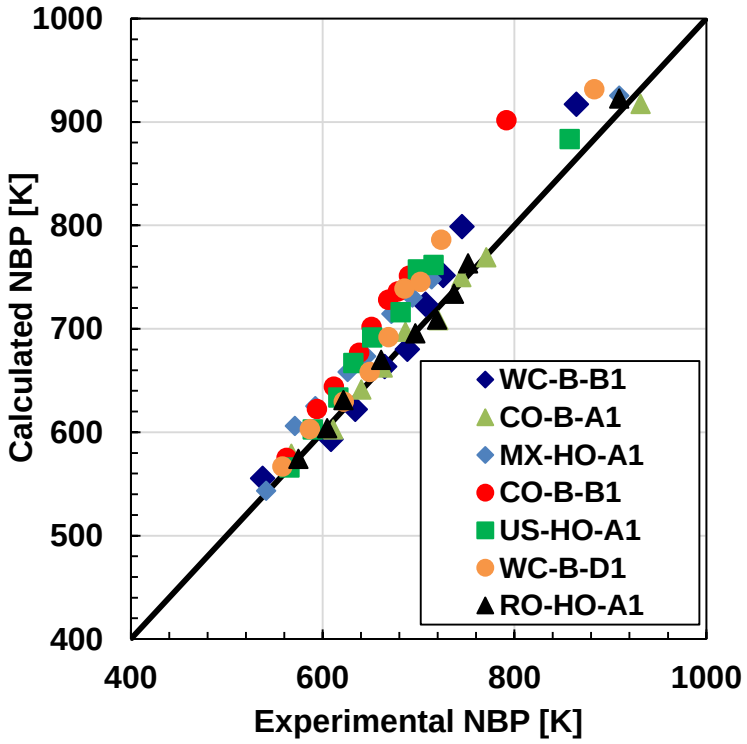

Figure 6.4. NBP predictions obtained from Soreide's correlation using experimental SG and MW values.

Before proposing a new correlation, the best performing (Soreide) and most commonly used (Lee-Kesler) correlations were evaluated to determine what features made one correlation better than the other. Figure 6.5 shows the family of NBP curves that are obtained for several values of specific gravity and molecular weight. The Lee-Kesler correlation does not have an asymptotic NBP at infinite MW causing the observed over-prediction in NBP values for higher MW cuts, Figure 6.3B. The effect of specific gravity in this correlation is smaller than the effect of the MW, and it is used mainly to produce a family of curves with similar shape that converge to the specific gravity and molecular weight of a low boiling point paraffin.

On the other hand, Soreide's correlation produces a family of curves that have a maximum asymptotic NBP for an infinite MW and SG, Equation 2.5 and Figure 6.3 (right). Here the effect of density is again smaller than the effect of MW. However, at MW values lower than 280 g/mol, the predicted NBP increases with increasing density while above 280 g/mol, the trend reverses. This reversal likely reflects the change in aromaticity from lower MW to higher MW cuts but, of more relevance here, it mathematically forces the predicted NBP values to approach an asymptote, avoiding unrealistic NBP predictions for heavy cuts.

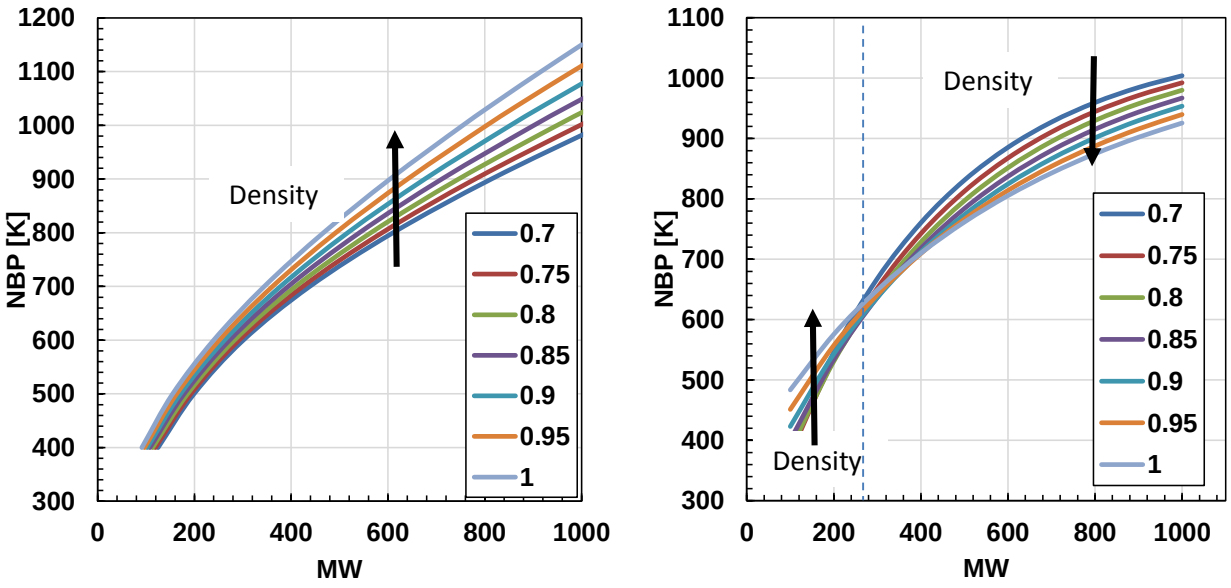

Figure 6.5. NBP curves obtained using left) the Lee-Kesler and right) Soreide correlations.

It was proposed to keep the structure of the Soreide correlation and retune it for heavy components using the experimental data collected in this study. To make the modified Soreide correlation applicable to a wide range of distillation cuts, the proposed correlation was fitted to a development dataset which included the NBP of 300 pure components as well as the 63 heavy distillation cuts. The pure components included paraffins, isoparaffins, naphthenes, aromatics and polycondensed aromatic structures. The final correlation is given by:

$$T_b = 1805 - 1131 * MW^{-0.049} * SG^{1.5258} * D/1.8$$

$$D = \exp(-0.005 * MW - 2.675 * SG + 0.003 * MW * SG) \quad (6.1)$$

where T_b is the normal boiling temperature in K. Equation 6.1 was based on boiling point data in the temperature range from 300 to 900 K. The shape of the equation allows prediction of NBP values not higher than 1300 K for high molecular weight and specific gravity values outside the established range.

Figure 6.6 presents the dispersion plots of the NBP predictions for the distillation cuts from the original and modified versions of the Soreide correlation. The NBP error bars were calculated from the propagation of the experimental errors for SG and MW. MW errors were the major contributor to the errors in the predictions. Figure 6.7 is a dispersion plot for the NBP of pure components ranging from paraffins to polycondensed aromatic structures. The average absolute and relative deviations and bias for the original and modified Soreide correlations are summarized in Table 6.2 and the maximum deviations in Table 6.3. The new correlation improved the average and maximum deviations for both pure hydrocarbons and the heavy distillation cuts, and significantly reduced the bias (from 3.1 to 1.6%).

The original version of the Soreide correlation is an excellent generally applicable predictive correlation for the NBP of distillation cuts. However, as was discussed in Chapter 2, small errors in the predicted NBP can produce significant errors in phase behavior predictions. Therefore, the improvements in the NBP predictions using the new correlation are expected to help provide more accurate phase behavior predictions for heavy oil and bitumen samples.

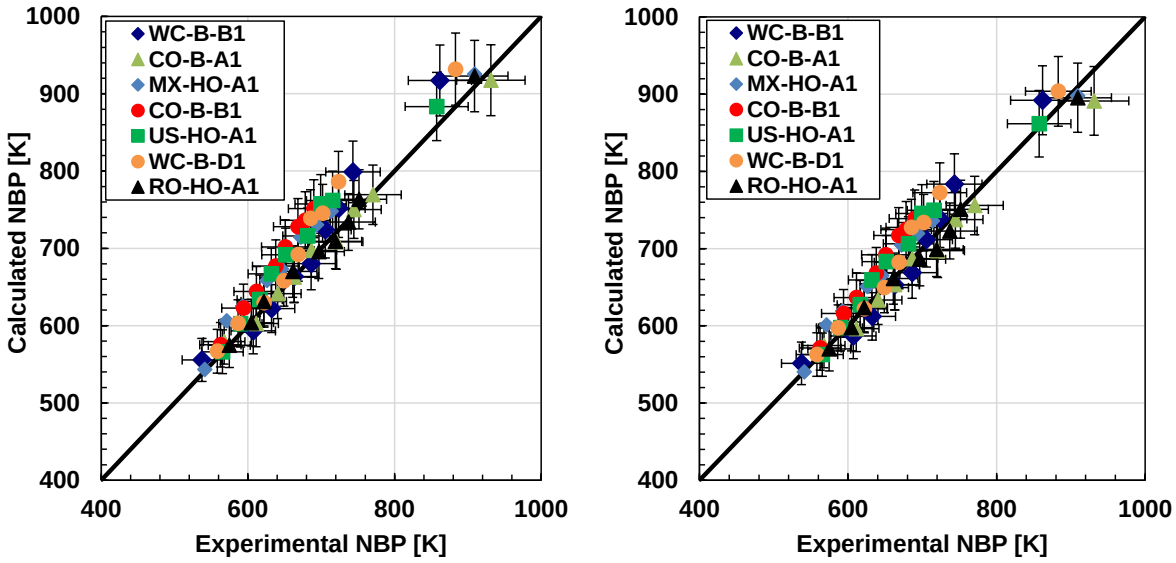

Figure 6.6. Dispersion plots for the NBP of the development dataset distillation cuts determined from: left) the original Soreide correlation; right) the modified Soreide correlation.

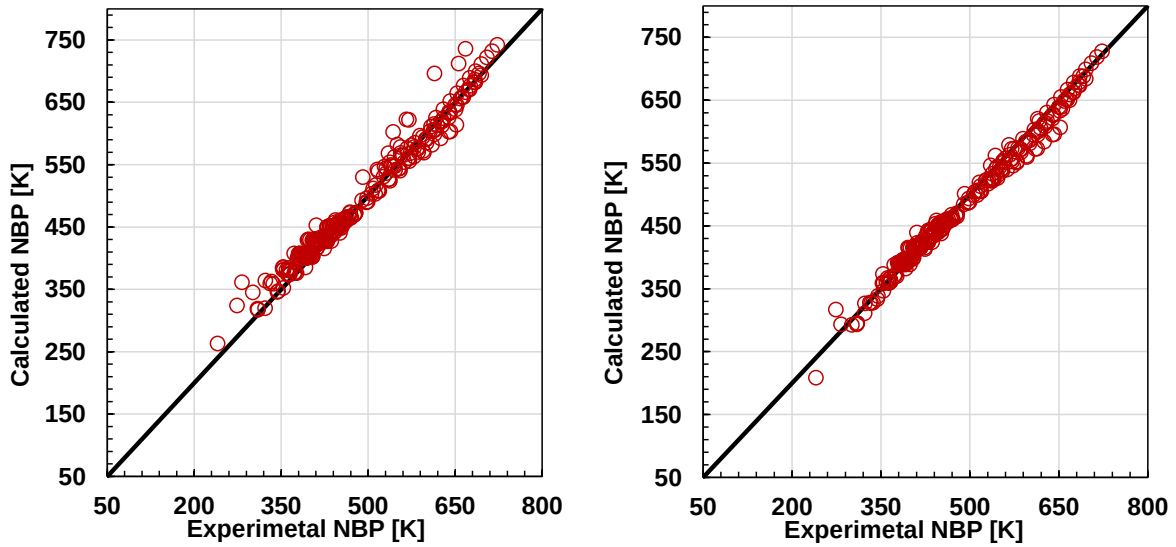

Figure 6.7. Dispersion plots for the NBP of the development dataset pure hydrocarbons determined from: left) the original Soreide correlation; right) the modified Soreide correlation.

Table 6.2. Average absolute and relative deviations and bias from the original and modified Soreide correlation for NBP for the development dataset.

Oil Sample	Original Soreide			Modified Soreide		
	AAD [K]	ARD [%]	Bias [%]	AAD [K]	ARD [%]	Bias [%]
WC-B-B1	23	3.2	2.1	19	2.8	0.8
CO-B-A1	7.2	1.0	-0.02	14	1.9	-1.2
MX-HO-A1	29	4.4	4.4	22	3.3	3.5
CO-B-B1	43	3.6	3.3	20	2.7	1.7
US-HO-A1	30	4.3	3.9	22	2.9	2.2
WC-B-D1	30	4.5	4.5	20	2.6	3.0
RO-HO-A1	6.6	4.2	3.7	21	2.9	2.4
Pure Components	13	2.9	2.0	8.9	1.9	0.02
Overall	**15**	**3.0**	**2.2**	**11**	**2.0**	**0.4**

Table 6.3. Maximum absolute and relative deviations from the original and modified Soreide correlation for NBP of the development dataset.

Oil Sample	Original Soreide		Modified Soreide	
	MAAD [K]	MARD [%]	MAAD [K]	MARD [%]
WC-B-B1	56	7.5	40	5.4
CO-B-A1	14	2.1	40	4.3
MX-HO-A1	43	6.4	33	5.3
CO-B-B1	61	9.0	49	7.3
US-HO-A1	58	8.3	46	6.6
WC-B-D1	63	8.7	49	6.8
RO-HO-A1	14	1.6	21	2.9
Pure Components	82	28	47	16
Overall	**82**	**28**	**49**	**16**

The original and modified Soreide correlations were evaluated against an independent test dataset obtained from the literature (Sturm and Shay, 2000; Smith, 2007; Fang *et al.*, 2003) and provided in Tables 6.5 to 6.9. The dataset included 100 cuts encompassing a wide range of aromaticity and paraffinicity dictated by the bulk H/C ratios values. Note, no experimental error was presented by the authors. Fang *et al.* (2003) provided data for three oils but combined the data into a single table without distinguishing between the oils, hence the specific gravity of each bulk sample is not reported for these oils.

Table 6.4. Molecular weight, specific gravity, H/C atomic ratio, and normal boiling point of ANS oil with bulk SG=0.89 and H/C=1.7 (Sturm and Shay, 2000).

Molecular Weight [g/mol]	Specific Gravity	H/C Ratio	Normal Boiling Point [K]
152	0.8095	1.90	469.2
245	0.8456	1.84	519.2
248	0.8633	1.79	547.0
263	0.8696	1.81	574.8
271	0.8867	1.77	630.3
434	0.9021	1.75	644.2
442	0.9296	1.72	699.8
518	0.9437	1.66	755.3
573	0.9628	1.61	810.9
683	0.9678	1.58	866.4
850	0.9830	1.55	922.0

Table 6.5. Molecular weight, specific gravity, H/C atomic ratio, and normal boiling point of ALT oil with bulk SG=0.81and H/C=1.9 (Sturm and Shay, 2000).

Molecular Weight [g/mol]	Specific Gravity	H/C Ratio	Normal Boiling Point [K]
148	0.7649	2.00	469.3
225	0.7853	2.08	519.3
231	0.7945	2.07	547.0
264	0.8003	2.08	574.8
289	0.8044	2.06	630.4
338	0.8203	1.95	644.3
401	0.8338	2.05	699.8
457	0.8413	2.07	755.4
551	0.8577	2.01	810.9
750	0.8741	2.03	866.5
1018	0.8848		922.0

Table 6.6. Molecular weight, specific gravity, H/C atomic ratio, and normal boiling point of SJV oil with bulk SG=0.91and H/C=1.5 (Sturm and Shay, 2000).

Molecular Weight [g/mol]	Specific Gravity	H/C Ratio	Normal Boiling Point [K]
171	0.8532	1.86	469.2
207	0.8745	1.80	519.2
228	0.8914	1.76	547.0
244	0.9124	1.70	574.8
272	0.9317	1.64	630.3
283	0.9483	1.58	644.2
335	0.9604	1.58	699.8
432	0.9872	1.50	755.3

540	1.0034	1.47	810.9
640	1.015	1.45	866.4
718	1.0274	1.44	922.0

Table 6.7. Molecular weight, specific gravity, H/C atomic ratio, and normal boiling point of HVGO with bulk SG=1.02 and H/C= 1.47(Smith, 2007).

Molecular Weight [g/mol]	Specific Gravity	Normal Boiling Point [K]
288	0.9232	616.15
287	0.9456	632.15
304	0.9592	660.65
328	0.9672	685.65
359	0.9714	710.65
402	0.9770	735.65
451	0.9796	760.65
578	0.9948	785.65

Table 6.8. Molecular weight, specific gravity, and normal boiling point of Iran, Russia, China oils (Fang *et al*, 2003).

Molecular Weight [g/mol]	Specific Gravity	Normal Boiling Point [K]	Molecular Weight [g/mol]	Specific Gravity	Normal Boiling Point [K]
95	0.7066	355.5	171	0.8114	467.7
95	0.7255	357.2	162	0.8004	477.7
108	0.7370	377.2	163	0.8069	478.3
108	0.7374	377.5	162	0.8178	481.5
107	0.7303	380.5	171	0.8135	490.7
107	0.7466	381.1	201	0.8568	502.4
120	0.7585	385.4	180	0.8192	503.7

120	0.7573	402.7	180	0.8199	506.8
120	0.7639	406.6	187	0.8305	509.2
119	0.7545	407.7	199	0.8336	526.6
134	0.7764	411.0	199	0.8312	530.1
133	0.7742	427.4	205	0.8430	530.9
130	0.7756	429.1	199	0.8362	531.7
131	0.7769	431.0	210	0.8408	542.4
133	0.7824	431.3	221	0.8441	556.7
131	0.7650	433.3	226	0.8522	556.8
132	0.7786	433.6	220	0.8457	557.4
133	0.7797	434.9	232	0.8524	559.3
139	0.7808	437.1	243	0.8681	577.7
134	0.7810	437.4	249	0.8597	582.1
136	0.7823	439.8	244	0.8554	583.3
137	0.7837	443.0	256	0.8644	595.0
139	0.7851	445.7	267	0.8789	601.2
147	0.7894	446.2	272	0.8737	607.0
147	0.7879	452.0	268	0.8740	610.5
155	0.7972	455.4	295	0.8854	624.4
146	0.7866	457.2	299	0.8837	629.6
147	0.7990	457.3	296	0.8827	634.3
159	0.8187	461.1	325	0.8973	646.8

Figure 6.8 presents the dispersion plots of the NBP predictions for the test dataset from the original and modified versions of the Soreide correlation. The average absolute and relative deviations and bias for the original and modified Soreide correlations are summarized in Table 6.9 and the maximum deviations in Table 6.10. Overall the improvement is slight but nonetheless the maximum deviations are decreased for the majority of the cuts. The improvement is a more significant success than appears at first glance. The modified correlation was optimized for heavy

cuts and yet provides improved predictions for the more conventional test dataset oils (SG ranging from 0.81 to 1.02). Hence, the modified Soreide correlation is capable of predicting normal boiling points for pure components, light to medium oils, and can be used with confidence for heavy oil and bitumen samples. The average deviations with this correlation were less than 5% with a bias approaching zero.

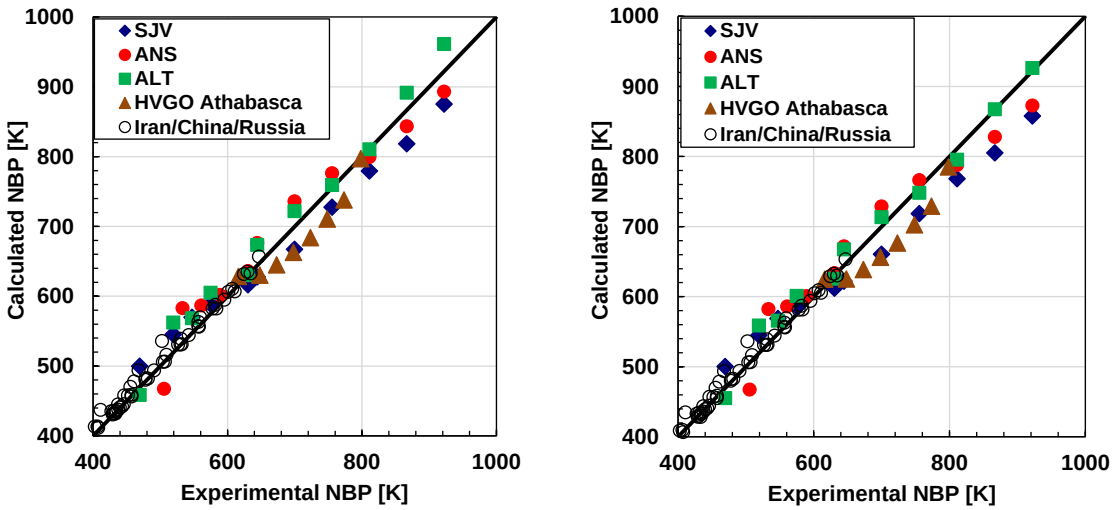

Figure 6.8. Dispersion plots for the NBP of the test dataset determined from: left) the original Soreide correlation; right) the modified Soreide correlation.

Table 6.9. Average absolute and relative deviations and bias from the original and modified Soreide correlations for the NBP of the test dataset.

Oil Sample	Original Soreide			Modified Soreide		
	AAD [K]	ARD [%]	Bias [%]	AAD [K]	ARD [%]	Bias [%]
ANS	26	4.1	2.8	24	4.2	1.9
ALT	21	3.2	2.8	15	2.6	1.4
SJV	28	4.2	-0.9	34	4.9	-1.7
HVGO	26	3.6	-2.6	28	4.0	-3.6
Iran/Russia/China	6.8	1.5	1.5	5.4	1.2	0.9
Overall	**14**	**2.5**	**1.3**	**14**	**2.3**	**0.5**

*The AAD and ARD for each sample are the deviations for the data for that sample only.
*The overall AAD and ARD are for the entire test dataset.

Table 6.10. Maximum absolute and relative deviations from the original and modified Soreide correlations for the NBP of the test dataset.

Oil Sample	Original Soreide		Modified Soreide	
	MAAD [K]	MARD [%]	MAAD [K]	MARD [%]
ANS	50	9.4	49	9.2
ALT	43	8.3	39	7.6
SJV	48	6.5	65	7.1
HVGO	39	5.4	47	6.5
Iran/Russia/China	34	7.3	34	6.7
Overall	**50**	**9.4**	**65**	**9.2**

6.2 Molecular Weight

For mixtures of pure components, the molecular weight can be determined from the composition of the mixture and the known component molecular weights as follows:

$$M = \sum_i x_i M_i \tag{2.4}$$

where x_i and M_i correspond to the mole fraction and molecular weight of component i. For petroleum cuts, there are a vast number of components and the exact composition of the mixture is not known. Instead, the average molecular weight of the cut must be measured or determined from a correlation.

There are many correlations for the prediction of molecular weight from NBP or from a combination of several properties such as NBP and SG, or viscosity and SG. The correlations that use viscosity are usually implemented only when no reliable NBP data were available because the non-Newtonian behavior of the viscosity of heavy cuts is difficult to determine and leads to unreliable predictions. Most correlations relate MW to both NBP and SG.

The correlations available in the literature for NBP were provided in Table 2.3 and include the Goosens, Katz Firoozabadi (KF), Twu *et al.*, Lee Kesler (LK), and Hauri and Sage (H-S), original Raizi Daubert (oldRD), Winn Mobil (WM), Rao Bardon (RB) and new Riazi Daubert (newRD)

correlations. The correlations were tested on the experimental MW data of the heavy oil cuts using their measured SG and NBP as inputs. The measured data are reported in Appendix B. Figure 6.9 shows the measured and correlated MW versus NBP for the WC-B-B1 distillation cuts. Figure 6.10 presents the deviations of all of the above correlations for all of the oils. The average and maximum absolute and relative deviations and the bias obtained for each correlation are reported in Table 6.11. Detailed results for each sample are summarized in Appendix G.

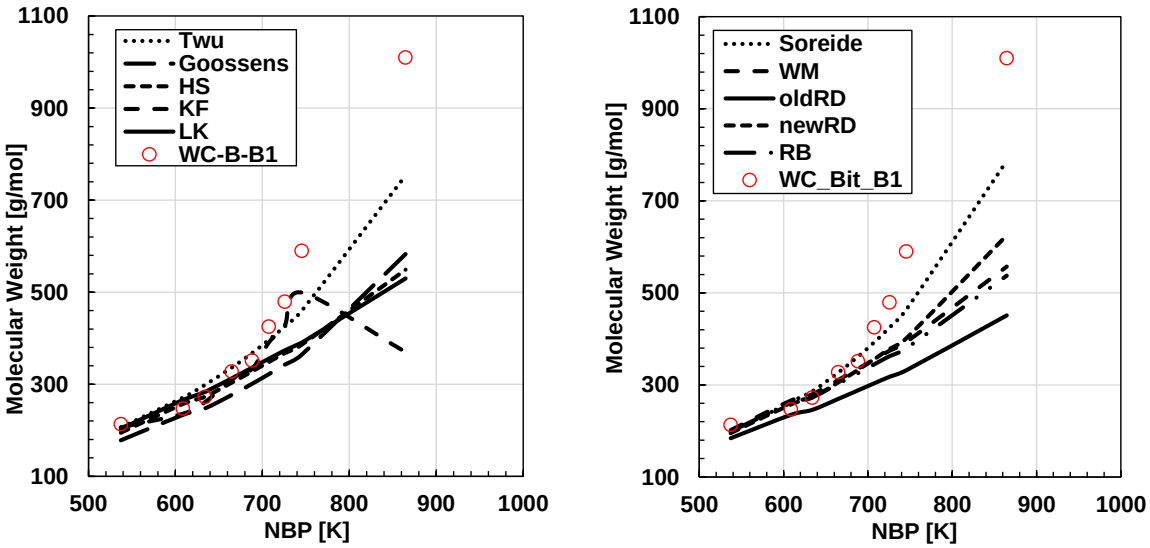

Figure 6.9. Measured and correlated MW versus NBP for the WC-B-B1 distillation cuts. left) Twu, Goosens, Hauri and Sage (H-S), Katz Firoozabadi (KF), Lee Kesler (LK), correlations; right) Soreide, Winn Mobil (WM), original Raizi Daubert (oldRD), new Riazi Daubert (newRD), and Rao Bardon (RB) correlations.

The best predictions for MW were obtained from the Soreide and Twu correlations. However, most of the correlations under-predict the MW with an even greater bias than observed with the NBP correlations. The Katz Firoozabadi correlation (KF) exhibits non-physical behavior: at carbon numbers around 45, which correspond to boiling temperatures near 750K, it has a maximum that is probably due to the polynomial form of the equation.

All the correlations were developed from datasets that included only light to medium petroleum cuts and here are being used outside their range of applicability. As observed for the NBP, all of the correlations have an increasing deviation from the low to the high boiling cuts. Part of the increased bias can be attributed to differences in MW measurements. MW was measured by vapor pressure osmometry (VPO) in this thesis but freezing point depression methods are often used in the literature. MW from freezing point depression are often lower than VPO measurements (Altgelt and Boduszynski, 1994). Nonetheless, most of the deviation is attributed to extrapolating the correlations beyond their range of applicability. This issue will be addressed when the test dataset is examined later.

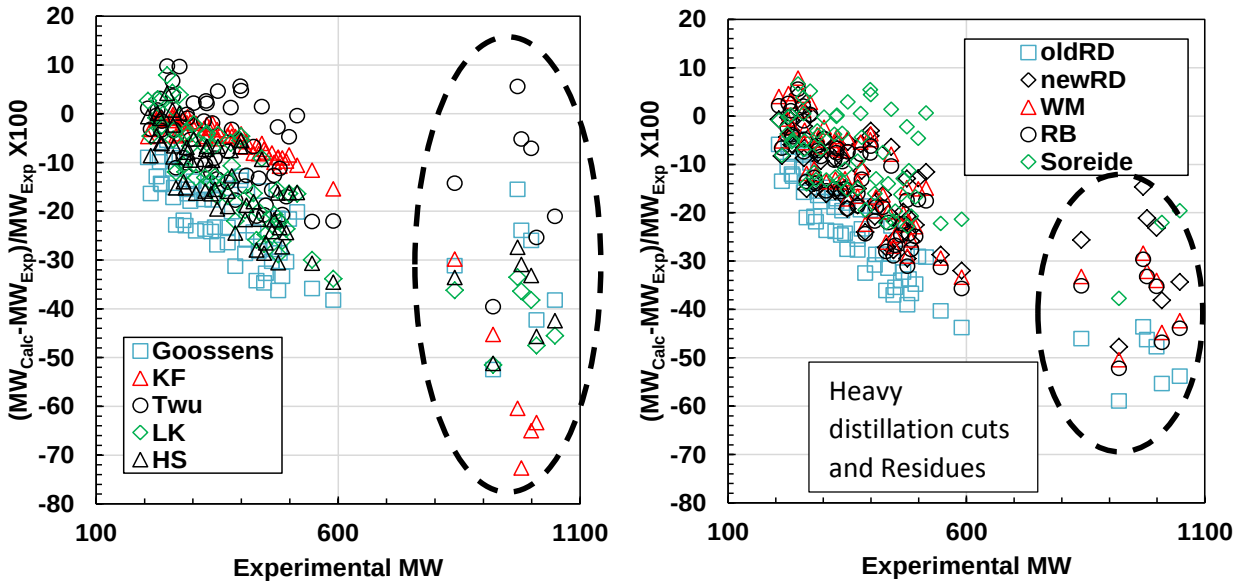

Figure 6.10. Relative error obtained for predicted MW using experimental SG and NBP values: left) Goosens, Katz Firoozabadi (KF), Twu, Lee Kesler (LK), and Hauri and Sage (H-S) correlations; right) original Raizi Daubert (oldRD), Winn Mobil (WM), Rao Bardon (RB) and new Riazi Daubert (newRD). The errors for the Soreide correlation are shown in Figure 6.11.

Table 6.11 Average absolute and relative deviations, maximum absolute and relative deviations, and bias for NBP obtained using correlations from literature for the development dataset.

Correlation	AAD [K]	ARD [%]	MAAD [K]	MARD [%]	Bias [%
Soreide	49	9.8	347	38	-8.6
LK	90	15.5	480	52	-14.7
old RD	134	25.8	564	59	-25.8
new RD	78	14.7	439	48	-14.5
Goossens	108	22.3	483	53	-22.3
HS	91	16.5	471	51	-16.4
KF	85	11.2	971	93	-11.2
WM	86	15.1	464	51	-14.2
RB	93	16.7	480	52	-16.3
Twu	48	9.4	364	40	-7.3

Figure 6.11 presents the dispersion plots of the MW predictions for the development dataset distillation cuts from the original and modified versions of the Soreide correlation. The MW error bars were calculated from the propagation of the experimental errors for SG and NBP. Figure 6.12 is a dispersion plot for the MW of pure components ranging from paraffins to polycondensed aromatic structures. The average absolute and relative deviations and bias for the original and modified Soreide correlations are summarized in Table 6.12 and the maximum deviations in Table 6.13. The new correlation improved the average and maximum deviations for both pure hydrocarbons and the heavy distillation cuts, and significantly reduced the bias (from -5.5 to -0.4%).

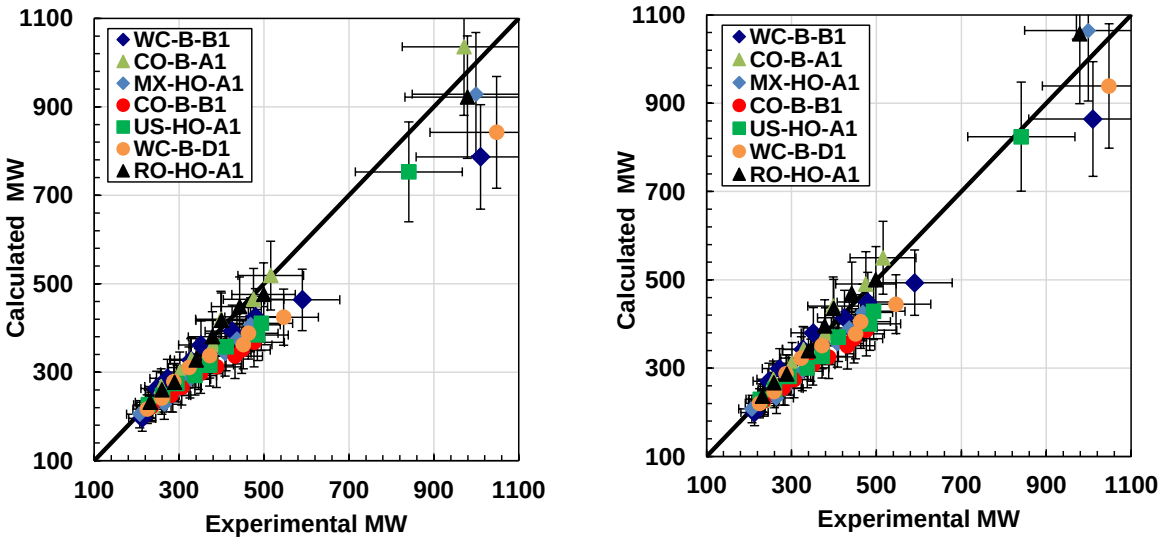

Figure 6.11. Dispersion plots for the MW of the development dataset distillation cuts determined from: left) the original Soreide correlation; right) the modified Soreide correlation.

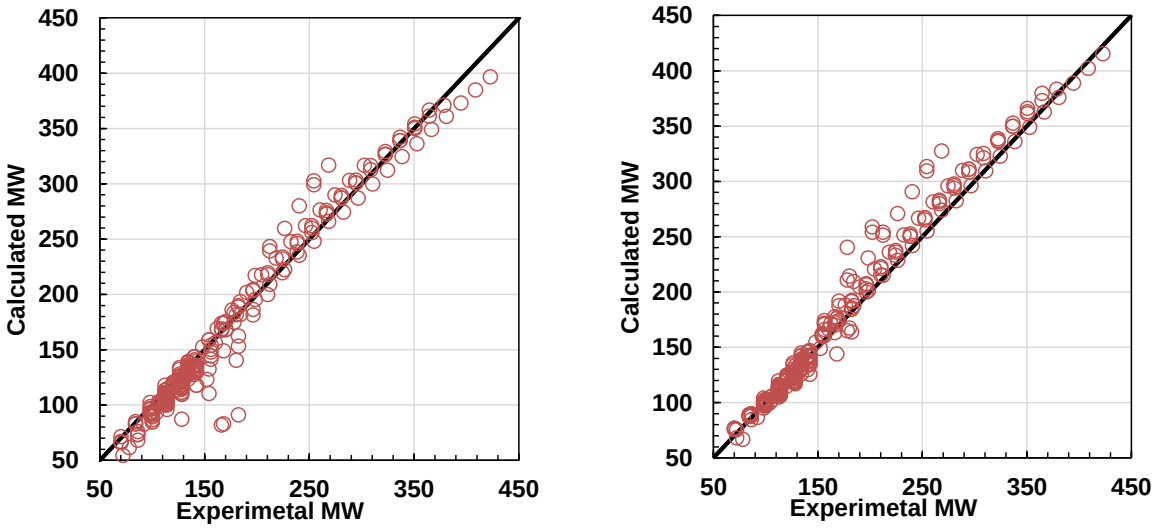

Figure 6.12. Dispersion plots for the MW of the development dataset pure hydrocarbons determined from: a) the original Soreide correlation; b) the modified Soreide correlation.

Table 6.12. Average absolute and relative deviations and bias from the original and modified Soreide correlation for MW for the development dataset.

Oil Sample	Original Soreide			Modified Soreide		
	AAD [g/mol]	ARD [%]	Bias [%]	AAD [g/mol]	ARD [%]	Bias [%]
WC-B-B1	55	9.5	-6.3	45	8.7	-2.8
CO-B-A1	15	3.2	0.4	39	6.3	5.0
MX-HO-A1	46	11.4	-11.4	38	9.7	-8.6
CO-B-B1	96	16.6	-16.6	86	14.5	-14.5
US-HO-A1	52	11.4	-11.4	39	9.1	-9.1
WC-B-D1	64	11.7	-11.7	47	9.0	-9.0
RO-HO-A1	15	2.8	-1.3	17	3.2	2.3
Pure Components	12	7.5	-4.9	8	4.6	0.6
Overall	**19**	**7.8**	**-5.5**	**14**	**5.3**	**-0.4**

Table 6.13. Maximum absolute and relative deviations from the original and modified Soreide correlation for MW of the development dataset.

Oil Sample	Original Soreide		Modified Soreide	
	MAAD [g/mol]	MARD [%]	MAAD [g/mol]	MARD [%]
WC-B-B1	127	21.4	103	17.4
CO-B-A1	21	5.3	37	9.2
MX-HO-A1	66	16.1	57	13.9
CO-B-B1	109	22.9	96	20.0
US-HO-A1	101	20.8	89	18.4
WC-B-D1	122	22.3	106	19.5
RO-HO-A1	24	4.7	31	7.7
Pure Components	194	95.9	57	35.4

The original and modified Soreide correlations were evaluated against the same independent test dataset obtained from the literature for the NBP correlations, Tables 6.4 to 6.8. The MW were

calculated using the reported SG and MW. Figure 6.13 presents the dispersion plots of the MW predictions for the test dataset from the original and modified versions of the Soreide correlation. The average absolute and relative deviations and bias for these correlations are summarized in Table 6.14 and the maximum deviations in Table 6.15. As observed for the NBP prediction, although the overall improvement is slight, the maximum deviations are decreased for the majority of the cuts. Again, the results demonstrate that the modified Soreide correlation is capable of correlating MW for pure components, light to medium oils, and can be used with confidence for heavy oil and bitumen samples. The average deviations with this correlation were less than 14% with a bias approaching zero.

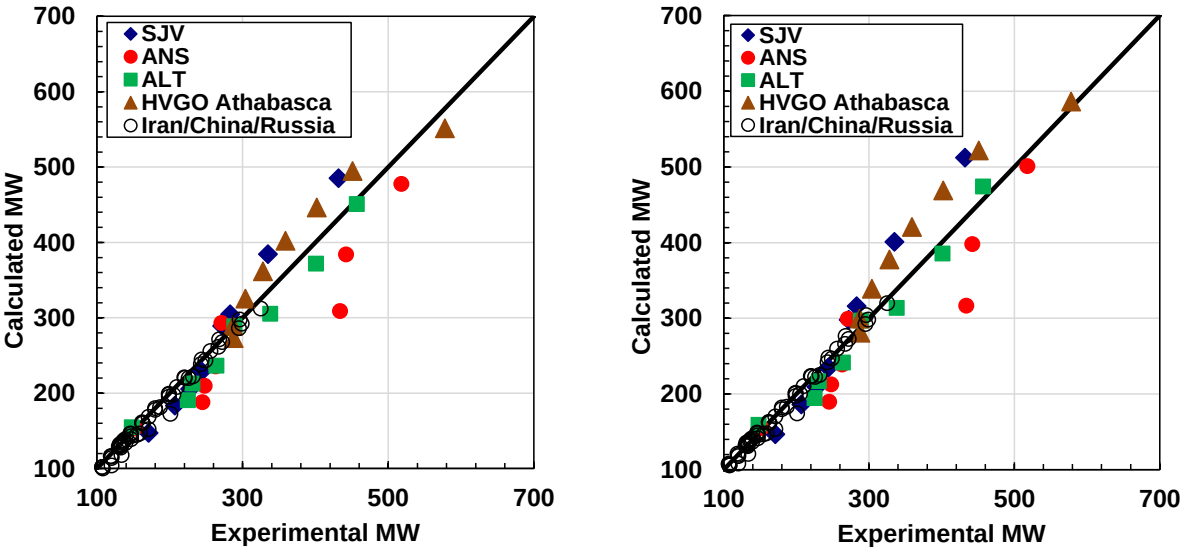

Figure 6.13. Dispersion plots for the MW of the test dataset determined from: right) the original Soreide correlation; left) the modified Soreide correlation.

Table 6.14. Average absolute and relative deviations and bias from the original and modified Soreide correlations for the MW of the test dataset.

Oil Sample	Original Soreide			Modified Soreide		
	AAD [g/mol]	ARD [%]	Bias [%]	AAD [g/mol]	ARD [%]	Bias [%]
ANS	46	13.4	-11.2	43	12.7	-10.2
ALT	19	7.0	-5.9	19	6.9	-3.9
SJV	28	10.3	-0.1	34	11.7	1.8
HVGO	29	7.6	3.4	35	9.5	8.6
Iran/Russia/China	5	3.1	-2.9	4	2.3	-1.8
Overall	**14**	**5.4**	**-3.2**	**14**	**5.1**	**-1.5**

Table 6.15. Maximum absolute and relative deviations from the original and modified Soreide correlations for the MW of the test dataset.

Oil Sample	Original Soreide		Modified Soreide	
	MAAD [g/mol]	MARD [%]	MAAD [g/mol]	MARD [%]
ANS	1245	28.8	121	27.8
ALT	34	15.2	32	14.4
SJV	53	14.7	74	18.3
HVGO	44	12.0	65	15.8
Iran, Russia, China	29	14.1	29	14.3

6.3 Specific Gravity

As shown in Chapter 2, there are several correlations to predict SG that use different input variables. These variables range from simply MW and characterization factors (Jacoby, 1952; Soreide, 1989; Whitson, 1983) to refractive index combined with either MW or boiling point

(Riazi and Daubert, 2005). Elemental analysis was also used as correlating variable to predict SG (Gray, 2002; Katz and Firoozabadi, 1978).

The correlations were tested on the experimental MW of the heavy oil cuts using their measured properties as inputs. Measured data are reported in Appendix B. Figure 6.14 shows the measured and correlated SG versus MW for the WC-B-B1 distillation cuts. Figure 6.15a and Figure 6.15b, respectively, show the errors for the methods that require a characterization factor and the methods that do not use characterization factors and instead use other physical properties. The average and maximum average and relative deviations and bias are presented in Table 6.16. The deviations and bias for each sample are summarized in Appendix G.

The SG predictions are much more accurate than the NBP and MW predictions. However, excluding the residue fraction, all of the correlations (except for RD MW, RI and K-F) exhibit a trend in the error with the maximum over-prediction occurring for the light cuts and the maximum under-prediction occurring for the heavy cuts. Note, since the K-F correlation preserves the same shape as the distillation cuts experimental density, it will be used in Chapter 8 to develop an improved specific gravity distribution. Interestingly, the Gray correlation performed similarly to the other correlations although it only used elemental analysis as an input.

Not surprisingly, the correlations with the characterization factor had lower deviations and bias on average than the other methods. The smallest deviations and bias were found with the Jacoby (1982) correlation because it provided better predictions for the residues. The maximum deviation with this correlation was only 6% but the systematic trend in the errors suggest that the correlation can be improved upon.

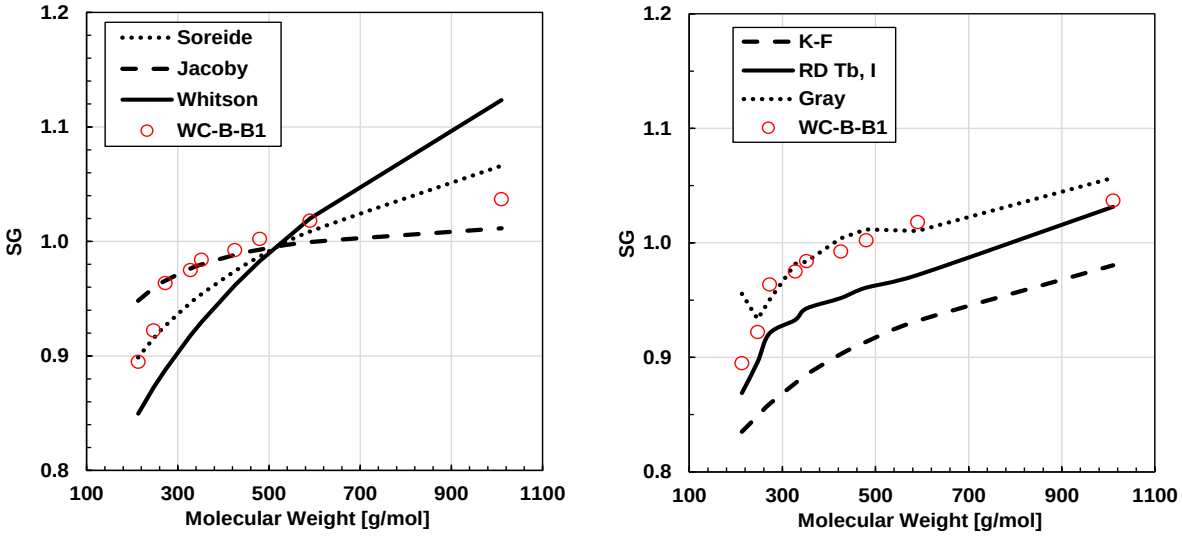

Figure 6.14. Measured and correlated SG versus MW for the WC-B-B1 distillation cuts. Left) Soreide, Jacoby, Whitson; right) Katz Firoozabadi (K-F), Riazi and Daubert using boiling point and refractive index as inputs (RD Tb, I), and Gray.

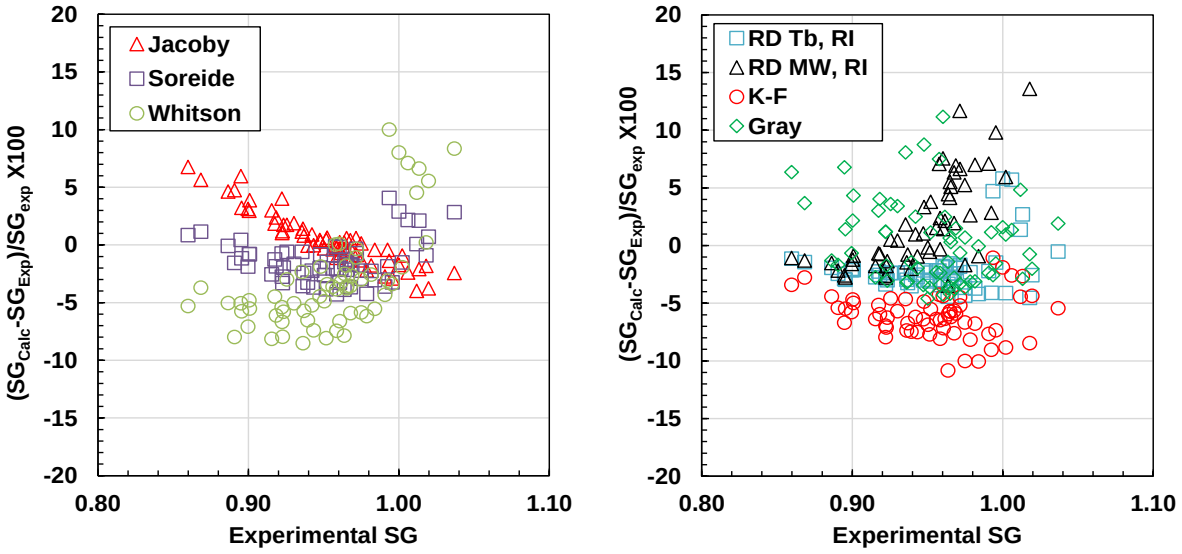

Figure 6.15. Relative error obtained for predicted SG using correlations with characterization factors (left: Soreide, Jacoby, Whitson) and correlations with physical properties (right: Katz Firoozabadi (K-F), Riazi and Daubert using boiling point and refractive index as inputs (RD Tb, I), and Gray) as input parameters.

Table 6.16 Absolute and relative deviations for SG obtained using correlations from literature.

Correlation	AAD	ARD [%]	MAAD	MARD [%]	Bias [%]
Soreide	0.02	2.0	0.04	4.3	1.5
Whitson	0.05	4.9	0.09	8.5	3.4
Jacoby	0.02	1.8	0.06	6.8	-0.5
RD Tb, RI	0.03	2.8	0.06	5.8	2.2
RD MW, RI	0.09	8.8	0.64	63.3	-7.6
K-F	0.06	6.1	0.10	10.8	6.1
Gray	0.03	3.1	0.11	11.2	-0.3

Since the best results were obtained with characterization factors, this approach is tested first. To facilitate the discussion, the correlations are provided in Equations 2.16 to 2.18:

Soreide: $$SG = 0.28554 + Cf * (MW - 65.94185)^{0.129969} \quad (2.16)$$

Whitson: $$SG = 6.0108 * MW^{0.17947} * Kw^{-1.18241} \quad (2.17)$$

Jacoby: $$SG = 0.8468 - \frac{15.8}{MW} + Ja * (0.2456 - \frac{1.77}{MW}) \quad (2.18)$$

In Equations 2.16 to 2.18 to obtain the SG of the pseudocomponents, the inputs are the MW of the pseudocompnents and the characterization factors J_a, C_f, and K_w which are tuned to fit the correlation to the bulk density. For the Jacoby correlation J_a varies between 0 and 1 for petroleum fractions; the 0 value indicates a 100% paraffinic compound and 1 represents a 100% aromatic compound. Soreide developed a similar characterization factor that ranges between 0.27 and 0.33 depending on the oil; the lower end corresponds to paraffinic structures and the higher end to aromatic ones. Similarly, the Whitson correlation requires the commonly used K_w (Watson Factor) which can range from 10 to 13 for distillation cuts.

The characterization factors are not only used to match bulk properties but also, to some extent account for the relative aromaticity of the oil. Figure 6.16 shows the relationship between SG and

MW for different values of J_a, C_f and K_w., The Jacoby correlation preserves the same shape at all characterization factors while the Whitson and Soreide correlations shift the shape of the curves as the characterization factors change. The main differences are in how rapidly the SG changes with MW and the magnitude of the SG at high MW. The Whitson correlation has the slowest change in SG at low MW and predicts unrealistically high SG at large values of MW. Soreide and Jacoby predict realistic SG at large MW but still do not correctly capture the change in SG with MW.

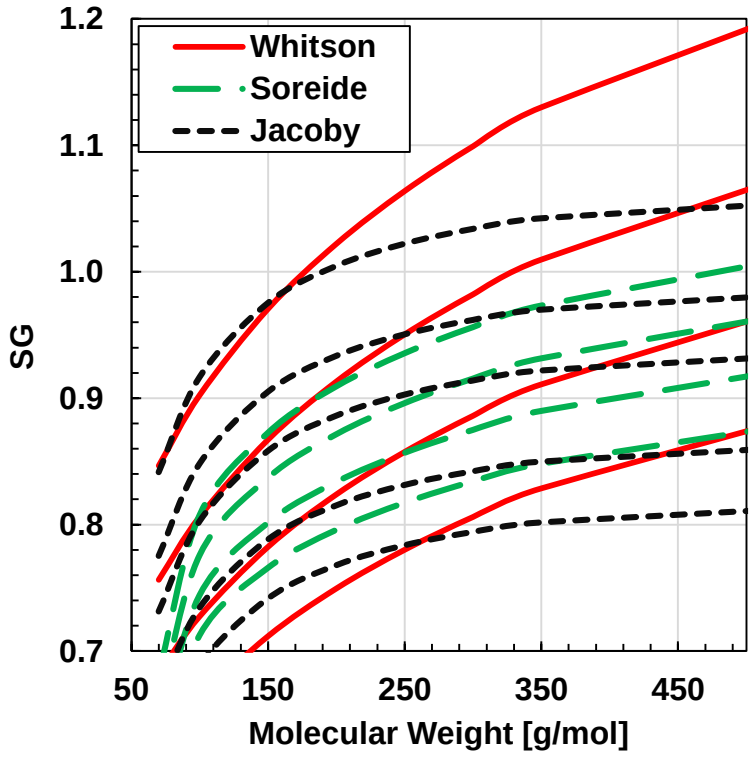

Figure 6.16. Specific gravity versus molecular weight for Whitson correlation (solid lines for Watson factors of 10, 11, 12, and 13), Soreide correlation (dashed line for C_f of 0.27, 0.29, 0.31 and 0.33), and the Jacoby correlation (dotted line for J_a of 0.0, 0.25, 0.5, 0.75, and 1.0).

An alternative parameter to describe compositional changes within the oil is the H/C atomic ratio. This measurable property is directly related to the aromaticity of cuts and ranges from approximately 2 to less than 1 from paraffinic to aromatic molecules. A new correlation is

proposed with a similar mathematic form to the Jacoby correlation but with MW and the H/C ratio as inputs, Equation 6.2:

$$SG_i = \left(2.0591 - \left(\frac{H}{C}\right)_{bulk}\right)\left(0.5717 - \frac{4.802}{MW_i}\right) + \left(2.0591 - \frac{1.27985}{\left(\frac{H}{C}\right)_{bulk}}\right)\left(0.6171 - \frac{24.68}{MW_i}\right) \quad (6.2)$$

where $(H/C)_{bulk}$ is the H/C ratio of the bulk sample distilled, in this case the maltenes, and MW_i and SG_i are the molecular weight and specific gravity of each cut, respectively.

Dispersion plots for the Jacoby correlation and the proposed correlation to H/C ratio (Equation 6.2) are shown in Figures 6.17 (left) and 6.17 (right), respectively. The average absolute and relative deviations and bias for the two correlations are summarized in Table 6.17 and the maximum deviations in Table 6.18. The new correlation better matched the density trend from light to heavy cuts, resulting in lower average and maximum deviations than the Jacoby correlation.

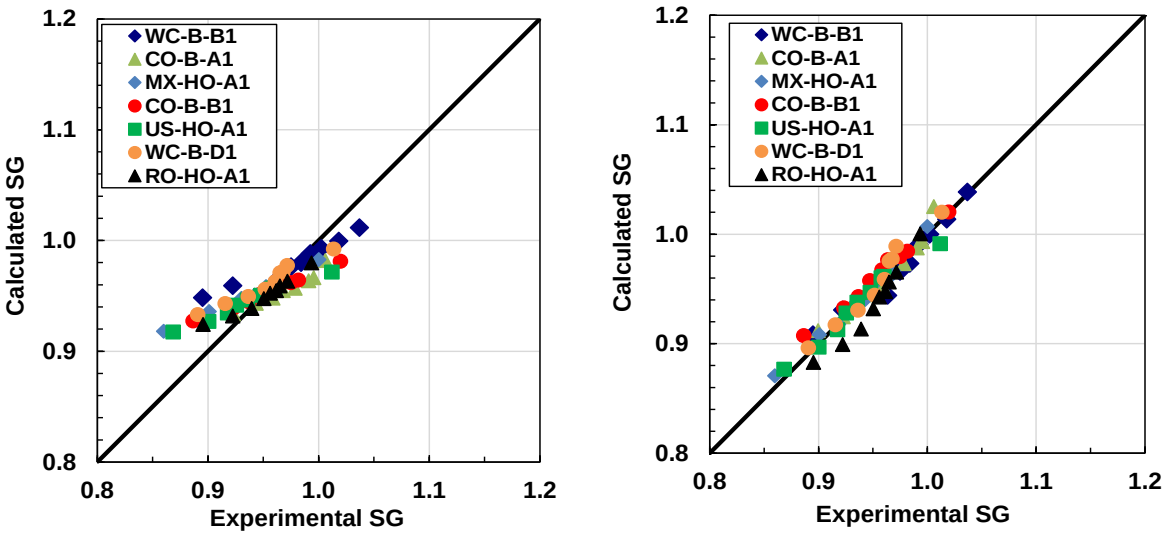

Figure 6.17. Dispersion plots for the SG of the development dataset determined from: left) the Jacoby correlation; right) the proposed correlation to H/C ratio (Eq. 6.2).

Table 6.17. Average absolute and relative deviations and bias from the Jacoby correlation and the proposed correlation to H/C ratio (Eq. 6.2) for the SG of the development dataset.

Oil Sample	Jacoby			Equation 6.2		
	AAD	ARD [%]	Bias [%]	AAD	ARD [%]	Bias [%]
WC-B-B1	0.02	1.8	-0.5	0.01	1.4	1.0
CO-B-A1	0.02	1.9	0.9	0.01	0.7	0.2
MX-HO-A1	0.02	2.1	-1.5	0.01	0.6	-0.3
CO-B-B1	0.02	1.7	0.0	0.01	0.7	-0.5
US-HO-A1	0.02	2.0	-1.0	0.01	0.6	-0.1
WC-B-D1	0.01	1.5	-1.0	0.01	0.6	-0.1
RO-HO-A1	0.01	1.0	0.0	0.01	1.3	1.2
Overall	**0.02**	**1.7**	**-0.4**	**0.01**	**0.8**	**0.2**

Table 6.18 Maximum absolute and relative deviations from the Jacoby correlation and the proposed correlation to H/C ratio (Eq. 6.2) for the SG of the development dataset.

Oil Sample	Jacoby		Equation 6.2	
	MAAD	MARD [%]	MAAD	MARD [%]
WC-B-B1	0.05	6.0	0.02	2.5
CO-B-A1	0.03	3.1	0.01	1.3
MX-HO-A1	0.06	6.8	0.01	1.8
CO-B-B1	0.04	4.6	0.02	2.3
US-HO-A1	0.05	5.6	0.01	1.5
WC-B-D1	0.04	4.7	0.01	1.3
RO-HO-A1	0.03	3.2	0.02	2.5

An important check for the proposed correlation is that predicted SG of the cuts are consistent with the bulk SG of the whole sample (the deasphalted oil). The SG of the bulk oil was calculated from the correlated SG of the cuts assuming ideal mixing (zero excess volume) as follows:

$$SG_{Bulk} = \left(\sum_{i=1}^{N} \frac{w_i}{SG_i} \right)^{-1} \quad (2.4)$$

The measured and calculated bulk SG for each oil are compared in Figure 6.18. The overall absolute average and relative deviations were 0.003 and 0.31%, respectively. For the majority of the oils, the error of calculated bulk density is within the experimental error (±0.5%) of the measurements. Note, the H/C ratios of the cuts can be tuned with a constant multiplier so that the calculated bulk SG matches the measured value.

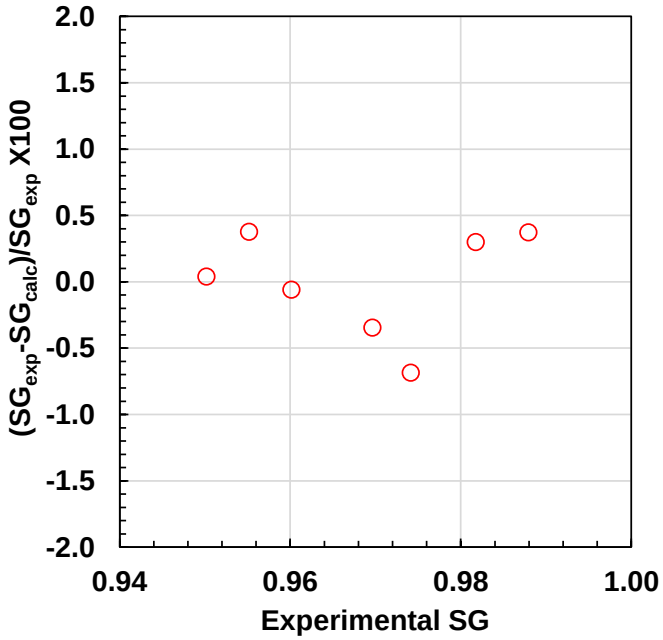

Figure 6.18. Error plot obtained between the calculated and experimental bulk specific gravity of seven different heavy oil and bitumen samples using Equation 6.2

The Jacoby equation and the proposed correlation (without tuning) were evaluated against the same independent test dataset obtained from the literature for the NBP correlations, Tables 6.4 to 6.7. Figure 6.19 is a dispersion plot of the correlated versus measured SG and the relative deviations and bias and the maximum deviations are summarized in Tables 6.19 to 6.20. Overall, the proposed correlation predicted SG with an average absolute relative deviation less than 1.4%; compared with Jacoby correlation the new equation was able to predict the SG with an improvement of almost 50%. The average maximum absolute deviations using Equation 6.2 were lower (3.1 %) than the ones obtained with Jacoby correlation (6.0 %). The deviations obtained

with Equation 6.2 for the test data set are larger than found for the development dataset but less than the deviations found with the other correlations. This performance is very good considering that the correlation was developed and optimized for heavy cuts.

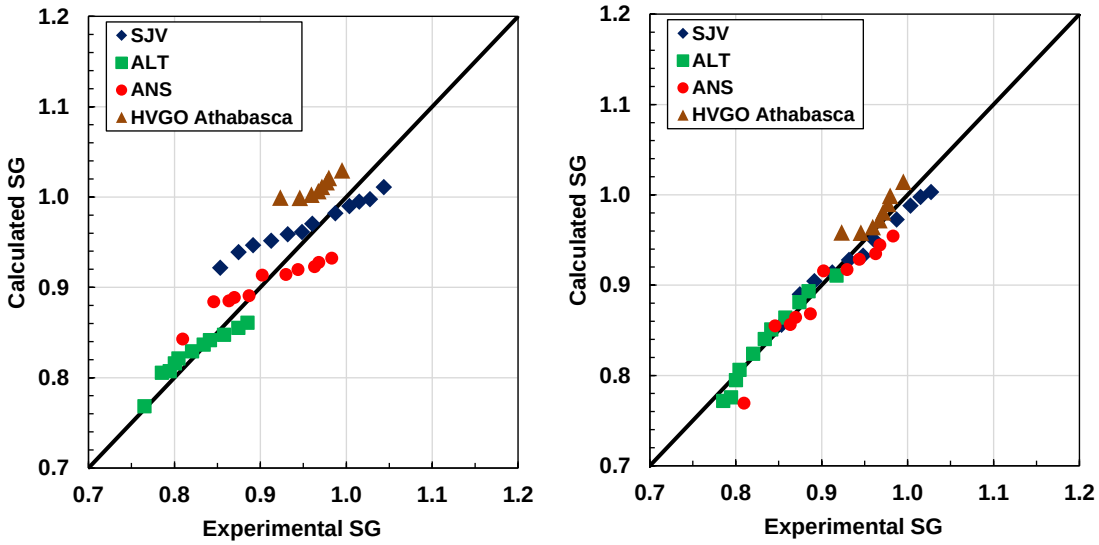

Figure 6.19. Dispersion plot for the SG of the test dataset determined from Jacoby (left) and the Eq. 6.2 (right).

Table 6.19. Average absolute and relative deviations and bias from the Jacoby correlation and the proposed correlation to H/C ratio (Eq. 7.2) for the SG of the test dataset.

Oil Sample	Jacoby			Equation 6.2		
	AAD	ARD [%]	Bias [%]	AAD	ARD [%]	Bias [%]
ANS	0.03	2.7	1.2	0.02	2.0	2.0
ALT	0.01	1.5	-0.1	0.01	0.9	-0.2
SJV	0.03	3.5	-2.2	0.01	1.3	0.6
HVGO	0.05	4.8	-4.8	0.01	1.6	-1.6
Overall	**0.03**	**3.1**	**-1.4**	**0.01**	**1.4**	**0.1**

Table 6.20. Maximum absolute and relative deviations from the Jacoby correlation and the proposed correlation to H/C ratio (Eq. 6.2) for the SG of the test dataset.

Oil Sample	Jacoby		Equation 6.2	
	MAAD	MARD [%]	MAAD	MARD [%]
ANS	0.05	5.15	0.04	5.0
ALT	0.02	2.69	0.02	2.3
SJV	0.07	8.04	0.02	2.3
HVGO	0.08	8.25	0.04	3.8

6.4 Specific Gravity and H/C Ratio

The proposed correlation for the SG of distillation cuts requires the bulk H/C ratio as an input. H/C ratio is a useful property in its own right for assessing the aromaticity and heating value of an oil. It is also used as a parameter in upgrading models. However, the H/C ratio is not commonly measured for crude oils and their cuts. Riazi (2005) presented a correlation to calculate the C/H ratio as a function of boiling point and specific gravity. However, in this study it was found that a simpler relation between specific gravity and H/C ratio exists for several distillation cuts. It is more convenient to correlate H/C ratio to a single and more commonly measured property such as the bulk specific gravity.

First consider the distribution of H/C ratios in different crude oils. The measured elemental composition for all the petroleum cuts is provided in Appendix G. Figure 6.20 presents the H/C ratio of the distillation cuts versus their cumulative weight percent distilled. The lightest oil (RO-HO-A1) has the highest H/C ratios compared with the more aromatic oils such as WC-B-B1 and CO-B-A1. As expected, the H/C ratio decreases for the higher boiling point cuts. As discussed in Chapter 2, the lower boiling point cuts are less dense and richer in saturated hydrocarbons (high H/C ratio), while the heavier cuts are denser and more aromatic (low H/C ratio). The H/C ratio is inversely proportional to SG, Figure 6.21, and the properties were correlated as follows:

$$\left({}^{H}/_{C}\right)_i = \frac{1.7661 - SG_i}{0.50337} \tag{6.3}$$

where $(H/C)_i$ and SG_i are the H/C ratio and specific gravity of the petroleum cut. Figure 6.22 is dispersion plot of the correlated versus measured SG and the deviations and bias are summarized in Table 6.21. In Figure 6.20 and 7.21, although the trends are clear within an oil and between the two properties, some scatter is observed that can be attributed to the uncertainty of the measurements for both specific gravity (0.5%) and elemental analysis (0.3%).

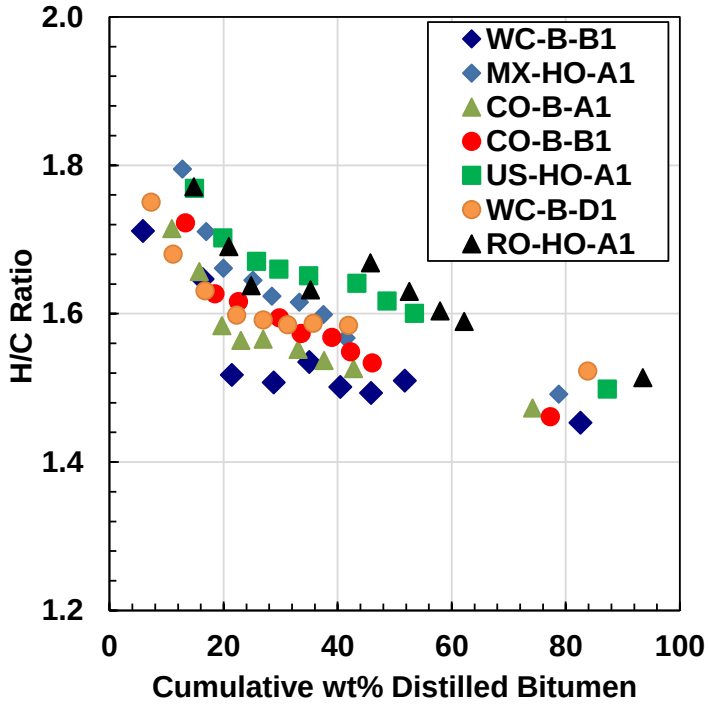

Figure 6.20. H/C ratio of the DVFA distillation cuts versus cumulative weight percent distilled.

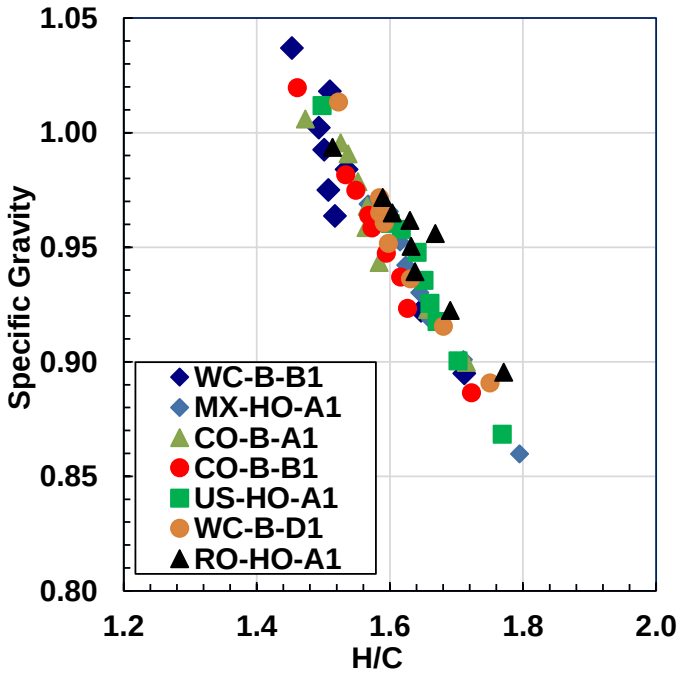

Figure 6.21. H/C ratio of the DVFA distillation cuts versus the specific gravity.

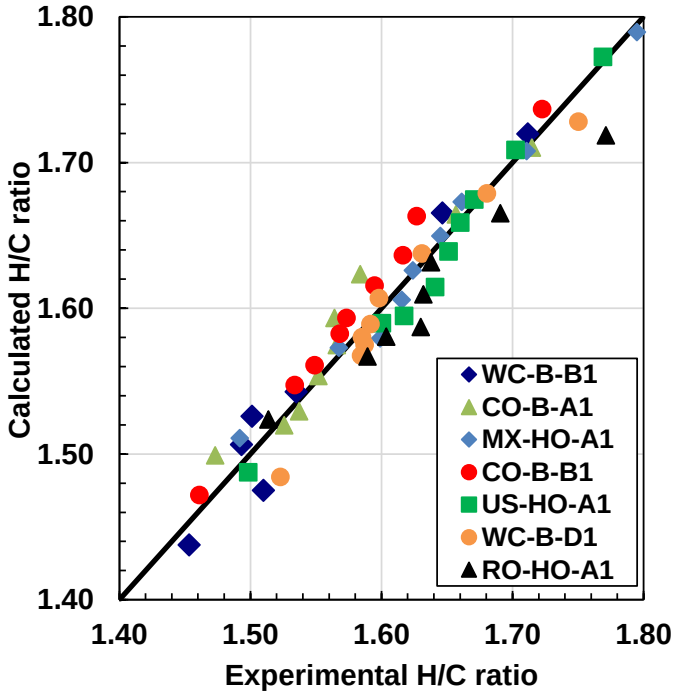

Figure 6.22. Dispersion plot for the H/C ratio of the development dataset determined from the proposed correlation (Eq. 6.3).

Table 6.21. Average and maximum absolute and relative deviations and bias from the proposed correlation (Eq. 6.3) for the H/C ratio of the development dataset.

Oil Sample	AAD	ARD [%]	MAAD	MARD [%]	Bias [%]
WC-B-B1	0.02	1.1	0.03	2.3	0.2
CO-B-A1	0.01	0.9	0.04	2.5	0.7
MX-HO-A1	0.01	0.6	0.02	1.3	0.1
CO-B-B1	0.02	1.1	0.04	2.2	1.1
US-HO-A1	0.01	0.7	0.03	1.6	-0.5
WC-B-D1	0.01	0.8	0.04	2.5	-0.6
RO-HO-A1	0.03	1.5	0.05	3.0	-1.4
TOTAL	**0.02**	**1.0**	**0.04**	**2.2**	**-0.04**

The proposed correlation was evaluated against the oils from the independent test dataset for which H/C ratios were available (ANS, ALT and SJV), Tables 6.4 to 6.7. Figure 6.23 is a dispersion plot of the correlated versus measured H/C ratio and the deviations and bias are summarized in Table 6.22. Overall, for the test data set, the proposed correlation is within 4.6 % of the measured values. The main contributor to this error is due to the drastic under-prediction of the H/C ratios for the ALT oil, which was the least dense and most paraffinic of the three oils. For the other oils, SJV and ANS, the relative deviations were considerably lower (less than 1.9 %) and comparable to the absolute deviations obtained for the development dataset with a slight difference of 0.015.

To further investigate the issue with the ALT oil, the H/C ratio of each cut was plotted versus SG to determine if the oil had the expected trend of decreasing H/C ratio from low to high boiling cuts, Figure 6.24. Surprisingly and unlike the other two oils, the content/C ratio of the ALT oil distillation cuts remained constant. It appears that this oil consists mainly of saturated hydrocarbons and the higher boiling cuts contain larger saturated molecules but no additional aromatic species; hence, the H/C ratio does not change.

The direct correlation of H/C ratio to SG (or vice versa) appears to apply to typical petroleum cuts where both size and aromaticity increases in higher boiling cuts. For this type of mixture, the bulk

H/C ratios required for the previously proposed SG correlation, Equation 6.2, can be determined using Equation 6.3 when experimental bulk H/C ratios are not available. For very paraffinic oils, both MW and H/C ratio are required, Equation 6.2.

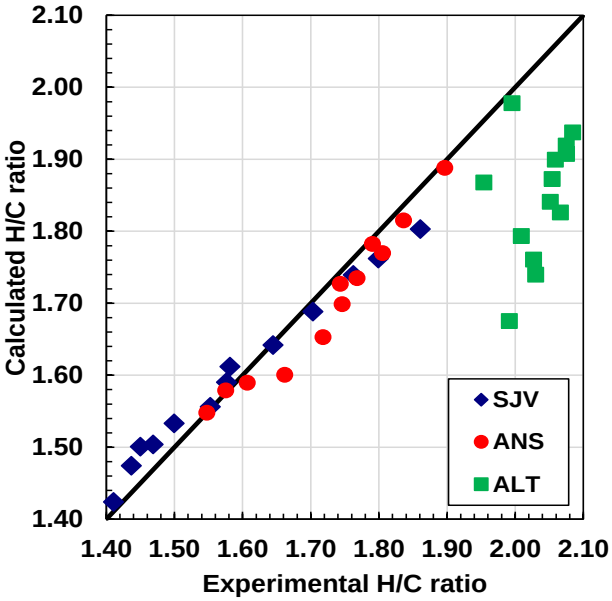

Figure 6.23. Dispersion plot for the H/C ratio of the test dataset determined from the proposed correlation (Eq. 6.3).

Table 6.22. Average and maximum absolute and relative deviations and bias from the proposed correlation (Eq. 6.3) for the H/C ratio of the test dataset.

Oil Sample	SG	AAD	ARD [%]	MAD	MARD [%]	Bias [%]
ANS	0.8911	0.04	2.2	0.14	10.5	-0.5
ALT	0.8179	0.21	10.2	0.32	15.7	-10.2
SJV	0.9772	0.03	1.7	0.06	3.5	0.6
TOTAL	**--**	**0.08**	**4.7**	**0.17**	**9.9**	**-3.1**

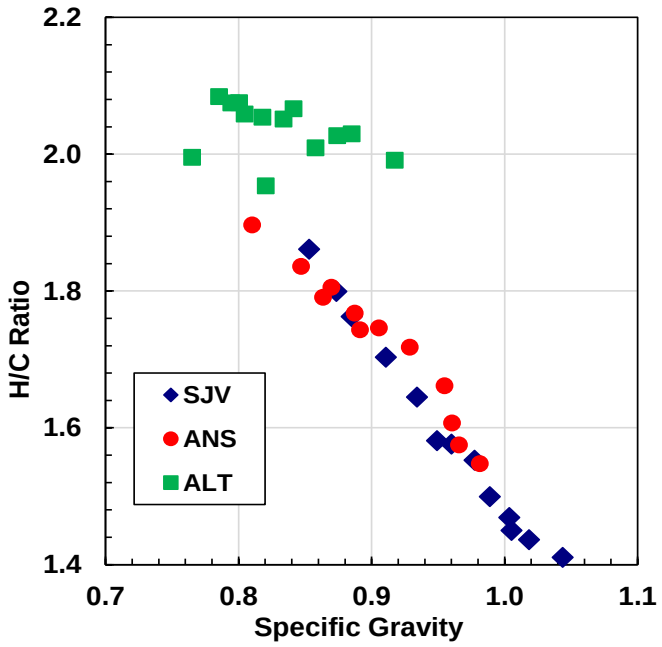

Figure 6.24. H/C ratio for the test dataset distillation cuts versus the specific gravity.

6.5 Density, Molecular Weight and Refractive Index

In some cases, such as in-line process measurements, it is easier to measure refractive index than density. As discussed in Chapter 2, density is a function of the refractive index, F_{RI}. Hence, an accurate correlation to obtain SG from F_{RI} is required because most property correlations are based on SG. Some of the correlations available in the literature relating density and F_{RI} were presented in Chapter 2 and include the One Third Rule and the Vargas and Chapman (2010) cubic correlation (VC). It was not clear from the literature review if a proportionality, linear, quadratic, or higher order relationship is sufficient to correlate SG and F_{RI}. A linear and quadratic correlation were developed and, along with the 1/3 Rule and VC correlations, were tested using the experimental data fromthe heavy oil cuts as well as SARA fraction and pure component data from Powers (2014). Measured data are reported in Appendix B.

Figure 6.25 shows density versus F_{RI} for the data collected in this project. It can be seen that an almost linear relation exists for petroleum cuts. A similar plot, Figure 6.26, was constructed for the pure components and SARA fractions (Powers, 2014) which shows the range where the distillation cuts fall. As expected, the cuts lie between saturates and paraffinic pure components

on the low end, and on the high end they are aligned with the aromatics from SARA fractions and pure components.

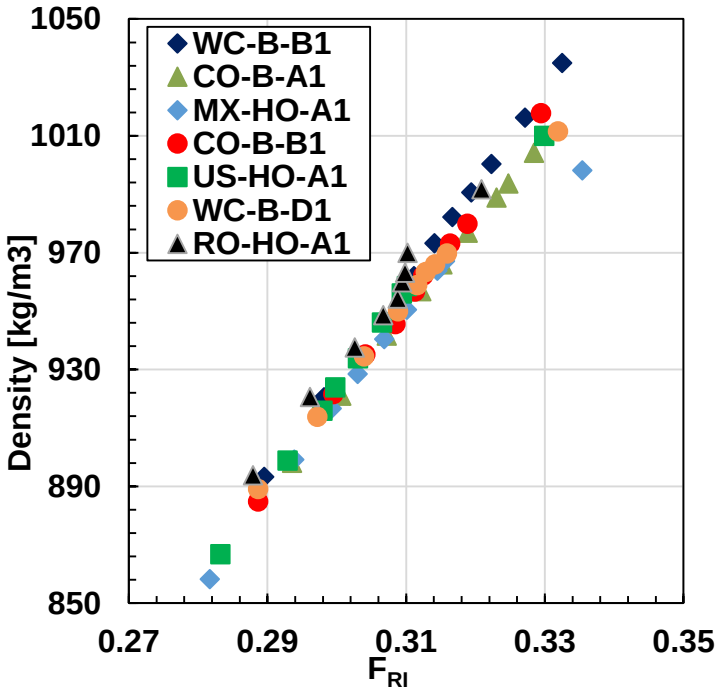

Figure 6.25. F_{RI} as a function of the density for the distillation cuts.

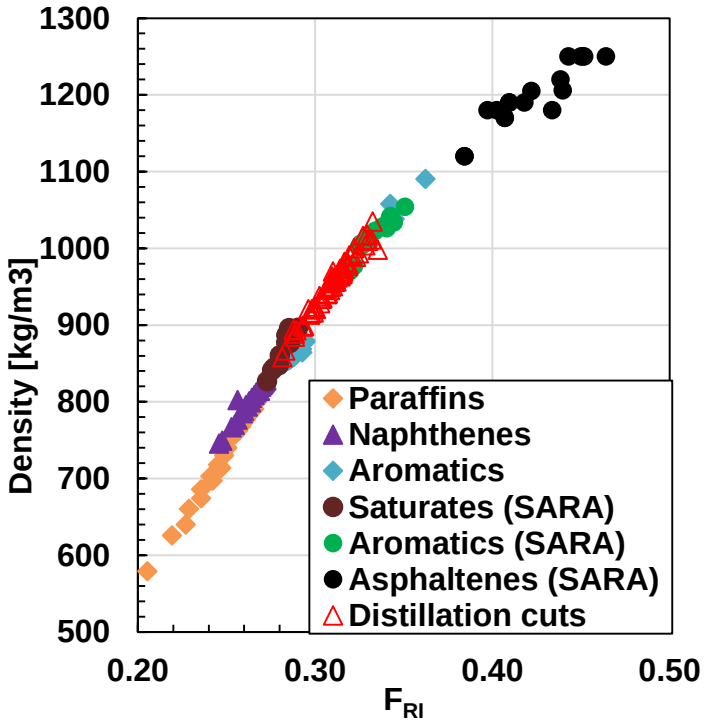

Figure 6.26. F_{RI} as a function of the density for pure components, SARA fractions and distillation cuts

A quadratic polynomial relation can describe the relation between F_{RI} and density. A quadratic correlation first developed by Powers (2014) was modified using all the components presented in Figure 6.23 to obtain the following:

$$F_{RI-20°C} = 3.384x10^{-7}\rho_{20°C}^2 - 2.835x10^{-4}\rho_{20°C} + 0.2737 \quad (6.4)$$

A simpler relation can be constructed between the F_{RI} and density, provided asphaltenes are not considered in the correlation. As mentioned previously and as can be seen in Figure 6.23, there is a linear relationship between the density and F_{RI} up to the aromatic fraction. The data excluding the asphaltenes was fitted to obtain the linear correlation shown in Equation 6.5:

$$F_{RI-20°C} = \frac{\rho_{20°C}/1000 + 0.1058}{3.4033} \quad (6.5)$$

Figure 6.27 compares the errors from one-third rule, Vargas and Chapman (2010, VC), and Equations 6.4 and 6.5. The average absolute and relative deviations, bias, and maximum deviations are presented in Table 6.23, 6.24 and 6.25 respectively. Compared with the one-third rule,

Equation 6.5 improves the relative deviation form 2.4 % to 1.2%. The maximum deviations were decreased for all the components of the test dataset when compared to the 1/3 Rule. The bias of Equation 6.5 had a value approaching to zero, which is similar to the one reported by the 1/3 Rule.

Equation 6.4 provides a deviation within 2.6% for the asphaltene refractive index compared with 5.4 and 3.6% from the 1/3 Rule and VC correlations. Similarly, the maximum deviations were decreased by 0.2% when compared to the VC equation, Equation 2.27. Note, the properties of the asphaltenes are subject to higher experimental errors and this could affect the overall performance of all the correlations presented/developed here. Overall, the linear correlation is sufficient for petroleum cuts excluding asphaltenes while a quadratic correlation is sufficient for pure hydrocarbons and all petroleum cuts.

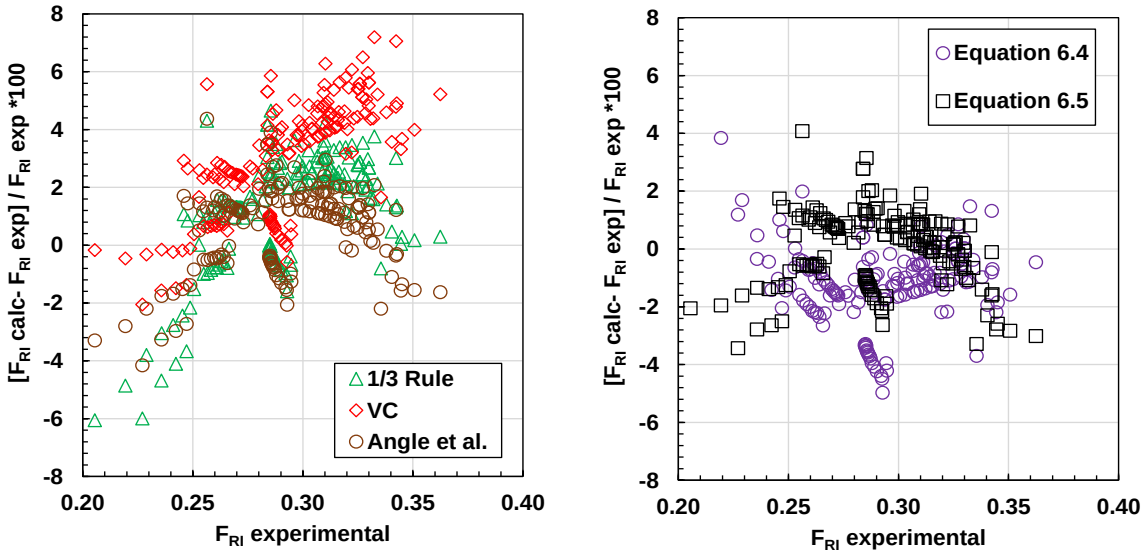

Figure 6.27. Relative error for the predicted F_{RI} of the development dataset using (left) the 1/3 rule, Vargas and Chapman (VC), and Angle *et al.* correlations, and (right) Equation 6.4, and 6.5 proposed in this work.

Table 6.23. Average relative and absolute deviations obtained using 1/3 Rule, Vargas and Chapman (VC) correlation, Equation 6.4 and 6.5 for the prediction of refractive index.

Compound	1/3 Rule		Angle *et al.*		VC		Eq. 6.4		Eq. 6.5	
	AAD	ARD [%]	AAD	ARD [%]	AAD	ARD [%]	AAD	ARD [%]	AAD	ARD [%]
Distillation cuts	0.008	2.6	0.005	1.52	0.014	4.4	0.003	1.0	0.002	0.7
Paraffins	0.005	2.3	0.003	1.45	0.002	0.8	0.005	2.0	0.003	1.3
Naphthenes	0.003	1.3	0.004	1.43	0.007	2.6	0.003	1.1	0.003	1.2
Aromatics	0.002	0.6	0.003	0.98	0.004	1.3	0.010	3.5	0.005	1.5
Saturates (SARA)	0.008	2.7	0.006	2.11	0.011	3.8	0.003	1.1	0.004	1.5
Aromatics (SARA)	0.006	1.8	0.003	0.85	0.016	4.7	0.003	0.9	0.003	0.9
Asph. (SARA)	0.024	5.4	0.033	7.71	0.015	3.6	0.011	2.6	-	-
Overall	**0.008**	**2.4**	**0.008**	**2.29**	**0.010**	**3.0**	**0.005**	**1.7**	**0.003**	**1.2**

Table 6.24. Bias obtained using 1/3 Rule, Vargas and Chapman (VC) correlation, Equation 6.4 and 6.5 for the prediction refractive index.

Compound	1/3 Rule	Angle *et al.*	VC	Eq. 6.4	Eq. 6.5
	Bias [%]	Bias [%]	Bias [%]	Bias [%]	Bias [%]
Distillation cuts	2.6	1.45	4.4	-0.9	0.5
Paraffins	-2.3	-1.40	0.1	-0.6	-1.2
Naphthenes	1.3	1.43	2.6	-0.7	1.2
Aromatics	-0.2	-0.86	1.2	-3.4	-1.5
Saturates (SARA)	2.7	2.11	3.8	-0. 9	1.5
Aromatics (SARA)	1.8	0.31	4.7	-0.9	-0.9
Asphaltenes (SARA)	-5.4	-7.71	3.4	-2.4	-
Overall	**0.06**	**-0.67**	**2.9**	**-1.4**	**-0.08**

Table 6.25. Maximum average relative and absolute deviations obtained using 1/3 Rule, Vargas and Chapman (VC) correlation, Equation 6.4 and 6.5 for the prediction of refractive index.

Compound	1/3 Rule		Angle *et al.*		VC		Eq. 6.4		Eq. 6.5	
	MAAD	MARD [%]	MAAD	MARD [%]	MAAD	MARD [%]	MAAD	MARD [%]	MAAD	MARD [%]
Distillation cuts	0.013	4.2	0.009	3.0	0.024	7.2	0.012	3.7	0.011	3.3
Paraffins	0.014	6.1	0.009	4.2	0.005	2.1	0.017	8.2	0.008	3.4
Naphthenes	0.011	4.3	0.011	4.4	0.014	5.6	0.005	2.0	0.010	4.1
Aromatics	0.013	4.7	0.011	3.9	0.017	5.9	0.006	2.2	0.009	3.2
Saturates (SARA)	0.010	3.0	0.006	2.1	0.024	7.1	0.015	5.0	0.011	3.0
Aromatics (SARA)	0.013	4.7	0.011	3.9	0.017	5.9	0.006	2.2	0.009	3.2
Asphaltenes (SARA)	0.048	10.3	0.058	12.6	0.029	7.3	0.031	7.1		
Overall	**0.017**	**5.3**	**0.017**	**4.9**	**0.018**	**5.8**	**0.013**	**4.3**	**0.010**	**3.4**

CHAPTER SEVEN: CORRELATION FOR VAPOR PRESSURE AND THERMAL PROPERTIES FOR HEAVY OILS AND BITUMEN

Vapor pressure and thermal data (heat capacity, heat of vaporization, and heat of combustion) are the backbone of the thermodynamic equilibrium calculations that, along with mass and energy balances, are required to design and simulate process units. However, it is challenging to determine the vapor pressure and thermal properties of heavy oils and bitumen because they contain high boiling point and high molecular weight compounds. These compounds have a very low volatility which is difficult to measure and challenging to extrapolate to typical operating pressures.

The vapor pressure and liquid heat capacity of the distillation cuts obtained using the DVFA-II were measured and the data were presented in Chapter 5 as part of the development of an interconversion method using constrained extrapolation of vapor pressure and heat capacity. In this chapter, the aim is to test correlations available in the literature against these data and recommend the best alternative for heavy oil and bitumen fractions. Since critical properties were not available for the cuts, only the correlations based on physical properties are tested here.

The heat of vaporization cannot be measured directly because the samples thermally decompose before reaching their normal boiling point. However, the heat of vaporization can be calculated from Cox equation that was fitted to vapor pressure data; the version is based on the direct relationship between vapor pressure and heat of vaporization through the Clapeyron equation. Although these derived property data cannot be regarded as experimental results, the calculated values are the best estimate available for heavy distillation cuts. The distillation cut data are compared with data from pure components and other crude oil mixtures. The correlations available in the literature are tested using this dataset and an alternative calculation linked with Clapeyron equation is proposed.

Finally, the heat of combustion data collected in this study for some distillation cuts are presented and the performance of correlations for the heat of combustion from elemental analysis is evaluated.

7.1 Vapor Pressure Correlations

As noted in Chapter 2, there are several correlations to predict vapor pressure that require either critical or physical properties as inputs. Only the correlations that use physical properties as input variables (Riazi, 2005; Maxwell and Bonnell, 1957) are evaluated here. Note, these correlations give the exact normal boiling point at 101325 Pa since it is an input to the equation. This constraint makes the correlations consistent with the TBP based oil characterization but not always accurate for vapor pressures below the normal boiling temperature.

Figure 7.1 compares the Riazi and M-B correlations versus the measured vapor pressure of the cuts from CO-B-B1 oil. Figure 7.2 presents the relative and absolute errors for the predicted vapor pressure values. Errors higher than 150% were observed for vapor pressures in the low and high temperature ranges for the distillation cuts. The error decreases exponentially as the pressure approaches atmospheric conditions. The high error at low pressures can be attributed to the use of reference components, such low boiling point paraffins, to develop the correlations. The extrapolation of these correlations outside their range of development is not recommended particularly at very low vapor pressure ranges (below 50000 Pa).

Note, for pressures below 1000 Pa, small magnitude deviations give high relative deviations. That is why in a relative deviation plot the errors appear to be excessively large. Since the literature correlations gave deviations higher than 300% for heavy oils distillation cuts, a new methodology to predict vapor pressure is proposed.

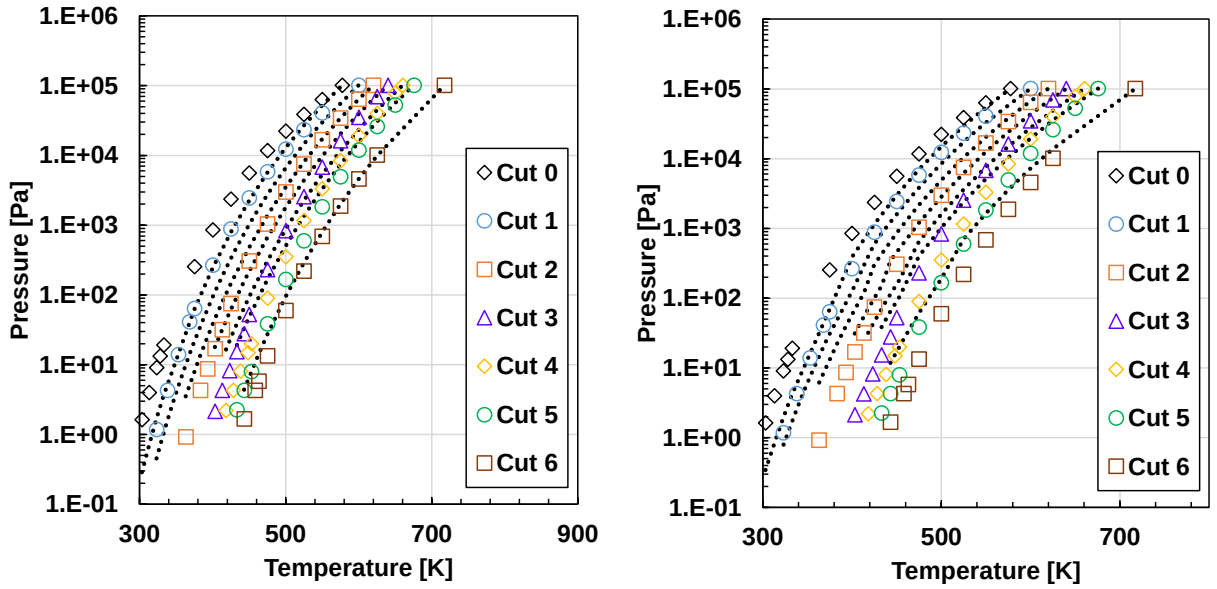

Figure 7.1. Measured and correlated vapor pressure using Riazi (left) and Maxwell and Bonnell (right) correlations for the oil sample CO-B-B1.

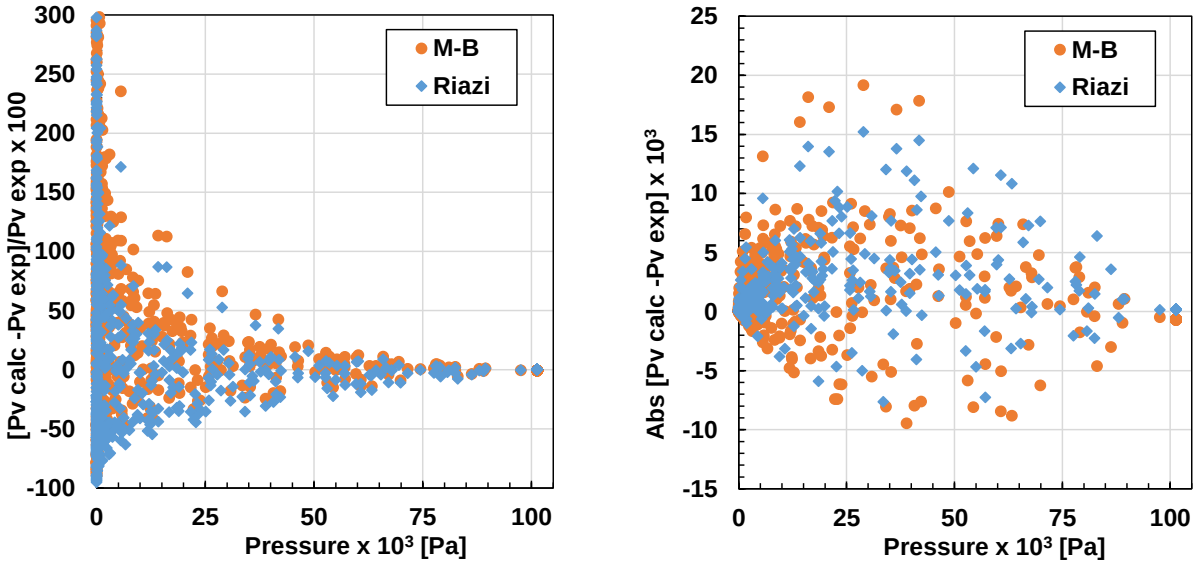

Figure 7.2. Relative (left) and absolute (right) deviations obtained for vapor pressure prediction using Riazi and M-B correlations for the 63 distillation cuts collected in this work.

Recall that the measured vapor pressure for the distillation cuts reported in Chapter 5 were simultaneously fitted with heat capacity data using the three parameter Cox equation. Figure 7.3 shows that the *average* values of the fitted parameters, do follow consistent trends versus

molecular weight. This, could form the basis of a correlation. The parameters have the following functional form in terms of the molecular weight:

$$A_0 = A_{01} + A_{02}\left[1 - \exp\left(-\frac{A_{03}MW}{100}\right)\right] \tag{7.1}$$

$$A_1 = A_{11}MW^2 + A_{12}MW + A_{13} \tag{7.2}$$

$$A_2 = A_{21} + A_{22}\left[1 - \exp\left(-\frac{A_{23}MW}{100}\right)\right] \tag{7.3}$$

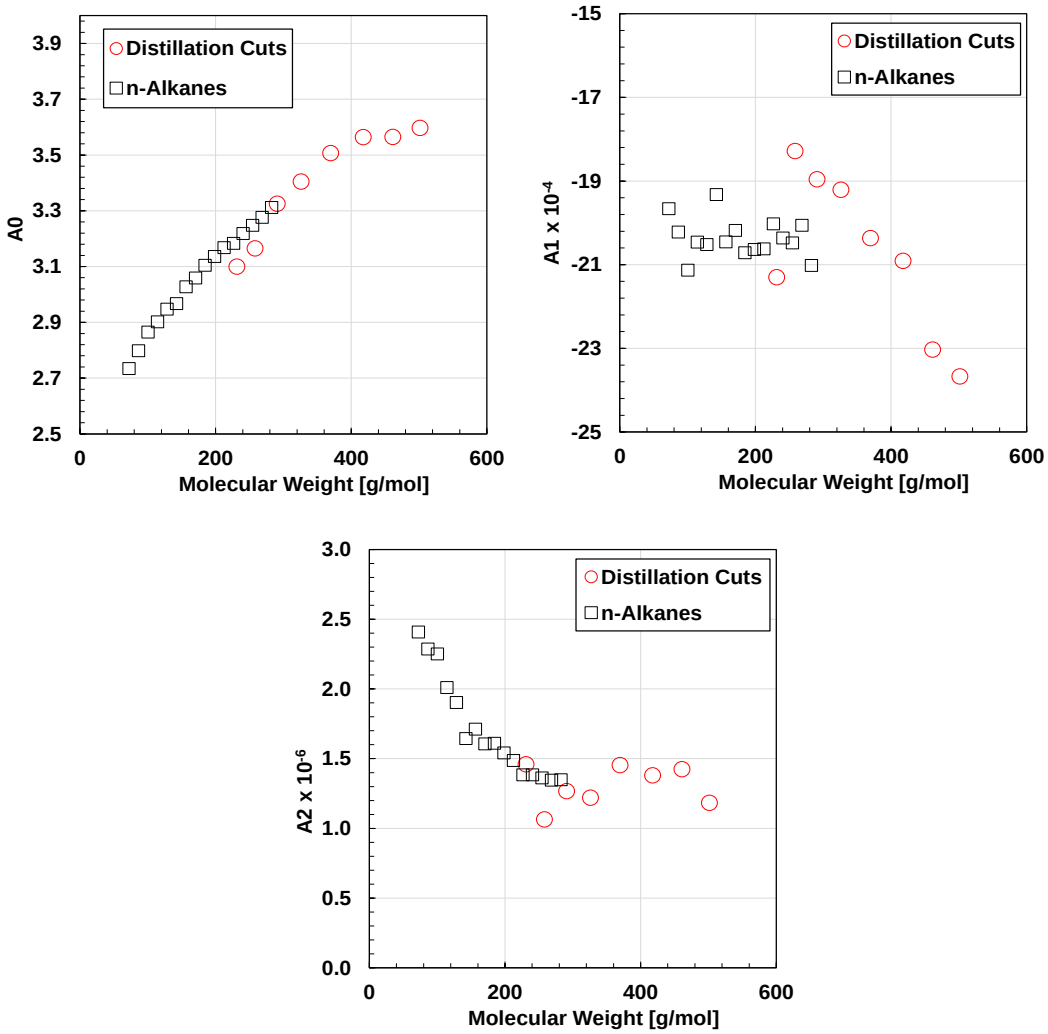

Figure 7.3. Trends obtained between molecular weight and Cox constants obtained in constrained extrapolation of vapor pressure and heat capacity a) constant A_0 b) constant A_1 and c) constant A_2

However, the average parameters are not constrained to provide the correct normal boiling point and do not fit the individual oil data. Therefore, the Cox correlation was constrained to match the NBP from the oil characterization by setting the reference temperature equal to the NBP as follows:

$$ln\left(\frac{P_{sat}}{P_b}\right) = \left(1 - \frac{T_{NBP}}{T}\right)\exp(A_0 + A_1 T + A_2 T^2) \tag{7.4}$$

where T_{NBP} is the normal boiling point. Finally, in order to better constrain the data fitting to obtain the correct shape of the vapor pressure curve, the following data were included:

1. measured vapor pressure (low pressure range)
2. experimental NBP obtained from oil characterization
3. synthetic data 'generated' from the Cox correlation using individually fitted Cox constants for each cut

The constants were then adjusted to minimize the following optimization function (OF) for the development dataset:

$$OF = \left[\frac{1}{n}\sum_{i=1}^{n}\left(P_{vi}^{calc} - P_{vi}^{exp}\right)^2\right] \tag{7.5}$$

where P_{vi}^{calc} and P_{vi}^{exp} are the calculated and the experimental vapor pressure respectively and n is the number of experimental points. The optimized constants are summarized in Table 7.1.

Table 7.1. Constants of Equations 7.1 to 7.3.

Constant: A_0		**Constant: A_1 [K^{-1}]**		**Constant: A_2[K^{-2}]**	
A_{01}	-1.7348	A_{11}	-0.00014	A_{21}	4.4414
A_{02}	5.3750	A_{12}	0.08681	A_{22}	-3.1774
A_{03}	0.9799	A_{13}	-33.3372	A_{23}	1.3091

The deviations for the predicted vapor pressure for the distillation cuts from the proposed correlation and for the RD and MB correlations are compared in Figure 7.4. Table 7.2 and Table

7.3 compares the average and maximum errors for each cut respectively. Using Equations 7.1 and 7.2 to 7.3, the vapor pressures of the distillation cuts were fitted with an average relative deviation of less than 64% compared with 150 and 263% obtained from Riazi and M-B correlations, respectively. Figure 7.4 shows that, despite the high errors in the low vapor pressure range, all correlations predict vapor pressures above 50000 Pa with a maximum deviation of 20%. The new correlation was able to keep this low error for a wider pressure range starting from pressures as low as 20000 Pa, assuming the circled points are outliers (as will be discussed later). Above 50000 Pa, the new correlation has an error of approximately 10% compared with 20% for M-B and Riazi correlations. A drawback of the new correlation is that errors of up to 100% are still obtained in the pressure range lower than 10000 Pa. However, practically speaking, predictions for a pressure range below 10000 Pa are not required for most industrial purposes.

The fact that the M-B correlation has the lowest error for the heaviest cut. This is probably because Tsonopoulos modified the temperature correction factor for coal liquid samples. Coal samples are expected to be more similar to the heaviest cut rather than to the intermediate cuts where less polyaromatic hydrocarbons are present.

Overall, for all of the correlations, the majority of the deviations were localized in Cuts 4 and 5. Although not explicitly shown in Table 7.2, these large deviations were mainly from the MX-HO-A1 oil sample (outliers in Figure 7.4). For cuts 4 and 5 of MX-HO-A1 oil, the measurement of vapor pressure required more cycles to reach a constant reading compared with the other oil distillation cuts. Hence, there may have been greater light-end losses causing a change in the initial composition of the distillation cuts.

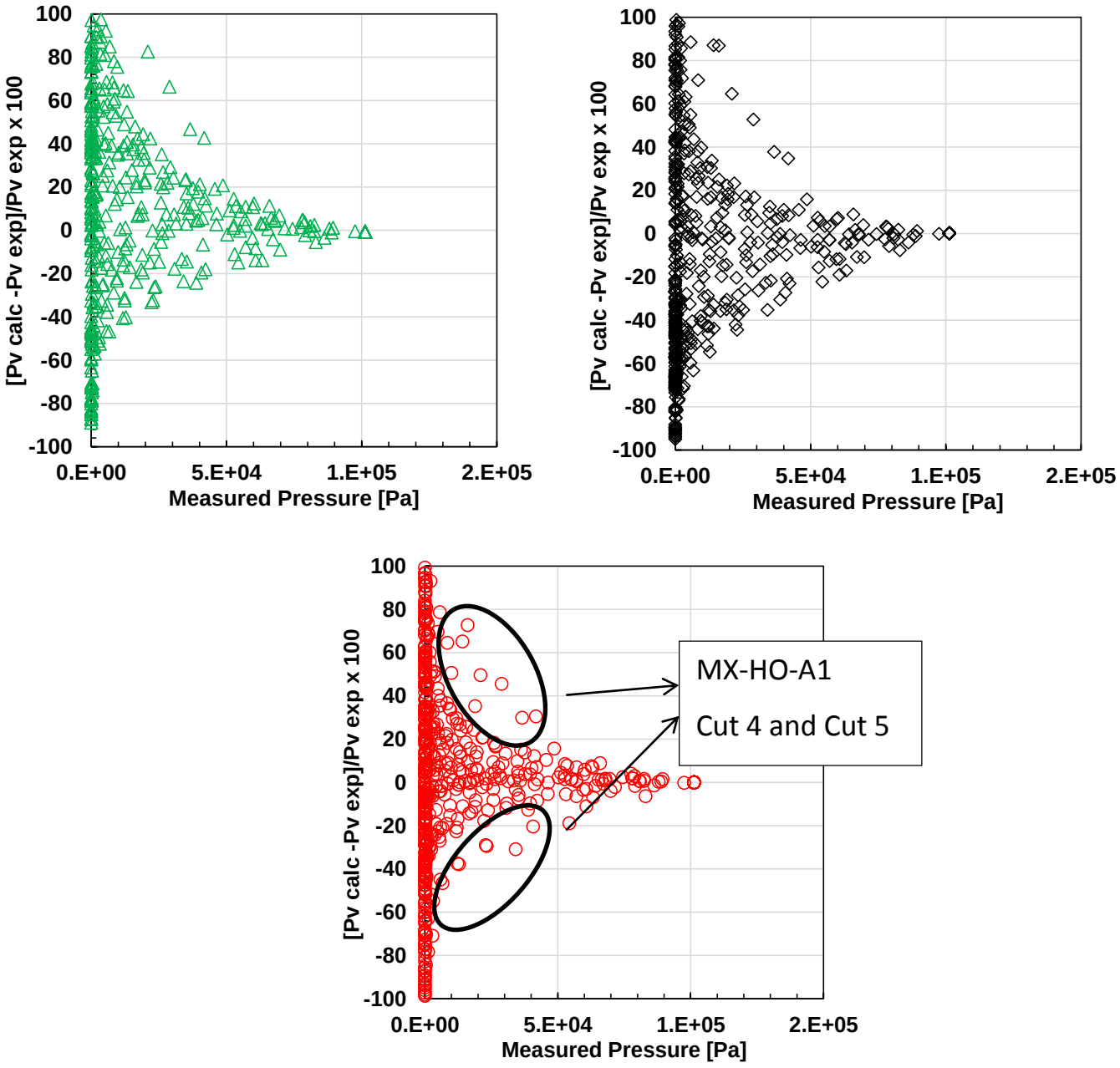

Figure 7.4. Dispersion plot for vapor pressures of the development dataset determined from the M-B (top left), Riazi (top right), and new correlation (bottom). Possible outliers are circled in the right hand plot.

Table 7.2. Average absolute and relative deviations obtained per cut from three different vapor pressure correlations.

Distillation Cut	Riazi			M-B			This study		
	Bias [%]	ARD [%]	AAD [Pa]	Bias [%]	ARD [%]	AAD [Pa]	Bias [%]	ARD [%]	AAD [Pa]
Cut 0	-22	43	1852	-12	41	1444	-8	26	811
Cut 1	38	92	1443	83	121	1390	13	52	948
Cut 2	154	181	1304	273	289	1853	54	79	1046
Cut 3	135	151	944	277	278	1501	21	42	572
Cut 4	324	334	1202	651	651	2355	82	102	783
Cut 5	313	316	1267	702	703	2425	111	125	1214
Cut 6	3	42	841	113	114	703	22	32	591
Cut 7	-41	41	1597	20	31	577	45	49	480
Overall	**113**	**150**	**1306**	**263**	**278**	**1531**	**42**	**63**	**806**

Table 7.3. Average absolute and relative deviations obtained per cut from three different vapor pressure correlations.

Distillation Cut	Riazi		MB		This study	
	MARD [Pa]	MAAD [%]	MARD [Pa]	MAAD [%]	MARD [Pa]	MAAD [%]
Cut 0	162	11897	157	9462	119	4915
Cut 1	595	11549	894	8449	249	8339
Cut 2	1466	12106	2556	10118	750	10564
Cut 3	1424	5064	2196	9244	297	4747
Cut 4	3876	13799	8326	17308	1294	10927
Cut 5	5911	15227	13806	19173	1984	13151
Cut 6	248	7097	716	5283	174	5479
Cut 7	68	8864	135	3670	370	6657
Overall	**1719**	**10700**	**3598**	**10338**	**655**	**8097**

The correlations were tested on a test dataset that was separated into the following four groups to better determine the type of samples for which the correlations give the most accurate vapor pressure predictions.

1) a paraffinic set of distillation cuts from the ALT oil (Sturm and Shay, 2000).
2) an intermediate set of distillation cuts from the ANS oil (Sturm and Shay, 2000).
3) an aromatic set of distillation cuts from the SJV oil (Sturm and Shay, 2000).
4) a Western Canadian Bitumen, its de-asphalted fraction, and eicosane (Castellanos *et al.*, 2012).

Figure 7.5 presents the dispersion plot that compares the fit obtained for the four test datasets using Riazi, M-B, and the new correlation. Tables 7.4 to 7.7 report the absolute and average deviations for each set individually. The maximum deviations are summarized in Appendix H. Overall, the M-B and the new correlation perform better than the Riazi correlation. The Riazi correlation, as indicated by the author, is a good correlation for vapor pressures near the normal boiling point. It is not surprising that it performs poorly for datasets outside this range. The performance of the M-B correlation is slightly better for the first three datasets but the new correlation provides significantly better predictions for the heaviest cuts and for the fourth, most aromatic, dataset. As intended, the new correlation is well suited to predict the vapor pressure of heavy petroleum fractions. Note, the new correlation must be used with caution for samples with molecular weight values less than 200 g/mol since this was the lowest MW in the set of distillation cuts used to develop the new correlation.

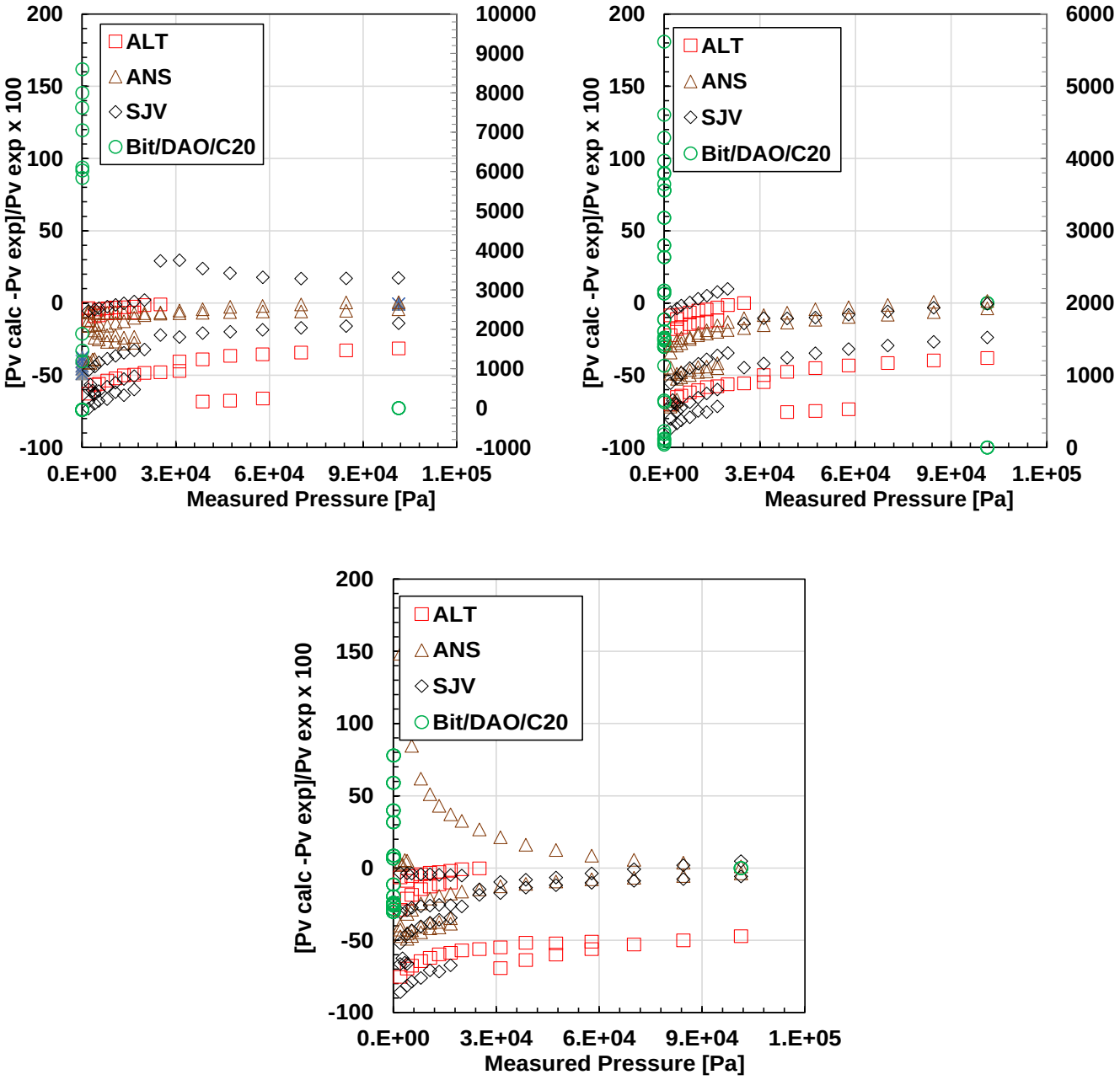

Figure 7.5. Dispersion plot for vapor pressures from the test dataset determined from the M-B (top left), Riazi (top right), and the new correlation (bottom). The secondary axis in top plots was required to observe errors for the fourth group in the test dataset.

Table 7.4. Average absolute and relative deviations obtained for first group in the test dataset from three different vapor pressure correlations.

Sample	This study		M-B		Riazi	
	ARD [%]	AAD [Pa]	ARD [%]	AAD [Pa]	ARD [%]	AAD [Pa]
ALT/Cut 550-600	9	1300	5	1000	10	1600
ALT/Cut 650-750	48	8500	32	6100	38	7100
ALT/Cut 750-850	62	4400	52	3700	60	4300
ALT/Cut 850-950	52	1900	67	2500	75	2800
Overall	**44**	**3900**	**41**	**3400**	**52**	**4200**

Table 7.5. Average absolute and relative deviations obtained for the second group in the test dataset from three different vapor pressure correlations.

Sample	This study		M-B		Riazi	
	ARD [%]	AAD [Pa]	ARD [%]	AAD [Pa]	ARD [%]	AAD [Pa]
ANS/Cut 320-450	30	4000	7	3300	11	5300
ANS/Cut 550-600	13	2900	5	2300	14	4200
ANS/Cut 750-850	44	3700	24	2300	49	4100
ANS/Cut 850-950	4	120	40	1200	69	2100
Overall	**38**	**4300**	**36**	**4200**	**47**	**5200**

Table 7.6. Average absolute and relative deviations obtained for the third group in the test dataset from three different vapor pressure correlations.

Sample	This study		M-B		Riazi	
	ARD [%]	AAD [Pa]	ARD [%]	AAD [Pa]	ARD [%]	AAD [Pa]
SJV/Cut 450-650	29	6300	41	8700	51	10100
SJV/Cut 500-550	7	3500	11	3000	18	6000
SJV/Cut 600-650	8	1600	20	3000	7	1100
SJV/Cut 650-750	72	14000	64	14000	75	15500
SJV/Cut 750-850	86	5600	81	5300	90	6000
SJV/Cut 850-950	35	1600	45	1300	76	2300
Overall	**42**	**5600**	**44**	**5800**	**53**	**7000**

Table 7.7. Average absolute and relative deviations obtained for the fourth group in the test dataset from three different vapor pressure correlations.

Sample	This study		M-B		Riazi	
	ARD [%]	AAD [Pa]	ARD [%]	AAD [Pa]	ARD [%]	AAD [Pa]
Bitumen WC-B-B1	33	17	1500	600	800	200
Maltenes WC-B-B1	91	13	7000	600	4200	400
Eicosane	26	1	40	1	120	2
Overall	**50**	**10**	**2900**	**400**	**1700**	**200**

An attempt was made to correlate the Cox constants with NBP instead of MW; however, the deviations were significantly higher compared with the correlations using MW for both the development and test datasets. The correlation with MW also includes NBP through Eq. 7.4, while a correlation to NBP only has the one input. It may be possible that two input variables are required to accurately predict vapor pressure. Note, if molecular weight is not available as part of the characterization data, it can be calculated from Equation 6.1 using NBP and SG as inputs.

7.2 Liquid Heat Capacity

As introduced in Chapter 2, the most commonly used correlations available in the literature to determine the liquid heat capacity at constant pressure from physical properties are the Lee-Kesler (1976), Dagostar (2013), and Tsonopoulos (1986) correlations. The correlations were tested on a development dataset that included the following distillation cuts for which liquid heat capacity were available:

- WC-B-B1 Cut 0 to Cut 6
- CO-B-A1 Cut 0 to Cut 6
- MX-B-A1 Cut 0 to Cut 4
- CO-B-B1 Cut 0 to Cut 3

Figure 7.6 shows the measured and correlated liquid heat capacities, C_p^{liq}, versus temperature for the WC-B-B1 distillation cuts as an example. Figure 7.7 presents the deviations for all of the above correlations from the measured C_p^{liq} of the distillation cuts. The average and maximum absolute and relative deviations and the bias obtained for each correlation are reported in Table 7.8.

The lowest relative deviations and bias was observed for the Lee-Kesler (1976) correlation. The lowest deviations obtained with the Lee-Kesler correlation were for the lightest fractions (Cut 0 and Cut 1); however, the deviations significantly increased from the low to high boiling fractions reaching a maximum relative deviations of 12%. The Dagostar (2013) correlation, which uses elemental analysis as input, had the highest deviation, 6.3%. The poor performance of the Dagostar correlation can be attributed to the significant diversity in structures within a single distillation cut. Recall that this correlation was developed with pure components and does not account for molecular polydispersity. The Tsonopoulos (1986) correlation had a higher average deviation than the Lee-Kesler correlation (4.5% versus 3.6%) but had the lowest maximum average and relative deviations (0.14 J/mol K and 7.3% respectively).

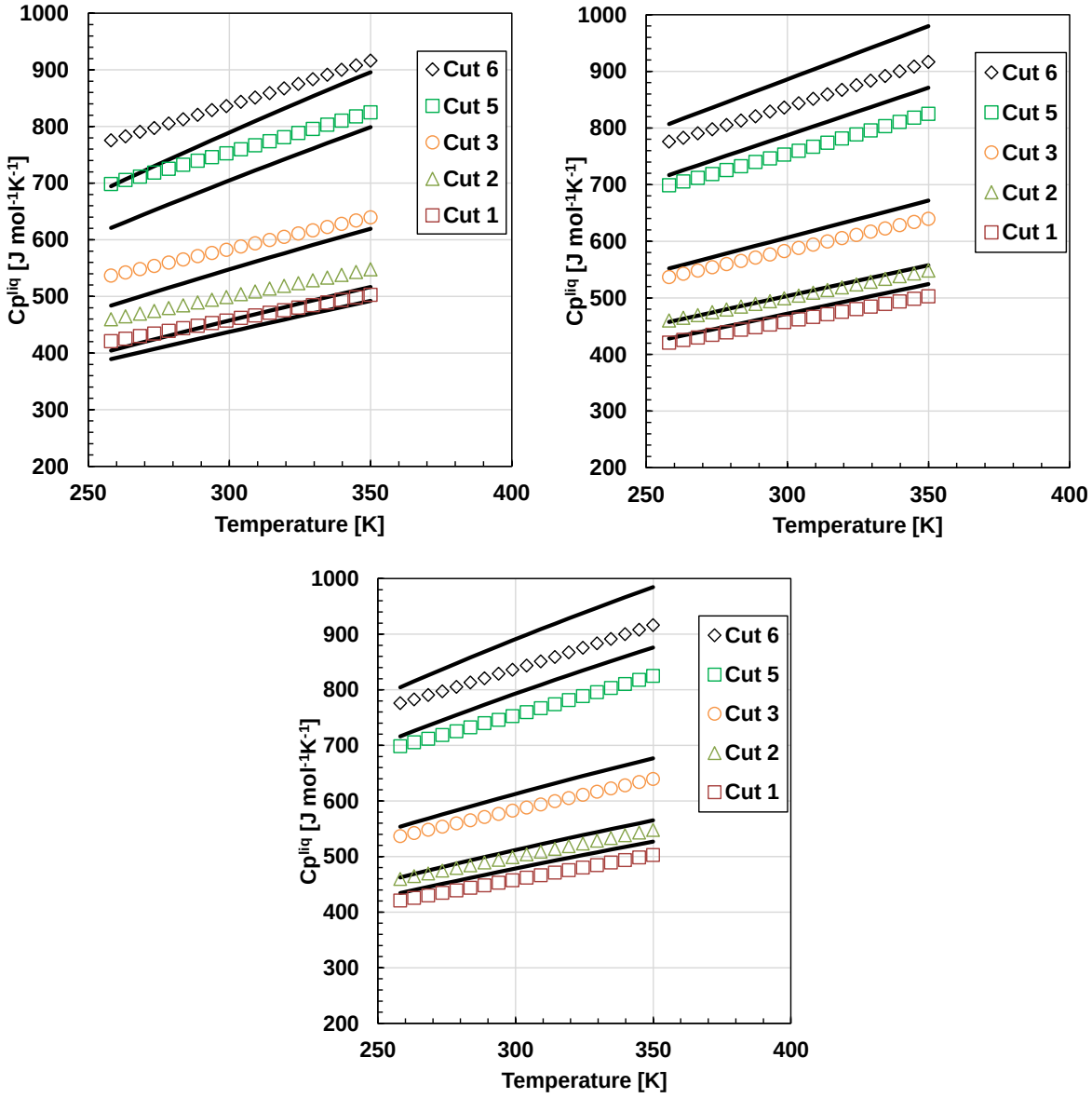

Figure 7.6. Measured and correlated C_p^{liq} versus Temperature for the WC-B-B1 distillation cuts using Lee-Kesler (top left), Tsonopoulos (top right) and Dagostar (bottom) correlations.

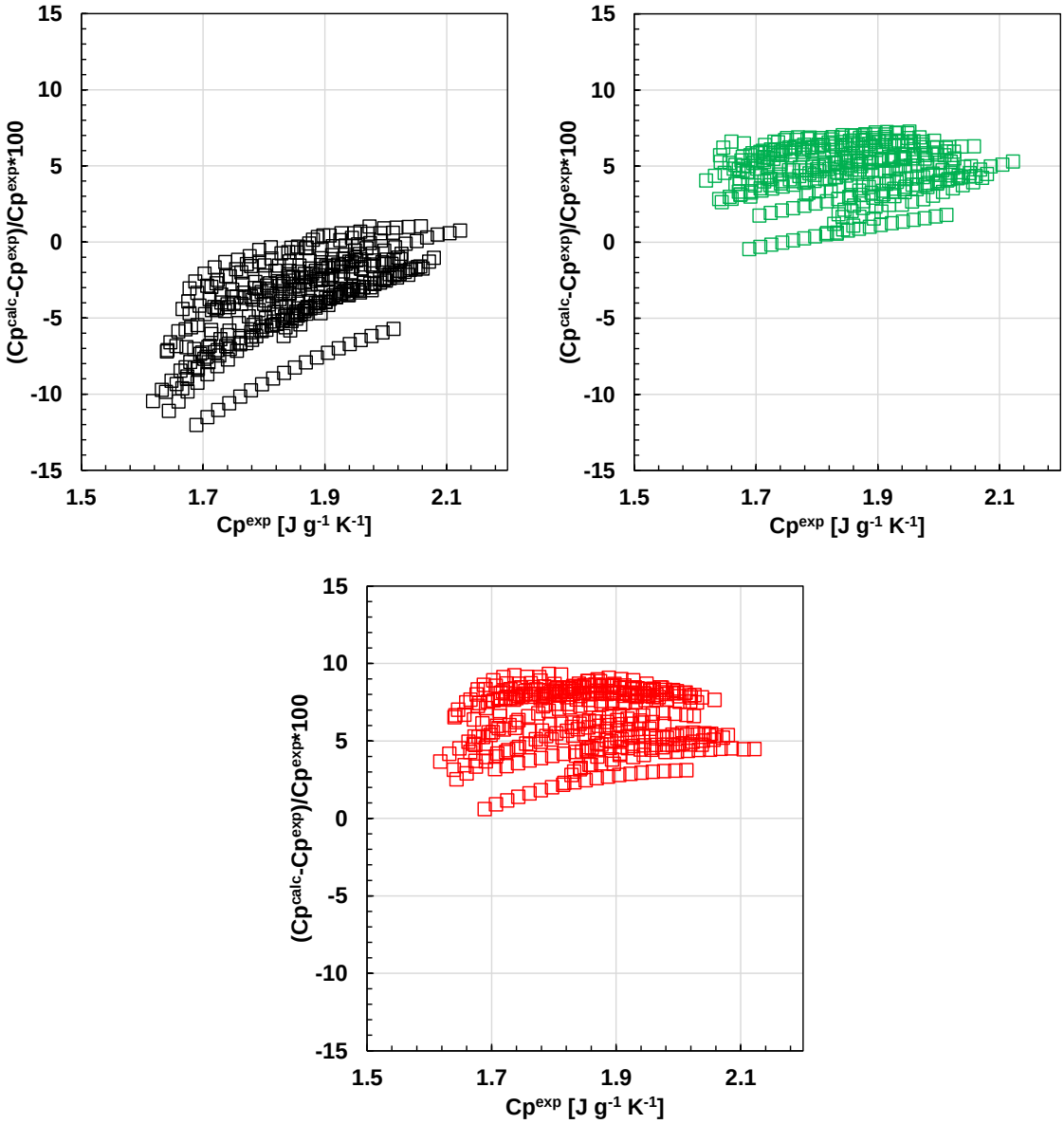

Figure 7.7. Relative error obtained for predicted Cp^{liq} using Lee-Kesler (left), Tsonopoulos (centre) and Dagostar (right) correlations.

Table 7.8. Average absolute and relative deviations, maximum absolute and relative deviations, and bias for Cp^{liq} obtained using correlations from literature for the development dataset.

Correlation	AAD [J/g K]	ARD [%]	MAAD [J/g K]	MARD [%]	Bias [%]
Lee-Kesler	0.07	3.6	0.14	8.3	-3.6
Tsonopoulos	0.08	4.5	0.13	6.6	4.4
Dagostar	0.12	6.3	0.15	8.1	6.1

Overall the correlations do not accurately predict the heat capacity of the high boiling fractions. However, the Tsonopoulos correlation had a systematic error that can be decreased by tuning the correlation to a more aromatic and high boiling point dataset. The Tsonopoulos correlation is provided below:

$$C_p^{liq} = (A_1 + A_2 K_w) * \left[A_3 - A_4 SG + (A_5 - A_6 SG)\left(\frac{T}{1000} - A_7\right)\right] \tag{7.6}$$

where K_w is the Watson factor, SG is the specific gravity and T is the temperature in K. Note that this correlation uses the Watson Factor; therefore, NBP and SG are required inputs. The correlation was retuned by adjusting the constant to fit the development dataset. The new sets of constants for the retuned correlation are given in Table 7.9.

For cases where distillation data are not available, an alternative to Equation 7.6 was proposed with SG and H/C ratio as inputs. The correlation was first introduced in Chapter 5 and is presented again below for the sake of convenience:

$$C_p^{liq} = (A_1 + A_2 C_S) * \left[A_3 - A_4 SG + (A_5 - A_6 SG)\left(\frac{T}{1000} - A_7\right)\right] \tag{5.15}$$

$$C_S = \exp\left(-\frac{2.214}{H/C}\right) \tag{5.16}$$

The constants are presented in Table 7.9. Note, both correlations have the same set of constants from A2 to A7 and only a slight modification of constant A1 in Equation 7.6 was required to make it a function of H/C ratio (Eq. 5.15 and 5.16). Do recall, as shown in Chapter 6, the H/C ratio is an alternative characterization factor to the Watson factor, K_w, and it seems to better capture the relative structural changes within the oil. If elemental compositions are not available, the H/C ratio can be determined from SG using Equation 7.3.

Table 7.9. Constants for original (Equation 7.6), refitted Tsonopoulos, and modified (Equation 5.15) Tsonopoulos correlations for specific liquid heat capacity.

Coefficient	Original	Retuned	Modified
A_1	0.28299	1.621	1.539
A_2	0.23605	0.007	0.007
A_3	0.645	0.733	0.733
A_4	0.05959	0.076	0.076
A_5	2.32056	4.401	4.401
A_6	0.94752	2.341	2.341
A_7	0.25537	0.092	0.092

Figure 7.8 presents the relative deviation plots of the C_p^{liq} predictions for the development dataset from the original and modified versions of the Tsonopoulos correlation. The average absolute and relative deviations and bias for the original and modified Tsonopoulos correlations are summarized in Table 7.10 and the maximum deviations in Table 7.11. The retuned and new correlations significantly improved the heat capacity predictions for the development dataset, reducing the ARD to approximately 1% and the maximum deviations from 4.5% to approximately 2.3%. Although not shown explicitly in Table 7.10, for Equation 7.6 and 5.15, the highest deviations were observed in the lightest distillation cuts (Cut 0). This cut is distinct in chemistry from the other cuts; as it is paraffinic while the others have more aromatic content. While elemental

composition is the dominant contribution to heat capacity, molecular structure also has an effect. The proposed correlations appear to be slightly biased towards aromatic and mixed chemistry cuts and is less accurate for low boiling paraffinic cuts.

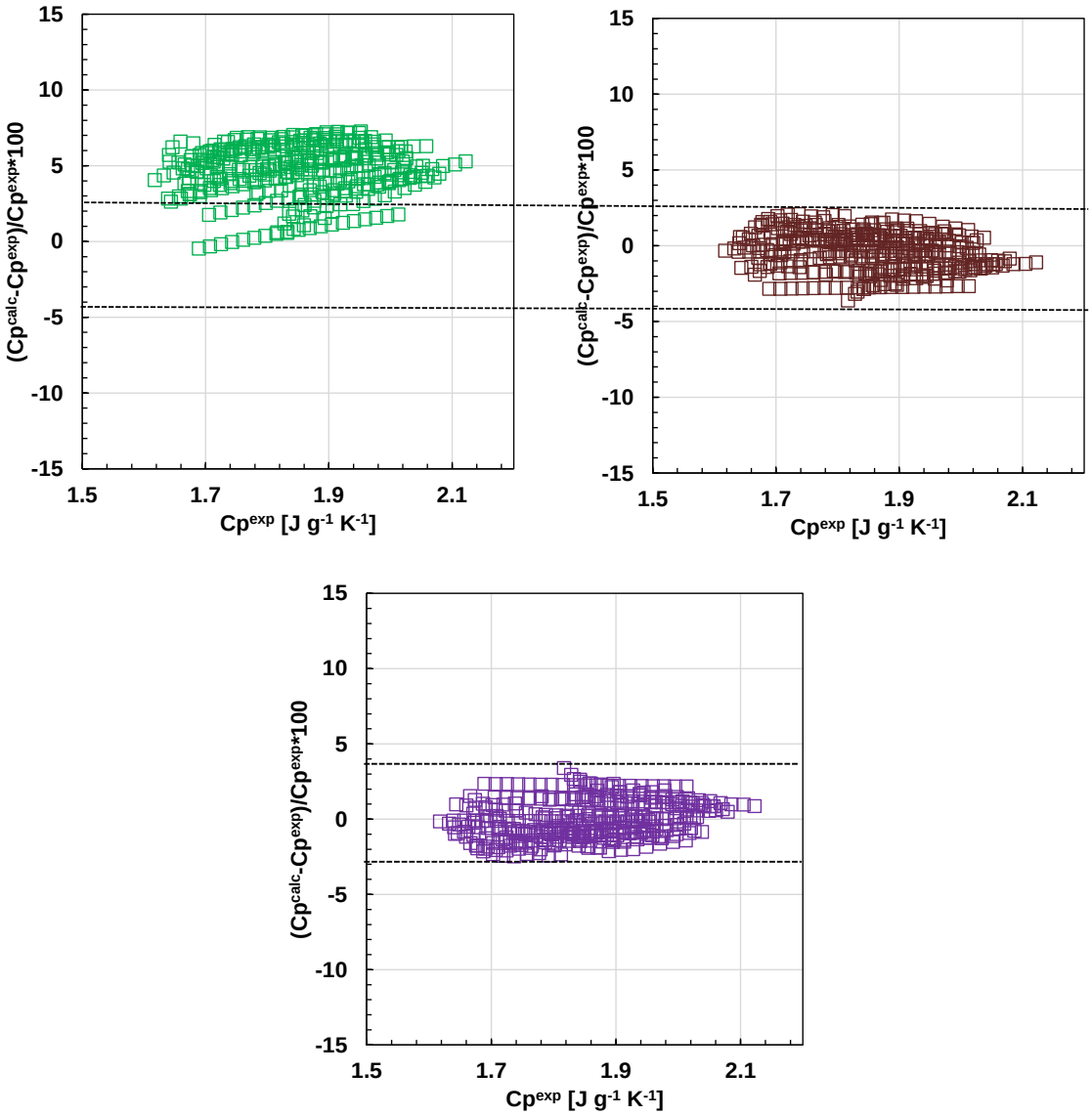

Figure 7.8. Relative error obtained for predicted C_p^{liq} of the development dataset using original Tsonopoulos using Watson factor (top left), retuned Tsonopoulos (top right), and modified Tsonopoulos using H/C ratio (bottom) correlations.

Table 7.10 Average absolute and relative deviations and bias from the retuned Tsonopoulos using Watson factor and modified Tsonopoulos using H/C ratio correlations for C_p^{liq} for the development dataset.

Oil Sample	Retuned (Kw)			Modified (H/C)		
	ARD [%]	AAD [J/g K]	Bias [%]	ARD [%]	AAD [J/g K]	Bias [%]
WC-B-B1	1.2	0.02	-1.1	1.0	0.02	0.6
CO-B-A1	1.1	0.02	0.5	1.3	0.02	-0.9
MX-HO-A1	1.5	0.03	-1.5	1.2	0.02	1.2
CO-B-B1	0.5	0.01	0.2	0.6	0.01	-0.6
Overall	**1.1**	**0.02**	**-0.5**	**1.0**	**0.02**	**0.1**

Table 7.11. Maximum average absolute and relative deviations and bias from the retuned Tsonopoulos using Watson factor and modified Tsonopoulos using H/C ratio correlations for C_p^{liq} for the development dataset.

Oil Sample	Retuned (Kw)		Modified (H/C)	
	MARD [%]	MAAD [J/g K]	MARD [%]	MAAD [J/g K]
WC-B-B1	2.9	0.05	2.4	0.04
CO-B-A1	2.3	0.05	2.5	0.04
MX-HO-A1	3.6	0.07	2.7	0.06
CO-B-B1	1.0	0.02	1.3	0.03
Overall	**2.4**	**0.05**	**2.2**	**0.04**

The original, retuned, and modified Tsonopoulos correlations were evaluated against an independent test dataset that included distillation cuts for the following oils:

- MX-B-A1 cut 5 to cut 7
- CO-B-B1 cut 4 to cut 6
- Mayan Oil (Fulem *et al.*, 2008)

The test dataset was small because several physical properties were required to test both correlations simultaneously and few datasets in the literature included C_p^{liq}, NBP, SG, and H/C ratio.

Figure 7.9 is a dispersion plot for the original, retuned, and modified Tsonopoulos correlations applied to the test dataset. The deviations are summarized in Table 7.12 and 7.13. The proposed correlations significantly improve the predictions of the liquid heat capacity (AARD of 1.5% compared with 6% from the original Tsonopoulos correlation). The maximum deviations were reduced to less than 2% compared with 7% from the original correlation. Both the retuned (Equation 7.6) and modified (Equation 5.15) correlations predict the heat capacities to within the experimental error of the measurements (≈1%). The modified correlation has a better performance for a wider range of liquid heat capacities with the lowest average and maximum deviations and lowest bias. Note for the distillation cuts, both correlations have a deviation of less than 0.2%. A greater difference is observed for the Mayan crude oil where the modified correlation outperforms the retuned correlation by 1.6%. The retuned and modified correlations appear to be well suited for heavy oils but have not been tested on conventional oils.

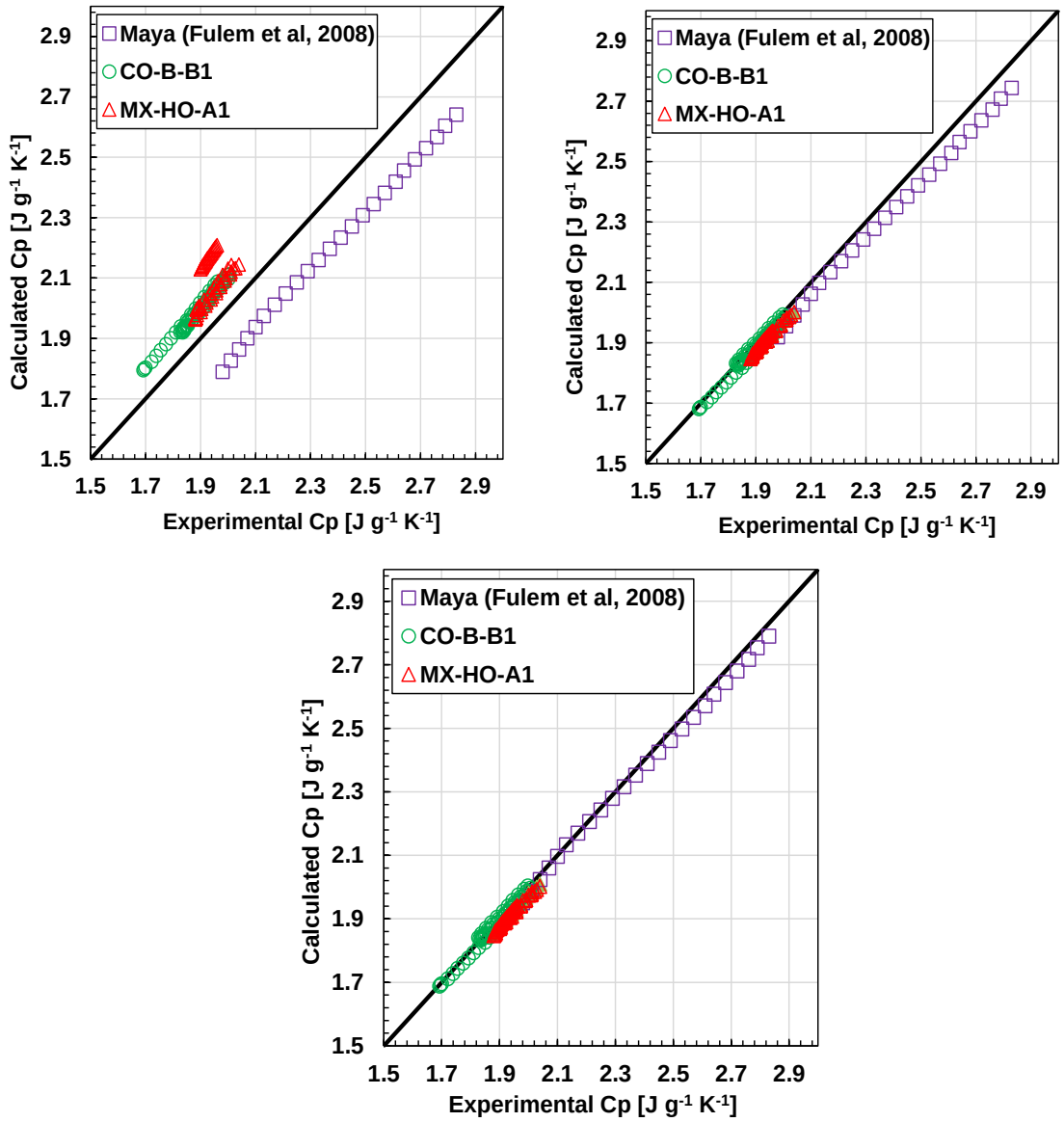

Figure 7.9. Dispersion plots for the C_p^{liq} of the test dataset determined from: original Tsonopoulos using Watson factor (top left), retuned Tsonopoulos (top right), and modified Tsonopoulos using H/C ratio (bottom) correlations.

Table 7.12. Average relative deviation obtained for original, retuned and modified versions of Tsonopoulos correlations for the test dataset.

Oil Sample	Original Tsonopoulos			Retuned (Kw)			Modified (H/C)		
	AAD [J/g K]	ARD [%]	Bias [%]	AAD [J/g K]	ARD [%]	Bias [%]	AAD [J/g K]	ARD [%]	Bias [%]
Maya (Fulem *et al*, 2008)	0.18	7.5	-7.5	0.06	2.5	-2.5	0.02	0.9	-0.9
MX-HO-A1	0.10	5.1	5.1	0.03	1.6	-1.6	0.02	1.3	-1.3
CO-B-B1	0.10	5.4	5.4	0.01	0.4	-0.2	0.01	0.4	0.3
Overall	**0.13**	**6.0**	**1.0**	**0.03**	**1.5**	**-1.4**	**0.02**	**0.9**	**-0.6**

Table 7.13. Maximum average relative deviation obtained for original, retuned and modified versions of Tsonopoulos correlations for the test dataset.

Oil Sample	Original Tsonopoulos		Retuned (Kw)		Modified (H/C)	
	MAAD [J/g K]	MARD [%]	MAAD [J/g K]	MARD [%]	MAAD [J/g K]	MARD [%]
Maya (Fulem *et al*, 2008)	0.19	9.6	0.09	3.2	0.04	1.6
MX-HO-A1	0.11	5.9	0.04	1.8	0.03	1.5
CO-B-B1	0.11	5.7	0.02	0.9	0.02	0.9
Overall	**0.14**	**7.1**	**0.05**	**2.0**	**0.03**	**1.3**

7.3 Heat of Vaporization

In Chapter 2 several correlations were presented that could be used to determine the heat of vaporization at the normal boiling point (Riazi, 2005; Vetere, 1995; Gopinathan, 2001; and Fang, 2005). To test the correlations, it was first necessary to generate heat of vaporization data. Unfortunately, the enthalpy of vaporization of a heavy hydrocarbon cannot be measured directly at its normal boiling point because heavy hydrocarbons decompose below this temperatures (at

atmospheric pressure). Instead, as noted in Chapter 5, it can be calculated from vapor pressure data through the Clausius-Clapeyron equation,

$$-\frac{\Delta H^{vap}}{R} = \frac{dP_{sat}}{d(1/T)} \quad (5.1)$$

Since the parameters of the Cox equation were obtained from the fitting of both vapor pressure and heat capacity, this same set of parameters can be used to determine ΔH^{vap} using Equations 7.7 and 7.8, which are a derived form of the Cox equation for the heat of vaporization:

$$\Delta H^{vap} = R[T_b + (T - T_b) * (A_1 T + A_2 T^2)]\exp(A_0 + A_1 T + A_2 T^2) \quad (7.7)$$

When $T=T_b$, this equation reduces to:

$$\Delta H_{nbp}^{vap} = \text{R}\, T_b \exp(A_0 + A_1 T_b + A_2 T_b^2)\,/1000 \quad (7.8)$$

The heats of vaporization determined using Equation 7.8 are provided in Appendix H. The 'experimental' ΔH^{vap} follows the expected trends with temperature and molecular weight, Figure 7.10, for Cuts 1, 3 and 6 from WC-B-B1. The values of ΔH^{vap} decrease as the temperature increases and approaches the normal boiling point. The higher the temperature of the fluid, the higher the kinetic energy of the molecules relative to the intermolecular forces. Therefore to break intermolecular forces at a higher temperature requires less energy than at a lower temperature. The heat of vaporization trend increases from the lowest boiling to highest boiling cuts as their MW increases. The attractive forces between the molecules tend to be greater for larger molecules and therefore they have larger heats of vaporization.

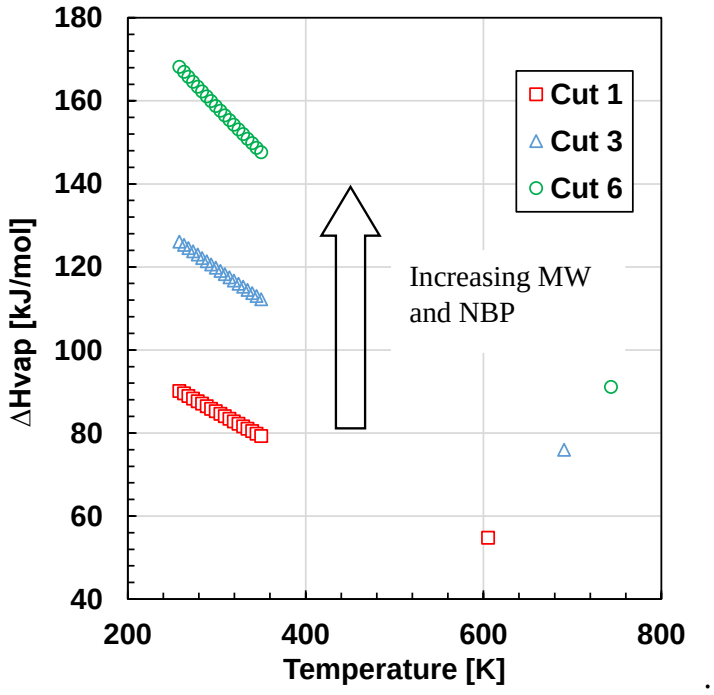

Figure 7.10. Heat of vaporization of three distillation cuts from WC-B-B1 versus temperature.

Note, the 'experimental' heats of vaporization may not correspond to the actual experimental values due to the assumptions made during the development of Equation 5.1. To check the results, the ΔH_{nbp}^{vap} values for the distillation cuts are compared with the known heats of vaporization of pure components versus molecular weight, Figure 7.11. Note, there are two trends for pure components, one for the paraffinic compounds and another for aromatic and PAH compounds. The PAHs follow a different trend because the intermolecular attraction between aromatic rings is relatively strong. Hence, their heat of vaporization is greater than those of paraffinic and naphthenic compounds of the same molecular weight. Although the data for the distillation cuts are scattered, their calculated heats of vaporization fall between the two trends as is expected based on their mixed chemistry. The distillation cuts shift from near paraffinic values to near aromatic values from lighter to heavier cuts, consistent with the increasing aromaticity of the cuts. Since no experimental data are available for the cuts, the deviation for ΔH_{nbp}^{vap} from the actual value was assumed to be within the reported values for *n*-alkanes from Ruzicka *et al.* (2004); that is, less than 6%.

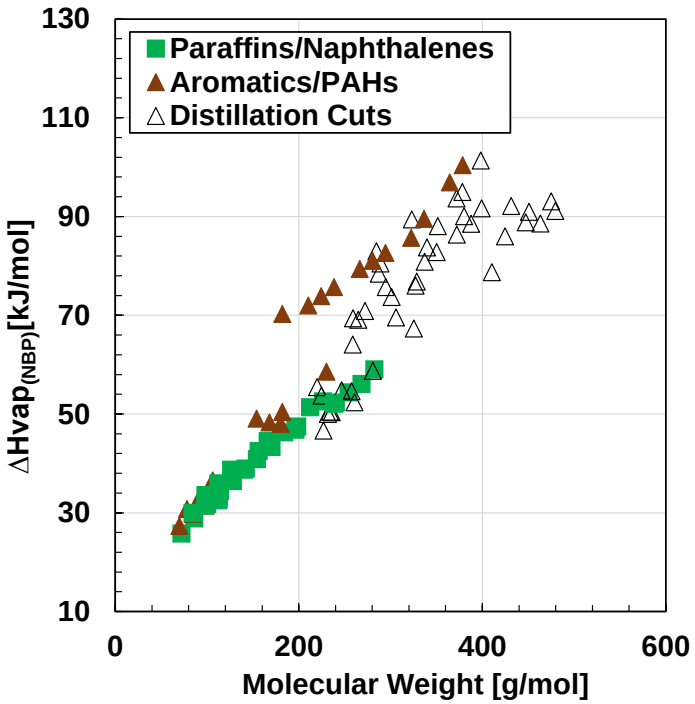

Figure 7.11. Heat of vaporization at the normal boiling point versus molecular weight for pure hydrocarbons and the DVFA distillation cuts.

The heats of vaporization from this study as well as for selected pure hydrocarbons, Table 7.14, were used to test the correlations obtained from the literature and to develop a new correlation. The deviations of the literature correlations developed by Riazi (2005), Vetere (1995), Gopinathan (2001) and Fang (2005) are shown in Figure 7.12 and summarized in Table 7.15. Although not shown explicitly in Table 7.15, the highest deviations for all the correlations were obtained for the distillation cuts and the aromatic/PAHs. These high errors likely arise because there were no aromatic compounds in the datasets used to develop these correlations. Also, as shown in Figure 7.11, if the PAHs are neglected as part of the dataset, the predicted heat of vaporization will correspond to the lower trend observed for the paraffinic and naphthenic compounds and the heat of vaporization of PAHs will be significantly under-predicted. Hence, there is potential to develop an improved correlation for the heat of vaporization correlations of heavy cuts.

Table 7.14. Development dataset for ΔH_{nbp}^{vap} of pure components and distillation cuts

Component	Data Points	Reference
n-Alkanes/Naphthanes	35	Ruzicka and Majer, 1993, Yaws, 2003
Aromatics/PAHs	28	Fang *et al.*, 2003, Yaws, 2003
Distillation cuts	63	this study

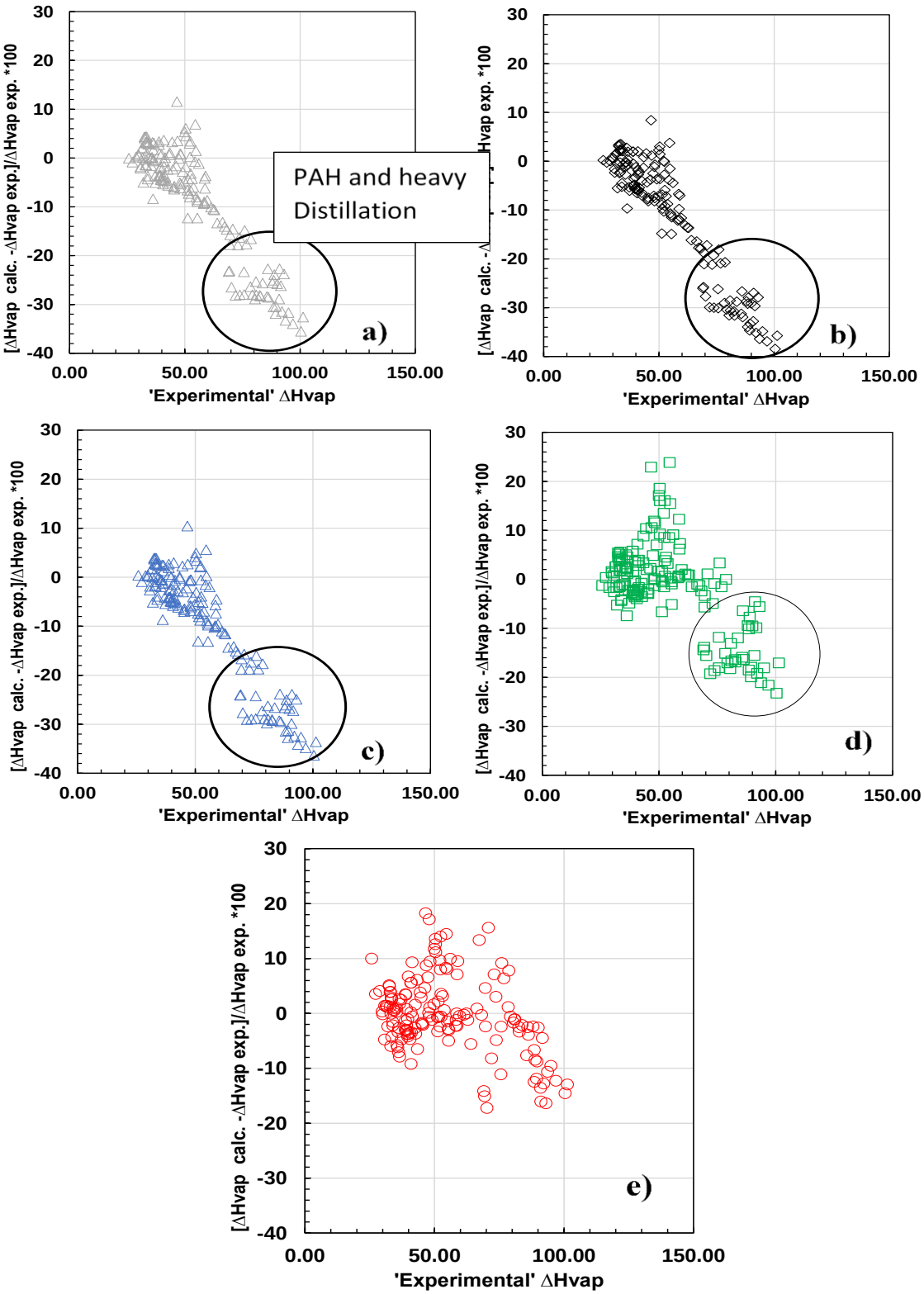

Figure 7.12. Relative error for the predicted heat of vaporization for the development dataset from the Riazi (a), Vetere (b), Gopinathan (c), Fang (d), and proposed (e) correlations.

Table 7.15. Average absolute and relative deviations, maximum absolute and relative deviations, and bias for heat of vaporization obtained using correlations from literature for the development dataset.

Correlation	AAD [kJ/mol]	ARD [%]	Bias [%]	MAAD [kJ/mol]	MARD [%]
Riazi	9.4	11.9	-9.9	23.6	24.5
Vetere	10.4	13.1	-12.0	26.3	27.3
Gopinathan	9.7	12.3	-10.7	24.4	25.2
Fang	6.2	9.0	-1.9	17.0	20.5

To develop a new correlation, the heats of vaporization for the dataset shown in Table 7.14 were first recalculated using Equation 7.8 with the generalized equations for Cox constants (Eq. 7.1 to 7.3). Figure 7.13 shows that the heats of vaporization of the distillation cuts were predicted with deviations of less than 7%. However, the paraffins and naphthenes were systematically under-predicted for compounds with molecular weight lower than 350 g/mol, with deviations as high as 50%. The heats of vaporization of heavy PAHs were similarly under-predicted. Not surprisingly, this approach predicted the heats of vaporization of the distillation cuts (from which the average parameters were obtained) with reasonably accuracy. However, it does not perform well for pure components.

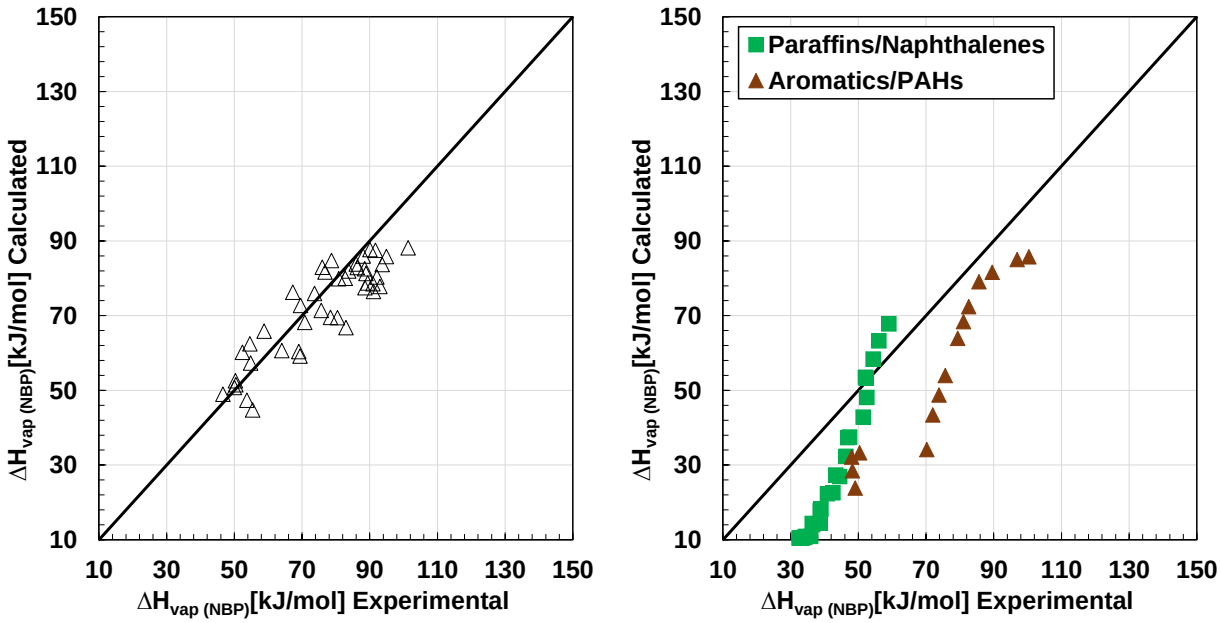

Figure 7.13. Dispersion plots for the calculated and predicted heat of vaporization at the normal boiling point for the distillation cuts (left) and pure components (right) using Equations 7.9, 7.4 to 7.6

The deviations between the predicted and "experimental" heats of vaporization were found to correlate to MW and SG, and the majority of the deviations were observed at molecular weights lower than 300 g/mol. The main trend in the deviations correlated to MW and a MW based correction factor was found to eliminate the paraffinic and naphthenic deviations. A secondary correlation based on SG was required to correct the under-prediction of the heat of vaporization for PAHs. The corrected version of Equation 7.8 for MW<300 g/mol is given by:

$$\Delta H_{nbp}^{vap} = \mathrm{R}\, T_b \exp(A_0 + A_1 T_b + A_2 T_b^2)/1000 - CF_1 \tag{7.9}$$

$$CF_1 = \frac{-25.03}{1 + \exp[(MW - 198.92)/CF_2)]} \tag{7.10}$$

$$CF_2 = 25.32 + \frac{2.02}{1.996 + \exp[SG - 9.327]} \tag{7.11}$$

where R is 8.314 J/mol K, T_b is the normal boiling temperature in K, and A_0, A_1, and A_2 are generalized Cox constants given in Equations 7.1 to 7.3. For compounds with MW≥300, ΔH_{nbp}^{vap} is

provided by Equation 7.8. Figure 7.14 shows the dispersion plot for the new correlation applied to the development dataset and Table 7.16 summarizes the average and maximum deviations for each development data set. Note, the low MW compounds are now accurately predicted as well as the PAHs. The new correlation decreased the overall AARD to 7.5% compared with 9.0% for the best prediction from the literature correlations (Fang *et al.*, 2005). Also, a reduction in the maximum deviations (less than 16 %) as well as the overall bias (-1.5 %) compared with results shown in Table 7.15.

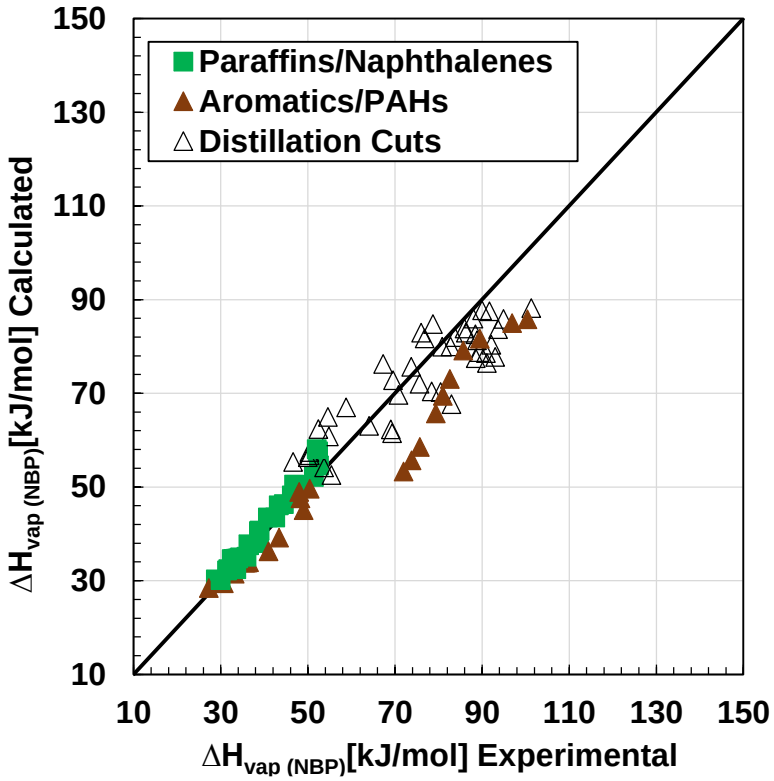

Figure 7.14. Dispersion plots for the calculated and predicted heat of vaporization at the normal boiling point using the proposed correlations for the pure components and distillation cuts.

Table 7.16. Average absolute and relative deviations, maximum absolute and relative deviations, and bias for heat of vaporization obtained using the proposed correlation for the development dataset.

Component	AAD [kJ/mol]	ARD [%]	Bias [%]	MAAD [kJ/mol]	MARD [%]
Paraffins/Naphthalenes	1.8	4.4	3.9	6.0	11.6
Aromatics/PAHs	6.2	8.9	-3.9	18.7	15.9
Distillation fractions	6.8	9.2	-1.5	15.2	19.1
Overall	4.9	7.5	-1.5	13.3	15.9

The proposed correlations as well as the literature correlations were tested for a set of distillation cuts from three different oils (Fang *et al.*, 2005). No distinction between the cuts was made by the author, therefore the combined results for all the 58 distillation cuts are presented. Figure 7.15 shows the dispersion plots obtained for all of the correlations and the deviations are summarized in Table 7.17. The new correlation performs better than all of the literature correlations, except the Fang correlation, with an average relative deviation less than 2.7%. The slightly better performance from Fang's correlation is not surprising because the test dataset used here is the same dataset that was used to develop the Fang correlation. The improvement over the other three correlations (Vetere, Riazi, and Gopinathan) is significant for heats of vaporization higher than 40 kJ/mol where these correlations under-predict the heat of vaporization by as much as 20%.

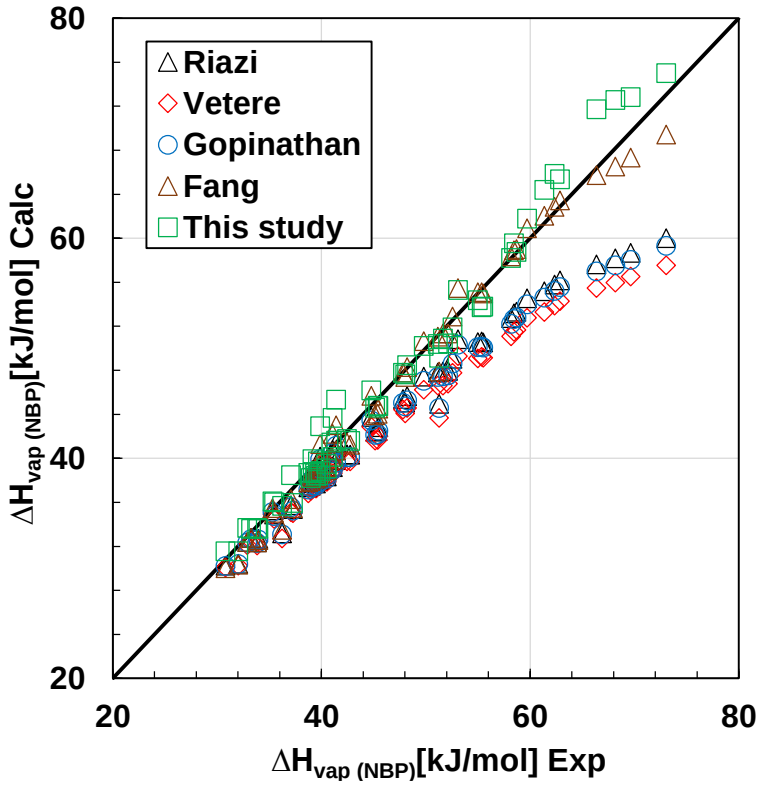

Figure 7.15. Dispersion plot for the test dataset using several correlations to predict heat of vaporization at the normal boiling point.

Table 7.17. Relative and absolute average deviations obtained for the test data set from literature correlations and proposed method in this study.

Correlation	AAD [kJ/mol]	ARD [%]	Bias [%]	MAAD [kJ/mol]	MARD [%]
Riazi	3.1	5.9	-5.9	13.0	17.8
Vetere	4.1	7.8	-7.8	15.5	21.2
Gopinathan	3.4	6.5	-6.5	13.7	18.8
Fang	1.0	2.3	-1.4	3.6	7.5
This study	1.3	2.6	0.6	5.2	9.5

Overall the main advantage of the proposed method is that it can be applied to a broader range of pure hydrocarbons and petroleum mixtures without compromising the accuracy of the low

molecular weight compounds. Although the predictions were improved by the new correlation, the physics behind the heat of vaporization for different chemical families are not fully described by only physical properties (see Figure 7.14). It is plausible that structural data showing the number of rings and double bonds could more accurately capture the attractive intermolecular forces that cause the heat of vaporization to have a different trends for the molecules with multiple aromatic rings and hetero-atomic molecules. Several studies (Kolska *et al.*, 2005, 2012; Marrero and Gani, 2001; Ma and Zhao, 1993; Drucos *et al.*, 1980, 1981, 1982, 1984) have shown the advantage of multilevel group contribution methods to predict heat values for wide ranges of chemical families. However, this approach is beyond the scope of this thesis which is focussed on correlations to physical properties. .

7.4 Heat of Combustion

As part of the project, the heats of combustion of some distillation cuts were measured at constant volume. The values are reported in Appendix H. Figure 7.16 compares the heat of combustion (high heating value-HHV) of the distillation cuts with pure components including paraffins, naphthenes, aromatics, and PAHs hydrocarbons. Figure 7.16 also shows how heat of combustion varies with the specific gravity for some of the oils used in this project. Overall, the data follows an expected trend with the lower boiling cuts (low SG) having higher heats of combustion than the higher boiling cuts (high specific gravity and higher heteroatom content).

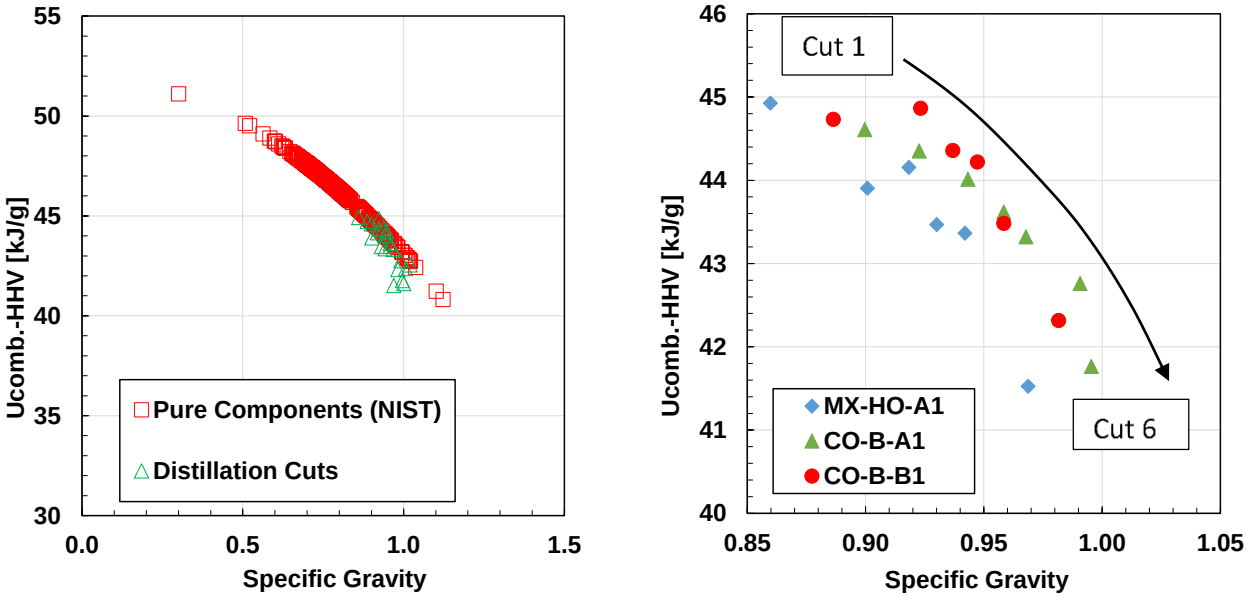

Figure 7.16. Variation of heat of combustion with specific gravity for pure components and distillation cuts (left) and data for three oil samples (right)

The correlations available in the literature for heat of combustion were provided in Table 2.8 and include the Tsonopoulos and Yan correlations. The correlations were tested on the experimental heats of combustion from the dataset listed in Table 7.18. Figure 7.17 presents the dispersion plot for both correlations. The error bars correspond to the 0.3% uncertainty from elemental analysis. Table 7.19 and 7.20 summarizes the average absolute and relative deviations, bias and maximum deviations.

Both correlations were able to predict the heat of combustion with similar accuracy: average deviations of 1.0% (0.4 kJ/g) for the Yan *et al.* (1988) correlation and 1.2% (0.5 kJ/g) for the Tsonopoulos (1986) correlation. It was observed that the major deviations were present in the coal liquid heat of combustion calculation. This higher error for coal liquids was also noted by the authors and may be an effect of higher errors in elemental analysis measurements, particularly for oxygen. Since the correlations have a sound fundamental basis and low error, a new correlation was not considered.

Table 7.18. Data set used to test the Tsonopoulos and Yan correlations.

Sample	Data Points	Reference
Distillation cuts	20	This Study
Heavy oil/ Bitumen	6	Yan *et al*., 1988
Coal Liquids	17	Jain and Sundararajan, 1981

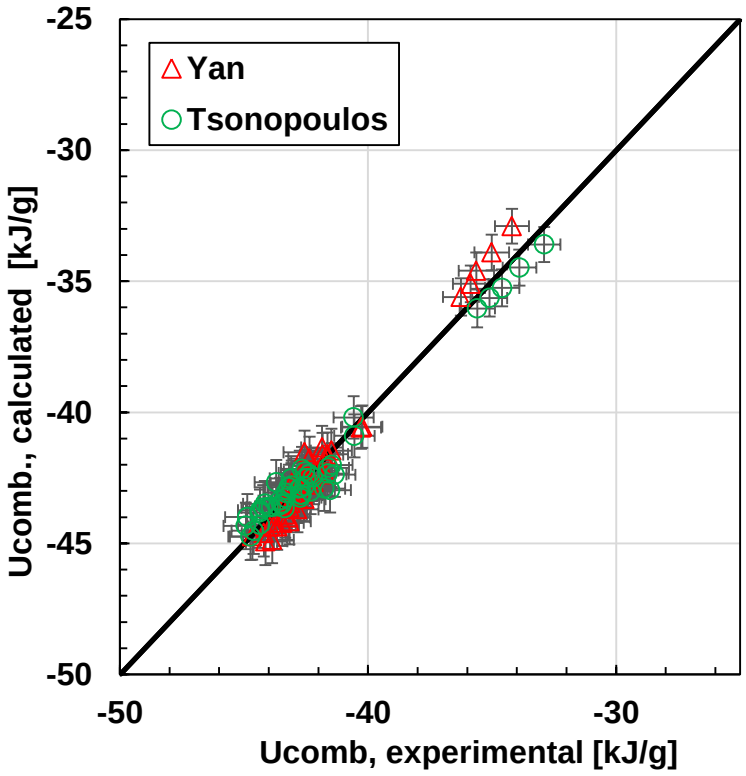

Figure 7.17. Comparison between the calculated and experimental heat of combustion from Yan and Tsonopoulos correlations.

Table 7.19. Average absolute and relative deviations obtained for the test data set.

Oil Sample	Yan			Tsonopoulos		
	Bias [%]	ARD [%]	AAD [kJ/mol]	Bias [%]	ARD [%]	AAD [kJ/mol]
Distillation Cuts	0.6	1.2	0.5	-0.2	1.0	0.4
Heavy Oil/Bitumen	0.1	0.3	0.1	-1.1	1.1	0.4
Coal Liquids	-0.7	1.6	0.6	-0.3	1.5	0.6
Overall	0.0	1.0	0.4	-0.5	1.2	0.5

Table 7.20. Maximum average absolute and relative deviations obtained for the test data set.

Oil Sample	Tsonopoulos		Yan	
	MARD [%]	MAAD [kJ/mol]	MARD [%]	MAAD [kJ/mol]
Distillation Cuts	2.5	1.0	2.5	1.0
Heavy Oil/Bitumen	1.3	0.4	0.8	0.3
Coal Liquids	1.2	0.5	1.5	0.5

CHAPTER EIGHT: IMPROVED CHARACTERIZATION OF HEAVY OILS AND BITUMEN SAMPLES

It is not always practical and economically viable to perform all the property measurements required to fully and accurately characterize a complex mixture like heavy oil. In many cases, the only information available for a heavy oil are its bulk properties (often only density) and a TBP curve from a distillation assay or from a simulated TBP curve obtained through gas chromatography analysis. The property correlations discussed in the previous chapters usually require two properties. Therefore, to initiate a pseudo-component based characterization, two property distributions are required: in this case, one for TBP and one for another property. Typically, density is selected as the second property and the form of its distribution is assumed. For instance, the exponential model is used for light reservoir fluids and the gamma model gives reasonable predictions for gas condensate systems (Whitson, 2000; Riazi, 2005). In this chapter, the existing methods to predict SG distributions are evaluated, a modification is proposed for one of the methods, and a new method is developed.

8.1 Specific Gravity Distribution Correlations

Methods to obtain specific gravity distributions from only boiling point data and bulk properties include the Bergman, constant Watson Factor, and Katz-Firoozabadi methods.

Bergman

Bergman used measured data for gas condensates with light plus fractions to relate specific gravity to the normal boiling point as follows:

$$SG = \frac{\left(0.4189 + 2.786x10^{-3}T_b - 8.685x10^{-6}T_b^2 + 1.306x10^{-8}T_b^3 - 7.092x10^{-12}T_b^4\right)}{0.9991} \quad (8.1)$$

Since this method was developed exclusively for light oils, it may not be suitable for heavy oils.

Constant Watson Factor (Cte Kw.)

The method proposed by Miquel and Castells (1993, 1994) is based on the assumption that the Watson factor is constant for all the pseudo-components of a mixture. Therefore, the SG of each pseudo-component is given by:

$$SG_i = \frac{T_{bi}^{1/3}}{K_w} \tag{8.2}$$

The Watson K factor, K_w, is calculated from the average boiling point and bulk specific gravity of the oil using the same equation. As noted by the authors, this method gives a good estimate for compounds with boiling point less than 500 K. Since for heavy oils and bitumens more than 30% of the sample has a boiling point higher than 500 K, this method may not accurately predict the SG distribution of a heavy petroleum sample. The Watson factor can also be adjusted to obtain the correct bulk SG (VMGSim User's Manual).

Katz-Firoozabadi (K-F)

Katz and Firoozabadi (1978) presented a set of properties for single carbon numbers up to C_{45}. Several authors correlated those values into polynomial functions of carbon number (Whitson, 1982; Naji, 2010). Whitson (1982) modified the set to improve the consistency of the predictions. Later Naji (2010) developed a similar set of equations as a function of the carbon number. The original K-F correlation is given by Equation 8.3:

$$SG_i = \frac{(0.5516 + 1.208x10^{-3}T_{bi} - 2.231x10^{-6}T_{bi}^2 + 2.265x10^{-9}T_{bi}^3 - 8.614x10^{-13}T_{bi}^4)}{0.9991} \tag{8.3}$$

However, the original version and its modifications could not be applied for components with carbon number greater than C_{45} or a normal boiling point higher that 850 K because a maximum occurred at these values.

Satyro and coworkers (2000) proposed a simpler expression by fitting data from 700 to 850 K range with specific gravity approaching a value of 1.05. They used the same data as was used to develop Equation 8.3, however, the form proposed by Satyro and coworkers eliminates the maximum in Equation 8.3. The final equation has the following form, Equation 8.4:

$$SG_i = \left(A + \frac{B}{T_{bi}}\right) \tag{8.4}$$

Equation 8.3 and 8.4 have a very limited range of applicability and tend to under-predict specific gravity values for heavy petroleum fractions. To overcome this problem, a constant multiplier is used to adjust the specific gravity distributions and match the bulk specific gravity. However, this multiplier is unique for each mixture and must be fitted for different samples.

All the previous methods were tested on two sets of distillation cuts listed in Table 8.1. Figure 8.1 shows the predicted SG distribution for all the methods mentioned before for one of the oils obtained in this study and one of the oils found in literature. Figure 8.2 shows the relative error plot. Table 8.2 presents the average and maximum absolute and relative deviations resulting for each dataset. The K-F correlation was not included in the error analysis because much of the data were above its range of applicability.

Table 8.1. Development dataset used to test literature correlations

Data set	No. of data points	Source
Deep vacuum distillation cuts	63	This study
Literature distillation cuts (SJV, ALT, ANS)	33	Strum and Shay, 2000

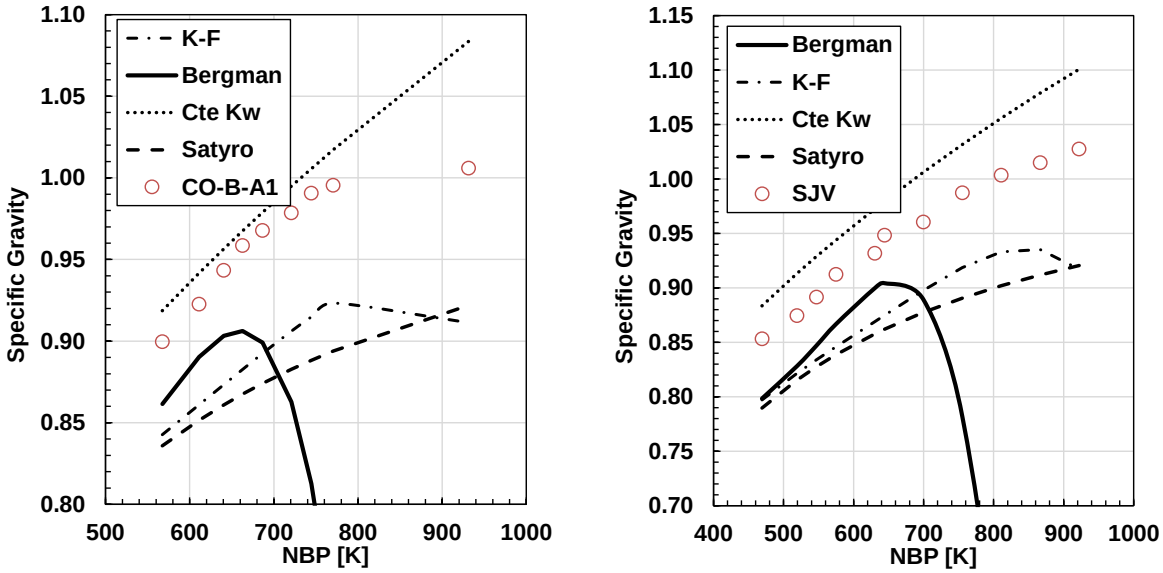

Figure 8.1. Measured and correlated SG versus NBP for the CO-B-A1 distillation cuts (left) and SJV distillation cuts (right) using Bergman, constant Watson factor (Cte. Kw), Katz Firoozabadi (K-F) and Satyro correlations.

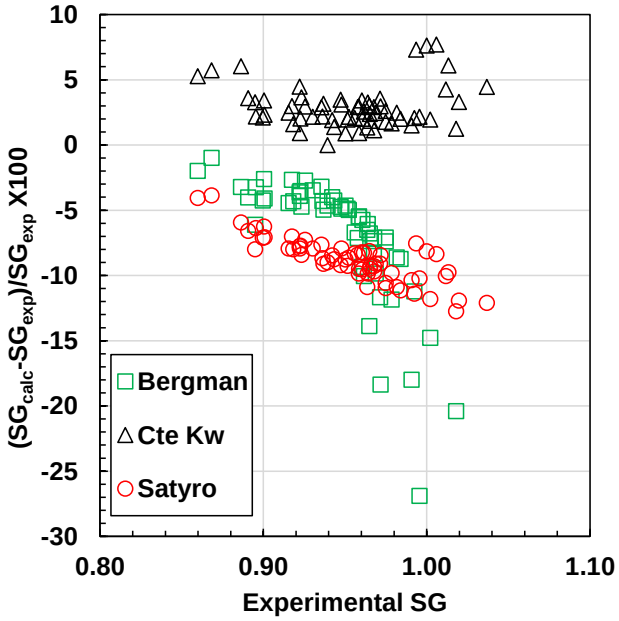

Figure 8.2. Relative error obtained for SG distribution predicted from the experimental NBP values using the Bergman, constant Watson factor (Cte. Kw) and Satyro correlations.

Table 8.2. Average absolute and relative deviations, maximum absolute and relative deviations, and bias for SG distributions obtained using correlations from literature for the development dataset.

Correlation	AAD	ARD [%]	Bias [%]	MAAD	MARD [%]
Bergman	0.24	25.1	-23.9	2.04	202.4
Cte Kw	0.03	2.8	2.5	0.05	5.8
Satyro	0.07	7.8	-6.7	0.13	12.7

The Bergman method has a maximum at approximately 650 K causing the predicted specific gravity to decrease as NBP increases, opposite to the correct trend. Not surprisingly, this correlation has the highest deviations, 25.1%. It is evident that the light plus fractions used to develop Bergman's correlations provided insufficient range to extrapolate accurately to heavy oil and bitumen samples. Note, this correlation was not designed to work for heavy oils and is only shown here for comparison.

The constant Watson factor is the best performing correlation with an average deviation of less than 2.8%. Note, in the middle range (near the average K_w of the oil), the predictions show the smallest deviations and in the low and high boiling range the deviations grow as the difference of this fractions from the whole sample are greater. The largest errors are generally for the residues.

The Satyro correlation under-predicts the SG and the deviations increase monotonically from the lowest to the highest boiling fraction. The under-predictions were expected since the development dataset of for this correlations consisted of pure components with a carbon number up to 45. Note, the correction proposed by Satyro and coworkers, completely eliminate the maximum observed in the original versions of this method. The average relative deviations were around 5% higher than using constant Watson factor. However, since the error grows monotonically a simple correction factor can be introduced for this correlation to improve its predictive capabilities.

Modified K-F/Satyro Method

The proposed correlation is based on the Satyro version of the K-F correlation and adds an additional term that acts as a multiplier to match the bulk specific gravity of the oil. The modified K-F correlation is given by Equation 8.5:

$$SG_i = \left(1.0563 + \frac{-125.114}{T_{bi}}\right) * \left(\frac{0.4493 + SG_{Bulk}}{1.3062}\right) \quad (8.5)$$

where T_{bi} is the normal boiling temperature of each pseudo-component in K and SG_{Bulk} is the specific gravity of the whole sample.

Figure 8.3 presents the dispersion plots of the SG predictions for the distillation cuts from Equation 8.5 and the best performing literature correlation, the constant Watson factor method. The average absolute and relative deviations and bias from the Constant Watson factor method and Equation 8.5 are summarized in Table 8.3 and the maximum deviations in Table 8.4. The new correlation improved the average and maximum deviations for both sets of distillation cuts (from 2.8% to 1.3%), and significantly reduced the bias (from 2.5 to 0.1%). Despite the good approximations obtained using Equation 8.5, most of the relative errors are higher than the experimental errors. Ideally, the SG predictions should be maintained within the experimental measurement errors (1%), in order to avoid significant propagation of errors during the characterization when predicting molecular weights and other thermal properties from the SG of each pseudo component. Therefore, a new correlation was proposed.

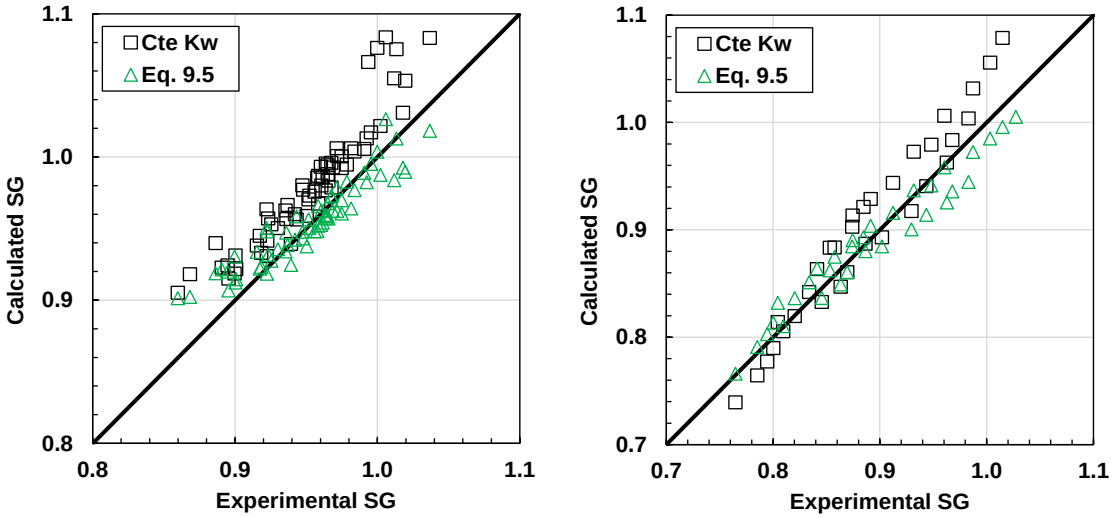

Figure 8.3. Dispersion plots for the SG distributions of the development dataset distillation cuts from this study (left) and literature (right) determined from the Constant Watson factor method and Equation 8.5.

Table 8.3. Average absolute and relative deviations and bias from the Constant Watson factor method and Equation 8.5 for SG for the development dataset.

Oil Sample	Cte. Kw			Equation 8.5		
	AAD	ARD [%]	Bias [%]	AAD	ARD [%]	Bias [%]
WC-B-B1	0.02	2.5	2.5	0.02	1.6	-0.3
CO-B-A1	0.02	2.3	2.3	0.01	1.3	1.3
MX-HO-A1	0.03	3.1	3.1	0.01	1.1	0.7
CO-B-B1	0.03	3.4	3.4	0.01	1.4	-0.3
US-HO-A1	0.03	3.5	3.5	0.01	1.2	0.1
WC-B-D1	0.03	3.0	3.0	0.01	1.0	1.0
RO-HO-A1	0.02	2.4	2.4	0.01	0.9	-0.6
ALT	0.02	2.3	0.5	0.01	1.6	1.6
ANS	0.01	1.0	-0.3	0.02	2.2	-2.2
SJV	0.04	4.7	4.7	0.01	1.2	-0.3
Overall	**0.03**	**2.8**	**2.5**	**0.01**	**1.3**	**0.1**

Table 8.4. Maximum absolute and relative deviations from the Constant Watson factor method and Equation 8.5 for SG for the development dataset.

Oil Sample	Cte. Kw		Equation 8.5	
	MAAD	MARD [%]	MAAD	MARD [%]
WC-B-B1	0.05	4.5	0.03	3.1
CO-B-A1	0.08	7.7	0.03	3.4
MX-HO-A1	0.08	7.6	0.04	4.8
CO-B-B1	0.05	6.0	0.03	3.7
US-HO-A1	0.05	5.7	0.03	3.9
WC-B-D1	0.06	6.1	0.03	3.5
RO-HO-A1	0.07	7.3	0.01	1.6
ALT	0.04	4.1	0.03	3.5
ANS	0.02	2.1	0.04	3.9
SJV	0.07	7.1	0.02	2.1
Overall	**0.06**	**5.8**	**0.03**	**3.3**

New Method

A correlation to improve the prediction of specific gravity for heavy distillation cuts was developed using the dataset showed in Table 8.1, and is given by:

$$SG_i = \left(0.6923 + 0.1962 * \left\{1 - \exp\left[-3.5003 * \left(\frac{T_{bi}}{1000} - 0.5209\right)\right]\right\}\right) + (SG_{DAO-Bulk} - 0.7830) \quad (8.6)$$

where $SG_{DAO\text{-}Bulk}$ corresponds to the specific gravity of the maltene fraction of the oil and T_{bi} is the normal boiling point of the pseudo-component in K.

The performance of Equation 8.6 is presented as a dispersion plot for the development datasets in Figure 8.4. Table 8.5 and 8.6 summarize the average and maximum absolute and relative errors

and bias obtained with Equation 8.6. Note, the overall performance was shown separately for the data from this study and from the literature to better observe where the improvement was obtained. For all the deep vacuum distillation cuts, the average absolute and relative deviations were less than 0.01 and 0.8%, respectively. The deviations were higher for the literature data with the highest deviations observed for the lightest oil included in the development dataset (ALT). It is possible that the higher dispersion in the low density range is due to experimental errors caused by high volatility of the samples. However, since there is no evidence to prove that the deviation is due to an experimental error, it is recommended to limit the application of Equation 8.6 to samples with specific gravities greater than 0.8. To better characterize an oil with bulk SG less than 0.81, as is the case of the oil ALT, it is recommended Equation 8.5 be used.

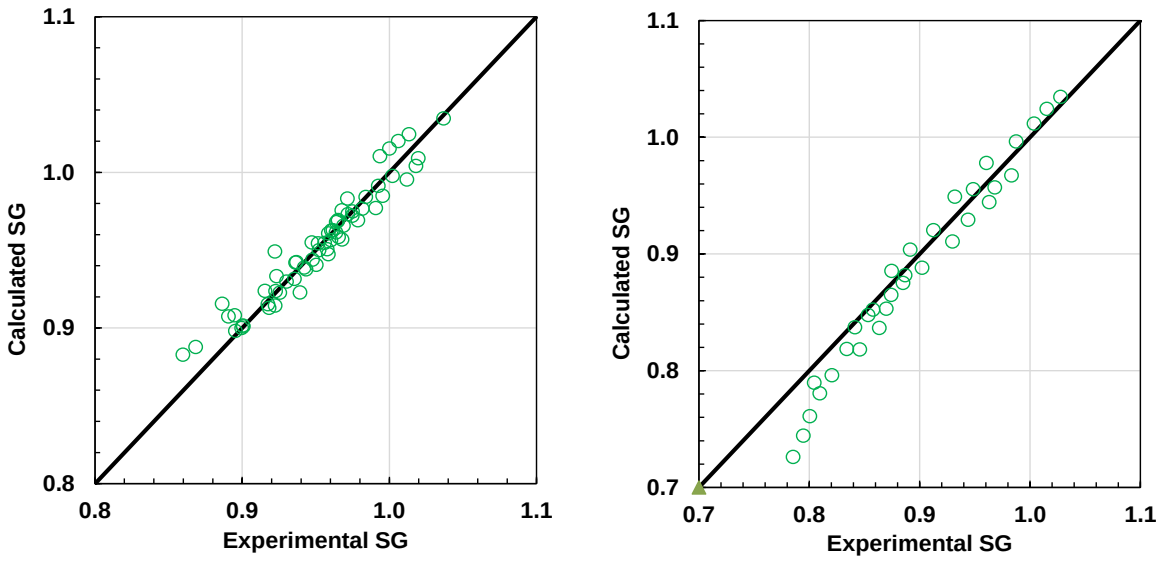

Figure 8.4. Dispersion plots for the SG distributions of the development dataset distillation cuts from this study (left) and literature (right) determined from Equation 8.6.

Table 8.5. Average absolute and relative deviations and bias using Equation 8.6 for SG for the development dataset.

Oil Sample	Equation 8.6		
	AAD	ARD [%]	Bias [%]
WC-B-B1	0.01	0.8	0.2
CO-B-A1	0.01	0.9	-0.5
MX-HO-A1	0.01	0.7	0.2
CO-B-B1	0.01	0.9	0.5
US-HO-A1	0.01	0.7	-0.2
WC-B-D1	0.01	0.8	0.8
RO-HO-A1	0.01	0.7	-0.1
Overall	**0.01**	**0.8**	**0.1**
ALT	0.03	3.5	-3.5
ANS	0.02	2.0	-2.0
SJV	0.01	1.1	1.0
Overall	**0.01**	**2.2**	**-1.5**

Table 8.6. Maximum absolute and relative deviations using Equation 8.6 for SG for the development dataset.

Oil Sample	Equation 8.6	
	MAAD	MARD [%]
WC-B-B1	0.03	2.9
CO-B-A1	0.01	1.4
MX-HO-A1	0.02	2.7
CO-B-B1	0.03	3.3
US-HO-A1	0.02	2.2
WC-B-D1	0.02	1.9
RO-HO-A1	0.02	1.8
Overall	**0.02**	**2.3**

ALT	0.08	10.0
ANS	0.03	3.6
SJV	0.02	1.9
Overall	**0.03**	**5.1**

Consistency Check for Equation 8.5 and 8.6

As mentioned before, the characterization methods should be consistent with the bulk properties. Therefore, the specific gravities calculated using Equations 8.5 and 8.6 were used to determine the bulk specific gravity of the oil as follows:

$$SG_{Bulk} = \left(\sum_{i=1}^{N} \frac{w_i}{SG_i} \right)^{-1} \tag{2.4}$$

The measured and calculated bulk specific gravities for each oil are compared in the dispersion plot, Figure 8.5. For the majority of the oils, the error of calculated bulk density is within the experimental error of the measurements (errors bars).

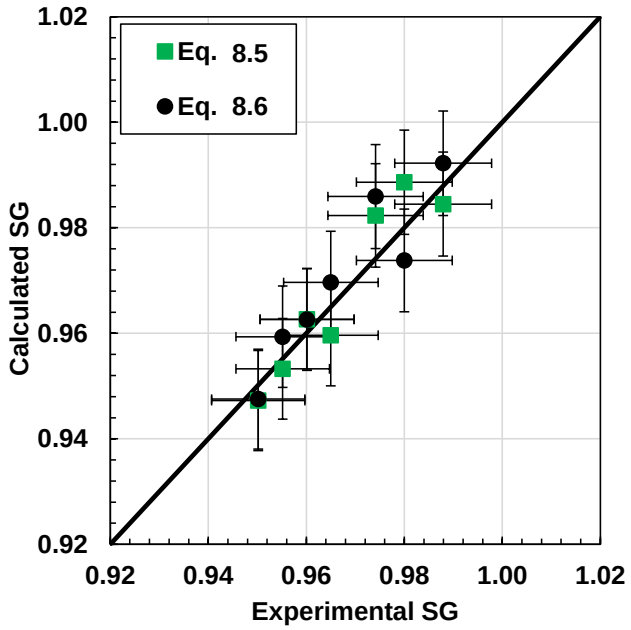

Figure 8.5. Dispersion plot comparing the calculated and experimental bulk specific gravity of seven different heavy oil and bitumen samples using Equations 8.5 and 8.6.

Note that some of the correlations developed here use the specific gravity of the deasphalted fraction of the bitumen as an input. This information is not always available since it requires prior deasphalting of the samples and this is not a routine procedure. It is more common to have the specific gravity of the whole mixture and the asphaltene content of that sample. Therefore, a simple relation between these two variables was developed to predict the specific gravity of the deasphalted oil, Equation 8.7:

$$SG_{DAO-Bulk} = \frac{SG_{Bit}}{0.9913 * wt\%Asp^{0.009133}} \tag{8.7}$$

where SG_{Bit} is the specific gravity of the heavy oil or bitumen sample and wt%Asp is the asphaltene content. The correlation fitted the SG of the maltenes for the oils in Table 8.1 with average absolute and relative deviation of 0.003 and 0.33% respectively. The previously developed methods, Equation 8.5 and 8.6, were tested using the calculated SG of the deasphalted oil. The average relative deviations for the development dataset was less than 1.3% and 1.4% for Equations 8.5 and 8.6, respectively, compared with 1.1 and 0.9% when the measured SG were used. Hence, Equation 8.7 can be used instead of the measured SG to estimate the SG distribution using Equation 8.5 or 8.6, without a significant loss in accuracy.

An Athabasca High Vacuum Gas oil (HVGO) was used to test Equations 8.5 and 8.6 (Smith, 2007). Note, the SG of the maltenes was not available and Equation 8.7 was used to estimate this value, however due to the low content of asphaltenes in HVGO both bitumen and DAO specific gravities were similar. The TBP curve and bulk properties were obtained from the literature (Smith, 2007). Figure 8.6 presents a dispersion plot of the predicted and measured specific gravity values from Equations 8.5 and 8.6. The average and maximum absolute and relative deviations and bias obtained for the HVGO from all the equations are summarized in Table 8.7. Both correlations predicted the data with a relative error near the experimental error. Equation 8.5 provided a slightly more accurate prediction probably because it was developed from a dataset that included pure components. Hence, it is more consistent through a wider range of specific gravities and boiling points.

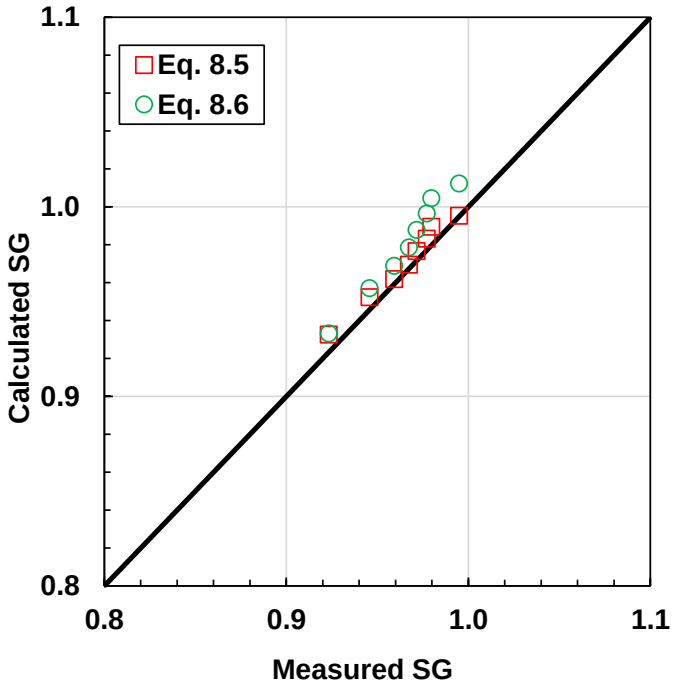

Figure 8.6. Predicted (from Equations 8.5 and 8.6) versus measured specific gravity for an Athabasca HVGO.

Table 8.7. Average absolute and relative deviations for the SG predicted with Equations 8.5 and 8.6 for an HVGO sample.

Method	AAD	ARD [%]	Bias [%]	MAAD	MARD [%]
Eq. 8.5	0.01	0.8	-0.8	0.01	1.4
Eq. 8.6	0.01	1.1	1.1	0.02	2.1

CHAPTER NINE: CONCLUSIONS AND RECOMMENDATIONS

9.1 Dissertation Contributions and Conclusions

The major contributions of this thesis are: 1) the development of a reproducible deep vacuum batch fractionation technique to generate distillation curves beyond the range of current commercial assays; 2) the measurement of the physical and thermal properties of the cuts obtained from the new apparatus - the heaviest cuts are a fraction of the fluid for which properties have not previously been measured; 3) the evaluation and modification of existing property correlations and development of new correlations, and; 4) a recommended correction to the ASTM D7169 method for the cumulative wt% distilled above an AET of 600 K.

9.1.1 Deep Vacuum Fractionation Apparatus (DVFA)

The DVFA, originally designed to measure vapor pressure and previously shown capable of fractionating heavy oils and bitumen (Castellanos, 2012), was modified and improved to produce reproducible and consistent distillation data and cuts with reproducible properties. The modifications introduced several challenges, the main one being the introduction of larger fittings which increased the potential for leaks. These issues were successfully resolved by introducing a T-shaped sample vessel with concentric adapters into the system. This simple rearrangement improved the fractionation, reduced the time of the experiment, and produced consistent distillation cuts. In addition, couplings using copper o-ring seals were used to minimize leaks in the system.

After the modifications, the apparatus was able to distill bitumen and heavy oils to up to 50 wt% without generating cracked samples. The repeatability for all the oils was on average less than 1.8% for the distillation curve, 0.2% for the density of the cuts, and 3% for the molecular weight of the cuts. Although the DVFA method is not practical for routine assays due to time and cost constraints, it was essential for the development of a methodology and correlations that can be used to characterize heavy oils based on conventional distillation data. First, the Gaussian extrapolation of conventional distillation data was validated. Second, a robust dataset of cut

properties was obtained and used to improve the property correlations for heavy oils. While the results have made the DVFA method redundant for routine assays, it is still recommended if a detailed and extensive analysis of the samples is required.

9.1.2 Interconversion Method to TBP Data for DVFA

The interconversion of the boiling temperatures measured in the DVFA to TBP was required for use in existing oil characterization procedures. An interconversion method based on the simultaneous fitting of vapor pressure and heat capacity with the Cox vapor pressure equation was successfully applied to the DVFA data. The same approach can be used to inter-convert data from any sub-atmospheric pressure distillation.

Other contributions that arose during the development of the inter-conversion method are:

1) the generation of experimental vapor pressure and liquid heat capacity data for heavy distillation cuts.
2) the confirmation that maltene distillation cuts follow a Gaussian distribution, which validates the characterization methodology for heavy oils proposed by Castellanos *et al.* (2011).
3) the development of new correlations to predict distillation curves of heavy oils from bulk properties.

9.1.3 Physical Property Distributions and Correlation

One of the major advantages of the deep vacuum fractionation apparatus was that real cuts could be collected for further analysis. Experimental values of heavy distillation cuts proved to be a valuable tool to improve, modify, or develop new correlations to obtain better property descriptions for heavy oils and bitumen.

Correlations to predict boiling point (NBP), specific gravity (SG) and molecular weight (MW) of heavy distillation cuts were developed. For the NBP and MW a modified version of Soreide's

correlation was used to better estimate these two properties. The average relative deviations for the development data set (DDS) were slightly decreased by 1% and 2.5% for the NBP and MW, respectively, when compared to the original Soreide correlation. The predicted NBP and MW for the test data set (TDS) was improved by 0.2% and 0.3%, respectively. In addition, a new correlation was proposed to predict SG from the H/C ratio and MW. The AARD was considerably improved from 1.7 to 0.8 for the DDS. The TDS confirmed the predictive capabilities of the new correlation with an AARD of less than 1.4%. The importance of the H/C ratio as a new characterization parameter was described and a correlation to predict it from SG was developed for cases where the measured H/C ratio was not available. The data was fitted within a 1% error.

A simple correlation between refractive index and SG was proposed. The DDS was fitted with an error of less than 1.2% compared with 2.3% for the best performing correlation from the literature. A clear relationship between density and refractive index was shown, validating the use refractive index as a substitute for density in equation of state modelling.

9.1.4 Vapor Pressure and Thermal Property Distributions and Correlation

The simultaneous fitting of vapor pressure and heat capacity to obtain NBP, provided a series of Cox constants. The values of these constants for the cuts of seven different oils were plotted against their MW and TBP. A trend was observed which was used to correlate Cox constants with MW and TBP, providing a new vapor pressure correlation that provided more accurate predictions for heavy cuts than the Maxwell-Bonnell and Riazi correlations. The new correlation improved the vapor pressure predictions for the heavier oils and bitumen with and AARD within 50%. The Maxwell-Bonnell equations performed better for the light cuts with a deviation of 41% compared with 44% from the correlation developed in this study.

The Tsonopoulos (1986) correlation for liquid heat capacity was modified to better fit the data collected as part of this thesis: first, with the Watson Factor and the SG of the cuts as input; second, with the H/C ratio and SG of the cuts as input. Both versions successfully predicted the liquid heat capacity by improving the AARD from 4.5 to around 1% for the DDS. Both retuned and modified correlations were tested and the best performance was obtained with the modified version that uses the H/C ratio as input parameter (0.8% compared with 1.5%). However, the second version is more

practical since it does not require boiling point data as an input parameter and, although it requires the H/C ratio, the ratio can be correlated to SG making the liquid heat capacity a function of only the SG.

Using the direct relationship between vapor pressure and enthalpy of vaporization through the Clapeyron equation, the previously calculated Cox constants were used to estimate enthalpy of vaporization. Although the data cannot be regarded as experimental, the calculated values gave the best estimate available for heavy distillation cuts. A new correlation to calculate the enthalpy of vaporization at the normal boiling point was developed. The overall AARD for the DDS was 7.5% compared with 9.5% from the best literature correlation. The proposed method predicted the enthalpy of vaporization over a wide range of MW and SG with deviations of less than 2.6% for the TDS.

The heats of combustion of some cuts were measured and the data were used to test the accuracy of current correlations using the elemental analysis. The Tsonopoulos (1986) and Yan *et al.* (1988) correlations predicted the heats of combustion (HHV) for heavy distillation cuts within 1%.

9.1.5 Characterization of Heavy Oils and Bitumen Samples

In this project, the distribution of many properties was measured for each oil. In practice, often only a distillation curve and bulk properties are available. The distribution of one other property is required for most correlations and SG was selected as this second property. Two methods were developed to generate property distributions from only bulk properties and TBP data. The first method was a modified version of the Katz-Firoozabadi correlation that included a new generalization of a correction factor proposed by Satyro and coworkers (2011). The second method was an equation developed specifically for heavy oils and bitumen samples, excluding pure components. Both methods showed an improvement from literature correlations by decreasing the deviations from 2.8% to 1.3% for the modified K-F method and to 0.8% for the new correlation. However, the application of this method is restricted to oils with SG higher than 0.8.

Once TBP and SG distributions are obtained, it is recommended to determine the MW using the modified version of Soreide's correlation (1989) and then the other physical and thermal properties

can be determined using the equations developed in this work. Hence, a complete oil characterization can be generated from only TBP and bulk SG data.

The final contribution of this project was in the area of simulated distillation, which has proven to be faster and more economical than physical distillation. First, the TBP from ASTM D7169 simulated distillation assays were shown to be in good agreement with spinning band distillation (SBD) data for the distillable part of the oil (up to 30 wt% of the oil). Beyond 30 wt% distilled, simulated distillation from ASTM D7169 diverged from the boiling point distribution obtained from the DVFA apparatus and corroborated with a Gaussian extrapolation of the SBD data. Note, 30 wt% distilled is the point at which the simulated distillation experimental temperature exceeded the estimated cracking temperature of heavy oils (~ 350 ˚C) and the cuts started to become more aromatic and polydisperse, A preliminary correction factor based on the bulk molar volume was recommended for simulated distillation data above 30 wt% distilled.

9.2 Recommendations

Recommendations for future project studies include the following:

1) Improve the insulation system for the deep vacuum fractionation apparatus to better control the temperature gradients and subsequently the internal temperature of the sample being distilled. This can be accomplished by either building an oven for the apparatus or making a custom-made mantle for all parts or sections of the apparatus with inbuilt temperature controllers.
2) Measure the liquid heat capacity of the remaining distillation cuts to fully test the predictive capabilities of the correlations developed in this work for more of the high boiling cuts
3) For all the correlations developed in this work, include a larger and more extensive dataset to increase the range of applicability for crude oils with different API values. Note, the aim of this study was to make the correlations particularly accurate for heavy oils and bitumen samples, however the accuracy for these fluids may be reduced if the range of the correlations is extended.

4) Improve the enthalpy of vaporization predictions by using group contribution methods to provide a better alternative to account for the aromatic ring and heteroatomic distribution within the oil that cannot be fully described by using only physical properties.
5) Measure the viscosity of the cuts and develop a predictive model for the viscosity of the whole sample. Note, this work is currently underway in a separate project.
6) Obtain ASTM D7169 and physical distillation data for additional heavy oils to test the proposed correction to simulated distillation data for a wider range of oils.
7) Implement the correlations proposed in this work in a software simulator to test if these correlation and the critical property predictions from existing correlations match available phase behaviour data. A final solution for phase behaviour prediction is not expected since there are other factors affecting the outcome of these models, such as the mixing rules for the co-volume and energy parameter and the equations used to obtain the binary interaction parameters for different crude oil/solvent systems. However, this work targeted one of the sources of error when using these models: the distribution of thermo-physical properties of heavy oil and bitumen samples.
8) Test the correlations for visbroken, thermocracked and hydrocracked samples to determine their applicability for downstream models.

References

2010 Survey of Energy Resources, World Energy Council, London, www.worldenergy.org.

Abu-Elgheit, M. B.; Elkholy, I. S.; Barakat, B. O. Distribution of Trace Metals in Petroleum and its Heavy Refinery Products. *Journal of Chemical Technology and Biotechnology*. **1981**, 31, pp. 760-764.

Aladwani, H. S.; Riazi, M. R. Some Guidelines for Choosing a Characterization Method for Petroleum Fractions in Process Simulators. *Chemical Engineering Research and Design*. **2005**, *83*(2), pp. 160-166.

Alboudwarej, H.; Akbarzadeh, K.; Svrcek, W. Y.; and Yarranton, H. W. A Generalized Regular Solution Model for Aphalthene Precipitation from n-Alkane Diluted Heavy Oils and Bitumens. Fluid Phase Equilibria, 232, **2005**, pp. 159-170.

Altgelt, K. H.; Boduszynski, M. M. Composition and Analysis of Heavy Petroleum Fractions. Ed Dekker. U.S.B. **1994.**

Ambrose, D.; Counsell, J. F.; Davenport, B. J. The Use of Chebyshev Polynomials for the Representation of Vapour Pressure between the Triple Point and the Critical Point. *J. Chem. Eng. Thermodyn.* **1970**, 2.

Ambrose, D.; Walton, J. Vapor pressures up to their critical temperatures of normal alkanes and 1-alkanols. *Pure Appl. Chem.* **1989**, 61, pp. 1395-1403.

Anderson, S. I.; Speight, J. G. Thermodynamic models for asphaltene solubility and precipitation. *J. Can. Pet. Eng.* **1999**, 22, pp. 53-66.

Anselne, M. J.; Teja, B. S., Critical Properties of Dilute Multi-Component Mixtures. *AIChE Journal.* **1990,** 36 (6), pp. 897.

Avlonitis, G; Mourikas, G.; Stamataki, S.; Tassios, D. A generalized correlation for the interaction coefficients of nitrogen hydrocarbon binary mixtures, *Fluid Phase Equilibria*, **1994**, Vol. 68, pp. 47-102.

Banerjee, D. K. Oil sands, heavy oils & bitumen: from recovery to refinery. Penwell Corp. U.S.B. **2012,** pp 32-33.

Barrera, D. M.; Ortiz, D. P. Yarranton, H. W. Molecular Weight and Densit Distributions of Asphaltenes from Crude Oils. *Energy and Fuels*. **2013**, 27, pp. 2474-2487.

Boduszynski, M. M. Composition of Heavy Petroleums 2- Molecular Characterization. *Energy Fuels*. **1988**, 2, pp. 597-613.

Boduszynski, M. M. Composition of Heavy Petroleums. .1. Molecular Weight, Hydrogen Deficiency, and Heteroatom Concentration as a function of Atmospheric Equivalent Boiling Point up to 1400 F. *Energy and Fuels*. **1987**, 1, pp. 2-11

BP Statistical Review of World Energy 2015. London, UK, June, **2015**

Bruno, T.; Smith, B. L. Enthalpy of Combustion of Fuels as a Function of Distillate Cut: Application of an Advanced Distillation Curve Method. *Energy and Fuels*. **2006**, 20, pp. 2109-2116.

Butler, R.M.; Mokrys, I.J. Solvent Analog Model of Steam-Assisted Gravity Drainage. *AOSTRA J. Res*, **1989,** 5, 17.

Carbognani, L.; Lubkowitz, J.; Gonzalez, M. F.; Pereira-Almao, P. High Temperature Simulated Distillation of Athabasca Vacuum Residue Fractions. Bimodal Distributions and Evidence for Secondary "On-Column" Cracking of Heavy Hydrocarbons. *Energy & Fuels*, 21, **2007,** pp. 2831-2839.

Castellanos, Díaz, O.; Schoeggl, F.; Yarranton, H. W.; Satyro, M. B.; Lovestead, T. M.; Bruno, T. J. Modeling the Vapour Pressure of Biodiesel Fuels. *World Academy of Science, Engineering and Technology.* **2012**, 65

Castellanos, O. Measurement and Modeling Methodology for Heavy Oil and Bitumen Vapor Pressure, University of Calgary, June **2012**.

Castellanos, O.; Modaresghazani, M.; Satyro, M. B.; Yarranton, H. W. Modelling the Phase Behavior of Heavy Oil and Solvent Mixtures. *Fluid Phase EquilibriB.* **2011**, 304 (1-2), pp.74- 85

Castellanos-Diaz, O.; Schoeggl, F.; Yarranton, H.; Satyro, M. Measurement of Heavy Oil and Bitumen Vapour Pressure for Fluid Characterization, *Industrial Engineering Chemistry Research Journal.* **2013**, 52(8), pp. 3027-3035

Castellanos-Diaz, O.; Sanchez-Lemus, M.C.; Schoeggl, F.F.; Satyro, M.A.; Taylor, S.D.; Yarranton, H.W. Deep-Vacuum Fractionation of Heavy Oil and Bitumen, Part I: Apparatus and Standardized Procedure, *Energy & Fuels*, 28 (5), **2014,** pp. 2857-2865.

Chirico, R.; Nguyen, B. Steele, W.; Strube, M. Vapor Pressure of n-Alkanes Revisited. New High Precision Vapor Pressure Data on n-Decanbe, n-Eicosane, and n-Octacosane. *J. Chem. Eng. DatB.* **1989**, 34, pp.149-156

Chopra, S.; Lines, L.; Schmitt, D. and Batzle, M. Heavy Oils: Reservoir Characterization and Production Monitoring. Geophysical Developments No. 13. *Society of Exploration Geophysicists*. U.S.B. , 2010; pp 1-7

Chueh, P. L.; Prausnitz, J. M. Vapor-liquid equilibria at high pressures: calculation of partial molar volumes in non-polar liquid mixtures. *AICHE J.*, Vol. 13, pp. 1099-1107.

Dagostar, N. Predicting Liquid phase Heat Capacity of Ill-defined Hydrocarbons. Doctoral Dissertation, University of Alberta, Edmonton, Canada, **2013**.

Deroo, G; Powell, B.; Tissot, B. The origin and migrations of petroleum in the Western Canadian Sedimentary Basin, Alberta- Geochemical and thermal maturation study. Geological Survey of Canada Bulletin. **1977.**

Dickson, F. E.; Kunesh, C. J.; McGinnis, E. L.; Petrakis, L. Used of electromagnetic resonance to characterize Vanadium-sulfur species in petroleum. *Anal. Chem.* **1972**, 42, 978.

Ducros, M.; Gruson, J. F.; Sannier, H. Estimation of the Enthalpies of Vaporization of Liquid Organic Compounds. Part 1. Alkanes, Cycloalkanes, Alkenes, Aromatic Hydrocarbons, Alcohols, Thiols, Chloro and Bromoalkanes, Nitriles, Esters, Acides and Aldehydes. *Thermochim. ActB.* **1980**, 36, 39.

Ducros, M.; Gruson, J. F.; Sannier, H. Estimation of the Enthalpies of Vaporization of Liquid Organic Compounds. Part 2. Ethers, Thioalkanes, Ketones and Amines. *Thermochim. ActB.* **1981**, 44, 131.

Ducros, M.; Sannier, H. Determination of vaporization enthalpies of liquid organic compounds. Part 4. Application to organometallic compounds. *Thermochim. ActB.* **1984**, 75 (3), 329.

Ducros, M.; Sannier, H. Estimation of the Enthalpies of Vaporization of Liquid Organic Compounds. Part 3. Unsaturated Hydrocarbons. *Thermochim. ActB.* **1982**, 54, 153.

Dunning, H. N.; Moore, J. W.; Bieber, H.; Williams, R. B. Porphyrin, Nickel, Vanadium and Nitrogen in Petroleum. *J. Chem. Eng. DatB.* **1960**, 5, 547.

Escobedo, J.; Mansoori, G. B. Viscometric principles of the onset of colloidal asphaltene flocculation in paraffinic oils and asphaltene micellization in aromatics. *SPE J.* **1998**, pp. 116-122.

Fang, W; Lei, Q; Lin, R. Enthalpies of vaporization of petroleum fractions from vapor pressure measurements and their correlation along with pure hydrocarbons. *Fluid Phase Equilibria*, **2003**, Vol. 205, pp. 149-161.

Fuhr, B. Heavy Oil and Bitumen Analytical Methods: Understanding Their Capabilities and Limitations. *Canadian Crude Quality Technical Association.* Alberta Research Counsil. **2008.**

Fulem M.; Laštovka, V.; Straka M.; Růžička K.; Shaw J. Heat Capacities of Tetracene and Pentacene. *J. Chem. Eng. DatB.* **2008**, 53, pp. 2175-2181

Gambill, W. R. Predict Critical Temperature. *Chem. Eng.* **1959** 66,181.

Gao, G; Daridon, J. L.; Saint-Guirons, H.; Xans, p.; Montel, F. A simple correlation to evaluate binary interaction parameters of the Peng-Robinson equation of state: binary light hydrocarbon systems, *Fluid Phase Equilibria*, **1992**, Vol. 774, pp. 85-93.

Goossens, B. G. Prediction of Molecular Weight of Petroleum Fractions. *Industrial and Engineering Chemistry Research*, **1996,** Vol. 35, pp. 985-988.

Gopinathan, N; Saraf, D. N. Predict heat of vaporization of crudes and pure components Revised II. *Fluid Phase Equilibria*, **2001**, Vol. 179, pp. 277-284.

Graboski, M. S.; Daubert, T. E. A modified Soave equation of state for phase equilibrium calculations. 2. Systems containing CO2, H2S, N2 and CO. *Ind. Eng. Chem. Proc. Des. Dev.*, **1978**, 17, pp. 448-454.

Gray, M. R. New technique defines the limits of upgrading heavy oils, bitumens. *Oil & Gas Journal*, **2002**, pp. 50-54.

Gray, M. R. Upgrading Petroleum Residues and Heavy Oils. Marcel Dekker. New York. **1994**.

Gupta, S.C.; Gittins, S.D.; Picherack, P. Field Implementation of Solvent Aided Process; CIPC Paper 2002-299, *Can. Int. Petr. Conf.*, Calgary, Alberta, June **2002**.

Hariu, O. H.; Sage, R. C. Crude Split Figured by Computer. *Hydrocarbon Processing*, **1969**, pp. 143-148.

Hepler, L. G. Thermochemical and Thermodynamic Properties. *AOSTRA technical Handbook of Oil Sands, Bitumens and Heavy Oils*. Series No. 6, Edmonton, **1989**.

Hodgson, G. W.; Baker, B. L. Vanadium, Nickel and Porphyrins in Thermal Geochemistry of Petroleum. *Am. Assoc. Petrol. Geol. Bull.* **1957**, 41.

HRES, BP- Heavy Oil; Heavy Oil vs. Light Oil; 2011.

Hsu, C. S.; Robinson, P. R. Practical advances in Petroleum Processing. Vol 1. Springer. U.S.B. **2006**. Ref 1, pp. 438.

International Petroleum Reserves and Resources, U.S. Energy Information Administration, http://www.eiB.gov/emeu/international/oilreserves.html

Jacoby, R. H.; Rzasa, M. J. Equlibrium Vaporization Ratios for Nitrogen, Methane, Carbon Dioxide, Ethane, and Hydrogen Sulfide in Absorber Oil/Natural Gas and Crude Oil/Natural Gas Systems. *Trans.*, AIME, **1952,** 195, 99.

Jain, S. R.; Sundararajan, R. New method of calculating calorific values from elemental compositions of fossil fuels. *Fuel*. **1981**, Vol 60, pp 1079-1082.

Johns, R. B. Biological Markers in the Sedimentary Record. Elsevier. Amsterdam. **1986**.

Kato, K.; Nagahama, K.; Hirata, M. Generalized interaction parameters for the Peng-Robinson equation of state: Carbon dioxide n-paraffin binary systems. *Fluid Phase Equilibria*, **1981**, Vol. 7, pp. 219-231.

Katz, D. L.; Firoozabadi, B. Predicting Phase Behavior of Condensate/Crude Oil Systems Using Methane Interaction Coefficients. *J. Pet. Tech.*, **1978,** 228, pp. 1649-1655.

Kesler, M. G.; Lee, B. I. Improve Prediction of Enthalpy of Fractions, *Hydrocarbon Processing*, **1976**. Vol. 55, pp. 153-158.

Kikic, I.; Vetere, B. Evaluation of several literature equations to predict vaporization enthalpies at the normal boiling point. *Fluid Phase EquilibriB.* **2011**, 309, pp. 151-154.

King, M. B. The Law of Corresponding States for Binary Gas and Liquid Mixtures. *Trans. Faraday So.***1957**, 53, 149.

King, M. B.; Al-Najar, H. A Method for Correlating and Extending Vapor Pressure Data to Lower Temperatures Using Thermal Data: Vapor Pressure Equations for some n-Alkanes at Temperatures below the Normal Boiling Point. *Chemical Engineering Science.* **1974**, 29, pp. 1003-1011

Kokal, S. L.; Najman, J. Sayegh, S. G. George, B. E. Measurement and correlation of asphaltene precipitation from heavy oils by gas injection. *J. Can. Pet. Technol.* **1992**, 31, 24.

Kolska, Z.; Ruzicka, V.; Gani, R. Estimation of the Enthalpy of Vaporization and the Entropy of Vaporization for Pure Organic Compounds at 298.15 K and at Normal Boiling Point Temperature by a Group Contribution Method. *Ind. Eng. Chem. Res.* **2005**, 44, pp. 8436-8454.

Kolska, Z; Zabransky, M.; Randova, B. Group Contribution Methods for Estimation of Selected Physico-Chemical Properties of Organic Compounds. *INTECH*. Chapter 6, **2012**.

Kordas, B.; Tsoutsouras, K.; Stamataki, S.; Tassios, D. A generalized correlation for the interaction coefficients of CO2-hydrocarbon binary mixtures. *Fluid Phase Equilibria*, **1994**, Vol. 93, pp. 141-166.

Korsten, H. Internally Consistent Prediction of Vapor Pressure and Related Properties. *Industrial and Engineering Chemical Research.* **2000**, 39, pp. 813-820.

Larter, S. R.; Head, I. M. Oil Sands and Heavy Oil: Origin and Exploitation, *Elements*, **2014**, Vol. 10, pp. 277-284.

Laštovka, V.; Shaw, J. M. Predictive correlations for ideal gas heat capacities of pure hydrocarbons and petroleum fractions, *Fluid Phase Equilibria* **2013**, 356, pp. 338-370

Leaute, R.P. Liquid Addition to Steam for Enhancing Recovery of Bitumen with CSS: Evolution of Technology from Research Concept to a Field Pilot at Cold Lake; SPE Paper 79011-MS, *SPE Int. Thermal Operations and Heavy Oil Symp. And Int. Horizontal Well Technol. Conf.*, Calgary, Alberta, November **2002**.

Lee, B. I.; Kesler, M. G.; A Generalized Thermodynamic Correlation Based on the Three-Parameter Corresponding States. *American Institute of Chemical Engineering Journal.* **1975**, 21, pp. 510-527.

Lixiong, L.; Kiran, E. Estimation of Critical Properties of Binary Mixtures Using Group Contribution Methods. *Chem. Eng. Comm* **1990**, 94, 131.

Lloyd, W. G.; Davenport, D. B. Applying Thermodynamics to Fossil Fuels: Heats of combustions from elemental compositions. *Journal of Chemical Education*. **1980**, Vol 57(1), pp. 56-60.

Ma, P.; Zhao, X. Modified Group Contribution Method for Predicting the Entropy of Vaporization at the Normal Boiling Point. *Ind. Eng. Chem. Res.* **1993**, 32, 3180.

Maham, Y.; Chodakowski, M. G.; Zhang, X.; Shaw, J. M. Asphaltene phase behavior; Prediction at a crossroads. *Fluid phase Equilib.* **2005**, 227, pp. 177-182.

Mansoori, G. B. Modeling of asphaltene and other heavy organic depositions. *J. Can. Pet. Eng.***1997**, 17, pp. 101-111.

Marrero, J.; Gani, R. Group-Contribution Based Estimation of Pure Substances. *Fluid Phase EquilibriB.* **2001**, pp. 183-184.

Maxwell, J. B.; Bonnell, L. S. Derivation and Precision of a New Vapor Pressure Correlation for Petroleum Hydrocarbons. *Ind. Eng. Chem. Res.* **1957,** *49*(7), pp. 1187-1196.

McKenna, B. M.; Donald, L; Fitzsimmons, J.; Juyal, P.; Spicer, V.; Standing, G; Marshall, B.; Rodgers, R. Heavy Petroleum Composition. 3. Asphaltene Aggregation. *Energy and Fuels*. **2013**, 27, pp. 1246-1256.

Mehrotra, B. K.; Sarkar, M.; and Svrcek, W. Y., Bitumen Density and Gas Solubility Prediction Using the Peng-Robinson Equation of State, AOSTRA Journal of Research, **1985**, pp. 216-229.

Merdrignac, I.; Espinat, D. Physicochemical Characterization of Petroleum Fractions: the State of Art. *Oil and Gas Science and Technology*. **2007**, 62, pp. 7-32.

Moffat, W. Private Communication, Analytical and Instrumentation Laboratory, University of Alberta, Edmonton, Canada, **2012**.

Mojelsky, T. W.; Montgomery, D. S.; Strausz, O. P. The Side Chains Associated with the Undistillable Aromatic and Resin Components of Athabasca Bitumen. AOSTRA J Res. **1986**, Vol 2, 177.

Moysan, J. M.; Paradowski, H.; Vidal, J. Prediction of phase behavior of gas containing systems with cubic equations of state. *Chem. Eng. Sci.*, **1986**, Vol. 41, pp. 2069-2074.

Mullins, O. C. Petroleomics and Structure-Function Relations of Crude Oils and Asphaltenes, in Asphaltenes, Heavy Oils and Petroleomics. New York. **2007**.

Mullins, O. C. Review of the Molecular Structure and Aggregation of Asphaltenes and Petroleomics. *SPE J.* **2008**, pp. 48-57.

Mullins, O. C.; Sheu, E. Y. Structures and Dynamics of Asphaltenes. Plenum Press. New York. **1998.**

Mullins, O. C.; Sheu, E. Y.; Hsmmsmi, B.; Marshall, B. G. Asphaltenes, Heavy Oils and Petroleomics. Springer Science + Business MediB. **2007**. pp 489-507.

Myers, H. S.; Fenske, M. R. Measurement and Correlation of Vapor Pressure Data for High Boiling Hydrocarbons. *Ind. Eng. Chem.* **1955**, 47(8), pp. 1652-1658.

Nars, T.N.; Ayodele, O.R. New Hybrid Steam Solvent Processes for the Recovery of Heavy Oil and Bitumen; SPE Paper 101717, 2*006 Abu Dhabi Int. Petr. Exhibition and Conf.*, Abu Dhabi, U.B.E., November 5-8, **2006.**

National Instruments, LabView 8.6, User Manual, National Instruments Corporation, Texas, **2008**.

Nenniger, J.B. Method and Apparatus for Stimulating Heavy Oil Production. Canadian Patent #2299790. **2005.**

Nishiumi, H.; Arai, T.; Takeuchi, K. Generalization of the binary interaction parameter of the Peng-Robinson equation of state by component family. *Fluid Phase Equilibria*, **1988**, Vol. 42, pp. 43-62.

Nji, G. N. Characterization of Heavy Oils and Bitumens. Doctoral Dissertation, University of Calgary, Calgary, Canada, **2010**.

Nji, G. N.; Svrcek, W. Y.; Yarranton, H. W.; Satyro, M. B. Characterization of Heavy Oils and Bitumens . 1. Vapor Pressure and Critical Constant Prediction Method for Heavy Hydrocarbons. *Energy Fuels*, **2008**, *43*(1), pp. 455-462.

Nji, G. N.; Svrcek, W. Y.; Yarranton, W. H.; Satyro, M. B. Characterization of Heavy Oils and Bitumens 2. Improving the Prediction of Vapor Pressures for Heavy Hydrocarbons at Low Reduced Temperatures Using the Peng−Robinson Equation of State. *Energy & Fuels*, **2009,** *23*(1), pp. 366-373.

Parhizgar, H.; Dehghani, M. R.; Eftekhari, B. Modeling of vaporization enthalpies of petroleum fractons and pure hydrocarbons using genetic programming. *Journal of Petroleum Science and Engineering*. **2013**, 112, pp. 97-104.

Parkash, S.; Moschopedis, S.; Speight, J. Physical properties and surface characteristics of asphaltenes. *Fuel*. **1979**, 58, pp. 877-882.

Payzant, J.D.; Hogg, B. M.; Montgomery, D.S.; Strausz, O.P. A Field Ionization Mass Spectrometric Study of the Maltene Fraction of Athabasca Bitumen. Part I- The saturates. AOSTRA J Res. **1985**, 1, 175.

Payzant, J.D.; Hogg, B. M.; Montgomery, D.S.; Strausz, O.P. A Field Ionization Mass Spectrometric Study of the Maltene Fraction of Athabasca Bitumen. Part II- The Aromatics. AOSTRA J Res. **1985**, 1, 183.

Poirier, M. B.; Bas, B. S. Characterization of Polynuclear Aromatic Hydrocarbons in Bitumen, Heavy Oil Fractions Boiling Above 350 C by Gas Chromatography-Mass Spectrometry. *Fuel*. **1984**, 63, 361.

Poling, B. E.; Prausnitz, J. M.; O'connell, J. P. Properties of gases and liquids, 5th edition, McGraw-hill, New York, **1987**.

Rao, V. K; Bardon, M. F. Estimating the molecular weight of petroleum fractions. *Ind. Eng. Chem. Proc. Des. Dev.*, **1985**, 24, 498.

Read, J.; Whiteoak, D. Shell Bitumen Handbook (5th Edition). ICE Publishing. **2003**.

Reynolds, J. G.; Biggs, W. R. Characterization of vanadium compounds in selected crudes II. Electron paramagnetic resonance studies of the first coordination spheres in Porphyrin and non-porphyrin fractions. *Liq. Fuels Tech.* **1985**, 4, pp. 425-448.

Riazi, M. R. Characterization and Properties of Petroleum Fractions, 1st Edition, *ASTM international*, U.S.B., **2005**

Riazi, M. R.; Daubert, T. E. Analytical Correlations Interconvert Distillation-Curve Types. *Oil & gas J.*, **1986,** 50.

Riazi, M. R.; Daubert, T. E. Simplify property predictions. *Hydro. Pro.* 115, **1980**.

Ringen, S.; Lanum, J; Miknis, F. P. Calculating heating values from elemental compositions of fossil fuels. *Fuel*. **1979**, Vol 58, pp. 69-71.

Rodgers, R. P.; McKenna, B. M. Petroleum Analysis. *Anal. Chem.* **2011**, 83, pp. 4665-4687.

Růžička, K.; Majer, V. Simple and Controlled Extrapolation of Vapor Pressures towards the Triple Point. *AIChE J.* **1996**, 42 (6), pp.1723-1740

Růžička, K.; Majer, V. Simultaneous Correlation of Vapor Pressures and Thermal Data: Application to 1-Alkanols. *Fluid Phase Equilibria.* **1986**, 28, pp. 253-264

Růžička, K.; Majer, V. Simultaneous Treatment of Vapor Pressures and Related Thermal Data between the Triple and Normal Boiling Temperatures for n -Alkanes C5 – C20. *J Phys. Chem*. **1994,** 23

Růžička, K; Fulem, M.; Private Communication, Institute of Chemical Technology, Prague, **2012**.

Sanchez, M.C., Schoeggl, F.F., Taylor, S.D., Fulem, M., Yarranton, H.W. Deep Vacuum Fractionation of Heavy Oil and Bitumen: Part 2 Interconversion Method, *Energy & Fuels*, 28, **2014**, pp. 2866-2873.

Sbaite, P.; Batistella, C. B.; Winter, B.; Vasconcelos, C. J. G.; Maciel, M. R. W.; Filho, R. M.; Gomes, B. True Boiling Point Extended Curve of Vacuum Residue Through Molecular Distillation. *Petroleum Science and Technology*, **2006,** *24*(3-4), pp. 265-274.

Setti, L.; Lanzaniri, G.; Pifferi, P. G.; Spagna, G. Further Research into the Aerobic Degradation of *n*-Alkanes in a Heavy Oil by a Pure Culture of a *Pseudomonas* SP. *Chemosphere*. **1993**, 26, pp. 1151-1157.

Shaw, J. M. Towards common generalized phase diagrams for asphaltene containing hydrocarbon fluids. *ACS Pet. Chem. Div. Prepr*. **2002**, 47, pp. 338-342.

Smith, R. L.; Watson, K. M. Boiling Points and Critical Properties of Hydrocarbon Mixtures. *Ind. Eng. Chem*. **1937,** 29, 1408.

Smith, D. F. Petroleomics Applications of Fourier Transform Ion Cyclotron Resonance Mass Spectrometry: Crude Oil and Bitumen Analysis, Florida State University, October **2007.**

Soreide, I. Improved Phase Behavior Predictions of Petroleum Reservoir Fluids from a Cubic Equation of State. Doctoral Dissertation, Norwegian Inst. Of Technology, Trondheim, Norway, **1989**.

Speight, J. G. Handbook of Petroleum Analysis. John Wiley and Sons, Inc. U.S.B. **2001.**

Speight, J. G. Oil Sand Production Processes. Elsevier Inc. U.S.B. **2013**; pp 1-12.

Straka, M.; Růžička, K.; Růžička, V. Heat Capacities of Chloroanilines and Chloronitrobenzenes. *J. Chem. Eng. DatB.*, **2007**, 52, pp. 1375-1380

Strausz, O. P.; Lown, E. M. The Chemistry of Alberta Oil Sands, Bitumen and Heavy Oils. *Alberta Energy Research Institute*. Calgary, Alberta, **2003.**

Sturm, G. P.; Shay, J. Y. Comprenhensive Report of API Crude Oils Characterization Measurements – Downstream Segment; *API Technical Report 997*. 1st Ed., August, **2000**.

Technical Data Book – Petroleum Refining, third edition, API, New York, **1977.**

Treibs, B. Organic Mineral Substances. II. Ocurrence of Chlorophyl derivatives in an Oil Shale of the Upper Triasic. *Justus Liegbis Ann. Chem.* **1934**, 509, 103.

Tsonopoulos, C.; Heidman, J. L.; Thermodynamic and Transport Properties of Coal Liquids. John Wiley & Sons, Inc., New York, **1986**, pp. 99-113.

Twu, C. H. An Internally Consistent Correlation for Predicting the Critical Properties and Molecular Weight of Petroleum and Coal-Tar Liquids. *Fluid Phase Equilibria*, **1984,** 16,137.

Van Nes, K.; Van Western, H. B. Aspects of Constitution of Minerals Oils, Elsevier New York. **1951.**

Velasco, B.; Roman, F. L.; White, J. B.; Mulero, B. A predictive vapor-pressure equation. *J. Chem. Thermodynamics*. **2008**, 40, pp. 789-797.

Vetere, B. Methods to predict the vaporization enthalpies at the normal boiling temperature of pure compounds revisited. *Fluid Phase Equilibria*, **1995**, Vol.106, No.1-2, pp. 1-10.

Vetere, B. The Riedel Equation. *Ind. Eng. Chem. Res.* **1991**, 30, pp. 2487-2492.

Vickers, A. K. Higher-Temperature Simulated Distillation with DB-HT Sim Dis Columns. Applications. *Agilent Technologies Inc.,* Hydrocarbon Processing, October **2002**, USA.

Villalanti, D. C.; Raia, J. C.; Maynard, J. B. High-temperature Simulated Distillation Applications in Petroleum Characterization. *Encyclopedia of Analytical Chemistry*. **1995.**

Whitson, C. H. Characterizing Hydrocarbon plus Fraction. SPEJ, *Trans*, AIME**, 1983**, 275, pp. 683-694.

Whitson, C.H. Effect of physical properties estimation on equation-of-state predictions. SPE 1120, presented at the *57th Annual Fall Technical Conference and Exhibition of the Society of Petroleum Engineers of AIME*, New Orleans, LA, **1982**.

Yan, H. K.; Zhou,y.; Hepler, L. G. Heats of Combustion of Light and Heavy Oils, *Oilfield Chemistry*. **1998**, 5, 208.

Yarranton, H. W.; Fox, W. B.; Svrcek, W. Y. Effect of Resins on Asphaltene Self-Association and Solubility. *The Canadian Journal of Chemical Engineering*. **2007**, 85, pp. 635-642.

Yaws, Carl L.Yaws' Handbook of Thermodynamic and Physical Properties of Chemical Compounds. Knovel. **2003**, online version available at: http://app.knovel.com/hotlink/toc/id:kpYHTPPCC4/yaws-handbook-thermodynamic/yaws-handbook-thermodynamic

Zais, E. J. *An Improved Binary Interaction Model For The Prediction of Critical Pressures of Multi-component Hydrocarbon Systems*, The University of Texas at Austin, Austin, TX, (1972).

Zhao L. Steam Alternating Solvent Process. SPE Paper 86957, *SPE Int. Thermal Operations and Heavy Oil Symp.*, Bakersfield, California **2004**.

Zou, X. Y.; Shaw, J. M. Dispersed phases and dispersed phase deposition issues arising in asphaltene rich hydrocarbon fluids. *J. Pet. Sci. Technol.* **2004**, 22, pp.759-771.

APPENDIX A: TREATMENT OF DISTILLATION DATA TO OBTAIN TBP FOR HEAVY OILS

Two main points regarding physical (SBD), simulated (ASTM D7169), and TBP data are reviewed in this chapter. First, a validation of SBD data as TBP data will be presented. Then a preliminary correction factor as a function of the bulk specific gravity and molecular weight for simulated distillation will be proposed to correct the predicted boiling point of the heavy ends of a sample.

A.1. Is SBD Data Equivalent to a TBP Curve?

A TBP is defined as the boiling temperature measured at distillation conditions that provide the highest degree of separation possible for a petroleum fluid; that is, at high reflux ratios and a large number of theoretical plates. The standard laboratory conditions for a TBP curve are a distillation column with 15-100 theoretical plates and a 5:1 reflux ratio (Villalanti *et al.*, 1997; Riazi, 2005; ASTM D2882). For samples with wide boiling ranges, such as heavy oils, the only physical distillations considered to provide TBP data are the ASTM D2892 and D5236 methods after inter-conversion to AET. ASTM D2892 is an atmospheric distillation while D5236 is a vacuum distillation.

One approach to verify that the SBD provides TBP data is then to compare an SBD boiling curve with those obtained with ASTM D5236. Unfortunately, for the crude oils used in this study, ASTM D2892 and D5236 were not measured due to the cost associated with the experiments. An alternative approach is to compare the SDB distillations with high temperature simulated distillations (ASTM D7169). ASTM D7169 is an extension of the ASTM D2887 method for petroleum cuts and mixtures containing boiling range material above 811 K (538 ˚C). Villalanti and coworkers (Villalanti *et al.*, 1997, 2000; Golden *et al.*, 1995) compared ASTM D7169 results with physical distillations (ASTM D2892 and D5236) for 100 crudes ranging in API gravity from light to heavy. Overall, they concluded that the difference was less than 2% mass between the initial boiling point and a cut temperature of 650 K. However, for boiling temperatures above 650 K they observed a deviation between physical and simulated distillation. They attributed this difference to the change between physical distillations from atmospheric (D2892) to vacuum

(D5236) conditions. Another important observation was that the simulated distillation was consistently higher than the physical distillation and the deviations grew larger and at a lower temperature form the light to the heavy samples

Keeping these results in mind, a comparison up to a temperature of 650 K was made between the SBD data and the ASTM D7169 data. Figure A.1 presents the SBD and ASTM D7169 data collected for the oil WC-B-D1. The SBD data are in good agreement with the ASTM D7169 distillation, confirming that the SBD AET correspond to TBP data. This was also the case for the other three oils for which ASTM 7169 was measured (see Figure A.2). The average absolute and relative deviation was less than 2.1% and 8 K, respectively.

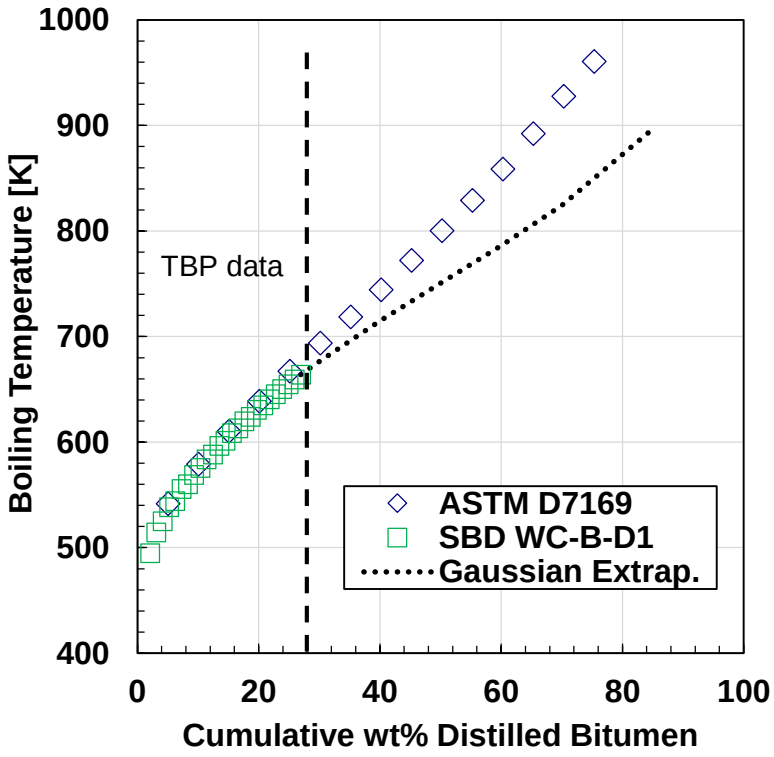

Figure A.1. Comparison between experimental SBD and ASTM 7169 data for a the WC-B-D1 sample.

Figure A.2. Comparison between experimental SBD and ASTM 7169 data for a bitumen sample

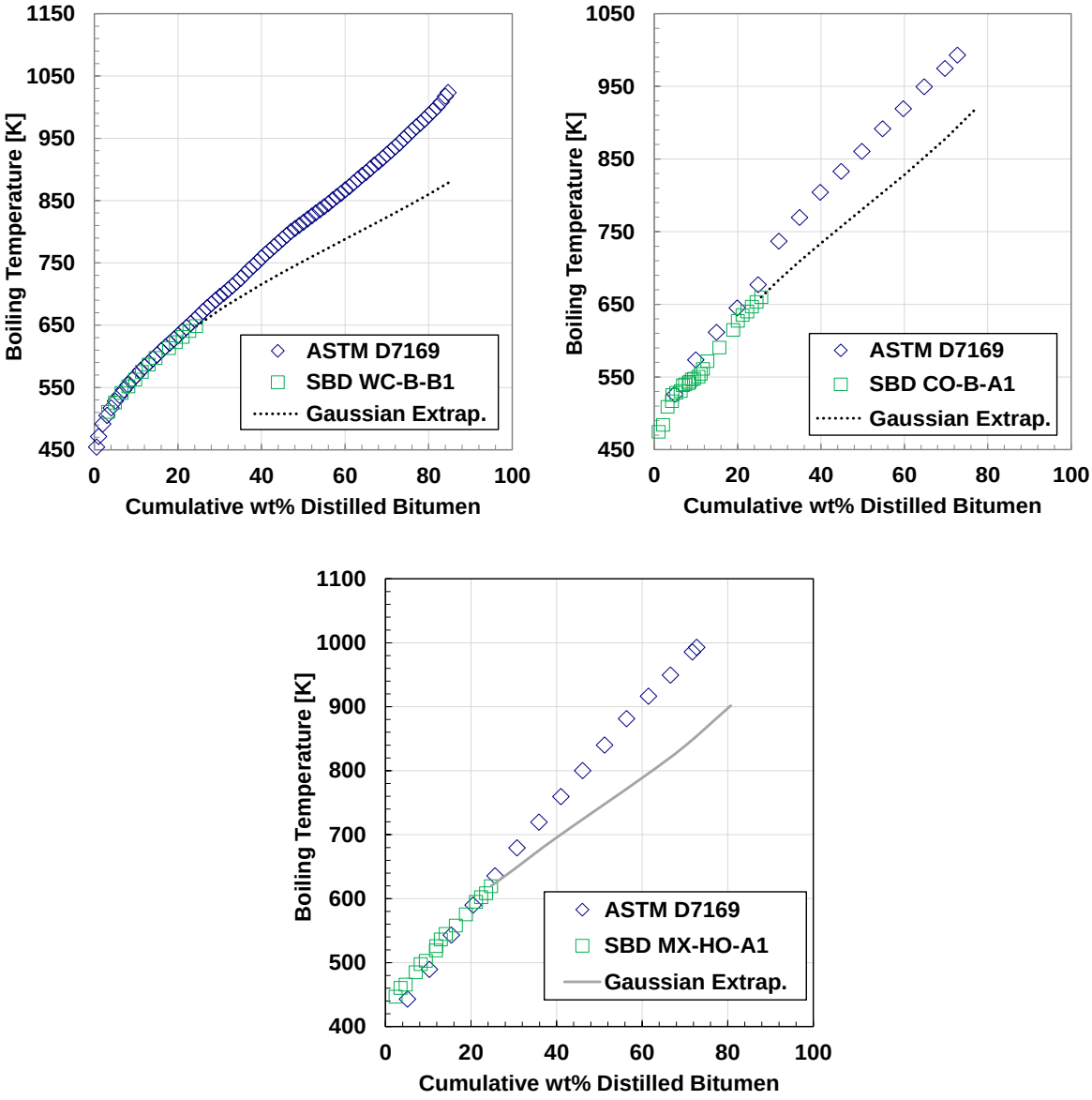

A.2. Correction of Simulated Distillation for Heavy Oils and Bitumen Samples

In this thesis, it was shown that the heavier distillation cuts followed the Gaussian extrapolation of the SBD data by the simultaneous correlation of vapor pressure and heat capacity. Also the study presented by Castellanos *et al.* (2011) demonstrated that when the maltene fraction is characterized using the entire ASTM D7169 data the phase behavior is incorrectly predicted, whereas if the characterization was performed using only the distillation data up to 40 wt% distilled

(~700 K) and a Gaussian extrapolation for the remainder of the maltenes, a better phase boundary prediction was obtained.

Figure A.1 shows that the Gaussian extrapolation deviates from ASTM D7169 data above a boiling temperature of 650 K, the same temperature Villalanti and coworkers observed higher discrepancies between physical and simulated distillation. They attributed the deviation to a switch from atmospheric and vacuum conditions. The most likely reason for the deviation is that the calibration standards used to correlate retention times and boiling points do not extrapolate to higher boiling cuts. Several authors (Boczkaj and Kaminski, 2013; Boczkaj and Przyjazny, 2011; Roussis and Fitzgerald, 2000; Durand *et al.*, 1999; Petroff *et al.*, 1987) have shown that the basic principle under which simulated distillation works does not apply to aromatic compounds (linearity between retention time and boiling point). The choice of the stationary phase also has a significant impact on whether or not there is agreement between the simulated and real distillation curves (Durand *et al.*, 1999).

Another possibility is that some cracking occurs at the high temperatures to which the samples are subjected in a high temperature SimDist. On-column thermal cracking has been demonstated with the appearance of a bimodal distribution of the chromatogram obtained using ASTM D7961 (Carbognani *et al.*, 2007). Using this bimodal response, Carbognani and coworkers (2007) were able to indicate the level of thermal maturity of the samples and to use the abundance of the second peak as an index of crackability. Other authors (Speight, 2001; Altgelt and Boduszynski, 1994) have also reported possible cracking of organic compounds due to the severe temperatures employed for elution of the heavy fraction of the samples (~703 K, 430˚C).

Hence, above a boiling temperature of 600 K the simulated boiling points require a correction to account for the incorrect boiling point predictions for the heavy ends. The following correction was designed to match the Gaussian extrapolation of the physical distillation obtained with SBD for three bitumen samples (WC-B-D1, CO-B-A1 and MX-HO-A1):

For TBP > 650 K:

$$T_{CF} = T_{SD} - x \qquad (A.1)$$

$$x = (-6.12x10^{-6}\, wt\%^2 + 0.346\, wt\% - 5.6)\left(\frac{MW_{Bulk}}{100 * SG_{Bulk}}\right) \qquad (A.2)$$

where T_{CF} (in K) is the corrected temperature that matches the boiling points corresponding to extrapolated SBD data, T_{SD} (in K) is the measured temperature using ASTM D7169, wt% is the cumulative weight percent of the corresponding T_{SD}, and MW_{Bulk} and SG_{Bulk} correspond to the molecular weight an specific gravity of the whole sample. Figure 8.9a presents a relative deviation plot for the fitted boiling points. The absolute and relative error of the fitted boiling temperatures were less than 13 K and 1.7 %, respectively, with a bias of 0.1%.

A fourth oil (WC-B-B1) was used to test Equations A.1 and A.2. Figure A.3 presents a relative deviation plot for the predicted boiling points. Note, the simulated distillation data collected for this sample was obtained from a different laboratory. The absolute and relative error of the fitted boiling temperatures were 5 K and 0.7 %, respectively, with a bias of 0.7%. Although the results are promising they are only preliminary. More data are required in order to build a more robust correction factor. Figure A.4 presents the plots of the corrected boiling temperature for the four oil samples used in this study.

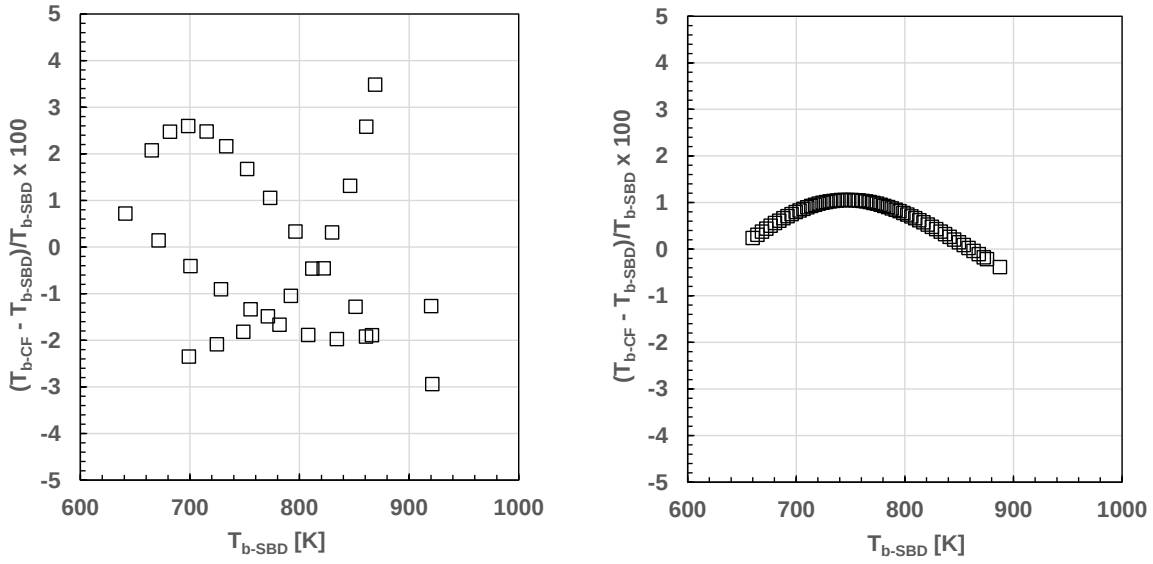

Figure A.3. Relative deviation obtained for the left) development data set and right) test data set.

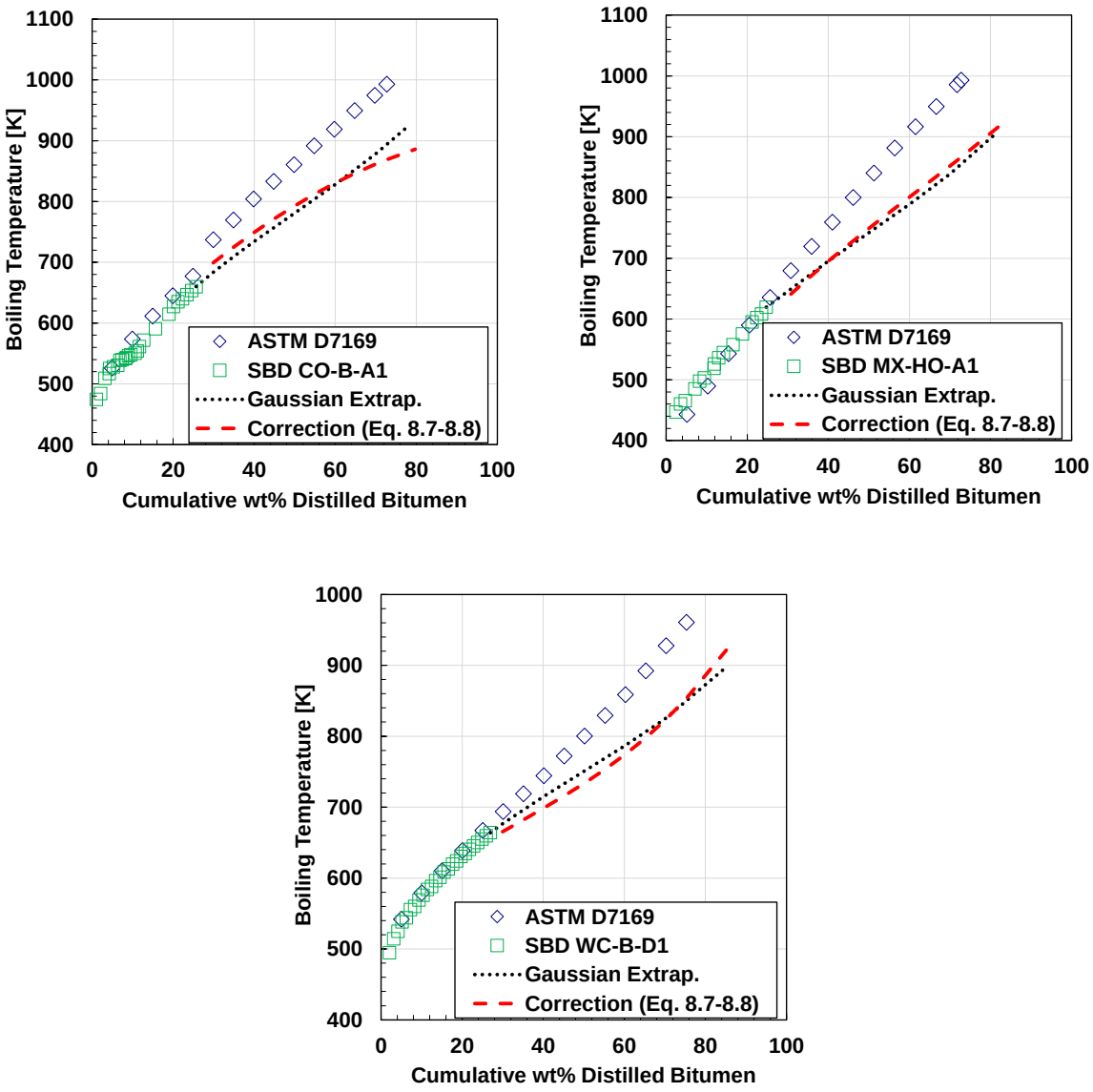

Figure A.4. Results obtained for the fitted boiling temperature of the development data set.

A.3. Deasphalted Specific Gravity Prediction

A simple correlation, Equation A.3 between bulk specific gravity and asphaltene content (wt%) was developed in this study with the goal of predicting the specific gravity of the deasphalted fraction of the mixture, which was required for some of the correlations developed in this study to predict physical properties.

$$SG_{DAO} = \left(\frac{SG_{Bulk}}{0.9534 * wt\%\ asp^{\,0.020266}}\right)^{1/0.0684} \qquad (A.3)$$

The specific gravity average absolute and relative deviations obtained with Equation A.3 were less than 0.006 and 0.6 % respectively.

APPENDIX B: DISTILLATION DATA FROM DVFA

Distillation data including density and molecular weight of each fraction is presented in Tables B.1 to B.6

Table B.1. Distillation data of CO-B-A1

Cut	Temperature [K]	Cumulative wt% Bitumen Distilled	Molecular Weight [g/mol]	Density [kg/m^3]
0	413	10.9	235.9	898.0
1	423	15.7	257.7	921.0
2	443	19.7	301.4	941.7
3	463	23.0	328.7	956.8
4	483	26.9	380.2	966.1
5	513	33.0	398.3	976.8
6	533	37.6	475.3	988.9
7	563	**42.8**	515.6	993.7
res	>563		971.0	1004.2

Table B.2. Distillation data of MX-HO-A1

Cut	Temperature [K]	Cumulative wt% Bitumen Distilled	Molecular Weight [g/mol]	Density [kg/m^3]
0	413	12.74	207.0	858.2
1	423	16.96	264.8	899.2
2	443	19.94	284.8	916.7
3	463	25.13	325.4	928.5
4	483	28.45	345.5	940.4
5	513	33.25	408.2	950.5
6	533	37.47	436.0	963.8
7	563	41.45	468.1	967.1
res	>563		999.0	1023.5

Table B.3. Distillation data of CO-B-B1

Cut	Temperature [K]	Cumulative wt% Bitumen Distilled	MolecularWeight [g/mol]	Density [kg/m^3]
0	413	13.32	233.9	884.8
1	423	18.45	280.8	921.7
2	443	22.60	306.1	935.2
3	463	29.76	350.3	945.6
4	483	33.60	387.8	956.8
5	513	38.98	431.7	962.2
6	533	42.23	447.3	973.1
7	563	46.03	476.4	979.9
res	>563		920.1	1017.8

Table B.4. Distillation data of US-OH-A1

Cut	Temperature [K]	Cumulative wt% Bitumen Distilled	Molecular Weight [g/mol]	Density [kg/m^3]
0	413	14.9	227.0	866.8
1	423	19.9	260.8	898.8
2	443	25.8	294.9	915.9
3	463	29.7	337.3	923.9
4	483	34.9	372.2	933.9
5	513	43.4	410.6	946.1
6	533	48.6	484.5	956.1
7	563	53.4	493.3	958.6
res	>563		841.1	1010.0

Table B.5. Distillation data of WC-B-D1

Cut	Temperature [K]	Cumulative wt% Bitumen Distilled	Molecular Weight [g/mol]	Density [kg/m^3]
0	413	7.3	224.8	889.1
1	423	11.1	259.3	913.8
2	443	16.7	287.4	934.5
3	463	22.3	323.2	949.9
4	483	26.9	372.1	958.9
5	513	31.2	451.0	963.4
6	533	35.7	463.3	966.0
7	563	41.9	546.0	969.8
res	>563		1047.8	1011.5

Table B.6. Distillation data of RO-HO-A1

Cut	Temperature [K]	Cumulative wt% Bitumen Distilled	Molecular Weight [g/mol]	Density [kg/m^3]
0	413	14.8	231.7	893.8
1	423	20.9	258.9	920.7
2	443	24.8	289.1	937.6
3	463	35.2	339.9	948.6
4	483	45.7	378.2	954.3
5	513	52.6	399.4	959.9
6	533	57.9	442.2	963.2
7	563	62.2	498.9	970.0
res	>563		978.9	991.8

APPENDIX C: . IDEAL GAS HEAT CAPACITY

Ideal gas heat capacity calculated for several fractions of seven different heavy oil and bitumen samples is presented in Tables B1 to B7

Table C.1. Calculated ideal molar heat capacity of WC-B-B1

Temperature [K]	C_p^{ig} [J mol^{-1} K^{-1}]					
	Cut 1	Cut 2	Cut 3	Cut 4	Cut 5	Cut 6
258.1	281.7	302.6	349.4	398.5	452.6	493.9
263.2	287.5	308.8	356.6	406.7	461.6	504.0
268.3	293.2	314.9	363.6	414.7	470.6	514.0
273.4	298.9	321.1	370.7	422.8	479.6	524.1
278.5	304.6	327.2	377.8	430.9	488.6	534.1
283.6	310.3	333.4	384.9	438.9	497.6	544.1
288.7	315.9	339.5	392.0	447.0	506.5	554.1
293.8	321.6	345.6	399.0	455.0	515.5	564.1
298.9	327.3	351.7	406.1	463.0	524.4	574.1
304.0	332.9	357.8	413.1	471.1	533.3	584.1
309.1	338.5	363.9	420.1	479.0	542.2	594.0
314.2	344.2	369.9	427.1	487.0	551.1	604.0
319.4	349.7	376.0	434.1	495.0	559.9	613.8
324.5	355.3	382.0	441.0	502.9	568.7	623.7
329.6	360.9	388.0	448.0	510.8	577.5	633.5
334.7	366.4	393.9	454.9	518.6	586.2	643.3
339.8	371.9	399.9	461.7	526.5	594.9	653.1
344.9	377.4	405.8	468.6	534.3	603.6	662.8
350.0	382.8	411.7	475.4	542.0	612.3	672.4
355.1	388.3	417.6	482.2	549.8	0.0	682.1

Table C.2. Calculated ideal molar heat capacity of CO-B-A1

Temperature [K]	C_p^{ig} [J mol^{-1} K^{-1}]						
	Cut 0	Cut 1	Cut 2	Cut 3	Cut 4	Cut 5	Cut 6
261.5	272.6	295.6	339.0	367.5	426.2	444.3	526.0
265.0	276.4	299.8	344.1	372.7	430.8	449.7	533.2
270.0	281.8	305.6	350.7	379.8	439.0	458.3	543.4
275.0	287.2	311.4	357.3	387.0	447.3	466.9	553.6
280.0	292.6	317.2	363.9	394.1	455.6	475.6	563.9
285.0	298.0	323.0	370.5	401.3	463.8	484.2	574.1
290.0	303.3	328.8	377.1	408.4	472.1	492.8	584.3
295.0	308.7	334.5	383.7	415.5	480.3	501.4	594.5
300.0	314.0	340.3	390.2	422.6	488.5	509.9	604.6
305.0	319.3	346.0	396.8	429.7	496.7	518.5	614.8
310.0	324.6	351.7	403.3	436.8	504.9	527.0	624.9
315.0	329.9	357.4	409.8	443.8	513.0	535.5	635.0
320.0	335.1	363.0	416.3	450.8	521.1	544.0	645.0
325.0	340.4	368.7	422.7	457.8	529.2	552.4	655.1
330.0	345.6	374.3	429.2	464.8	537.3	560.8	665.1
335.0	350.8	379.9	435.6	471.8	545.3	569.2	675.0
340.0	355.9	385.5	442.0	478.7	553.3	577.6	684.9
345.0	361.1	391.0	448.3	485.6	561.3	585.9	694.8
350.0	366.2	396.6	454.7	492.4	569.2	594.2	704.6
354.8	371.1	402.1	460.3	498.9	577.0	602.2	713.8

Table C.3. Calculated ideal molar heat capacity of MX-HO-A1

Temperature [K]	C_p^{ig} [J mol^{-1} K^{-1}]							
	Cut 0	Cut 1	Cut 2	Cut 3	Cut 4	Cut 5	Cut 6	Cut 7
300.0	280.0	350.4	372.4	424.0	448.4	528.9	561.8	595.9
305.0	284.7	356.3	378.7	431.1	456.0	537.8	571.3	605.9
310.0	289.5	362.2	384.9	438.3	463.5	546.6	580.7	615.9
315.0	294.2	368.1	391.2	445.4	471.0	555.4	590.1	625.9
320.0	298.9	373.9	397.4	452.4	478.4	564.3	599.4	635.8
325.0	303.6	379.8	403.6	459.5	485.9	573.0	608.7	645.7
330.0	308.3	385.6	409.7	466.5	493.3	581.8	618.0	655.5
335.0	312.9	391.4	415.9	473.5	500.7	590.5	627.3	665.4
340.0	317.6	397.1	422.0	480.4	508.0	599.1	636.5	675.1
345.0	322.2	402.9	428.1	487.3	515.4	607.8	645.7	684.9
350.0	326.8	408.6	434.1	494.2	522.6	616.4	654.8	694.6
355.0	331.3	414.3	440.2	501.1	529.9	624.9	663.9	704.2
360.0	335.9	419.9	446.2	508.0	537.1	633.5	673.0	713.9
365.0	340.4	425.6	452.2	514.8	544.3	642.0	682.0	723.4
370.0	344.9	431.2	458.1	521.6	551.5	650.4	691.0	733.0
375.0	349.4	436.8	464.1	528.3	558.7	658.8	699.9	742.5
380.0	353.9	442.4	470.0	535.0	565.8	667.2	708.8	751.9
385.0	358.3	447.9	475.9	541.7	572.8	675.6	717.7	761.3
390.0	362.8	453.4	481.7	548.4	579.9	683.9	726.5	770.7
395.0	367.2	458.9	487.6	555.0	586.9	692.1	735.3	780.0

Table C.4. Calculated ideal molar heat capacity of CO-B-B1

Temperature [K]	C_p^{ig} [J mol^{-1} K^{-1}]						
	Cut 0	**Cut 1**	**Cut 2**	**Cut 3**	**Cut 4**	**Cut 5**	**Cut 6**
300.0	317.6	373.3	405.2	460.7	507.1	563.7	580.2
305.0	323.0	379.6	411.9	468.4	515.6	573.1	589.9
310.0	328.3	385.8	418.7	476.0	524.1	582.5	599.5
315.0	333.6	392.0	425.4	483.7	532.5	591.9	609.2
320.0	338.9	398.2	432.2	491.3	540.9	601.2	618.8
325.0	344.2	404.4	438.9	498.9	549.3	610.5	628.4
330.0	349.5	410.5	445.5	506.5	557.6	619.8	637.9
335.0	354.7	416.6	452.2	514.1	565.9	629.1	647.4
340.0	359.9	422.7	458.8	521.6	574.2	638.3	656.9
345.0	365.1	428.8	465.4	529.1	582.4	647.4	666.3
350.0	370.3	434.9	472.0	536.6	590.7	656.6	675.7
355.0	375.5	440.9	478.5	544.0	598.8	665.7	685.1
360.0	380.6	446.9	485.0	551.4	607.0	674.7	694.4
365.0	385.7	452.9	491.5	558.8	615.1	683.7	703.7
370.0	390.8	458.8	498.0	566.1	623.2	692.7	713.0
375.0	395.9	464.8	504.4	573.4	631.2	701.7	722.2
380.0	400.9	470.7	510.8	580.7	639.2	710.6	731.3
385.0	405.9	476.5	517.2	588.0	647.2	719.4	740.5
390.0	410.9	482.4	523.5	595.2	655.2	728.3	749.6
395.0	415.9	488.2	529.8	602.3	663.1	737.1	758.6

Table C.5. Calculated ideal molar heat capacity of US-OH-A1

Temperature [K]	C_p^{ig} [J mol^{-1} K^{-1}]							
	Cut 0	Cut 1	Cut 2	Cut 3	Cut 4	Cut 5	Cut 6	Cut 7
300.0	309.6	350.2	392.3	447.7	491.9	541.8	634.3	641.2
305.0	314.8	356.1	398.9	455.2	500.1	550.9	645.0	652.0
310.0	320.1	362.0	405.4	462.7	508.4	559.9	655.6	662.7
315.0	325.3	367.9	412.0	470.2	516.6	569.0	666.2	673.4
320.0	330.5	373.7	418.5	477.6	524.8	578.0	676.7	684.0
325.0	335.6	379.5	425.0	485.0	532.9	587.0	687.2	694.7
330.0	340.8	385.3	431.5	492.4	541.0	595.9	697.7	705.2
335.0	345.9	391.1	438.0	499.8	549.1	604.8	708.1	715.8
340.0	351.0	396.8	444.4	507.1	557.2	613.7	718.5	726.3
345.0	356.1	402.6	450.8	514.4	565.2	622.5	728.8	736.7
350.0	361.2	408.3	457.2	521.7	573.2	631.3	739.1	747.1
355.0	366.2	413.9	463.5	529.0	581.2	640.1	749.4	757.5
360.0	371.2	419.6	469.9	536.2	589.1	648.8	759.6	767.8
365.0	376.2	425.2	476.1	543.4	597.0	657.5	769.7	778.1
370.0	381.2	430.8	482.4	550.5	604.8	666.2	779.9	788.4
375.0	386.2	436.4	488.7	557.6	612.7	674.8	790.0	798.6
380.0	391.1	442.0	494.9	564.7	620.4	683.4	800.0	808.7
385.0	396.0	447.5	501.1	571.8	628.2	691.9	810.0	818.8
390.0	400.9	453.0	507.2	578.8	635.9	700.4	820.0	828.9
395.0	405.8	458.5	513.4	585.8	643.6	708.9	829.9	838.9

Table C.6. Calculated ideal molar heat capacity of WC-B-D1

Temperature [K]	C_p^{ig} [J mol^{-1} K^{-1}]							
	Cut 0	**Cut 1**	**Cut 2**	**Cut 3**	**Cut 4**	**Cut 5**	**Cut 6**	**Cut 7**
300.0	306.4	348.0	380.3	423.9	487.4	589.8	605.2	711.0
305.0	311.6	353.9	386.6	431.0	495.5	599.7	615.3	722.9
310.0	316.8	359.7	393.0	438.0	503.6	609.5	625.4	734.8
315.0	321.9	365.5	399.3	445.1	511.8	619.3	635.5	746.6
320.0	327.0	371.3	405.6	452.1	519.8	629.1	645.5	758.4
325.0	332.2	377.1	411.9	459.1	527.9	638.8	655.5	770.2
330.0	337.2	382.8	418.2	466.1	535.9	648.6	665.5	781.9
335.0	342.3	388.6	424.4	473.1	543.9	658.2	675.4	793.6
340.0	347.4	394.3	430.7	480.0	551.9	667.9	685.3	805.2
345.0	352.4	399.9	436.9	486.9	559.8	677.5	695.2	816.8
350.0	357.4	405.6	443.0	493.8	567.7	687.0	705.0	828.3
355.0	362.4	411.2	449.2	500.6	575.6	696.6	714.8	839.8
360.0	367.3	416.8	455.3	507.4	583.4	706.0	724.5	851.3
365.0	372.3	422.4	461.4	514.2	591.2	715.5	734.2	862.7
370.0	377.2	428.0	467.5	521.0	599.0	724.9	743.8	874.0
375.0	382.1	433.5	473.5	527.7	606.7	734.2	753.4	885.3
380.0	387.0	439.1	479.5	534.4	614.4	743.6	763.0	896.5
385.0	391.8	444.5	485.5	541.1	622.1	752.9	772.5	907.7
390.0	396.7	450.0	491.5	547.7	629.7	762.1	782.0	918.9
395.0	401.5	455.5	497.4	554.3	637.3	771.3	791.5	930.0

Table C.7. Calculated ideal molar heat capacity of RO-HO-A1

Temperature [K]	C_p^{ig} [J mol^{-1} K^{-1}]							
	Cut 0	**Cut 1**	**Cut 2**	**Cut 3**	**Cut 4**	**Cut 5**	**Cut 6**	**Cut 7**
300.0	318.0	349.9	386.8	454.9	509.2	532.5	586.6	660.3
305.0	323.4	355.8	393.3	462.5	517.7	541.4	596.4	671.3
310.0	328.8	361.6	399.8	470.1	526.3	550.3	606.2	682.3
315.0	334.1	367.5	406.2	477.6	534.8	559.2	616.0	693.2
320.0	339.5	373.3	412.6	485.2	543.2	568.0	625.7	704.2
325.0	344.8	379.1	419.0	492.7	551.7	576.8	635.4	715.0
330.0	350.1	384.9	425.4	500.2	560.1	585.6	645.0	725.9
335.0	355.3	390.7	431.7	507.7	568.4	594.3	654.6	736.7
340.0	360.6	396.4	438.0	515.1	576.8	603.0	664.2	747.5
345.0	365.8	402.1	444.3	522.5	585.1	611.7	673.7	758.2
350.0	371.0	407.8	450.6	529.9	593.3	620.3	683.2	768.9
355.0	376.2	413.5	456.9	537.2	601.6	628.9	692.7	779.5
360.0	381.4	419.1	463.1	544.5	609.8	637.4	702.1	790.1
365.0	386.5	424.7	469.3	551.8	617.9	646.0	711.5	800.7
370.0	391.6	430.3	475.4	559.0	626.1	654.5	720.8	811.2
375.0	396.7	435.9	481.6	566.3	634.2	662.9	730.1	821.7
380.0	401.8	441.4	487.7	573.5	642.2	671.3	739.4	832.1
385.0	406.8	447.0	493.8	580.6	650.3	679.7	748.6	842.5
390.0	411.9	452.5	499.9	587.7	658.2	688.1	757.8	852.8
395.0	416.9	457.9	505.9	594.8	666.2	696.4	767.0	863.1

APPENDIX D: LIQUID HEAT CAPACITY

Measured liquid heat capacity of the fractions is presented in Tables C1 to C4. Tables C5 to C7 contain the calculated liquid heat capacities using Eq. 5.15 introduced in Chapter 5.

Table D.1. Measured liquid molar heat capacity of WC-B-B1

Temperature [K]	C_p^{liq} [J mol^{-1} K^{-1}]					
	Cut 1	Cut 2	Cut 3	Cut 4	Cut 5	Cut 6
258.1	420.9	459.8	536.7	612.4	698.6	775.7
263.2	425.5	464.7	542.4	619.0	705.4	782.7
268.3	430.0	469.6	548.1	625.5	711.7	790.4
273.4	434.6	474.5	553.8	632.0	718.6	797.4
278.5	439.1	479.4	559.5	638.5	725.5	805.1
283.6	443.7	484.3	565.3	645.1	732.4	812.9
288.7	448.2	489.2	571.0	651.6	739.8	820.6
293.8	452.8	494.1	576.7	658.1	746.0	828.9
298.9	457.3	499.0	582.4	664.6	752.7	835.9
304.0	461.8	503.9	588.1	671.2	759.7	843.4
309.1	466.4	508.8	593.8	677.7	766.7	851.2
314.2	470.9	513.6	599.6	684.2	773.9	859.1
319.4	475.5	518.5	605.3	690.8	781.3	867.1
324.5	480.0	523.4	611.0	697.3	788.4	875.4
329.6	484.6	528.3	616.7	703.8	795.7	883.4
334.7	489.1	533.2	622.4	710.3	803.2	891.5
339.8	493.7	538.1	628.1	716.9	810.5	899.9
344.9	498.2	543.0	633.9	723.4	817.9	908.1
350.0	502.8	547.9	639.6	729.9	825.0	916.5

Table D.2. Measured liquid molar heat capacity of CO-B-A1

Temperature [K]	C_p^{liq} [J mol^{-1} K^{-1}]						
	Cut 0	Cut 1	Cut 2	Cut 3	Cut 4	Cut 5	Cut 6
261.5	395.9	429.4	504.1	549.4	624.3	653.5	791.9
265.0	398.1	431.8	503.8	555.7	629.7	655.8	795.5
270.0	401.7	435.6	505.7	558.2	640.8	661.0	801.6
275.0	405.6	439.8	510.6	555.8	649.6	669.3	809.0
280.0	409.7	444.3	515.6	559.8	651.5	682.6	817.4
285.0	414.6	449.4	521.4	566.0	651.9	693.2	826.1
290.0	419.2	454.2	526.9	572.0	657.8	691.5	837.1
295.0	422.8	458.4	531.9	576.8	664.5	697.3	846.4
300.0	427.4	464.1	538.3	584.7	671.6	704.6	852.6
305.0	434.1	470.2	543.1	589.3	678.5	712.3	861.3
310.0	437.9	474.7	548.2	594.8	686.3	720.0	869.9
315.0	442.2	477.7	555.2	601.8	693.2	727.2	878.4
320.0	445.6	481.9	560.1	607.3	699.6	733.9	887.1
325.0	450.2	488.3	565.1	613.6	706.1	741.5	896.2
330.0	454.7	493.0	570.8	619.7	713.2	748.5	903.9
335.0	459.8	498.4	576.3	625.2	720.0	755.3	911.8
340.0	465.0	503.6	582.7	631.7	727.2	762.6	921.3
345.0	469.8	508.7	587.6	637.7	733.8	770.5	930.6
350.0	474.7	513.4	593.3	643.8	741.1	777.5	939.8
354.8	479.1	518.4	598.4	649.4	747.6	784.4	948.6

Table D.3. Measured liquid molar heat capacity of MX-HO-A1

C_p^{liq} [J mol^{-1} K^{-1}]									
Temp. [K]	**Cut 0**	**Temp. [K]**	**Cut 1**	**Temp. [K]**	**Cut 2**	**Temp. [K]**	**Cut 3**	**Temp. [K]**	**Cut 4**
265.0	376.0	281.4	485.3	291.3	522.7	299.0	602.9	300.9	631.8
270.0	378.4	285.0	488.1	295.0	525.5	300.4	603.9	305.0	636.0
275.0	381.3	290.0	492.5	300.0	529.9	305.0	608.2	310.0	641.4
280.0	384.4	295.0	495.2	305.0	534.3	310.0	613.4	315.0	646.9
285.0	388.2	300.0	501.4	310.0	538.9	315.0	618.8	320.0	652.4
290.0	392.5	305.0	504.7	315.0	543.6	320.0	624.1	325.0	658.3
295.0	394.4	310.0	508.1	320.0	548.4	325.0	629.9	330.0	665.1
300.0	398.9	315.0	513.6	325.0	553.4	330.0	636.4	335.0	671.3
305.0	402.5	320.0	518.1	330.0	559.2	335.0	642.4	340.0	676.7
310.0	405.1	325.0	522.9	335.0	564.3	340.0	647.6	345.0	682.5
315.0	409.6	330.0	527.2	340.0	568.8	345.0	652.8	350.0	688.9
320.0	413.5	335.0	531.5	345.0	573.5	350.0	658.4	355.0	695.3
325.0	417.1	340.0	535.7	350.0	578.4	355.0	664.4	358.0	699.5
330.0	420.7	345.0	540.1	355.0	583.5	357.9	667.9		
335.0	424.5	350.0	544.6	357.9	586.8				
340.0	428.0	355.0	548.5						
345.0	431.6	358.1	550.6						
350.0	435.6								
355.0	439.2								
357.7	441.8								

Table D.4. Measured and calculated liquid molar heat capacity of CO-B-B1

C_p^{liq} [J mol^{-1} K^{-1}]											
Temp. [K]	**Cut 0**	**Temp. [K]**	**Cut 1**	**Temp. [K]**	**Cut 2**	**Temp. [K]**	**Cut 3**	**Temp. [K]**	**Cut 5***	**Cut 6***	**Cut 7***
262.4	400.8	275.0	482.6	289.0	545.6	300.0	630.5	300.0	759.9	808.4	860.6
265.0	402.8	276.0	484.2	290.3	546.7	301.5	631.5	305.0	766.6	815.6	868.5
270.0	406.5	280.0	489.4	295.0	551.9	305.0	635.4	310.0	773.3	822.9	876.4
275.0	410.3	285.0	495.1	300.0	557.9	310.0	641.4	315.0	780.2	830.3	884.5
280.0	414.4	290.0	500.3	305.0	562.2	315.0	647.6	320.0	787.1	837.7	892.6
285.0	419.2	295.0	504.4	310.0	568.1	320.0	653.8	325.0	794.2	845.3	900.8
290.0	423.8	300.0	511.4	315.0	574.1	325.0	660.3	330.0	801.3	853.0	909.1
295.0	427.7	305.0	514.7	320.0	579.6	330.0	667.7	335.0	808.5	860.7	917.5
300.0	431.5	310.0	519.0	325.0	585.9	335.0	674.4	340.0	815.8	868.5	926.0
305.0	437.0	315.0	525.2	330.0	591.2	340.0	680.5	345.0	823.2	876.5	934.5
310.0	439.8	320.0	530.9	335.0	596.1	345.0	686.6	350.0	830.7	884.5	943.2
315.0	443.8	325.0	537.0	340.0	601.4	350.0	693.1	355.0	838.3	892.6	951.9
320.0	450.3	330.0	542.0	345.0	606.6	355.0	699.6	360.0	845.9	900.8	960.8
325.0	454.8	335.0	546.4	350.0	612.8	357.9	703.8	365.0	853.7	909.1	969.7
330.0	458.0	340.0	551.8	355.0	618.0			370.0	861.5	917.5	978.7

335.0	461.5	345.0	556.4	357.8	621.3	375.0	869.4	925.9	987.9
340.0	467.1	350.0	562.1			380.0	877.4	934.5	997.1
345.0	471.9	355.0	567.3			385.0	885.5	943.2	1006.4
350.0	476.6	357.6	568.9			390.0	893.7	951.9	1015.7
355.0	481.3					395.0	902.0	960.7	1025.2

***Predicted values using Eq. 5.16**

Table D.5. Calculated liquid molar heat capacity of US-OH-A1

Temperature [K]	C_p^{liq} [J mol^{-1} K^{-1}]							
	Cut 0	**Cut 1**	**Cut 2**	**Cut 3**	**Cut 4**	**Cut 5**	**Cut 6**	**Cut 7**
300.0	439.8	474.1	559.4	638.7	702.5	773.9	907.8	919.6
305.0	443.1	480.0	564.0	644.0	708.4	780.4	915.6	927.6
310.0	446.5	485.9	568.7	649.4	714.4	787.0	923.6	935.8
315.0	450.0	491.8	573.5	654.8	720.4	793.7	931.6	944.0
320.0	453.5	497.6	578.3	660.4	726.6	800.6	939.8	952.4
325.0	457.1	503.4	583.2	666.0	732.9	807.5	948.0	960.9
330.0	460.8	509.1	588.2	671.8	739.2	814.5	956.4	969.5
335.0	464.6	514.8	593.3	677.6	745.7	821.7	964.9	978.2
340.0	468.4	520.5	598.5	683.5	752.2	828.9	973.5	987.0
345.0	472.3	526.1	603.7	689.5	758.9	836.2	982.2	995.9
350.0	476.3	531.7	609.0	695.6	765.6	843.7	991.0	1004.9
355.0	480.3	537.3	614.4	701.7	772.4	851.2	1000.0	1014.0

360.0	484.4	542.8	619.8	708.0	779.3	858.8	1009.0	1023.3
365.0	488.6	548.2	625.4	714.3	786.3	866.6	1018.2	1032.6
370.0	492.8	553.7	631.0	720.7	793.4	874.4	1027.5	1042.1
375.0	497.2	559.1	636.7	727.3	800.6	882.4	1036.9	1051.7
380.0	501.6	564.4	642.4	733.8	807.9	890.4	1046.4	1061.4
385.0	506.1	569.8	648.3	740.5	815.3	898.5	1056.0	1071.2
390.0	510.6	575.0	654.2	747.3	822.8	906.8	1065.7	1081.1
395.0	515.2	580.3	660.2	754.2	830.3	915.1	1075.5	1091.1

Table D.6. Calculated liquid molar heat capacity of WC-B-D1

Temperature [K]	C_p^{liq} [J mol^{-1} K^{-1}]							
	Cut 0	**Cut 1**	**Cut 2**	**Cut 3**	**Cut 4**	**Cut 5**	**Cut 6**	**Cut 7**
300.0	435.0	460.3	542.4	605.7	696.6	843.3	865.8	1018.3
305.0	438.8	466.2	546.9	610.9	702.7	850.6	873.3	1027.2
310.0	442.2	472.0	551.5	616.2	708.8	858.0	880.9	1036.3
315.0	445.6	477.8	556.2	621.6	714.9	865.5	888.6	1045.4
320.0	449.1	483.5	561.0	627.0	721.2	873.2	896.5	1054.7
325.0	452.7	489.2	565.8	632.5	727.6	880.9	904.4	1064.0
330.0	456.3	494.8	570.7	638.1	734.0	888.7	912.4	1073.5
335.0	460.1	500.5	575.7	643.7	740.5	896.6	920.6	1083.2
340.0	463.8	506.0	580.8	649.5	747.1	904.6	928.8	1092.9
345.0	467.7	511.6	585.9	655.3	753.8	912.8	937.2	1102.8
350.0	471.6	517.1	591.1	661.2	760.6	921.0	945.6	1112.8

355.0	475.6	522.5	596.4	667.1	767.5	929.3	954.2	1122.9
360.0	479.7	528.0	601.7	673.2	774.4	937.8	962.9	1133.1
365.0	483.9	533.4	607.1	679.3	781.5	946.3	971.7	1143.5
370.0	488.1	538.7	612.6	685.5	788.6	955.0	980.5	1153.9
375.0	492.4	544.0	618.1	691.7	795.8	963.7	989.5	1164.5
380.0	496.7	549.3	623.8	698.1	803.1	972.5	998.6	1175.3
385.0	501.1	554.5	629.5	704.5	810.5	981.5	1007.8	1186.1
390.0	505.6	559.7	635.2	711.0	818.0	990.6	1017.1	1197.1
395.0	510.2	564.9	641.1	717.5	825.5	999.7	1026.5	1208.1

Table D.7. Calculated liquid molar heat capacity of RO-HO-A1

Temperature [K]	C_p^{liq} [J mol^{-1} K^{-1}]							
	Cut 0	**Cut 1**	**Cut 2**	**Cut 3**	**Cut 4**	**Cut 5**	**Cut 6**	**Cut 7**
300.0	450.8	458.2	545.6	646.2	723.0	757.4	835.0	940.0
305.0	454.2	464.1	550.1	651.5	728.8	763.6	842.0	947.9
310.0	457.6	469.9	554.8	656.8	734.7	770.0	849.1	956.0
315.0	461.1	475.7	559.5	662.3	740.7	776.4	856.3	964.2
320.0	464.6	481.5	564.3	667.9	746.8	783.0	863.6	972.5
325.0	468.3	487.2	569.2	673.5	753.0	789.7	871.1	980.9
330.0	472.0	492.9	574.1	679.2	759.3	796.4	878.6	989.5
335.0	475.8	498.5	579.1	685.1	765.7	803.3	886.3	998.1
340.0	479.6	504.1	584.2	691.0	772.2	810.3	894.0	1006.9
345.0	483.6	509.7	589.4	697.0	778.9	817.4	901.9	1015.8

350.0	487.6	515.2	594.6	703.1	785.6	824.5	909.9	1024.9
355.0	491.7	520.7	599.9	709.3	792.4	831.8	918.0	1034.0
360.0	495.9	526.1	605.2	715.5	799.4	839.2	926.2	1043.3
365.0	500.1	531.5	610.7	721.9	806.4	846.7	934.6	1052.7
370.0	504.5	536.9	616.2	728.4	813.6	854.3	943.0	1062.3
375.0	508.9	542.2	621.8	734.9	820.9	862.0	951.6	1071.9
380.0	513.3	547.5	627.5	741.6	828.3	869.8	960.2	1081.7
385.0	517.9	552.8	633.2	748.3	835.7	877.7	969.0	1091.6
390.0	522.5	558.0	639.0	755.1	843.3	885.8	977.9	1101.6
395.0	527.2	563.2	644.9	762.0	851.0	893.9	986.9	1111.7

APPENDIX E: EXPERIMENTAL VAPOR PRESSURE DATA

Measured vapor pressure of the fractions is presented in Tables D1 to D7. The constants obtained from the constrained extrapolation are summarized in Table D8

Table E.1. Measured vapor pressure for distillation fractions of WC-B-B1

Cut	T [K]	P [Pa]	Cut	T [K]	P [Pa]	Cut	T [K]	P [Pa]
1	313.2	0.5	2	333.2	0.06	3	323.2	0.002
1	333.2	2.5	2	353.2	0.6	3	353.2	0.05
1	343.2	5.3	2	373.2	2.3	3	393.2	2.2
1	353.2	11.7	2	393.2	8.6	3	413.2	7.2
1	363.2	25.5	2	413.2	33.8	3	433.2	23
4	403.2	0.7	5	423.2	2.2	6	433.2	1.3
4	413.2	1.3	5	433.2	3.6	6	443.2	2.1
4	423.2	2.2	5	443.2	6	6	453.2	3.5
4	433.2	3.8	5	458.2	12.1			
4	443.2	6.4						

Table E.2. Measured vapor pressure for distillation fractions of CO-B-A1

Cut	T [K]	P [Pa]	Cut	T [K]	P [Pa]	Cut	T [K]	P [Pa]	Cut	T [K]	P [Pa]
0	318	2.5	1	323	1.1	2	343	1.1	3	383	1.2
0	328	5.6	1	333	2.3	2	353	2.1	3	393	2.2
0	333	8.4	1	343	4.6	2	363	4.0	3	403	3.9
0	343	19.3	1	353	9.1	2	373	7.5	3	413	7.0
0			1	363	18.4	2	383	13.7	3	423	12.1
4	403	1.2	5	433	1.3	6	443	1.3			
4	413	2.2	5	443	2.2	6	453	2.2			
4	423	3.7	5	453	3.5	6	458	2.8			
4	433	6.2	5	463	5.7	6	463	3.5			
4	443	10.2									

Table E.3. Measured vapor pressure for distillation fractions of MX-HO-A1

Cut	T [K]	P [Pa]	Cut	T [K]	P [Pa]	Cut	T [K]	P [Pa]	Cut	T [K]	P [Pa]
0	305.2	1.4	1	343.2	1.2	2	373.2	1.2	3	393.2	1.3
0	313.2	2.6	1	353.2	2.3	2	383.2	2.3	3	403.2	2.3
0	323.2	6.1	1	363.2	4.6	2	393.2	4.2	3	413.2	3.9
0	333.2	14.2	1	373.2	9.0	2	403.2	7.5	3	423.2	6.6
			1	383.2	17.7	2	413.2	13.0	3	433.2	11.0
4	413.2	1.3	5	443.2	1.7	6	443.2	1.7	7	448.2	1.8
4	423.2	2.2	5	448.2	2.1	6	448.2	2.2	7	453.2	2.3
4	433.2	3.7	5	453.2	2.8	6	453.2	2.8	7	458.2	2.8
4	443.2	6.1				6	463.2	4.4	7	463.2	3.5

Table E.4. Measured vapor pressure for distillation fractions of CO-B-B1

Cut	T [K]	P [Pa]	Cut	T [K]	P [Pa]	Cut	T [K]	P [Pa]	Cut	T [K]	P [Pa]
0	303.2	1.6	1	323.2	1.2	2	363.2	0.9	3	403.2	2.1
0	313.2	4.0	1	338.2	4.3	2	383.2	4.3	3	413.2	4.3
0	323.2	9.1	1	353.2	14.0	2	393.2	8.7	3	423.2	8.2
0	328.2	13.3	1	368.2	41.1	2	403.2	16.9	3	433.2	15.4
0	333.2	19.1	1	383.2	109.3	2	413.2	31.8	3	443.2	27.8
4	418.2	2.2	5	433.2	2.3	6	443.2	1.7			
4	428.2	4.3	5	443.2	4.3	6	458.2	4.3			
4	438.2	8.1	5	453.2	8.0	6	463.2	5.8			
4	448.2	14.9									
4	453.2	20.0									

Table E.5. Measured vapor pressure for distillation fractions of US-OH-A1

Cut	T [K]	P [Pa]	Cut	T [K]	P [Pa]	Cut	T [K]	P [Pa]	Cut	T [K]	P [Pa]
0	302.2	1.5	1	313.2	0.3	2	383.2	2	3	403.2	2.1
0	313.2	3.8	1	343.2	4.3	2	393.2	4.2	3	413.2	4.2
0	318.2	5.8	1	363.2	19.6	2	403.2	8.3	3	423.2	8.1
0	323.2	8.5	1	383.2	74.7	2	413.2	15.6	3	433.2	15
			1	393.2	136.1						
4	413.2	2.2	5	423.2	2.2	6	433.2	2.2	7	433.2	2.2
4	423.2	4.2	5	433.2	4.3	6	443.2	4.2	7	443.2	4.2
4	433.2	8	5	443.2	8	6	453.2	7.8	7	453.2	7.7
4	438.2	10.9	5	453.2	14.5	6	463.2	14.1			

Table E.6. Measured vapor pressure for distillation fractions of WC-B-D1

Cut	T [K]	P [Pa]	Cut	T [K]	P [Pa]	Cut	T [K]	P [Pa]	Cut	T [K]	P [Pa]
0	313.2	1.7	1	343.2	0.8	2	383.2	2.0	3	403.2	1.1
0	323.2	4.2	1	363.2	4.2	2	393.2	4.2	3	423.2	4.2
0	333.2	9.3	1	373.2	8.6	2	403.2	8.1	3	433.2	7.8
0	338.2	13.6	1	383.2	16.8	2	413.2	15.1	3	443.2	14.2
	343.2	19.6	1	393.2	31.0		423.2	26.9			
4	433.2	3.0	5	443.2	3.1	6	443.2	2.2	7	443.2	2.2
4	438.2	4.2	5	448.2	4.2	6	453.2	4.2	7	453.2	4.2
4	443.2	5.7	5	453.2	5.6	6	458.2	5.7	7	463.2	7.6
4	448.2	7.8	5	463.2	10.1	6	463.2	7.6			

Table E.7. Measured vapor pressure for distillation fractions of RO-HO-A1

Cut	T [K]	P [Pa]	Cut	T [K]	P [Pa]	Cut	T [K]	P [Pa]	Cut	T [K]	P [Pa]
0	313.2	1.7	1	343.2	0.8	2	383.2	2.1	3	413.2	2.2
0	323.2	4.1	1	363.2	4.2	2	393.2	4.2	3	423.2	4.2
0	333.2	9.2	1	373.2	8.7	2	403.2	8.4	3	433.2	8.0
0	338.2	13.4	1	383.2	17.3	2	413.2	15.9	3	443.2	14.6
	343.2	19.1	1	393.2	32.4		423.2	28.8		453.2	26.0
4	433.2	2.2	5	443.2	2.3	6	443.2	2.3	7	443.2	2.3
4	443.2	4.3	5	453.2	4.3	6	453.2	4.3	7	453.2	4.2
4	453.2	7.9	5	458.2	5.8	6	463.2	7.8	7	463.2	7.7
4	463.2	14.2	5	463.2	7.8						

Table E.8. Parameters for Cox equations used to fit vapor pressure and $\Delta C^{'exp}$ with P_0 set to 101325 Pa for the eight oils characterized in this work

Sample	Cut	A_0	A_1 x 10^{-4}	A_2 x 10^{-6}	T_b [K]
WC-B-B1	1	3.11221	-22.21270	1.69391	605.03
	2	3.21997	-21.65373	1.79536	651.16
	3	3.30326	-23.05355	1.82732	690.60
	4	3.44185	-22.25477	1.70515	698.03
	5	3.51200	-23.61439	1.68252	706.73
	6	3.54805	-26.63337	2.03107	743.27
CO-B-A1	0	3.03826	-20.90684	1.52903	583.90
	1	3.03583	-21.41957	1.50693	630.96
	2	3.13523	-22.96500	1.63447	662.54
	3	3.28486	-20.99280	1.63595	676.86
	4	3.34154	-24.06453	2.16413	710.32
	5	3.43789	-20.96773	1.72373	724.04
	6	3.54117	-23.65263	1.66748	748.31
MX-HO-A1	0	3.15065	-18.77709	1.30126	537.97
	1	3.33299	-18.45701	1.18662	580.00
	2	3.43547	-15.76080	0.89250	600.00
	3	3.38597	-18.70039	0.87783	626.10
	4	3.62043	-16.42552	1.05355	630.00
	5	3.72662	-17.27968	1.08588	650.67
	6	3.52580	-21.60550	1.15697	743.91
	7	3.57652	-21.25255	0.97102	748.37
CO-B-B1	0	3.06663	-23.22736	1.49441	577.52
	1	3.18426	-22.41889	1.17258	600.00
	2	3.36047	-18.67288	1.03968	620.00
	3	3.49478	-17.82440	0.95283	640.00

	4	3.55921	-19.86677	1.22121	660.38
	5	3.62346	-20.55609	1.23245	675.60
	6	3.59308	-21.16838	1.21716	717.43
US-HO-A1	0	3.07951	-22.84177	1.56285	570.55
	1	3.12333	-16.27584	0.58643	591.32
	2	3.36762	-17.68206	1.05620	627.90
	3	3.45084	-18.09667	1.01993	650.00
	4	3.51787	-20.50515	1.35065	662.00
	5	3.50544	-21.61711	1.24991	699.58
	6	3.57981	-24.02399	1.27938	724.04
	7	3.58040	-24.40041	1.25377	730.36
WC-B-D1	0	3.15140	-20.21226	1.37550	556.14
	1	3.22183	-13.36731	0.64219	583.22
	2	3.37584	-18.13824	1.20763	625.16
	3	3.46817	-17.58520	1.12370	655.05
	4	3.54972	-18.84684	1.19256	670.00
	5	3.63159	-21.19822	1.24781	690.00
	6	3.62578	-21.52190	1.21851	706.00
	7	3.66026	-24.42117	1.13626	735.00
RO-HO-A1	0	3.10731	-21.87253	1.49821	576.60
	1	3.14183	-13.87169	0.66331	603.98
	2	3.37906	-17.86694	1.23924	620.17
	3	3.44240	-18.24768	1.09803	667.99
	4	3.51507	-20.61720	1.49350	692.00
	5	3.51059	-21.16420	1.43574	718.20
	6	3.53713	-22.62613	1.40093	731.00
	7	3.56891	-24.63554	1.36926	750.00

APPENDIX F: SPINNING BAND DISTILLATION DATA AND CORRESPONDING GAUSSIAN EXTRAPOLATION.

F.1. Experimental SBD

This section presents the experimental TBP curves obtained using SBD as well as the Gaussian extrapolation up to the asphaltene region. Both sets of data are included in the same table for the oils. The data corresponding to Gaussian Extrapolation is marked with a start (*)

Table F.1. Experimental and extrapolated SBD data for WC-B-B1

Normal Boiling Temperature [K]	wt % Distilled	Normal Boiling Temperature [K]	wt % Distilled
510.6	3.1	622.8	18.9
525.6	4.7	631.2	20.5
541.1	6.3	640.5	22.0
551.8	7.9	648.4	23.6
562.6	9.4	661.9	28.0*
574.9	11.0	697.2	37.5*
586.7	12.6	730.3	47.2*
597.2	14.2	763.3	57.0*
613.0	17.3	864.8	82.6*

Table F.2. Experimental and extrapolated SBD data for CO-B-A1

Normal Boiling Temperature [K]	wt % Distilled	Normal Boiling Temperature [K]	wt % Distilled
474.7	1.1	554.4	9.8
484.1	1.9	561.4	10.2
509.1	2.8	571.9	11.2
516.9	3.7	590.7	13.7
525.5	3.8	593.6	14.7
528.4	4.7	610.5	15.7
530.7	5.6	618.2	16.6
538.8	6.0	625.7	17.6
540.0	6.5	633.0	18.6
541.6	7.3	675.2	25.0
543.4	7.4	744.2	37.5*
546.8	7.9	792.2	47.2*
547.9	8.4	840.0	57.0*
550.6	9.3	931.5	74.2*

Table F.3. Experimental and extrapolated SBD data for MX-HO-A1

Normal Boiling Temperature [K]	wt % Distilled	Normal Boiling Temperature [K]	wt % Distilled
441.4	2.2	576.0	17.7
454.5	3.3	587.0	18.8
462.9	4.4	591.5	19.9
476.0	5.5	602.8	21.0
482.3	6.6	606.4	22.1
495.7	7.7	624.9	24.4
503.4	8.9	632.2	25.5
516.8	10.0	639.2	26.6
524.6	11.1	646.2	27.7
537.3	12.2	643.0	28.0*
542.1	13.3	693.9	37.5*
551.8	14.4	741.7	47.2*
559.9	15.5	789.3	57.0*
568.3	16.6	909.2	78.8*

Table F.4. Experimental and extrapolated SBD data for CO-B-B1

Normal Boiling Temperature [K]	wt % Distilled	Normal Boiling Temperature [K]	wt % Distilled
451.5	2.0	597.7	19.1
474.3	3.0	597.4	20.1
484.4	4.0	607.1	21.1
503.1	5.0	614.6	22.1
506.9	6.0	618.6	23.1
517.7	7.0	623.3	24.1
521.7	8.0	626.8	25.1
536.6	9.0	632.0	26.1
540.8	10.0	633.1	27.1
551.3	11.0	638.1	28.1
556.3	12.0	640.7	29.1
566.4	13.0	671.5	40.0*
571.7	14.0	701.9	50.0*
577.7	15.0	732.3	60.0*
582.3	16.0	764.9	70.0*
589.3	17.1	791.7	77.3*
591.5	18.1		

Table F.5. Experimental and extrapolated SBD data for US-HO-A1

Normal Boiling Temperature [K]	wt % Distilled	Normal Boiling Temperature [K]	wt % Distilled
449.2	1.9	597.2	21.4
469.8	2.9	601.6	22.3
480.4	3.7	605.8	23.2
491.7	4.6	610.0	24.2
496.4	5.6	614.0	25.1
506.5	6.5	618.0	26.0
510.5	7.4	622.0	26.9
518.9	8.4	625.8	27.9
524.3	9.3	629.6	28.8
532.1	10.2	633.4	29.7
537.6	11.1	640.8	31.6
546.2	12.1	644.4	32.5
550.4	13.0	648.0	33.4
558.8	13.9	651.6	34.4
563.3	14.9	655.1	35.3
568.8	15.8	669.9	40.0*
574.2	16.7	704.1	50.0*
579.2	17.6	738.2	60.0*
582.8	18.6	774.7	70.0*
588.2	19.5	857.6	87.3*
592.8	20.4		

Table F.6. Experimental and extrapolated SBD data for WC-B-D1

Normal Boiling Temperature [K]	wt % Distilled	Normal Boiling Temperature [K]	wt % Distilled
494.7	1.9	624.0	17.1
514.3	2.9	630.6	18.1
524.9	3.8	634.8	19.0
538.2	4.8	640.5	20.0
544.0	5.7	645.4	20.9
555.4	6.7	650.2	21.9
560.1	7.6	654.8	22.8
569.0	8.6	659.4	23.8
575.6	9.5	663.9	24.7
583.8	10.5	681.0	30.0*
588.1	11.4	717.2	40.0*
596.4	12.4	751.2	50.0*
601.1	13.3	785.1	60.0*
608.5	14.3	821.4	70.0*
613.0	15.2	883.3	83.8*
619.6	16.2		

Table F.7. Experimental and extrapolated SBD data for RO-HO-A1

Normal Boiling Temperature [K]	wt % Distilled	Normal Boiling Temperature [K]	wt % Distilled
471.3	1.9	618.3	24.2
484.9	2.9	621.9	25.2
496.7	3.9	628.0	26.2
512.6	4.8	630.0	27.1
517.1	5.8	635.1	28.1
524.6	6.8	638.5	29.1
529.2	7.8	644.1	30.0
537.2	8.7	647.3	31.0
539.7	9.7	651.2	32.0
550.2	10.7	654.0	32.9
554.5	11.6	658.4	33.9
561.9	12.6	660.7	34.9
567.0	13.6	664.8	35.8
573.4	14.5	666.3	36.8
577.5	15.5	668.8	37.8
584.9	16.5	673.5	38.8
588.0	17.4	678.6	40.7
596.3	19.4	711.0	50.0*
603.0	20.3	744.2	60.0*
606.4	21.3	779.7	70.0*
611.0	22.3	909.4	93.5*
614.2	23.3		

F.2. Results obtained from the interconverted data using the simplified interconversion method (Equation 5.18)

This section shows the quality of Equation 5.18 for the individual oils. For comparison, the Cox normal boiling points are presented too.

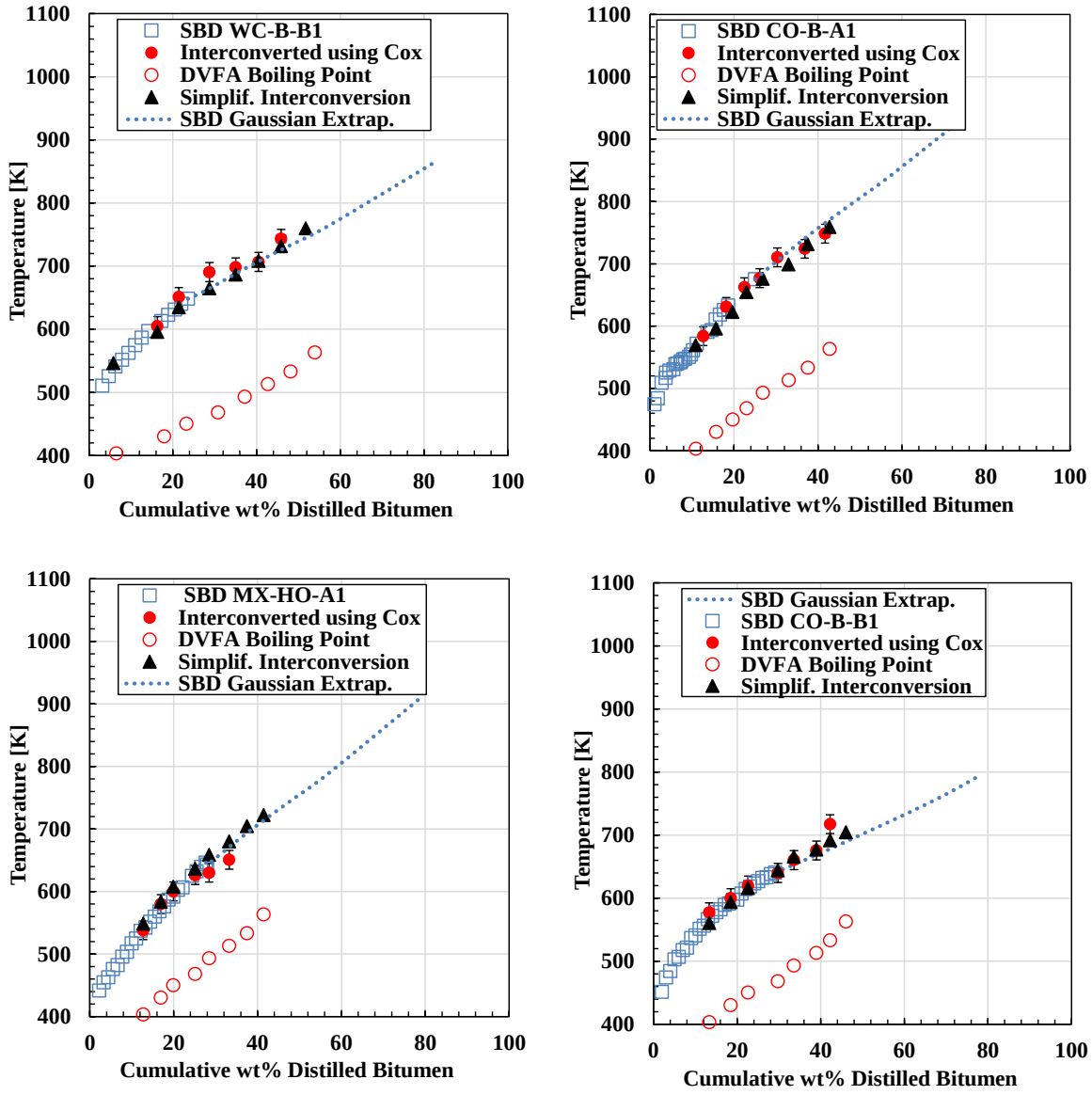

Figure F.1. Fitting obtained for the experimental NBP using simplified interconversion method for four oils.

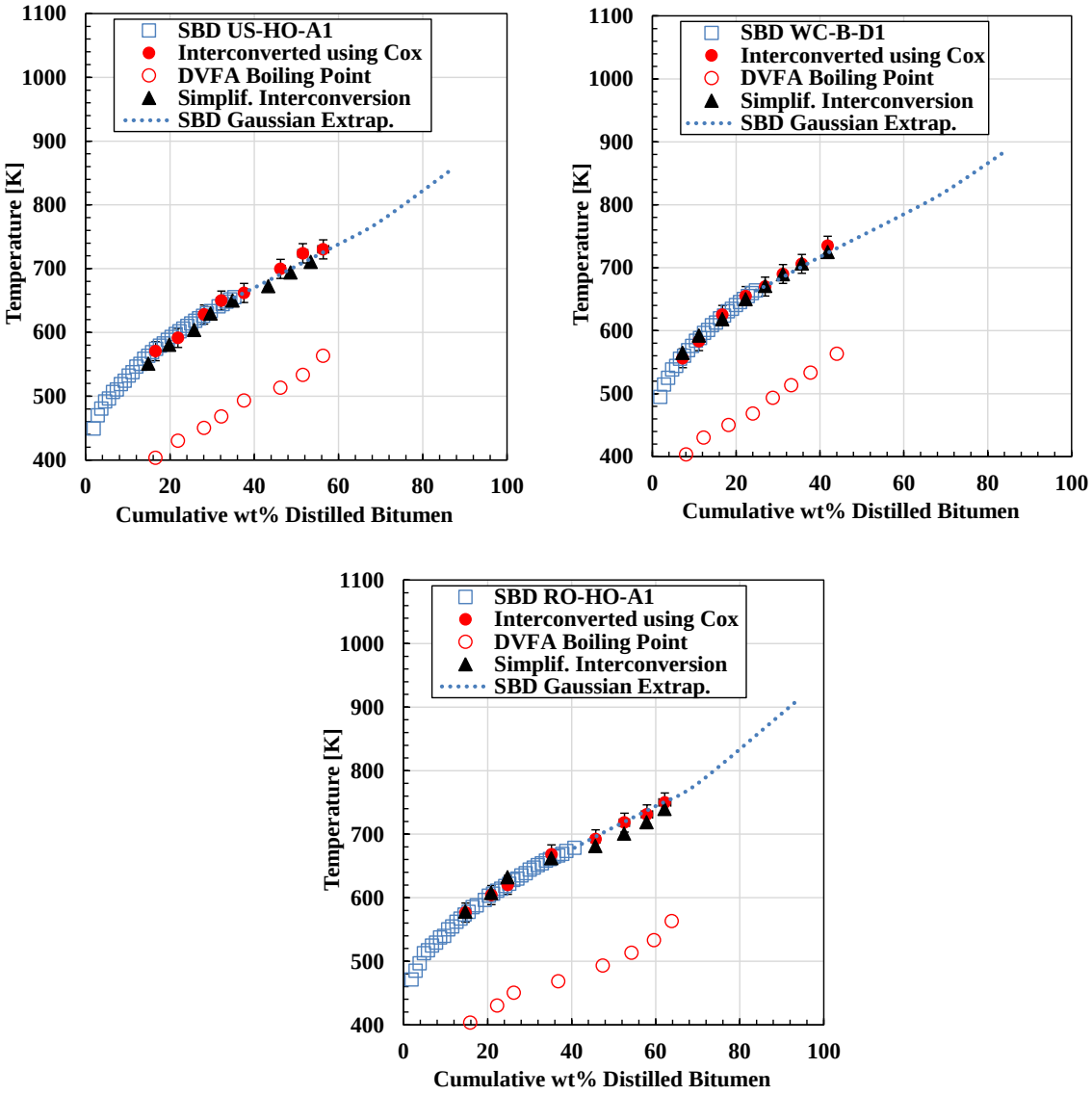

Figure F.2. Fitting obtained for the experimental NBP using simplified interconversion method for three oils.

APPENDIX G: PHYSICAL PROPERTIES

G.1. Normal boiling point

The absolute and relative error obtained in the prediction of NBP using correlations available in literature is reported per sample in Table G.1. The maximum deviations are summarized in Table G.2.

Table G.1 ARD and AAD obtained for the NBP of each bitumen and heavy oil distillation fractions using literature correlations

Oil	Soreide		L-K		RD		API	
Sample	AAD	ARD	AAD	ARD	AAD	ARD	AAD	ARD
WC-B-B1	22.6	3.1	137.7	9.9	37.4	5.4	72.5	5.4
CO-B-A1	7.2	1.0	83.2	5.7	33.6	4.6	33.6	2.6
MX-HO-A1	29.0	4.4	120.3	9.1	48.7	7.3	76.0	6.3
CO-B-B1	50.4	7.4	136.6	10.6	68.7	10.3	97.7	7.8
US-HO-A1	30.1	4.4	115.8	8.8	43.7	6.5	76.7	6.1
WC-B-D1	30.4	4.3	138.2	10.0	44.0	6.4	84.4	6.6
RO-HO-A1	6.6	0.9	78.6	5.4	24.6	3.3	32.8	2.5
TOTAL	**25.2**	**3.7**	**115.8**	**8.5**	**43.0**	**6.2**	**67.7**	**5.3**

Oil	oldRD		RB		Twu		Nji	
Sample	AAD	ARD	AAD	ARD	AAD	ARD	AAD	ARD
WC-B-B1	216.3	16.0	66.1	8.7	80.9	11.2	49.5	7.1
CO-B-A1	172.2	12.6	39.8	5.1	58.9	8.3	14.0	1.9
MX-HO-A1	204.8	16.0	59.6	8.4	78.0	11.6	16.5	2.3
CO-B-B1	221.9	17.7	72.0	10.2	92.9	13.7	52.0	7.8
US-HO-A1	202.7	15.9	59.0	8.2	78.4	11.4	31.5	4.8
WC-B-D1	229.7	17.5	68.3	9.2	85.6	12.2	23.9	3.5
RO-HO-A1	166.9	12.2	36.6	4.7	56.6	8.0	23.3	3.3
TOTAL	**202.1**	**15.4**	**57.4**	**7.8**	**75.9**	**10.9**	**30.1**	**4.4**

Table G.2 Maximum absolute and relative deviations for NBP obtained using correlations from literature.

Oil	Soreide		L-K		RD		API	
Sample	MAAD	MARD	MAAD	MARD	MAAD	MARD	MAAD	MARD
WC-B-B1	53.4	7.2	586.1	37.7	89.7	12.0	201.1	12.9
CO-B-A1	13.9	2.1	371.9	22.2	63.0	6.9	58.1	4.3
MX-HO-A1	42.8	6.4	432.6	26.4	74.6	11.1	102.9	8.5
CO-B-B1	110.2	13.9	548.0	38.5	98.0	14.2	263.8	18.5
US-HO-A1	58.2	8.3	370.2	24.0	86.5	12.4	131.5	10.4
WC-B-D1	62.7	8.7	552.7	34.8	88.9	12.6	171.1	11.3
RO-HO-A1	62.7	8.7	552.7	34.8	88.9	12.6	171.1	11.3

Oil	oldRD		RB		Twu		Nji	
Sample	MAAD	MARD	MAAD	MARD	MAAD	MARD	MAAD	MARD
WC-B-B1	690.3	44.4	233.7	27.0	690.3	44.4	233.7	27.0
CO-B-A1	499.6	29.8	130.1	14.0	499.6	29.8	130.1	14.0
MX-HO-A1	562.0	34.3	159.3	17.5	562.0	34.3	159.3	17.5
CO-B-B1	673.1	47.2	242.8	30.7	673.1	47.2	242.8	30.7
US-HO-A1	500.5	32.4	153.2	17.9	500.5	32.4	153.2	17.9
WC-B-D1	62.7	8.7	552.7	34.8	88.9	12.6	171.1	11.3
RO-HO-A1	62.7	8.7	552.7	34.8	88.9	12.6	171.1	11.3

G.2. Molecular weight

The absolute and relative error obtained in the prediction of MW using correlations available in literature is reported per sample in Tables G.3 to G.4. The maximum deviations are summarized in Table G.5 to G.6.

Table. G.3 Absolute and relative deviations for MW obtained using correlations from literature.

Oil Samle	Soreide		L-K		RD old		RD new		Goossens	
	AAD	ARD	AAD	ARD	AAD	ARD	AAD	ARD	AAD	ARD
WC-B-B1	83.8	13.7	102.7	16.1	143.2	25.0	90.4	14.7	118.6	21.6
CO-B-A1	47.9	9.0	64.9	10.5	114.1	21.8	41.5	8.0	70.6	15.9
MX-HO-A1	94.6	18.9	89.5	16.8	131.4	26.6	76.0	16.2	103.5	23.6
CO-B-B1	120.5	20.6	118.1	22.0	159.0	32.0	120.5	23.5	149.2	30.7
US-HO-A1	86.5	18.0	84.8	16.3	127.0	26.3	77.0	15.8	108.1	23.7
WC-B-D1	105.6	18.7	106.2	17.0	151.8	27.7	96.8	17.2	127.4	24.9
RO-HO-A1	55.2	9.6	63.0	9.8	111.8	21.2	43.7	7.6	75.8	16.1

Table. G.4 Absolute and relative deviations for MW obtained using correlations from literature.

Oil Sample	H-S		K-F		Winn-Mobil		Rao-Bardon		Twu	
	AAD	ARD	AAD	ARD	AAD	ARD	AAD	ARD	AAD	ARD
WC-B-B1	103.4	16.5	97.9	13.3	99.5	15.8	106.7	17.0	61.2	10.6
CO-B-A1	61.9	10.9	82.3	10.7	58.1	9.7	65.9	11.5	15.4	3.3
MX-HO-A1	89.6	17.9	91.7	12.5	84.9	16.5	91.4	17.9	41.7	10.0
CO-B-B1	125.8	24.3	62.4	8.9	117.9	22.1	125.8	24.0	92.8	17.5
US-HO-A1	87.1	17.3	44.6	7.2	81.3	15.9	88.3	17.4	52.8	11.1
WC-B-D1	109.6	18.8	127.5	14.7	102.4	16.7	110.8	18.6	60.3	10.1
RO-HO-A1	59.9	10.0	91.3	10.9	56.7	9.0	63.3	10.4	14.4	3.0

Table. G.5. Maximum absolute and relative deviations for MW obtained using correlations from literature.

Oil Sample	Soreide		L-K		RD old		RD new		Goossens	
	MAAD	MARD	MAAD	MARD	MAAD	MARD	MAAD	MARD	MAAD	MARD
WC-B-B1	146.6	24.8	480.1	47.5	559.0	55.3	384.9	38.1	427.3	42.3
CO-B-A1	35.3	14.9	325.8	33.6	423.4	43.6	142.4	14.7	150.9	21.5
MX-HO-A1	84.6	20.7	381.7	38.2	476.6	47.7	231.4	23.2	259.7	28.6
CO-B-B1	118.5	25.0	474.2	51.5	542.2	58.9	439.3	47.7	482.9	52.5
US-HO-A1	114.7	23.6	304.7	36.2	387.2	46.0	215.6	25.9	262.4	33.3
WC-B-D1	140.4	25.7	477.0	45.5	564.1	53.8	359.6	34.3	400.6	38.2
RO-HO-A1	39.6	11.6	356.6	36.4	452.9	46.3	206.5	21.1	234.4	23.9

Table. G.6. Maximum absolute and relative deviations for MW obtained using correlations from literature.

Oil Sample	H-S		K-F		Winn-Mobil		Rao-Bardon		Twu	
	MAAD	MARD	MAAD	MARD	MAAD	MARD	MAAD	MARD	MAAD	MARD
WC-B-B1	461.1	45.7	640.1	63.4	452.9	44.8	472.5	46.8	256.6	25.4
CO-B-A1	266.3	27.4	587.0	60.5	276.0	28.4	288.0	29.7	54.1	6.7
MX-HO-A1	331.5	33.2	649.3	65.0	340.2	34.1	352.1	35.2	71.3	14.9
CO-B-B1	471.4	51.2	416.7	45.3	464.4	50.5	480.1	52.2	364.4	39.6
US-HO-A1	282.4	33.6	250.9	29.8	279.7	33.3	295.7	35.2	120.1	20.7
WC-B-D1	445.0	42.5	971.3	92.7	444.3	42.4	460.3	43.9	220.8	22.1
RO-HO-A1	302.8	30.9	711.4	72.7	314.8	32.2	325.1	33.2	50.7	5.2

G.3. Specific Gravity

The absolute and relative error obtained in the prediction of SGusing correlations available in literature is reported per sample in Table G.7. The maximum deviations are summarized in Table G.8.

Table. G.7 Absolute and relative deviations for SG obtained using correlations from literature.

Oil Sample	Soreide		Withson		Jacoby	
	AAD	ARD	AAD	ARD	AAD	ARD
WC-B-B1	0.02	2.02	0.00	4.81	0.02	1.82
CO-B-A1	0.03	3.34	0.06	6.32	0.02	1.90
MX-HO-A1	0.02	1.74	0.05	5.00	0.02	2.13
CO-B-B1	0.02	1.70	0.04	4.28	0.02	1.68
US-HO-A1	0.01	0.63	0.03	2.76	0.02	2.00
WC-B-D1	0.02	2.30	0.06	6.04	0.01	1.50
RO-HO-A1	0.02	2.22	0.05	4.76	0.01	0.96

Oil Sample	RD Tb, I		RD MW, I		K-F		Gray	
	AAD	ARD	AAD	ARD	AAD	ARD	AAD	ARD
WC-B-B1	0.03	3.56	0.10	9.91	0.08	8.59	0.02	1.66
CO-B-A1	0.03	2.75	0.09	8.68	0.07	6.86	0.02	1.99
MX-HO-A1	0.02	2.58	0.09	9.16	0.05	5.08	0.03	2.80
CO-B-B1	0.03	3.10	0.08	7.67	0.06	6.00	0.03	2.97
US-HO-A1	0.02	1.98	0.07	6.87	0.04	4.42	0.06	5.87
WC-B-D1	0.03	2.69	0.10	10.46	0.06	5.83	0.03	3.30
RO-HO-A1	0.03	2.76	0.08	7.79	0.00	0.05	5.71	0.02

Table. G.8. Maximum absolute and relative deviations for SG obtained using correlations from literature.

Oil Sample	Soreide		Withson		Jacoby	
	MAAD	MARD	MAAD	MARD	MAAD	MARD
WC-B-B1	0.04	3.89	0.09	8.34	0.05	5.96
CO-B-A1	0.04	4.28	0.07	7.97	0.03	3.10
MX-HO-A1	0.03	2.88	0.08	8.00	0.06	6.76
CO-B-B1	0.02	2.43	0.06	5.80	0.04	4.62
US-HO-A1	0.01	1.26	0.05	4.80	0.05	5.64
WC-B-D1	0.04	3.86	0.08	8.52	0.04	4.74
RO-HO-A1	0.04	3.86	0.08	8.52	0.03	3.00

Oil Sample	RD Tb, I		RD MW, I		K-F		Gray
	MAAD	MARD	MAAD	MARD	MAAD	MARD	MAAD
WC-B-B1	0.05	4.53	0.58	55.51	0.10	10.83	0.06
CO-B-A1	0.06	5.72	0.52	51.99	0.08	8.16	0.03
MX-HO-A1	0.06	5.81	0.63	62.51	0.06	6.20	0.05
CO-B-B1	0.04	3.72	0.46	45.19	0.07	6.77	0.04
US-HO-A1	0.02	2.37	0.39	38.32	0.05	5.16	0.11
WC-B-D1	0.03	3.11	0.64	63.27	0.07	7.70	0.04
RO-HO-A1	0.03	3.11	0.64	63.27	0.07	7.70	0.04

G.4. Elemental analysis

The measured elemental composition of the petroleum fractions collected in this work are presented in Table G.9.

Table G.9. Measured elemental analysis for the distillation cuts

Sample	Cut	N wt%	C wt%	H wt%	S wt%	O wt%
WC-B-B1	0	0.43	84.75	12.18	2.74	0.31
	1	0.10	83.34	11.52	3.27	1.74
	2	0.00	83.59	10.65	4.41	2.01
	3	0.23	83.42	10.56	4.67	2.12
	4	0.27	84.08	10.84	4.72	1.95
	5	0.40	83.87	10.57	4.90	2.13
	6	0.36	83.35	10.45	5.63	1.81
	7	0.30	82.64	10.48	6.07	0.49
	Residue	0.56	81.99	10.00	6.75	1.94
CO-B-A1	0	0.10	86.17	12.41	1.27	2.00
	1	0.13	86.51	12.04	1.61	1.91
	2	0.16	86.22	11.47	2.04	2.04
	3	0.19	86.30	11.33	2.44	1.89
	4	0.23	85.66	11.26	2.42	2.04
	5	0.28	85.60	11.16	2.46	1.96
	6	0.39	85.22	11.00	2.76	1.87
	7	0.45	85.30	10.93	3.10	2.09
	Residue	0.70	84.90	10.50	3.44	2.21
MX-HO-A1	0	0.11	83.61	12.60	2.86	0.14
	1	0.13	83.18	11.95	3.86	0.33

	2	0.19	83.54	11.65	4.19	0.25
	3	0.24	83.79	11.57	4.16	0.30
	4	0.28	84.49	11.52	4.10	0.29
	5	0.24	84.51	11.46	4.14	0.29
	6	0.24	84.27	11.31	4.40	0.23
	7	0.28	83.75	11.02	4.82	0.34
	Residue	0.41	83.42	10.45	5.51	0.45
CO-B-B1	0	0.02	86.44	12.50	0.65	0.24
	1	0.04	86.29	11.79	1.27	0.24
	2	0.10	85.98	11.67	1.55	0.20
	3	0.12	85.94	11.51	1.72	0.27
	4	0.18	85.97	11.36	1.83	0.26
	5	0.20	85.88	11.31	1.82	0.29
	6	0.25	85.87	11.17	2.08	0.30
	7	0.29	85.39	11.00	2.42	0.31
	Residue	0.58	85.01	10.43	2.85	0.49
US-HO-A1	0	0.25	86.67	12.87	0.92	0.30
	1	0.29	86.35	12.34	1.52	0.34
	2	0.43	86.03	12.07	1.88	0.44
	3	0.54	85.94	11.98	1.88	0.39
	4	0.98	85.57	11.86	1.80	0.48
	5	1.17	85.86	11.83	1.59	0.50
	6	1.09	85.61	11.63	2.02	0.56
	7	1.36	85.26	11.46	2.33	0.46
	Residue	1.12	84.92	10.68	3.09	0.69

	0	0.02	86.12	12.66	0.91	0.07
	1	0.02	85.92	12.12	1.42	0.09
	2	0.03	85.74	11.74	2.07	0.14
	3	0.07	85.34	11.45	2.27	0.20
WC-B-D1	4	0.09	85.33	11.40	2.24	0.21
	5	0.13	85.37	11.36	2.24	0.18
	6	0.17	85.79	11.43	2.45	0.16
	7	0.20	85.48	11.37	2.71	0.21
	Residue	0.40	84.50	10.81	3.64	0.41
	0	0.43	86.68	12.89	0.00	0.06
	1	0.56	86.96	12.35	0.20	0.22
	2	0.45	86.90	11.95	0.21	0.39
	3	0.28	86.93	11.91	0.18	0.41
RO-HO-A1	4	0.55	86.82	12.16	0.15	0.28
	5	0.97	87.11	11.92	0.17	0.36
	6	0.81	86.98	11.71	0.21	0.42
	7	0.75	87.09	11.62	0.22	0.38
	Residue	0.70	87.03	11.06	0.27	0.74

APPENDIX H: VAPOR PRESSURE CORRELATION AND THERMAL DATA

H.1. Vapor Pressure Correlation

This appendix illustrates the deviations obtained when Equation 7.2 and 7.4 to 7.6 were used to fit the vapor pressure of the 63 distillation cuts from seven different heavy oil and bitumen samples. Tables H.1 to H.4 presents the bias for the test data set. Tables H.5 to H.8 summarizes the maximum average and relative deviations obtained for the tests data set.

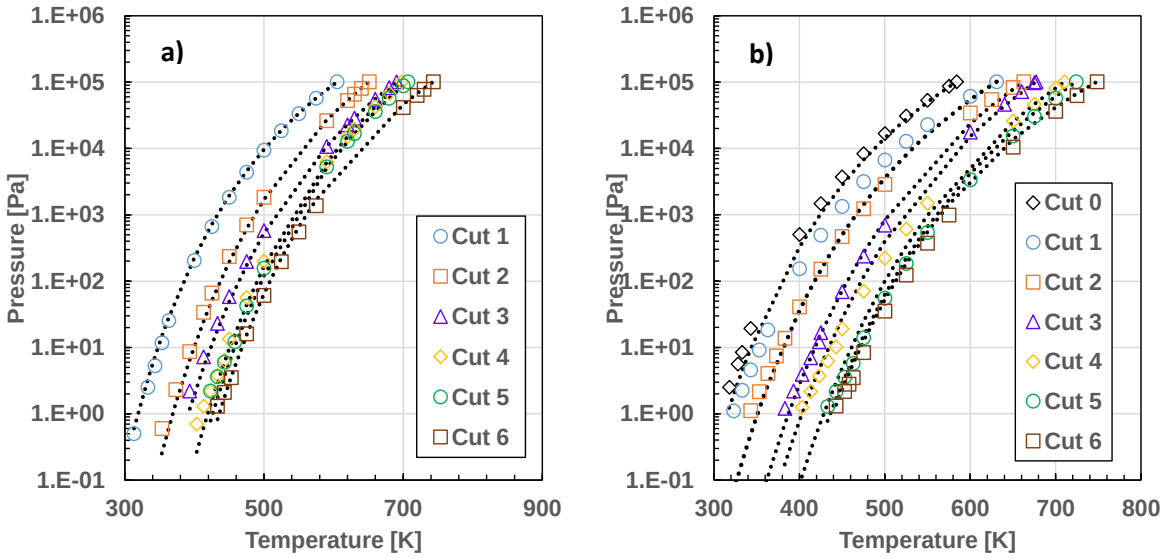

Figure H.1. Fitting obtained for a) WC-B-B1 and b) CO-B-A1 using Equation 7.2 and 7.4 to 7.6 to develop a new vapor pressure correlation for heavy petroleum fractions

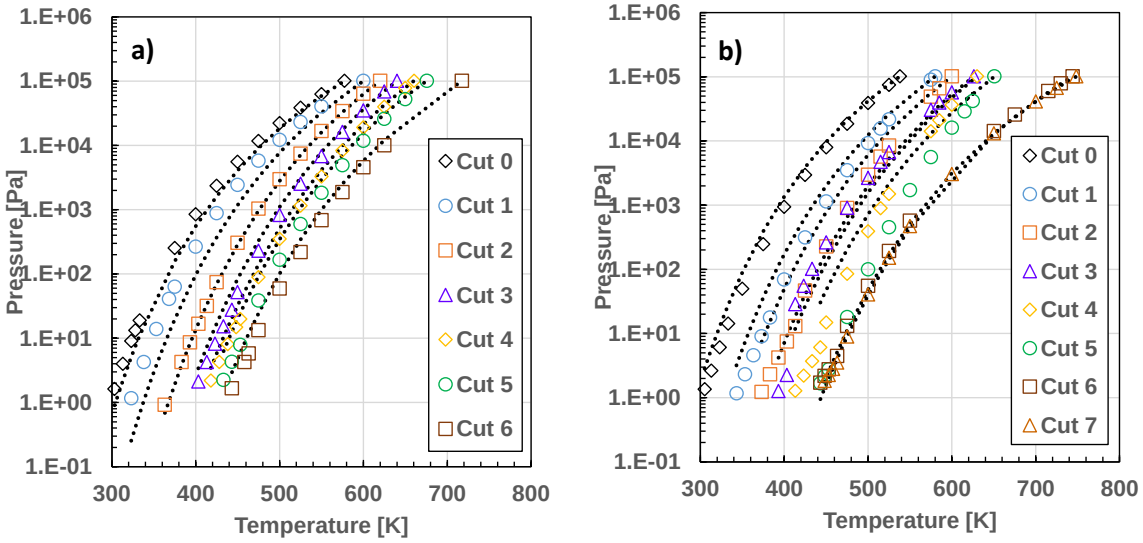

Figure H.2. Fitting obtained for a) MX-HO-A1and b) CO-B-B1using Equation 7.2 and 7.4 to 7.6 to develop a new vapor pressure correlation for heavy petroleum fractions

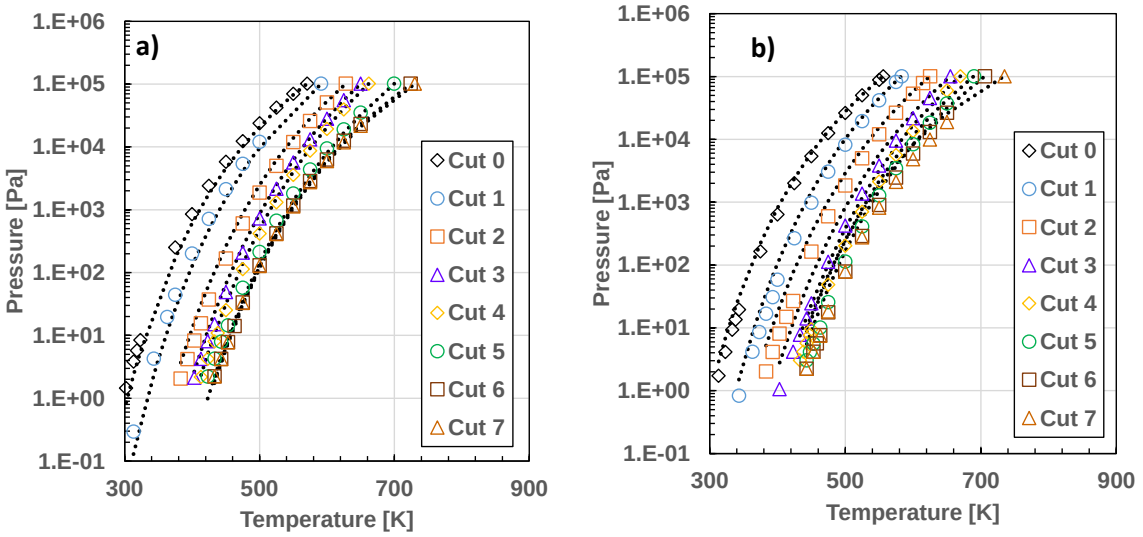

Figure H.3. Fitting obtained for a) US-OH-A1and b) WC-B-D1using Equation 7.2 and 7.4 to 7.6 to develop a new vapor pressure correlation for heavy petroleum fractions

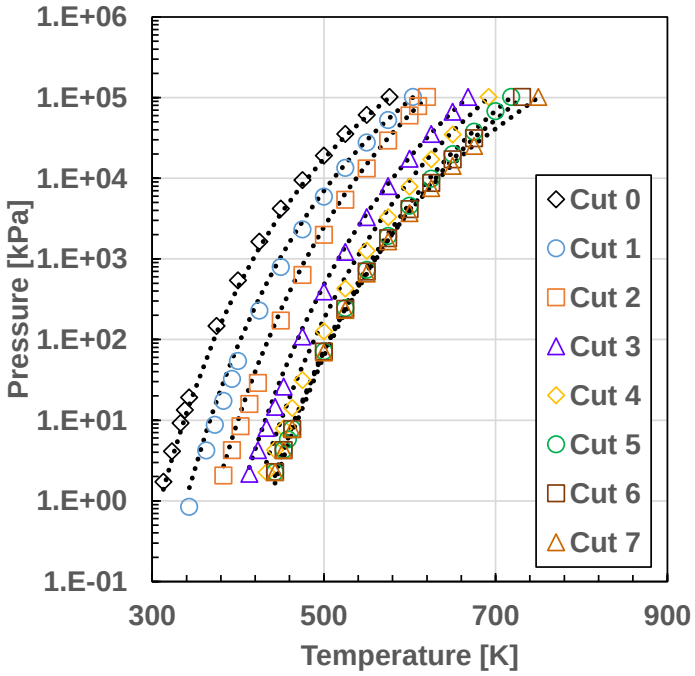

Figure H.4. Fitting obtained for RO-HO-A1 using Equation 7.2 and 7.4 to 7.6 to develop a new vapor pressure correlation for heavy petroleum fractions

Table H.1. Bias obtained for the first test data set from three different vapor pressure correlations.

Sample	This study	MB	Riazi
	Bias	Bias	Bias
ALT/Cut 550-600	-9	-5	-10
ALT/Cut 650-750	-48	-32	-38
ALT/Cut 750-850	-62	-52	-60
ALT/Cut 850-950	-52	-67	-75
Overall	-43	-39	-46

Table H.2. Bias obtained for the second test data set from three different vapor pressure correlations.

Sample	This study	MB	Riazi
	Bias	Bias	Bias
ANS/Cut 320-450	30	-5	-7
ANS/Cut 550-600	-13	-5	-13
ANS/Cut 750-850	-44	-24	-49
ANS/Cut 850-950	4	-40	-69
Overall	-6	-19	-35

Table H.3. Bias obtained for the third test data set from three different vapor pressure correlations.

Sample	This study	MB	Riazi
	Bias	Bias	Bias
SJV/Cut 450-650	-29	-41	-51
SJV/Cut 500-550	-7	-10	-16
SJV/Cut 600-650	1	20	-3
SJV/Cut 650-750	-72	-64	-75
SJV/Cut 750-850	-86	-81	-90
SJV/Cut 850-950	-53	-45	-76
Overall	-41	-37	-52

Table H.4. Bias obtained for the fourth test data set from three different vapor pressure correlations.

Sample	This study	MB	Riazi
	Bias	Bias	bias
Bitumen WC-B-B1	25	1513	804
Maltenes WC-B-B1	34	7036	3715
Eicosane	-26	-37	105
Overall	11	2837	1541

Table H.5. Maximum average absolute and relative deviations obtained for the first test dataset from three different vapor pressure correlations.

Sample	Riazi		MB		This study	
	MARD [%]	MAAD [Pa]	MARD [%]	MAAD [Pa]	MARD [%]	MAAD [Pa]
ALT/Cut 550-600	10	1628	5	1033	9	1262
ALT/Cut 650-750	38	7129	32	6091	48	8521
ALT/Cut 750-850	60	4294	52	3708	62	4393
ALT/Cut 850-950	75	2793	67	2519	52	1936
Overall	46	3961	39	3338	43	4028

Table H.6. Maximum average absolute and relative deviations obtained for the second test dataset from three different vapor pressure correlations.

Sample	Riazi		MB		This study	
	MARD [%]	MAAD [Pa]	MARD [%]	MAAD [Pa]	MARD [%]	MAAD [Pa]
ANS/Cut 320-450	11	5346	7	3343	30	4001
ANS/Cut 550-600	14	4155	5	2329	13	2947
ANS/Cut 750-850	49	4093	24	2260	44	3610
ANS/Cut 850-950	69	2056	40	1192	4	128
Overall	36	3912	19	2281	23	2671

Table H.7. Maximum average absolute and relative deviations obtained for the third test dataset from three different vapor pressure correlations.

Sample	Riazi		MB		This study	
	MARD [%]	MAAD [Pa]	MARD [%]	MAAD [Pa]	MARD [%]	MAAD [Pa]
SJV/Cut 450-650	51	10175	41	8719	29	6318
SJV/Cut 500-550	18	6024	11	3007	7	3492
SJV/Cut 600-650	7	1123	20	2997	8	1588
SJV/Cut 650-750	75	15503	64	13587	72	14708
SJV/Cut 750-850	90	5961	81	5296	86	5647
SJV/Cut 850-950	76	2268	45	1334	53	1569
Overall	53	6843	44	5823	42	5554

Table H.8. Maximum average absolute and relative deviations obtained for the fourth test dataset from three different vapor pressure correlations.

Sample	Riazi		MB		This study	
	MARD [%]	MAAD [Pa]	MARD [%]	MAAD [Pa]	MARD [%]	MAAD [Pa]
Bitumen WC-B-B1	804	189	1513	372	33	17
Maltenes WC-B-B1	3715	343	7036	608	91	13
Eicosane	105	22	42	1	23	1
Overall	1541	185	2864	327	49	10

H.2. Heat of Vaporization Data

The 'experimental' heats of vaporization for all the oils generated using the Cox constants obtained from simultaneous fitting of vapor pressure and liquid heat capacity are presented in the table below.

Table H.9. Heat of vaporization for the distillation cuts

Sample	Cut	ΔH^{vap}_{NBP} [kJ/mol]
WC-B-B1	1	54.8
	2	70.8
	3	76.0
	4	88.0
	5	86.0
	6	91.1
CO-B-A1	0	50.3
	1	54.6
	2	73.7
	3	76.8
	4	90.0
	5	101.3
	6	93.0
MX-HO-A1	0	55.4
	1	69.1
	2	83.0
	3	67.3
	4	105.6
	5	115.6
	6	79.9
	7	78.1
CO-B-B1	0	50.5

	1	58.8
	2	69.6
	3	82.8
	4	88.5
	5	92.1
	6	88.8
US-HO-A1	0	46.6
	1	52.4
	2	75.7
	3	80.9
	4	86.3
	5	78.7
	6	74.2
	7	71.6
WC-B-D1	0	53.7
	1	69.4
	2	78.4
	3	89.4
	4	93.7
	5	90.9
	6	88.5
	7	0.0
RO-HO-A1	0	50.0
	1	64.1
	2	80.5
	3	83.8
	4	94.9

5	91.7
6	84.5
7	75.3

H.3. Experimental Heat of Combustion for Distillation Cuts

The heat of combustions measurements correspond to the high heating value (HHV) and were measured at constant volume.

Table H.10. Heat of combustion for CO-B-A1 distillation cuts and deasphalted oil

Distillation Cut	HHV [kJ/g]
0	44.61
1	44.35
2	44.01
3	43.62
4	43.32
6	42.76
7	41.76
Residue	42.37
Maltenes	43.31

Table H.11. Heat of combustion for MX-HO-A1 distillation cuts and deasphalted oil

Distillation Cut	HHV [kJ/g]
0	44.93
1	43.9
2	44.16
3	43.47
4	43.37
7	41.53
Residue	41.62
Maltenes	42.73
Bitumen	41.34

Table H.12. Heat of combustion for CO-B-B1 distillation cuts and deasphalted oil

Distillation Cut	HHV [kJ/g]
0	44.73
1	44.86
2	44.36
3	44.22
4	43.48
5	43.22
6	42.01
7	42.32
Bitumen	42.56